EPICYCLIC HELICAL CHANNELS FOR PARAMETRIC RESONANCE IONIZATION COOLING

Final Report for Project starting 06/19/2010, ending 08/14/2013

Small Business: Muons, Inc.
552 N. Batavia Ave.
Batavia, IL 60510

Principal Investigator: Dr. Rolland Johnson

Research Institution: Thomas Jefferson National Accelerator Facility
Newport News, VA 23606

Research Inst. PI: Dr. Yaroslav Derbenev

Approved for public release; further dissemination unlimited. (Unclassified Unlimited)

PREPARED FOR THE UNITED STATES DEPARTMENT OF ENERGY

Work Performed Under grant DE-SC0002739

DISCLAIMER

This report was prepared as an account of work sponsored by an agency of the United States Government. Neither the United States Government nor any agency thereof, nor any of their employees, nor any of their contractors, subcontractors or their employees, makes any warranty, express or implied, or assumes any legal liability or responsibility for the accuracy, completeness, or any third party's use or the results of such use of any information, apparatus, product, or process disclosed, or represents that its use would not infringe privately owned rights. Reference herein to any specific commercial product, process, or service by trade name, trademark, manufacturer, or otherwise, does not necessarily constitute or imply its endorsement, recommendation, or favoring by the United States Government or any agency thereof or its contractors or subcontractors. The views and opinions of authors expressed herein do not necessarily state or reflect those of the United States Government or any agency thereof.

SBIR/STTR RIGHTS NOTICE

These SBIR/SITR data are furnished with SBIR/SITR rights under Grant No DE-SC0005589 and subgrant JSA-2011S025. For a period of four (4) years after acceptance of all items to be delivered under this grant, the Government agrees to use these data for Government purposes only, and they shall not be disclosed outside the Government (including disclosure for procurement purposes) during such period without permission of the grantee, except that, subject to the foregoing use and disclosure prohibitions, such data may be disclosed for use by support contractors. After the aforesaid four-year period, the Government has a royalty-free license to use and to authorize others to use on its behalf, these data for Government purposes, but is relieved of all disclosure prohibitions and assumes no liability for unauthorized use of these data by third parties. This Notice shall be affixed to any reproductions of these data in whole or in part. (End of Notice)

ABSTRACT

Proposed next-generation muon colliders will require major technical advances to achieve rapid muon beam cooling requirements. Parametric-resonance Ionization Cooling (PIC) is proposed as the final 6D cooling stage of a high-luminosity muon collider. In PIC, a half-integer parametric resonance causes strong focusing of a muon beam at appropriately placed energy absorbers while ionization cooling limits the beam's angular spread. Combining muon ionization cooling with parametric resonant dynamics in this way should then allow much smaller final transverse muon beam sizes than conventional ionization cooling alone. One of the PIC challenges is compensation of beam aberrations over a sufficiently wide parameter range while maintaining the dynamical stability with correlated behavior of the horizontal and vertical betatron motion and dispersion. We explore use of a coupling resonance to reduce the dimensionality of the problem and to shift the dynamics away from non-linear resonances. PIC simulations are presented.

EPICYCLIC HELICAL CHANNELS FOR PARAMETRIC RESONANCE IONIZATION COOLING CHANNELS

Table of Contents

ABSTRACT 2
Table of Contents 3
Motivation 4
Background 4
Technical Approach 5
Reports of Studies Supported by This Grant 9
Conclusions 9
Publications Supported by this grant 10
References 10
Appendix I: (IPAC10) Epicyclic Twin-Helix Magnetic Structure For Parametric-Resonance Ionization Cooling 11
Appendix II: (AAC10) Twin-Helix Channel for Parametric-resonance IC 14
Appendix III: (IPAC11) Parametric-Resonance Ionization Cooling In Twin-Helix 20
Appendix IV: (NAPAC11) Epicyclic Twin-Helix Ionization Cooling Simulations 23
Appendix V: (NAPAC11) EPIC Muon Cooling Simulations Using COSY Infinity 26
Appendix VI: (NAPAC11) Correcting Aberrations in Complex Magnet Systems for Muon Cooling Channels 29
Appendix VII: (COOL11) Helical Cooling Channel Developments 32
Appendix VIII: (IPAC12) Studies of fhe Twin Helix Parametric-Resonance Ionization Cooling Channel with COSY Infinity 36
Appendix IX: (IPAC12) Progress on Muon Parametric-Resonance Ionization Cooling Channel Development 39
Appendix X: (AAC12) Parametric-Resonance Ionization Cooling of Muon Beams 42
Appendix XI: (NuFact12) Progress Towards Parametric-Resonance Ionization Cooling in the Twin-Helix Channel 48
Appendix XII: (IPAC15) Skew-Quad Parametric-Resonance Ionization Cooling: Theory and Modeling 52
Appendix XIII: (IPAC15) Muon Tracking Studies in a Skew Parametric Resonance Ionization Cooling Channel 55
Appendix XIV: (arXiv:1205.3476) Parametric-Resonance Ionization Cooling 58
Appendix XV: (arXiv:1401.8256) Numerical Studies of Optimization and Aberration Correction Methods 102

Motivation

Bright muon beams have scientific, commercial, and homeland security applications. An important discovery machine made possible by such beams is an energy-frontier Muon Collider, made affordable by its technological innovations and compact size that allows it to sit on the Fermilab site. As a colliding beam particle, the muon offers many advantages to make up for its relatively short 2.2 μs lifetime. It is an elementary particle, so that all of its energy is available to create new states of matter such that a muon collider storage-ring can be ten times more effective than that of a hadron collider with the same diameter. It is 206.7 times more massive than an electron and therefore suffers little from electromagnetic radiation effects, which give an advantage over electron-positron colliders in the strength of bending magnets that can be used because of synchrotron radiation or in the initial-state energy resolution because of beamstrahlung.

Experiments at energy-frontier colliders require high luminosities of order 10^{34} cm^{-2} sec^{-1} or more in order to obtain reasonable rates for events having point-like cross sections. High luminosities require intense beams, small transverse emittances, and a small beta function at the collision point. For muon colliders, high beam intensities and small emittances are difficult and expensive to achieve because muons are produced diffusely and must be cooled drastically within their short lifetimes. The muon does not interact by the strong interaction, and its high mass relative to the electron means that it can pass through matter without hadronic or electromagnetic showers. Thus, it is the perfect candidate for ionization cooling, in which muons lose energy by passing through a low-Z material and only the longitudinal component is replaced by an RF cavity. This technique allows the angular spread of a beam of muons to be reduced in a very short time down to the limit determined by multiple scattering.

Background

Ionization cooling as it is presently envisioned will not cool the beam sizes sufficiently well to provide adequate luminosity without large muon intensities. For example, a muon-collider s-channel Higgs factory, a logical prerequisite to an energy frontier muon collider, would be compelling if the luminosity were high enough. The 4 MeV energy resolution needed to directly study the Higgs width is only possible with such a machine and the mass-dependent muon-Higgs coupling gives a factor of over 40,000 cross-section advantage relative to an electron collider. Numerical simulations of muon cooling channels based on technical innovations made and experimentally tested in this millennium have shown 6-d emittance reductions of almost 6 orders of magnitude. Parametric-resonance Ionization Cooling (PIC) can achieve an additional two orders of emittance reduction for an additional factor of 10 in luminosity [Appendices I-XV].

In addition, to the extent that the transverse emittances can be reduced further than with conventional ionization cooling, several problems can be alleviated. Lower transverse emittance allows reduced muon current for a given luminosity, which implies:

- a proton driver with reduced demands to produce enough proton power to create the muons,
- reduced site boundary radiation limits from muons decaying into neutrinos that interact with the earth,
- reduced detector background due to electrons from muon decay,

- reduced proton target heat deposition and radiation levels,
- reduced heating of the ionization cooling energy absorber,
- less beam loading and wake field effects in the accelerating RF cavities.

Smaller transverse emittance has virtues beyond reducing the required beam currents, namely:

- smaller higher-frequency RF cavities with higher gradient can be used for acceleration,
- beam transport is easier with smaller-aperture magnetic and vacuum systems,
- stronger collider interaction point (IP) focusing can be used, since that is limited by the maximum achievable beam extension prior to the IP.

Technical Approach

The limit on the minimum achievable emittances in muon ionization cooling comes from the equilibrium between the cooling process and multiple Coulomb scattering in the absorber material. The concept of Parametric-resonance Ionization Cooling (PIC) is to push this limit by an order of magnitude in each transverse dimension [Appendix XIV] by focusing the muon beam very strongly in both planes at thin absorber plates. This creates a large angular spread of the beam at the absorber locations, which is then cooled to its equilibrium value resulting in greatly reduced transverse emittances. Achieving adequately strong focusing using conventional magnetic optics would require unrealistically strong magnetic fields. Instead, PIC relies on a resonant process to provide the necessary focusing. A half-integer parametric resonance is induced in a cooling channel, causing focusing of the beam with the period of the channel's free oscillations.

The resonant perturbation changes the particles' phase-space trajectories at periodic locations along the channel from their normal elliptical shapes to hyperbolic ones as shown in Fig. 1. Thus, at certain periodic focal positions, the beam becomes progressively narrower in x and wider in x' as it passes down the channel. Without damping, the beam dynamics is not stable because the beam envelope grows with every period as illustrated in Fig. 2. Placing energy absorbers at the focal points stabilizes the beam motion by limiting the beam's angular divergence at those points through the usual ionization cooling mechanism. This dynamics then results in a strong reduction of the beam spot size at the absorber locations leading to transverse beam emittances that are an order of magnitude smaller than without the resonance. The longitudinal emittance is maintained constant by emittance exchange occurring due to dispersion at the absorber locations.

The normalized equilibrium transverse emittance achievable in PIC is given by [Appendix XIV]

$$\varepsilon_{\perp}^{n} = \frac{\sqrt{3}}{4\beta}(Z+1)\frac{m_e}{m_\mu}w$$

where $\beta = \upsilon / c$ is the relativistic factor, Z is the absorber material's atomic number, m_e and m_μ are the electron and muon masses, respectively, and w is the average absorber thickness in the beam direction.

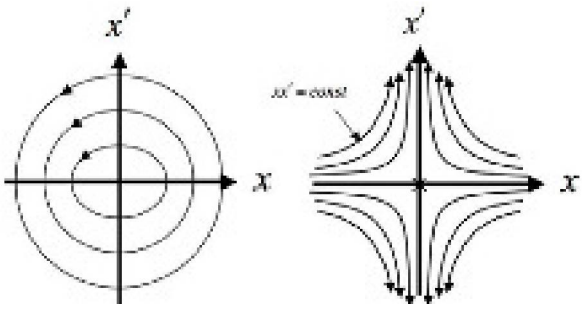

Fig. 1: Transformation of a particle's phase space motion by a half-integer parametric resonance: elliptical phase-space trajectories become hyperbolic. The trajectories are illustrated at the focal points.

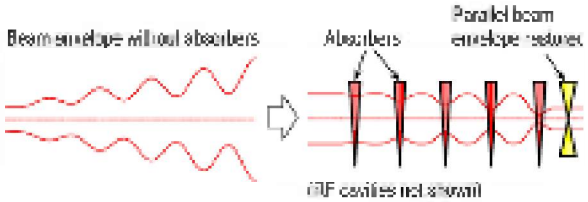

Fig. 2: Stabilizing effect of ionization cooling energy absorbers in a channel with a half-integer resonance.

The equilibrium beam size σ_a and angular spread θ_a at the absorber and the equilibrium momentum spread $\Delta p/p$ are given by [Appendix XIV]

$$\sigma_a^2 = \frac{1}{8}\frac{(Z+1)}{\gamma\beta^2}\frac{m_e}{m_\mu}w^2, \qquad \theta_a^2 = \frac{3}{2}\frac{(Z+1)}{\gamma\beta^2}\frac{m_e}{m_\mu}, \qquad (\Delta p/p)^2 = \frac{3}{8}\frac{(\gamma^2+1)}{\gamma\beta^2}\frac{m_e}{m_\mu}\frac{1}{\log}.$$

where γ is the muon relativistic energy factor and log is the Coulomb logarithm of ionization energy loss for fast particles. The expected PIC parameters for a 250 MeV/c muon beam are summarized in Table 1. Note that the absorbers are thicker at the beginning of the channel in order to produce a higher cooling rate of an initially large-emittance beam. As the beam cools propagating down the channel, the absorber thickness is gradually reduced in order to reach the minimum practical transverse emittance. Since the cooling rate gets lower for thinner absorbers, the minimum practical absorber thickness is determined by the practically acceptable beam loss due to muon decay.

TABLE 1. Expected PIC parameters.

Parameter	**Unit**	**Initial**	**Final**
Muon beam momentum, p	MeV/c	250	250
Number of particles per bunch, N_b	10^{10}	1	1
Be (Z = 4) absorber thickness, w	mm	20	2
Normalized transverse emittance (rms), $\varepsilon_x = \varepsilon_y$	μm	230	23
Beam size at absorbers (rms), $\sigma_a = \sigma_x = \sigma_y$	mm	0.7	0.1
Angular spread at absorbers (rms), $\theta_a = \theta_x = \theta_y$	mrad	130	130
Momentum spread (rms), $\Delta p/p$	%	2	2
Bunch length (rms), σ_z	mm	10	10

To attain simultaneous focusing in both planes at regular locations, the horizontal and vertical betatron oscillation periods must be commensurate with each other and with the channel's period, e.g. as illustrated in Fig. 3. A magnetic channel possessing such optical properties, called a twin helix channel, has been successfully developed and simulated [Appendices I-XI]. In a twin-helix channel, two equal-strength helical dipole harmonics with equal periods but opposite helicities are superimposed. Analogously to how combining two circularly-polarized waves produces a linearly-polarized one, the magnetic field in the midplane of this configuration is transverse to the plane. This means that the periodic orbit is flat and lies in the midplane. The horizontal and vertical motions are stable and uncoupled. A continuous straight quadrupole is added to the system in order to redistribute focusing between the horizontal and vertical dimensions.

Conceptually, the required magnetic field configuration can be obtained by winding two separate coaxial layers of helical conductors and coaxially superimposing a straight quadrupole as shown in Fig. 4(a). The helical conductors constituting the two layers have the same special periods and opposite helicities. Within each layer, the currents in the helical conductors vary azimuthally as $\cos(q)$. Note that the two layers do not have to have the same radius. The difference in the radii can be accounted for by adjusting the layers' currents. Another approach to producing the desired magnetic field is to combine two coaxial layers consisting of a series of tilted current loops overlaid with a coaxial straight quadrupole as shown in Fig. 4(b). The inclined loops comprising the two different layers are tilted in opposite directions. The current in the loops of each layer varies longitudinally as $\cos(kz)$. Such a technology, without longitudinal current variation, is used to make constant-field dipoles. Perhaps, a more practical approach to the channel's engineering design is to develop a conductor configuration that is centered on and follows the beam's periodic orbit.

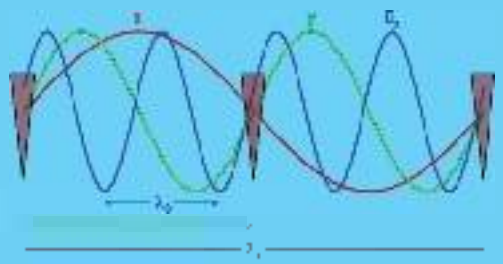

Fig. 3: Particle horizontal x and vertical y betatron trajectories and horizontal dispersion D_x for the case of correlated optics.

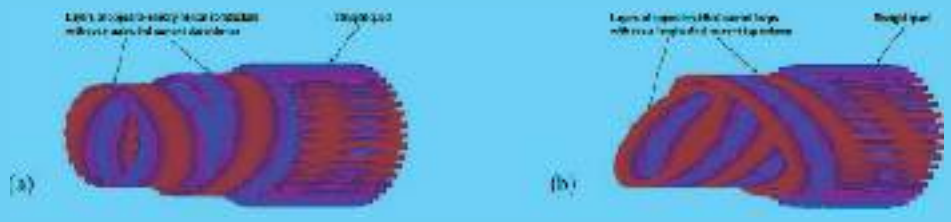

Fig. 4: Conceptual diagrams of possible practical implementations of the twin-helix channel. The color represents current variation in the conductors.

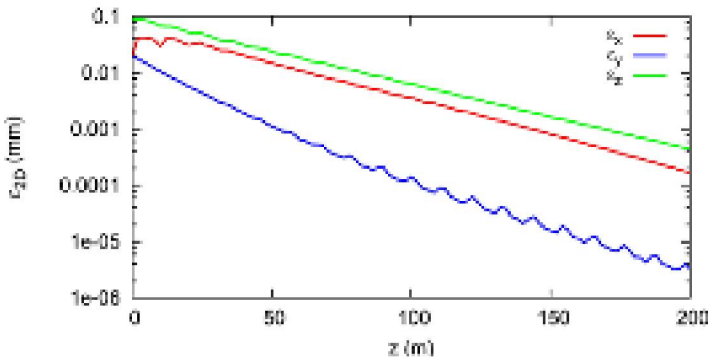

Fig. 5: Evolution of the horizontal ε_x, vertical ε_y, and longitudinal ε_z 2D emittances along a twin-helix channel ignoring stochastic effects.

Figure 5 shows the evolution of the three 2D emittances along a twin-helix channel obtained in a PIC simulation without stochastic effects using G4beamline that has been extended for this purpose. The initial emittance values were intentionally chosen relatively small in order to stay close to the linear regime. Since the stochastic effects are off, the emittances cool virtually to zero. An important condition necessary for implementation of PIC including stochastic effects is compensation of the beam smear from one focal point to another, to a degree where it is small compared to the focused beam size. Since the angular spread at the focal point is on the order of 100 mrad rms while the beam size is a fraction of a mm, this can be quite challenging.

Significant progress has been made on compensation of aberrations using helical multipole fields [Appendices IX, X] as illustrated in Fig. 6. A more systematic approach to aberration compensation is to use COSY Infinity, a matrix-based code, which works by expanding a particle's trajectory around a reference orbit to an arbitrary order in the 6D phase-space coordinates. Therefore, it can be used to unfold and analyze individual aberrations, which is well-suited for our purpose. COSY Infinity has been extended to include helical harmonics and to calculate the reference orbit in a twin helix. Work on compensating aberration using COSY Infinity has made a lot of progress [Appendices V, VI, VIII, XI, XV].

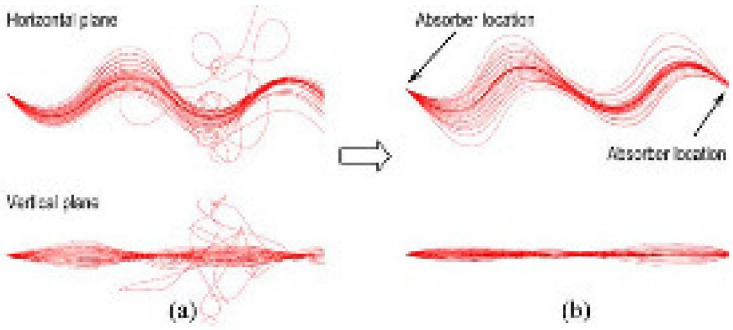

Fig. 6: Demonstration of aberration compensation in a twin helix up to a polar angle of 220 mrad; 250 MeV/c muon tracks are shown from one focal point to the next before (a) and after (b) aberration compensation using field harmonics up to decapole.

However, multipole fields in combination with correlated optics introduce another serious problem, namely, non-linear resonances causing loss of dynamical stability [Appendix XIII]. To illustrate this problem, consider the Hamiltonian term of a continuous harmonically-varying octupole field $H_{oct} = n_{oct}(6x^2y^2 - x^4 - y^4)/4$ where $n_{oct} \sim \cos(2\pi mz/L)$ is the normalized octupole strength, m is an integer, z is the longitudinal coordinate, L is the channel period length, $x \sim \cos(2\pi\nu_x z/L)$ and $y \sim \cos(2\pi\nu_y z/L)$ are the horizontal and vertical transverse betatron coordinates, respectively, and ν_x and ν_y are the horizontal and vertical betatron tunes, respectively. Multiple octupole harmonics are needed in a cooling channel to compensate spherical aberrations. However, as can be clearly seen from the Hamiltonian, with our choice of betatron tunes of $\nu_x = 0.25$ and $\nu_y = 0.5$, any octupole harmonic m causes resonances in both planes. Dispersion further complicates the resonance structure. Selecting different betatron tunes does not help; as long as the betatron periods are integer multiples of the channel period as required by PIC, multipole fields will tend to cause non-linear resonance. This makes it difficult to find a set of multipoles sufficient for aberration compensation that does not cause beam instabilities.

To overcome this problem, we developed the concept of Skew PIC [Appendices XIII, XIV]. We introduce coupling in a cooling channel in such a way that the point to point focusing needed for PIC is preserved but the canonical betatron tunes are shifted from their resonant values, i.e. the canonical phase advances in the two planes are shifted from $m\pi$ values. A simple way to think of it is that the beam is azimuthally rotated between consecutive focal points. This moves the dispersion and betatron motion away from non-linear resonances. It also offers a number of other benefits: (a) it allows for control of the dispersion size for chromatic compensation; (b) it reduces the dimensionality of the aberration compensation problem to just the radial dimension and therefore reduces the number of required compensating multipoles; (c) it equates the parametric resonance rates in the two planes, and therefore only one resonance harmonic is needed; (d) it equates the two cooling decrements in the two transverse dimensions.

Reports of Studies Supported by This Grant

The progress of the studies related to this grant was documented in contributions to the International and North American Particle Accelerator Conferences in 2010, 2011, 2012, and 2015, Workshops on Advanced Accelerator Concepts 2010 and 2012 and International Workshop on Neutrino Factories, Super Beams and Beta Beams 2012. These reprints are attached below as appendices.

Conclusions

PIC combines muon ionization cooling with parametric resonant dynamics to allow final equilibrium transverse beam emittances that are an order of magnitude smaller than those achievable with conventional ionization cooling alone. The 4 MeV energy resolution and the order of magnitude increased luminosity due to PIC will make a muon collider Higgs factory compelling.

Applying the same dynamics for Reverse Emittance Exchange (REMEX) will likewise make a compelling energy frontier muon collider. REMEX uses beryllium wedge absorbers to exchange longitudinal with transverse emittances. Smaller transverse emittances create

larger luminosity while the longitudinal emittance grows up to the point that the bunch length starts to reduce the luminosity due to the hourglass effect. Thus, PIC and REMEX together can provide two orders of magnitude luminosity increase of a muon collider.

A special continuous-field twin-helix magnetic channel with correlated behavior of the horizontal and vertical betatron motions and dispersion was developed for PIC. A basic model of a PIC channel with absorbers and RF cavities was setup in G4beamline. The model's validity was confirmed by PIC simulations with stochastic effects off. Compensation of beam aberrations is required for a complete demonstration of PIC with stochastic effects on. Difficulties with aberration corrections have stymied the development of a practical PIC channel. However, recent development of a fully transversely-coupled optical solution (Skew PIC) shows great promise.

Publications Supported by this grant

Publications supported by this grant are reproduced in the appendices. Particularly noteworthy are:

[1] Ya. S. Derbenev et al., arXiv:1205.3476v1 [physics. acc-ph]. [Appendix IX]
[2] J.A. Maloney, "parametric-resonance ionization cooling for muon beams in the twin helix channel", Ph.D. dissertation. http://www.niu.edu/physics/academic/grad/theses/JamesMaloney_PhD2013.pdf
[3] J.A. Maloney et al., submitted to PRST-AB. [Appendix XV]

References

[1] Six-dimensional muon beam cooling using a homogenous absorber: Concepts, beam dynamics, cooling decrements, and equilibrium emittances in a helical dipole channel", Y. Derbenev and R. Johnson, Phys. Rev. STAB 8, 041002 (2005)
[2] G4beamline, T. Roberts, http://www.muonsinc.com

EPICYCLIC TWIN-HELIX MAGNETIC STRUCTURE FOR PARAMETRIC-RESONANCE IONIZATION COOLING*

V.S. Morozov#, Old Dominion University, Norfolk, VA, USA & Muons, Inc.
A. Afanasev, Hampton University & Muons, Inc.
Y.S. Derbenev, Jefferson National Accelerator Facility, Newport News, VA, USA
R.P. Johnson, Muons, Inc.

Abstract

Parametric-resonance Ionization Cooling (PIC) [1-3] is envisioned as the final 6D cooling stage of a high-luminosity muon collider. Implementing PIC imposes stringent constraints on the cooling channel's magnetic optics design. This paper presents a linear optics solution compatible with PIC. Our solution consists of a superposition of two opposite-helicity equal-period and equal-strength helical dipole harmonics and a straight normal quadrupole. We demonstrate that such a system can be adjusted to meet all of the PIC linear optics requirements while retaining large acceptance.

INTRODUCTION

Combining muon ionization cooling with parametric resonant dynamics should allow much smaller final transverse muon beam sizes than ionization cooling alone [1-3]. Thus, high luminosity would be achieved in a collider with fewer muons. Parametric ionization cooling is accomplished by inducing a parametric resonance in a muon cooling channel. The beam is then naturally focused with a period of the channel's free oscillations. Absorber plates for ionization cooling together with energy-restoring rf cavities are placed at the beam focal points. At the absorbers, ionization cooling maintains the angular spread constant while the parametric resonance causes a strong reduction of the beam spot size. This resonant cooling scheme should provide equilibrium transverse emittances that are at least an order of magnitude smaller than those achievable with conventional ionization cooling.

TWIN-HELIX CHANNEL

Correlated Optics Condition

To ensure the beam's simultaneous focusing in both horizontal and vertical planes, the horizontal oscillations' period λ_x must be equal to or be a low-integer multiple of the vertical oscillations' period λ_y. The PIC scheme also requires alternating dispersion D such that D is

- small at the beam focal points to minimize energy straggling in the absorber,
- non-zero at the absorber for emittance exchange,
- relatively large between the focal points to allow for aberration correction to keep the beam size small at the absorbers.

Given the above dispersion requirements, it is clear that λ_x and λ_y must also be low integer multiples of the dispersion period λ_D. Note that λ_x and λ_D should not be equal to avoid an unwanted resonance. Thus, the cooling channel's optics must have correlated values of λ_x, λ_y and λ_D:

$$\lambda_x = n\lambda_y = m\lambda_D , \qquad (1)$$

e.g. $\lambda_x = 2\lambda_y = 4\lambda_D$ or $\lambda_x = 2\lambda_y = 2\lambda_D$.

Orbital Dynamics

The PIC dynamics is very sensitive to magnetic fringe fields. One approach to finding a practical fringe-field-free solution is to use helical harmonics [4, 5]:

$$\begin{aligned} B_\varphi^n &= b_\varphi^n(|k|,\rho)\cos(n[\varphi - kz + \varphi_0^n]), \\ B_\rho^n &= b_\rho^n(|k|,\rho)\sin(n[\varphi - kz + \varphi_0^n]), \\ B_z^n &= \mathrm{sgn}(k)\, b_z^n(|k|,\rho)\cos(n[\varphi - kz + \varphi_0^n]), \end{aligned} \qquad (2)$$

where B_φ, B_ρ, and B_z are the azimuthal, radial, and longitudinal helical magnetic field components, respectively, n is the harmonic number (e.g. $n = 1$ is the dipole harmonic), and $k = 2\pi / \lambda_h$ is the helix wave number while λ_h is the helix period.

One extensively-studied system based on helical field is the Helical Cooling Channel (HCC) [4]. However, the HCC is not suitable for PIC because it has constant dispersion magnitude. It was suggested [2] that alternating dispersion could be created by superimposing the HCC with an opposite-helicity helical dipole field with a commensurate characteristic period. However, with this approach, the periodic orbit solution is somewhat complicated and producing sufficiently large acceptance seems problematic.

Here we study a somewhat different configuration of magnetic fields, however, retaining the principle of Ref. [2] of creating an alternating dispersion by superimposing two helical-dipole fields with commensurate periods. We use a superposition of two equal-strength helical dipole harmonics with equal periods and opposite helicities ($k_1 = -k_2$) as a basis for our PIC channel design. Analogously to how combining two circularly-polarized waves produces a linearly-polarized one, the magnetic field in the mid-(horizontal)-plane of this configuration is transverse to the plane. This means that the periodic orbit is flat and lies in the mid-plane. The horizontal and vertical motions are uncoupled. This is a

* Work supported by Muons, Inc.
# morozov@jlab.org

more conventional orbital dynamics problem than the one with a 3D reference orbit and coupled transverse motion.

Figure 1(a) shows an example of the periodic orbit solutions for 100 MeV/c μ^+ and μ^- in a twin-helix channel with 1 m period and 0.741 T magnetic field strength of each helical dipole harmonic. The periodic orbit was determined numerically by locating the fixed point in the phase space. For this procedure, one only needed to consider the x-x' horizontal phase space and the procedure was further simplified by selecting a longitudinal position where x' was zero. Figure 1(b) shows the dispersion as a function of the longitudinal position for the μ^+ solution shown in Fig. 1(a). Note that the dispersion has oscillatory behaviour required for PIC. Note also that the dispersion period is equal to the helix period, i.e. $\lambda_D = \lambda_h$.

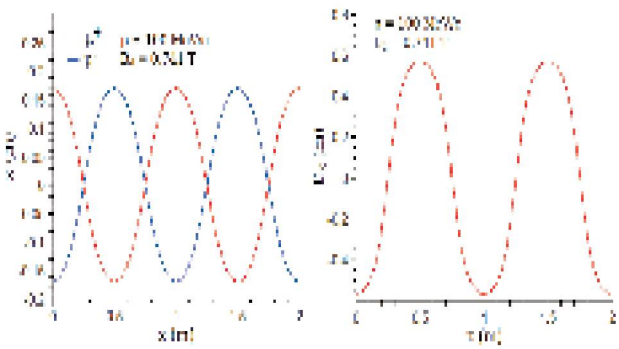

(a) (b)

Figure 1: (a) Periodic orbits of 100 MeV/c μ^+ and μ^- in a twin-helix channel with 1 m period and 0.741 T magnetic field strength of each helical dipole harmonic.
(b) Dispersion behavior as a function of the longitudinal position for the μ^+ solution in Fig. 1(a).

The transverse motion in a twin-helix consisting of two helical dipole harmonics only is stable around the periodic orbit in both dimensions as long as the helical dipole strength does not exceed a certain limiting value. Figures 2(a) and 2(b) show the periodic orbit's amplitude and the betatron tunes, respectively, vs. the helical dipole strength B_d for three different values of the helix period. In the calculations shown Figs. 2(a) and 2(b), the strength B_d was changed in small steps. On each step, the new periodic orbit was obtained as described above using the previous step's solution as the initial guess. The betatron tunes were extracted from a single-period linear transfer matrix, which was obtained numerically in terms of canonical coordinates. The canonical coordinates were calculated using an analytic expression for the helical magnetic field vector potential [5].

Since the dispersion period is determined by the helix period $\lambda_D = \lambda_h$, the correlated optics condition of Eq. (1) imposes the following conditions on the betatron tunes: $\nu_x = \lambda_h/\lambda_x = \lambda_h/(m\lambda_D) = 1/m$ and $\nu_y = \lambda_h/\lambda_y = \lambda_h/(m\lambda_D/n) = n/m$, e.g. $\nu_x = 0.5$, $\nu_y = 1$ or $\nu_x = 0.25$, $\nu_y = 0.5$. Examining Fig. 2(b) shows that it is not possible to satisfy these conditions by adjusting λ_h and B_d. Thus, we introduced a straight normal quadrupole to redistribute focusing between the horizontal and vertical dimensions. One subtlety is that, in addition to changing the focusing properties of the lattice, the quadrupole also changes the periodic reference orbit. The helical dipole strength B_d and the quadrupole gradient $\partial B_y/\partial x$ were iteratively adjusted until, at $B_d = 1.303$ T and $\partial B_y/\partial x = 1.153$ T/m, we achieved the correlated optics condition with $\nu_x = 0.25$ and $\nu_y = 0.5$. Having $\nu_x = 0.5$ and $\nu_y = 1$ would be more beneficial by allowing shorter spacing between the absorbers but it was not possible to adjust these tune values because of a strong parametric resonance at $\nu_y = 1$. We also attempted tuning the correlated optics condition by using a helical quadrupole pair instead of a straight quadrupole but that configuration did not seem compatible with the correlated optics requirements. Figure 3 shows the dependence of the betatron tunes on B_d at $\partial B_y/\partial x = 1.153$ T/m. The crossing lines indicate the correlated optics condition. Note that the straight quadrupole introduces an asymmetry into the magnetic field so that the correlated optics condition is satisfied for one muon charge only.

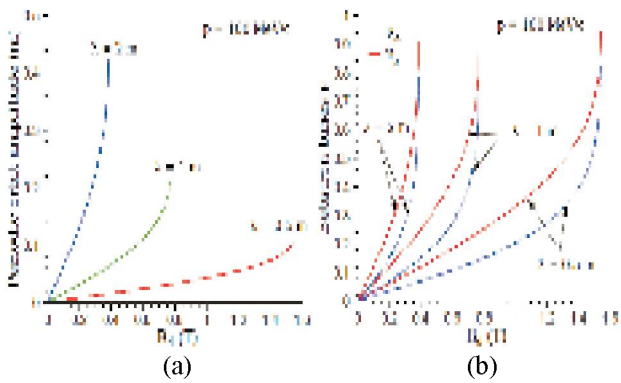

(a) (b)

Figure 2: Periodic orbit's amplitude (a) and horizontal and vertical betatron tunes (b) vs. the helical dipole strength.

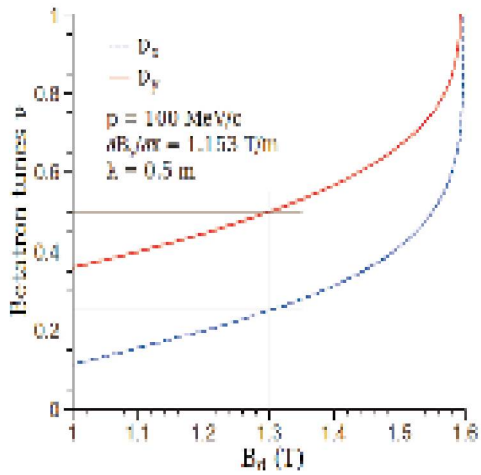

Figure 3: Horizontal and vertical betatron tunes vs. the helical dipole strength B_d at $\partial B_y/\partial x = 1.153$ T/m.

We next studied the dependence of the periodic orbit and of the betatron tunes on the muon momentum. We found that, with correlated optics, the dispersion

amplitude $D_{x\ max}$ = p $\partial x_{max}/\partial p$ was 0.098 m and the horizontal and vertical chromaticities were ξ_x = p $\partial \nu_x/\partial p$ = -0.646 and ξ_y = -0.798, respectively. The correlated optics parameters scale with the muon momentum and helix period in the following way:

$$B_d \propto p/\lambda, \quad \partial B_y/\partial x \propto p/\lambda^2, \\ x_{\max}, D_x \propto \lambda, \quad \xi_x, \xi_y \propto \text{const}. \tag{3}$$

G4beamline simulation

To estimate the dynamic aperture of the correlated optics channel, we tracked 10^5 100 MeV/c muons through 100 periods of the channel using the GEANT-based G4beamline program. The initial muon beam was monochromatic, parallel and uniformly distributed within a 5 cm × 5 cm square. Figures 4(a) and 4(b) show the initial and final transverse muon distributions, respectively. The initial positions of the particles that were not lost after 100 periods are shown in Fig. 4(a) in blue. Figures 4(a) and 4(b) suggest a very large dynamic aperture and therefore high transmission efficiency of the twin-helix channel.

Possible Practical Implementation

In practice, the required magnetic field configuration can be obtained by installing two separate helical dipoles producing equal field strengths within the channel's aperture [5] and then superimposing a straight quadrupole. The helical dipoles should be aligned along the symmetry axis and should have the same spatial periods and opposite helicities. Alternatively, the desired magnetic fields can be obtained by combining two series of tilted current loops with their currents varied along the symmetry axis.

Next steps

We will next consider compensation of chromatic and spherical aberrations. It has been demonstrated in [3] that chromatic terms can be compensated using two sextupole harmonics $n_s(s) = n_{s1} \sin(ks) + n_{s2} \sin(2ks)$ where k is the helix wave number. The spherical aberrations can be compensated [3] using three octupole harmonics $n_o(s) = n_{o1} + n_{o2} \cos(ks) + n_{o3} \cos(2ks)$. Thus, we will next study the non-linear optics effects of these sextupole and octupole parameters.

PIC requires x-y coupling for equalization of the cooling decrements [3]. Coupling can be introduced in the twin-helix channel by inducing an x-y coupling resonance or by slightly offsetting the spatial period of one of the helical harmonics in the harmonics pair.

CONCLUSION

We designed a muon beam "twin-helix" channel with linear optics suitable for parametric ionization cooling. The channel is a superposition of two opposite-helicity equal-period equal-strength helical dipole harmonics and a straight normal quadrupole. We demonstrated that such a system can be adjusted to meet all of the PIC linear optics requirements. Our tracking simulations suggest that the twin-helix channel has very large dynamics aperture. There is a straightforward practical implementation of such a channel.

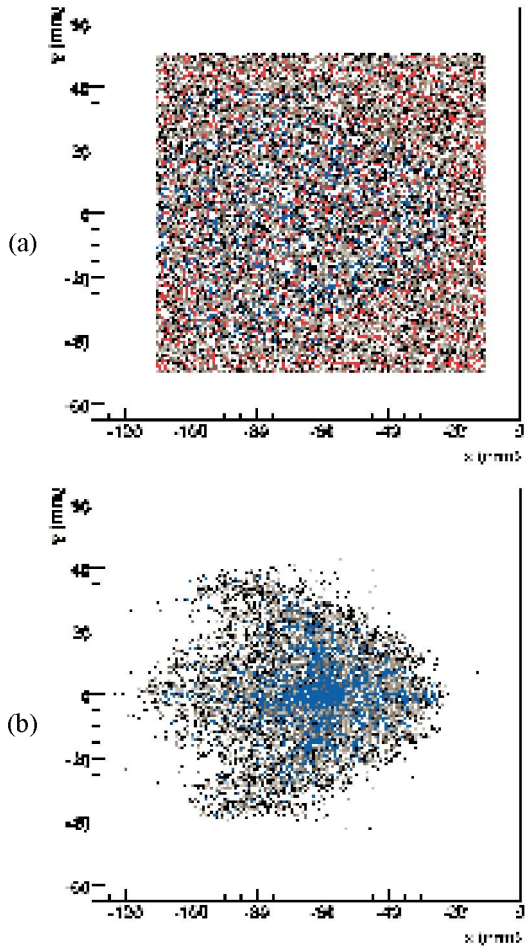

Figure 4: Initial (a) and final (b) transverse muon beam distributions in a G4beamline tracking study.

REFERENCES

[1] Y.S. Derbenev and R.P. Johnson, *Parametric-resonance Ionization Cooling and Reverse Emittance Exchange for Muon Colliders*, Proc. COOL05, AIP. Conf. Proc. 821 (2006), p. 420.

[2] Y.S. Derbenev and R.P. Johnson, *Advances in Parametric-resonance Ionization Cooling*, Proc. EPAC08, Genoa, Italy (2008), pp. 2838-2840; A. Afanasev, Y.S. Derbenev and R.P. Johnson, *Aberration-free Muon Transport Line for Extreme Ionization Cooling: a Study of Epicyclic Helical Channel*, *ibid.*, p. WEPP147.

[3] Y.S. Derbenev and R.P. Johnson, *Parametric-resonance ionization cooling*, in preparation.

[4] Y.S. Derbenev and R.P. Johnson, Phys. Rev. ST Accel. Beams 8, 041002 (2005).

[5] T. Tominaka *et al.*, Nucl. Instrum. Meth. A 459, 398 (2001).

Twin-Helix Channel for Parametric-Resonance Ionization Cooling

V.S. Morozov[a,d], A. Afanasev[b,d], Y.S. Derbenev[c], and R.P. Johnson[d]

[a]*Old Dominion University, Norfolk, Virginia 23529, USA*
[b]*Hampton University, Hampton, Virginia 23668, USA*
[c]*Thomas Jefferson National Accelerator Facility, Newport News, Virginia 23606, USA*
[d]*Muons, Inc., Batavia, Illinois 60510, USA*

Abstract. Parametric-resonance Ionization Cooling (PIC) [1-3] is envisioned as the final 6D cooling stage of a high-luminosity muon collider. Implementing PIC imposes stringent constraints on the cooling channel's magnetic optics design. This paper presents a linear optics solution compatible with PIC. Our solution consists of a superposition of two opposite-helicity equal-period and equal-strength helical dipole harmonics and a straight normal quadrupole. We demonstrate that such a system can be adjusted to meet all of the PIC linear optics requirements while retaining large acceptance.

Keywords: parametric resonance ionization cooling.
PACS: 29.27.-a, 29.20.-c, 14.60.Ef, 41.85.Lc

INTRODUCTION

Combining muon ionization cooling with parametric resonant dynamics should allow much smaller final transverse muon beam sizes than ionization cooling alone [1-3]. Thus, high luminosity would be achieved in a collider with fewer muons. The Parametric-resonance Ionization Cooling (PIC) concept is illustrated in Fig. 1(a). PIC is accomplished by inducing a parametric resonance in a muon cooling channel. The beam is then naturally focused with a period of the channel's free oscillations. Absorber plates for ionization cooling together with energy-restoring rf cavities are placed at the beam focal points. At the absorbers, ionization cooling maintains the angular spread constant while the parametric resonance causes a strong reduction of the beam spot size as illustrated in Fig. 1(b). This resonant cooling scheme should provide equilibrium transverse emittances that are at least an order of magnitude smaller than those achievable with conventional ionization cooling [3].

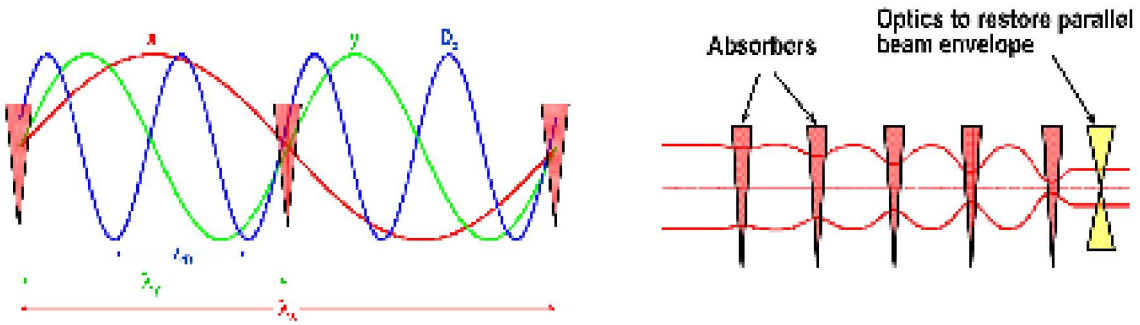

FIGURE 1. (a) Conceptual diagram of a PIC channel showing particle's horizontal (x) and vertical (y) betatron trajectories along with horizontal dispersion D_x. (b) Beam envelope in a PIC channel illustrating stabilizing absorber effect and beam spot size reduction at the focal points.

Downloaded 10 May 2012 to 129.57.115.212. Redistribution subject to AIP license or copyright; see http://proceedings.aip.org/about/rights_permissions

TWIN-HELIX CHANNEL

Correlated Optics Condition

To ensure the beam's simultaneous focusing in both horizontal and vertical planes, the horizontal oscillation period λ_x must be equal to or be a low-integer multiple of the vertical oscillation period λ_y. The PIC scheme also requires alternating dispersion D such that D is

- small at the beam focal points to minimize energy straggling in the absorber,
- non-zero at the absorber for emittance exchange to maintain constant longitudinal emittance,
- relatively large between the focal points to allow for aberration correction to keep the beam size small at the absorbers.

Given the above dispersion requirements, it is clear that λ_x and λ_y must also be low integer multiples of the dispersion period λ_D. Note that λ_x and λ_D should not be equal to avoid an unwanted resonance. Thus, the cooling channel optics must have correlated values of λ_x, λ_y and λ_D:

$$\lambda_x = n\lambda_y = m\lambda_D \tag{1}$$

e.g. $\lambda_x = 2\lambda_y = 4\lambda_D$ or $\lambda_x = 2\lambda_y = 2\lambda_D$.

Orbital Dynamics

The PIC dynamics is very sensitive to magnetic fringe fields. One approach to finding a practical fringe-field-free solution is to use helical harmonics [4, 5]:

$$\begin{aligned}
B_\varphi^n &= \left(\frac{2}{nk}\right)^{n-1} \left.\frac{\partial^{n-1} B_\varphi^n}{\partial \rho^{n-1}}\right|_0 \cos(n[\varphi - kz + \varphi_0^n])\,[I_{n-1}(nk\rho) - I_{n+1}(nk\rho)], \\
B_\rho^n &= \left(\frac{2}{nk}\right)^{n-1} \left.\frac{\partial^{n-1} B_\varphi^n}{\partial \rho^{n-1}}\right|_0 \sin(n[\varphi - kz + \varphi_0^n])\,[I_{n-1}(nk\rho) + I_{n+1}(nk\rho)], \\
B_z^n &= -2\left(\frac{2}{nk}\right)^{n-1} \left.\frac{\partial^{n-1} B_\varphi^n}{\partial \rho^{n-1}}\right|_0 \cos(n[\varphi - kz + \varphi_0^n])\, I_n(nk\rho),
\end{aligned} \tag{2}$$

where B_φ, B_ρ, and B_z are the azimuthal, radial, and longitudinal helical magnetic field components, respectively, n is the harmonic number (e.g. $n = 1$ is the dipole harmonic), and $k = 2\pi / \lambda_h$ is the helix wave number while λ_h is the helix period.

One extensively-studied system based on helical field is the Helical Cooling Channel (HCC) [4]. However, the HCC is not suitable for PIC because it has constant dispersion magnitude. It was suggested [2] that alternating dispersion could be created by superimposing the HCC with an opposite-helicity helical dipole field with a commensurate characteristic period. However, with this approach, the periodic orbit solution is somewhat complicated and producing sufficiently large acceptance seems problematic.

Here we study a somewhat different configuration of magnetic fields, however, retaining the principle of Ref. [2] of creating an alternating dispersion by superimposing two helical-dipole fields with commensurate periods. We use a superposition of two equal-strength helical dipole harmonics with equal periods and opposite helicities ($k_1 = -k_2$) as a basis for our PIC channel design. Analogously to how combining two circularly-polarized waves produces a linearly-polarized one, the magnetic field in the mid-(horizontal)-plane of this configuration is transverse to the plane. This means that the periodic orbit is flat and lies in the mid-plane. The horizontal and vertical motions are uncoupled. This is a more conventional orbital dynamics problem than the one with a 3D reference orbit and coupled transverse motion.

Figure 2(a) shows an example of the periodic orbit solutions for 100 MeV/c μ^+ and μ^- in a twin-helix channel with 1 m period and 0.741 T magnetic field strength of each helical dipole harmonic. The periodic orbit was

Downloaded 10 May 2012 to 129.57.115.212. Redistribution subject to AIP license or copyright; see http://proceedings.aip.org/about/rights_permissions

determined numerically by locating the fixed point in the phase space. For this procedure, one only needed to consider the x-x' horizontal phase space and the procedure was further simplified by selecting a longitudinal position where x' was zero. Figure 2(b) shows the dispersion as a function of the longitudinal position for the μ^+ solution shown in Fig. 2(a). Note that the dispersion has oscillatory behavior required for PIC. Note also that the dispersion period is equal to the helix period, i.e. $\lambda_D = \lambda_h$.

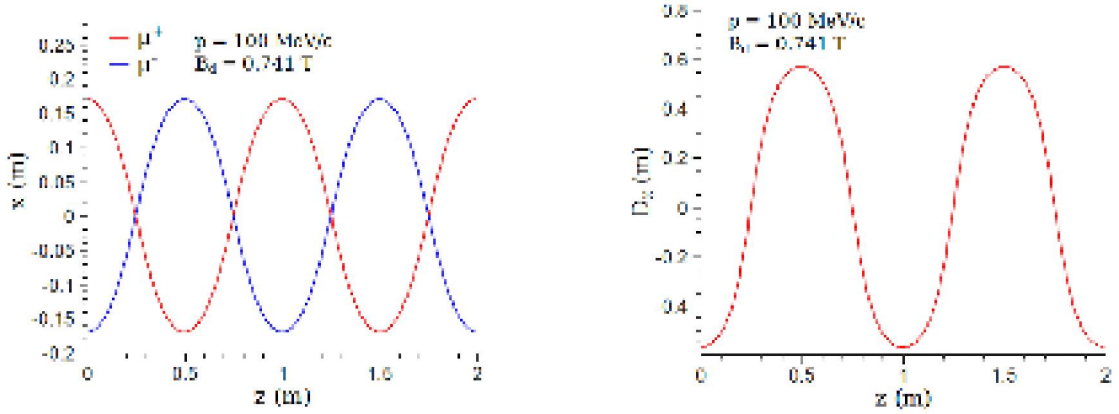

FIGURE 2. (a) Periodic orbits of 100 MeV/c μ^+ and μ^- in a twin-helix channel with 1 m period and 0.741 T magnetic field strength of each helical dipole harmonic. (b) Dispersion behavior as a function of the longitudinal position for the μ^+ solution in Fig. 2(a).

The transverse motion in a twin-helix consisting of two helical dipole harmonics only is stable around the periodic orbit in both dimensions as long as the helical dipole strength does not exceed a certain limiting value. Figures 3(a) and 3(b) show the periodic orbit amplitude and the betatron tunes, respectively, vs. the helical dipole strength B_d for three different values of the helix period. In the calculations shown in Figs. 3(a) and 3(b), the strength B_d was changed in small steps. On each step, the new periodic orbit was obtained as described above using the previous step's solution as the initial guess. The betatron tunes were extracted from a single-period linear transfer matrix, which was obtained numerically in terms of canonical coordinates. The canonical coordinates were calculated using an analytic expression for the helical magnetic field vector potential [5].

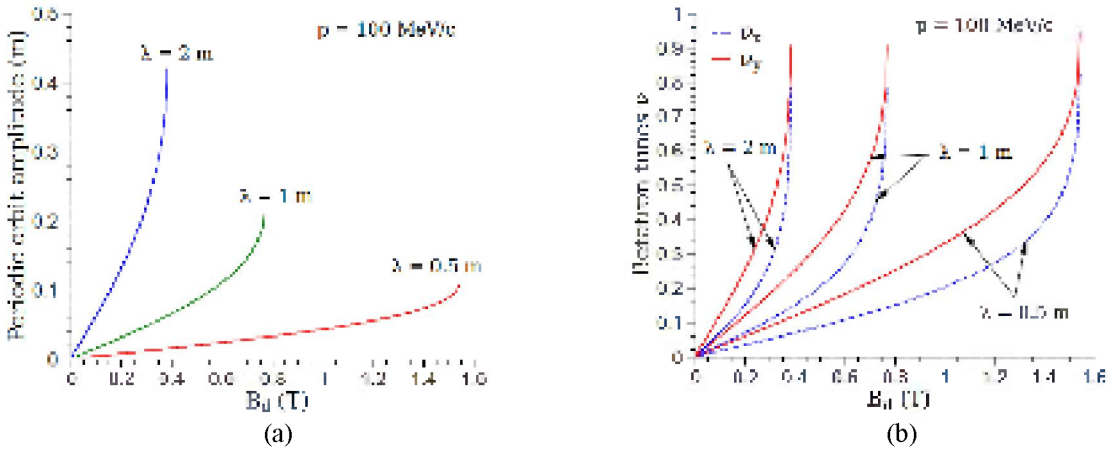

FIGURE 3. Periodic orbit amplitude (a) and horizontal and vertical betatron tunes (b) vs. the helical dipole strength.

Since the dispersion period is determined by the helix period $\lambda_D = \lambda_h$, the correlated optics condition of Eq. (1) imposes the following conditions on the betatron tunes: $\nu_x = \lambda_h/\lambda_x = \lambda_h/(m\lambda_D) = 1/m$ and $\nu_y = \lambda_h/\lambda_y = \lambda_h/(m\lambda_D/n) = n/m$, e.g. $\nu_x = 0.5$, $\nu_y = 1$ or $\nu_x = 0.25$, $\nu_y = 0.5$. Examining Fig. 3(b) shows that it is not possible to satisfy these conditions by adjusting λ_h and B_d. Thus, we introduced a straight normal quadrupole to redistribute focusing

Downloaded 10 May 2012 to 129.57.115.212. Redistribution subject to AIP license or copyright; see http://proceedings.aip.org/about/rights_permissions

between the horizontal and vertical dimensions. One subtlety is that, in addition to changing the focusing properties of the lattice, the quadrupole also changes the periodic reference orbit. The helical dipole strength B_d and the quadrupole gradient $\partial B_y/\partial x$ were iteratively adjusted until, at $B_d = 1.303$ T and $\partial B_y/\partial x = 1.153$ T/m, we achieved the correlated optics condition with $\nu_x = 0.25$ and $\nu_y = 0.5$. Having $\nu_x = 0.5$ and $\nu_y = 1$ would be more beneficial by allowing shorter spacing between the absorbers but it was not possible to adjust these tune values because of a strong parametric resonance at $\nu_y = 1$. We also attempted tuning the correlated optics condition by using a helical quadrupole pair instead of a straight quadrupole but that configuration did not seem compatible with the correlated optics requirements. Figures 4(a) and 4(b) show the dependence of the betatron tunes on B_d at $\partial B_y/\partial x = 1.153$ T/m and on $\partial B_y/\partial x$ at $B_d = 1.303$ T, respectively. The crossing lines indicate the correlated optics condition. Note that the straight quadrupole introduces an asymmetry into the magnetic field so that the correlated optics condition is satisfied for one muon charge only.

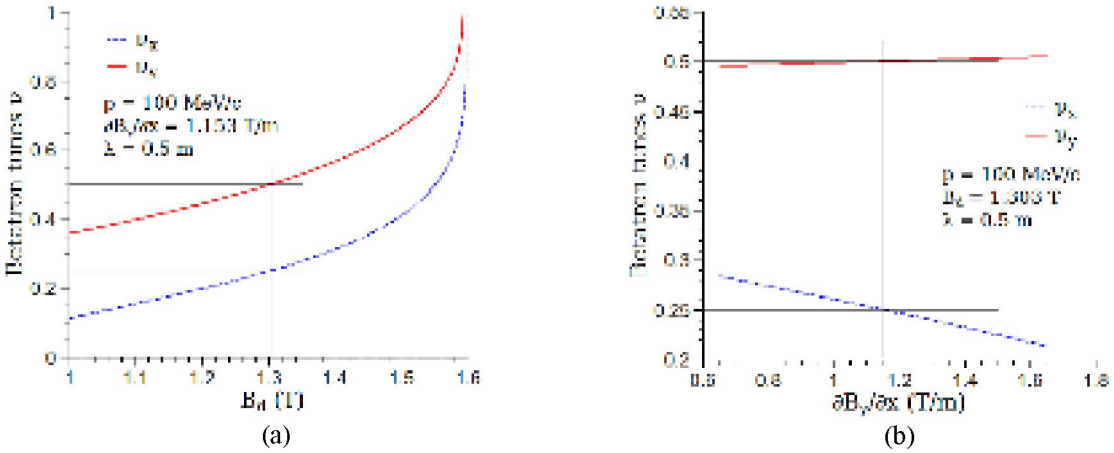

FIGURE 4. Horizontal and vertical betatron tunes vs. the helical dipole strength B_d at $\partial B_y/\partial x = 1.153$ T/m (a) and the straight quadrupole gradient $\partial B_y/\partial x$ at $B_d = 1.303$ T (b).

We next studied the dependence of the periodic orbit and of the betatron tunes on the muon momentum as shown in Figs. 5(a) and 5(b). These studies demonstrated large momentum acceptance of the twin-helix channel. We found that, with correlated optics, the dispersion amplitude $D_{x\,max} = p\,\partial x_{max}/\partial p$ was 0.098 m and the horizontal and vertical chromaticities were $\xi_x = p\,\partial\nu_x/\partial p = -0.646$ and $\xi_y = -0.798$, respectively. The correlated optics parameters scale with the muon momentum and helix period in the following way:

$$B_d \propto p/\lambda; \quad \partial B_y/\partial x \propto p/\lambda^2; \quad x_{\max}, D_x \propto \lambda; \quad \xi_x, \xi_y \propto \text{const.} \tag{3}$$

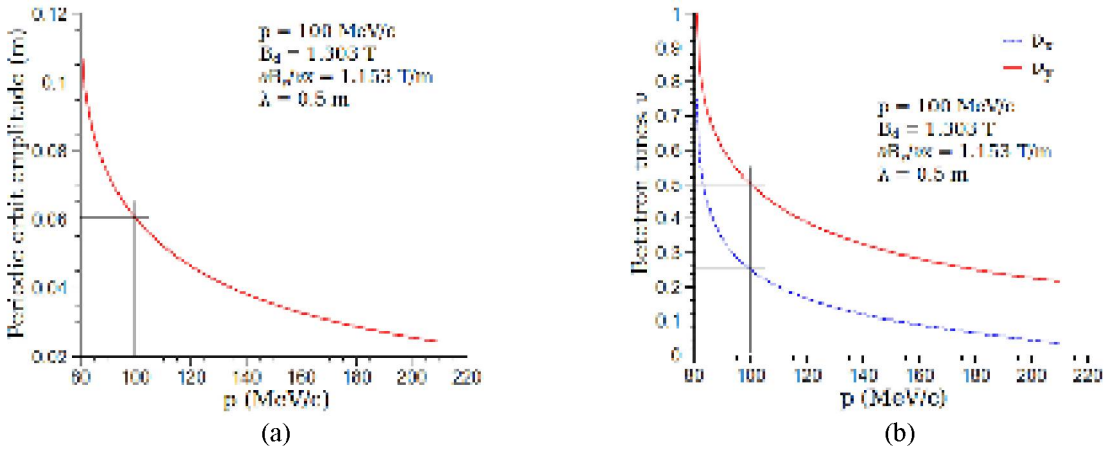

FIGURE 5. Periodic orbit amplitude (a) and betatron tunes (b) vs. the muon momentum with correlated optics.

Downloaded 10 May 2012 to 129.57.115.212. Redistribution subject to AIP license or copyright; see http://proceedings.aip.org/about/rights_permissions

G4beamline Simulation

To estimate the dynamic aperture of the correlated optics channel, we tracked 10^5 100 MeV/c muons through 100 periods of the channel using the GEANT-based G4beamline program [6]. The initial muon beam was monochromatic, parallel and uniformly distributed within a 10 cm × 10 cm square. Figures 6(a) and 6(b) show the initial and final transverse muon distributions, respectively. The initial positions of the particles that were not lost after 100 periods are shown in Fig. 6(a) in blue. Figures 6(a) and 6(b) suggest a very large dynamic aperture and therefore high transmission efficiency of the twin-helix channel.

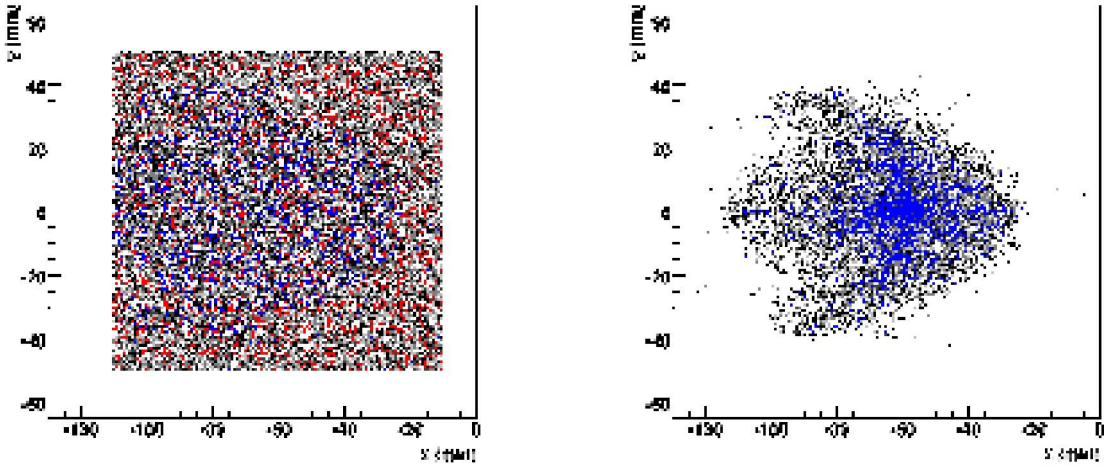

(a) (b)

FIGURE 6. Initial (a) and final (b) transverse muon beam distributions in a G4beamline tracking study.

Possible Practical Implementation

In practice, the required magnetic field configuration can be obtained by winding two separate coaxial layers of helical conductors and coaxially superimposing a straight quadrupole as shown in Fig. 7(a). The helical conductors constituting the two layers have the same special periods and opposite helicities. Within each layer, the currents in the helical conductors vary azimuthally as $\cos(\phi)$. Note that the two layers do not have to have the same radius. The difference in the radii can be accounted for by adjusting the layers' currents. Another approach to producing the desired magnetic field is to combine two coaxial layers consisting of series of tilted current loops and overlay a coaxial straight quadrupole as shown in Fig. 7(b). The inclined loops comprising the two different layers are tilted in opposite directions. The current in the loops of each layer varies longitudinally as $\cos(kz)$. Such a technology, without longitudinal current variation, is used for making constant-field dipoles.

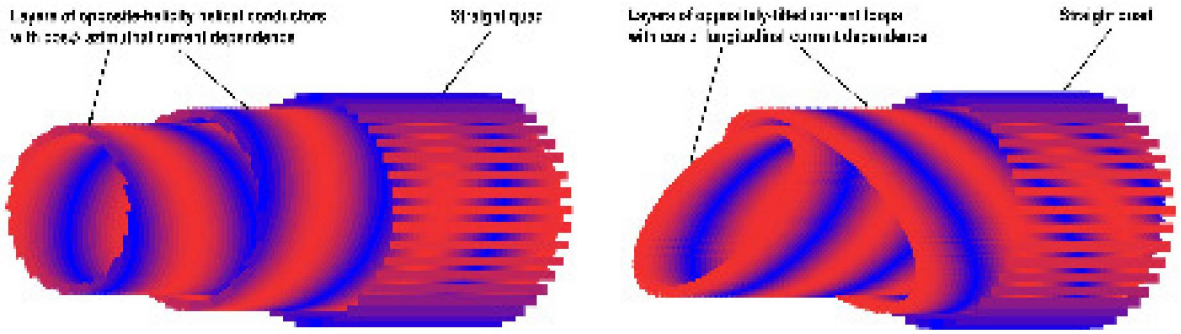

(a) (b)

FIGURE 7. Conceptual diagrams of possible practical implementations of the twin-helix channel (a) using a combination of two helical conductor layers and a straight quadrupole and (b) using a combination of two layers of tilted current loops and a straight quadrupole. The colors represent current variation in the conductiors.

Downloaded 10 May 2012 to 129.57.115.212. Redistribution subject to AIP license or copyright; see http://proceedings.aip.org/about/rights_permissions

Next Steps

We next plan to introduce wedge absorbers and rf cavities in the simulations. We will first demonstrate cooling without a parametric resonance, which should produce a result similar to the conventional ionization cooling. We will then introduce a parametric resonance and investigate its effect on cooling. We expect to show improvement in the equilibrium emittances due to the parametric resonance even prior to aberration compensation.

We will then consider compensation of chromatic and spherical aberrations. We plan to reduce the number of aberration compensation condition by taking advantage of the orbital motion symmetries naturally occurring in the correlated optics. Figure 1(a) shows that the particle's horizontal betatron trajectory is symmetric with respect to the point located half-way between two adjacent absorbers while the vertical betatron trajectory and dispersion are anti-symmetric with respect to the same point. These symmetry properties automatically eliminate many of the aberrations. It has been demonstrated in [3] that chromatic terms can be compensated using two sextupole harmonics $n_s(s) = n_{s1} \sin(ks) + n_{s2} \sin(2ks)$ where k is the helix wave number. The spherical aberrations can be compensated [3] using three octupole harmonics $n_o(s) = n_{o1} + n_{o2} \cos(ks) + n_{o3} \cos(2ks)$. Thus, we will next study the non-linear optics effects of these sextupole and octupole parameters.

PIC requires x-y coupling for equalization of the cooling decrements [3]. Coupling can be later introduced in the twin-helix channel by inducing an x-y coupling resonance or by slightly offsetting the spatial period of one of the helical harmonics in the harmonics pair.

CONCLUSION

We designed a muon beam "twin-helix" channel with linear optics suitable for parametric ionization cooling. The channel is a superposition of two opposite-helicity equal-period equal-strength helical dipole harmonics and a straight normal quadrupole. We demonstrated that such a system can be adjusted to meet all of the PIC linear optics requirements. Our tracking simulations suggest that the twin-helix channel has very large dynamic aperture. There is a straightforward practical implementation of such a channel.

ACKNOWLEDGMENTS

This work was supported by Muons, Inc.

REFERENCES

1. Y.S. Derbenev and R.P. Johnson, "Parametric-resonance Ionization Cooling and Reverse Emittance Exchange for Muon Colliders" in *COOL 05*, AIP Conference Proceedings 821, 2006, p. 420.
2. Y.S. Derbenev and R.P. Johnson, "Advances in Parametric-resonance Ionization Cooling" in Proceedings of *EPAC 08*, Genoa, Italy, 2008, pp. 2838-2840; A. Afanasev, Y.S. Derbenev and R.P. Johnson, "Aberration-free Muon Transport Line for Extreme Ionization Cooling: a Study of Epicyclic Helical Channel", *ibid.*, p. WEPP147.
3. Y.S. Derbenev and R.P. Johnson, "Parametric-resonance ionization cooling", in preparation.
4. Y.S. Derbenev and R.P. Johnson, *Phys. Rev. ST Accel. Beams* **8**, 041002 (2005).
5. T. Tominaka *et al.*, *Nucl. Instrum. Meth.* A **459**, 398 (2001).
6. G4beamline, http://g4beamline.muonsinc.com

Downloaded 10 May 2012 to 129.57.115.212. Redistribution subject to AIP license or copyright; see http://proceedings.aip.org/about/rights_permissions

PARAMETRIC-RESONANCE IONIZATION COOLING IN TWIN-HELIX*

V.S. Morozov#, Ya.S. Derbenev, Jefferson Lab, Newport News, VA, USA
A. Afanasev, Hampton University, Hampton, VA, USA
R.P. Johnson, Muons, Inc., Batavia, IL, USA
B. Erdelyi, J.A. Maloney, Northern Illinois University, DeKalb, IL, USA

Abstract

Parametric-resonance Ionization Cooling (PIC) is proposed as the final 6D cooling stage of a high-luminosity muon collider. For the implementation of PIC, we developed an epicyclic twin-helix channel with correlated optics. Wedge-shaped absorbers immediately followed by short rf cavities are placed into the twin-helix channel. Parametric resonances are induced in both planes using helical quadrupole harmonics. We demonstrate resonant dynamics and cooling with stochastic effects off using GEANT4/ G4beamline. We illustrate compensation of spherical aberrations and benchmark COSY Infinity, a powerful tool for aberration analysis and compensation.

INTRODUCTION

Combining muon ionization cooling with parametric resonant dynamics should allow much smaller final transverse muon beam sizes than conventional ionization cooling alone [1-2]. Thus, high luminosity would be achieved in a collider with fewer muons. Parametric-resonance Ionization Cooling (PIC) is accomplished by inducing a half-integer parametric resonance in a muon cooling channel. The beam is then naturally focused with a period of the channel's free oscillations. The channel is designed [3-5] with correlated values of the horizontal and vertical betatron periods so that focusing occurs in both planes simultaneously. Absorber plates for ionization cooling followed by energy-restoring RF cavities are placed at the beam focal points. At the absorbers, ionization cooling limits the angular spread while the parametric resonance causes a strong reduction of the beam spot size. The normalized equilibrium transverse emittance achievable in this resonant cooling scheme is given by [2]

$$\varepsilon_{\perp}^{n} = \frac{\sqrt{3}}{4\beta}(Z+1)\frac{m_e}{m_\mu}w\,, \qquad (1)$$

where $\beta = \upsilon / c$ is the relativistic velocity factor, Z is the absorber material's atomic number, m_e and m_μ are the electron and muon masses, respectively, and w is the average absorber thickness in the beam direction. Compared to the conventional ionization cooling, the emittance of Eq. (1) is reduced by at least an order of magnitude by a factor [2]

$$\frac{\pi}{\sqrt{3}}\frac{w}{\lambda_x} = \frac{\pi}{2\sqrt{3}}\frac{\gamma'_{acc}}{\gamma'_{abs}}\,, \qquad (2)$$

where λ_x is the period of the horizontal betatron oscillations and γ'_{acc} and γ'_{abs} are the RF acceleration and intrinsic absorber energy loss rates, respectively. The equilibrium beam size σ_a and angular spread θ_a at the absorber and the equilibrium momentum spread $\Delta p/p$ are given by [2]

$$\sigma_a^2 = \frac{1}{8}\frac{(Z+1)}{\gamma\beta^2}\frac{m_e}{m_\mu}w^2\,, \qquad (3)$$

$$\theta_a^2 = \frac{3}{2}\frac{(Z+1)}{\gamma\beta^2}\frac{m_e}{m_\mu}\,, \qquad (4)$$

$$(\Delta p/p)^2 = \frac{3}{8}\frac{(\gamma^2+1)}{\gamma\beta^2}\frac{m_e}{m_\mu}\frac{1}{\log}\,, \qquad (5)$$

where γ is the muon relativistic energy factor and log is the Coulomb logarithm of ionization energy loss for fast particles. For instance, for 250 MeV/c muons in a cooling channel with 5 mm thick Be absorbers, Eqs. (1) and (3)-(5) give $\varepsilon_{\perp}^{n} \approx 60$ μm·rad, $\sigma_a \approx 0.2$ mm, $\theta_a \approx 130$ mrad, and $\Delta p/p \approx 0.02$.

PARAMETRIC RESONANCE

To induce a half-integer parametric resonance, we earlier [5] used short lumped quadrupole magnets. That scheme, however, was primarily used for demonstration purposes. Its practical implementation would be difficult and the quadrupole fringe fields could potentially drive beam resonances and produce aberrations. Moreover, inducing a resonance in one plane was causing a dynamic instability in the other plane [5]. This simple model helped to gain a qualitative understanding of the parametric resonance driving scheme. We then used a pair of opposite-helicity but otherwise identical helical quadrupoles [6, 7] to excite a parametric resonance in each plane. The periodicity of the helical quadrupole pair was twice shorter than the respective betatron period [5]. Locations of the focal points were set with respect to the main twin helix by adjusting the parametric quadrupole phases using the fact that the focal point is located 1/8 of the respective betatron period from the maximum of the

* Supported in part by DOE SBIR grant DE-SC0005589.
Notice: Authored by Jefferson Science Associates, LLC under U.S. DOE Contract No. DE-AC05-06OR23177. The U.S. Government retains a non-exclusive, paid-up, irrevocable, world-wide license to publish or reproduce this manuscript for U.S. Government purposes.
morozov@jlab.org

Copyright © 2011 by IPAC'11/EPS-AG — cc Creative Commons Attribution 3.0 (CC BY 3.0)

quadrupole field [5]. Using this approach, we were able to independently induce a parametric resonance in each plane without causing instability in the other plane.

The horizontal and vertical phase-space trajectories of a 250 MeV/c μ^- at the desired absorber location with half-integer parametric resonances excited in both planes are shown by the red dots in the top and bottom parts of Fig. 1, respectively. The hyperbolic shape of the horizontal phase-space trajectory near the graph's center is indicative of a half-integer parametric resonance. The vertical phase-space motion is a little more complicated because it is strongly coupled to the horizontal motion. Regions of hyperbolic motion in the vertical phase space suggest that the particle goes in and out of the vertical parametric resonance depending on the particle's horizontal position. Tracking in this and later studies presented in this paper was done using the GEANT-based G4beamline program [8].

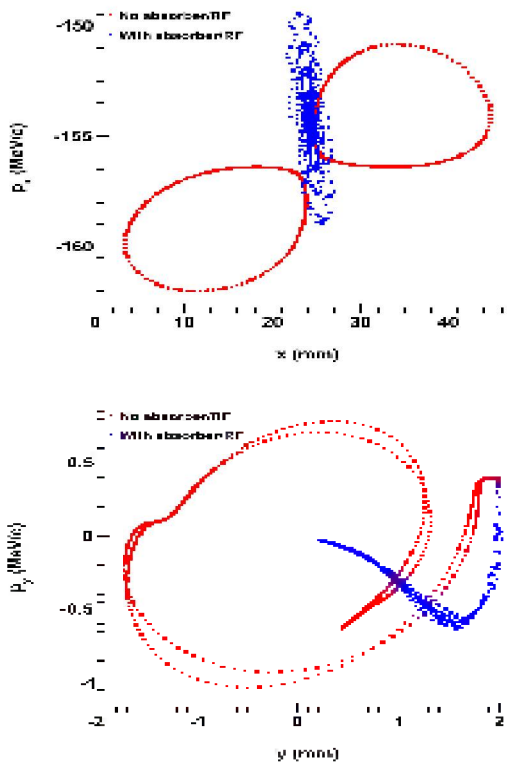

Figure 1: Horizontal (top) and vertical (bottom) phase-space trajectories with half-integer parametric resonances excited in both planes without (red) and with (blue) absorbers/RF. Stochastic effects are off.

COOLING SIMULATION

We next placed 2 cm thick Be wedge absorbers with a thickness gradient of 0.3 at the resonance focal points. Locations of the focal points were chosen at the places in the twin helix with 3 cm dispersion [5]. This dispersion value combined with the absorber thickness gradient should provide sufficient longitudinal cooling to maintain the momentum spread at a constant level [5]. The wedge absorbers were immediately followed by short 201 MHz RF cavities, which completely restored the absorber energy loss. At this level of study, the cavities were made unrealistically short to avoid large energy perturbations and to decouple from the transit time effects.

A 250 MeV/c μ^- was tracked through the system with stochastic effects turned off. The resulting horizontal and vertical phase-space trajectories at the absorber location are shown by the blue dots in Fig. 1 and compared to those without the absorbers/RF. Note an overall reduction of the size at an increase of the angular spread characteristic to PIC. Figure 2 shows evolution of the horizontal phase space along the cooling channel. Note the two distinct branches in the phase-space trajectory due to the half-integer parametric resonance.

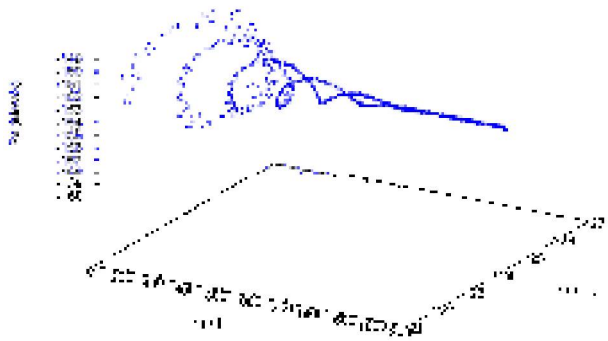

Figure 2: Evolution of the horizontal phase space along the cooling channel with absorbers/RF under the parametric resonance condition. Stochastic effects are off.

ABERRATION COMPENSATION

Horizontal Spherical Aberration

When the stochastic effects are turned on in the cooling simulation described above, the particle motion becomes unstable. This is due to aberration impact between consecutive focal points. Both chromatic and spherical aberrations must be compensated to a degree where they are small compared to the beam size at the absorber. Since, according to Eq. (4), the equilibrium angular spread in on the order of a hundred milliradians, the spherical aberrations must be precisely compensated over an angular range of a few hundred milliradians. This is a challenging task. However, some of the intrinsic symmetries of the correlated optics reduce the number of the aberration compensation conditions. The number of conditions can be further reduced by using a coupling resonance [2].

The conventional approach to aberration compensation is to correct aberrations sequentially from lower to higher order by successively introducing appropriate higher-order multipoles. However, it cannot be done in such a straightforward way in a twin helix since the reference orbit does not pass through the center of the magnetic system. Introducing a higher-order multipole in a twin helix feeds-down lower-order multipole components

Copyright © 2011 by IPAC'11/EPS-AG — cc Creative Commons Attribution 3.0 (CC BY 3.0)

along the orbit. Aberration compensation has to be done by adjusting different-order multipole components simultaneously. Here we demonstrate compensation of the horizontal spherical aberration using a straight octupole and a pair of helical decapoles. Their strengths were tuned using a generic fitting algorithm to minimize the smear of a monochromatic point-source beam with ±200 mrad horizontal angular spread after 2 helix periods. The μ^- tracks over 2 helix periods from one absorber location to another are shown before and after the compensation in Fig. 3. Figure 4 illustrates impact of the compensation on the channel's dynamic acceptance shown in terms of the initial horizontal and vertical momentum components, for which the particle later remains dynamically stable.

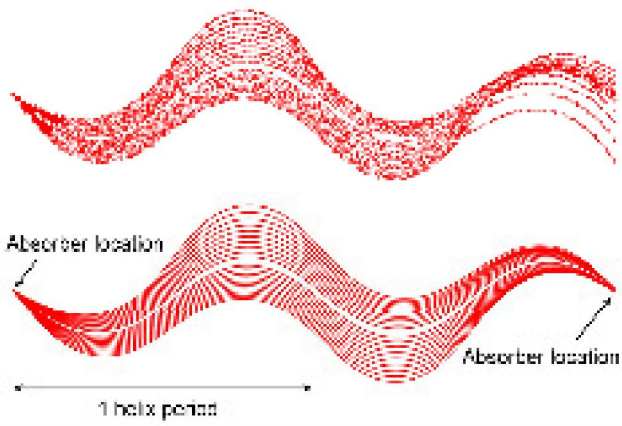

Figure 3: μ^- tracks distributed over ±200 mrad in the horizontal plane before (top) and after (bottom) compensation of the horizontal spherical aberration.

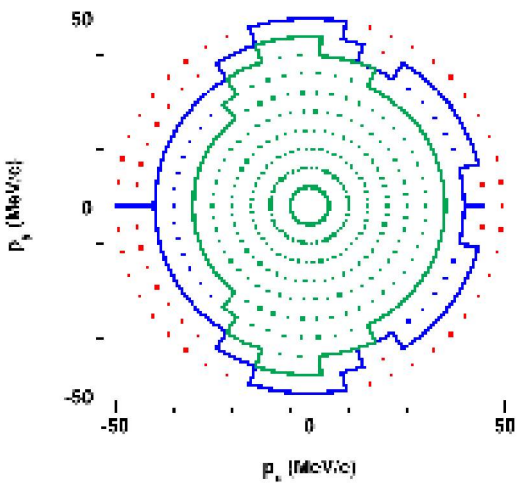

Figure 4: Dynamic acceptance in terms of the stable initial horizontal and vertical momentum components of a monochromatic point-source beam. The green and blue lines show the boundaries of the dynamic acceptance before and after the compensation, respectively.

COSY Infinity Benchmark

To systematically approach aberration correction, we plan on using COSY Infinity [9,10], a well-known code for aberration analysis and compensation. COSY works by expanding a particle's trajectory around a reference orbit to an arbitrary order in the 6D phase-space coordinates. Therefore, COSY is well-suited for our purpose. It has been extended to include helical harmonics and to calculate the reference orbit in a twin helix. The results of applying various orders of COSY to calculate the smear of a ±160 mrad monochromatic point-source beam after 2 helix periods are compared to a G4beamline simulation in Fig. 5 with a good agreement.

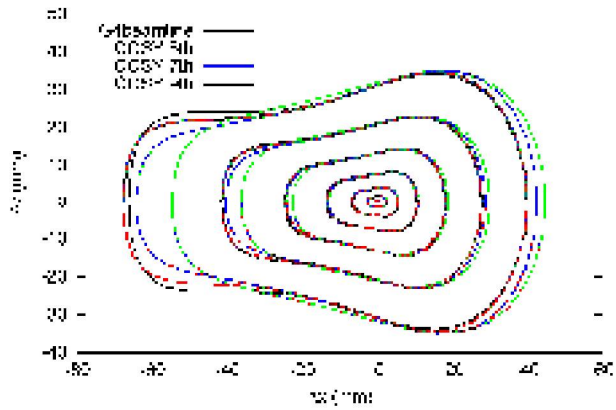

Figure 5: Beam smear due to spherical aberrations after 2 helix periods. G4beamline simulation is compared to various-order COSY Infinity calculations.

REFERENCES

[1] Y.S. Derbenev and R.P. Johnson, "Parametric-resonance Ionization Cooling and Reverse Emittance Exchange for Muon Colliders", in COOL'05, AIP Conf. Proc. 821, 2006, p. 420.
[2] Y.S. Derbenev and R.P. Johnson, "Parametric-resonance ionization cooling", in preparation.
[3] V.S. Morozov et al., "Epicyclic twin-helix magnetic structure for parametric-resonance ionization cooling", in Proc. IPAC'10, Kyoto, Japan.
[4] V.S. Morozov et al., "Twin-helix channel for parametric-resonance ionization cooling", in Proc. 2010 Adv. Acc. Conc. Workshop, Annapolis, MD.
[5] V.S. Morozov et al., "Epicyclic twin-helix ionization cooling simulations", in Proc. PAC'11, New York, NY, USA.
[6] Y.S. Derbenev and R.P. Johnson, PRST-AB 8, 041002 (2005).
[7] T. Tominaka et al., NIM A 459, 398 (2001).
[8] G4beamline, http://g4beamline.muonsinc.com
[9] K. Makino and M. Berz, "COSY Infinity version 9", Nuclear Instruments and Methods A558, 346 (2005).
[10] J.A. Maloney et al., "EPIC muon cooling simulations using COSY Infinity", in Proc. PAC'11, New York, NY, USA.

Copyright © 2011 by IPAC'11/EPS-AG — cc Creative Commons Attribution 3.0 (CC BY 3.0)

EPICYCLIC TWIN-HELIX IONIZATION COOLING SIMULATIONS*

V.S. Morozov#, Y.S. Derbenev, Jefferson Lab, Newport News, VA, USA
A. Afanasev, Hampton University, Hampton, VA, USA
R.P. Johnson, Muons, Inc., Batavia, IL, USA

Abstract

Parametric-resonance Ionization Cooling (PIC) is proposed as the final 6D cooling stage of a high-luminosity muon collider. For the implementation of PIC, we earlier developed an epicyclic twin-helix channel with correlated behavior of the horizontal and vertical betatron motions and dispersion. We now insert absorber plates with short energy-recovering units located next to them at the appropriate locations in the twin-helix channel. We first demonstrate conventional ionization cooling in such a system with the optics uncorrelated. We then adjust the correlated optics state and induce a parametric resonance to study ionization cooling under the resonant condition.

INTRODUCTION

Combining muon ionization cooling with parametric resonant dynamics should allow much smaller final transverse muon beam sizes than ionization cooling alone [1-2]. Thus, high luminosity would be achieved in a collider with fewer muons. Parametric-resonance Ionization Cooling (PIC) is accomplished by inducing a parametric ½-integer resonance in a muon cooling channel. The beam is then naturally focused with a period of the channel's free oscillations. Absorber plates for ionization cooling together with energy-restoring RF cavities are placed at the beam focal points. At the absorbers, ionization cooling limits the angular spread while the parametric resonance causes a strong reduction of the beam spot size. This resonant cooling scheme should provide equilibrium transverse emittances that are at least an order of magnitude smaller than those achievable with conventional ionization cooling [2].

IONIZATION COOLING SIMULATIONS

Twin-Helix Channel with Correlated Optics

The PIC concept requires [1-4] that, in the cooling channel, the horizontal free oscillation period λ_x is a low-integer multiple of the vertical free oscillation period λ_y while both λ_x and λ_y are low integer multiples of the dispersion oscillation period λ_D. We earlier developed the twin-helix channel [3, 4], which is compatible with the PIC requirements and can provide the following correlated values of λ_x, λ_y and λ_D:

$$\lambda_x = 2\lambda_y = 4\lambda_D . \qquad (1)$$

The twin-helix channel is a superposition of two opposite-helicity equal-period and equal-strength helical dipole harmonics [5, 6] and a straight normal quadrupole. The magnetic field strength at the center of each dipole harmonic B_d and the quadrupole field gradient $\partial B_y/\partial x$ corresponding to the correlated optics are given by

$$B_d = 6.515\cdot 10^{-3}\, p/\lambda \quad [T],$$
$$\partial B_y/\partial x = 2.883\cdot 10^{-3}\, p/\lambda^2 \quad [T/m], \qquad (2)$$

where p is the muon momentum in MeV/c and λ is the helix period in m. The optical properties of the twin-helix channel are well-understood [3, 4]. The periodic orbit amplitude x_{max}, dispersion amplitude $D_{x\,max}$ and horizontal and vertical chromaticities ξ_x and ξ_y corresponding to the correlated optics are given by

$$x_{\max} = 0.121\,\lambda \quad [m], \quad D_{x\,\max} = 0.196\,\lambda \quad [m],$$
$$\xi_x = -0.646, \quad \xi_y = -0.798. \qquad (3)$$

Equations (2) and (3) are used to obtain the twin helix correlated optics parameters for given muon momentum and helix period. Note that the twin-helix channel was earlier demonstrated [3, 4] to posses a large dynamic aperture even under the correlated optics state.

Simulation Setup

In a system with equally distributed partial cooling decrements of the three emittances and equal damping decrements of the beam size and angle spread at the absorber plates, the dispersion value at the absorber locations is given by [2]

$$D_{abs} = \frac{\Delta E_{abs}}{\partial \Delta E_{abs}/\partial x}\left(2 - \frac{4}{3}\beta^2\right), \qquad (4)$$

where ΔE_{abs} is the energy loss in the absorber, $\partial \Delta E_{abs}/\partial x$ is the energy loss gradient due to the absorber thickness gradient, and β is the muon relativistic factor. For instance, for a 2 cm thick Be wedge with a thickness gradient of 0.3, Eq. (4) gives a dispersion value of 3 cm.

The absorbers are placed every two periods of the twin helix, which is the shortest possible separation corresponding to a half of the period of the horizontal betatron oscillations and one period of the vertical betatron oscillations. The absorbers are centered on the reference trajectory and their axes are aligned with the reference momentum.

In the initial simulations without an induced parametric resonance, we used the parameters given above, where each absorber was immediately followed by a 2 cm long energy recovery region centered on and aligned with the

*Supported in part by DOE SBIR grant DE-SC0005589
#morozov@jlab.org

Copyright © 2011 by PAC'11 OC/IEEE — cc Creative Commons Attribution 3.0 (CC BY 3.0)

absorber axis. First, to avoid having to time RF cavities, we modeled energy recovery using regions of static electric field. We later replaced them with same-length RF cavities. The strength of the static electric field and the voltage gradient of the RF cavities were adjusted to completely compensate energy loss in the absorbers. The length of the energy recovery region was chosen to be short compared to the helix period in order to reduce the area where the muon momentum is different from its reference value and thus minimize perturbation of the reference orbit. Having short RF cavities also allows one to decouple from transit time effects. However, about 6.5 MeV energy loss from a 200 MeV/c muon in 2 cm of Be can be compensated with a realistic RF cavity. Optimizing the length of the cooling channel is not one of the goals of this conceptual study but, in a realistic channel, as large a fraction of the channel space as practically possible would be filled with absorbers and RF cavities.

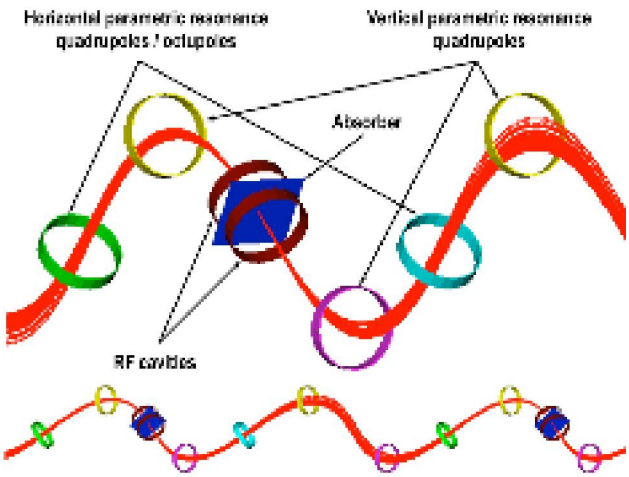

Figure 1: G4beamline event display showing an energy absorber, RF cavities, resonance driving quads, and octupole aberration correction magnets.

The half-integer parametric resonances in the later simulations were induced in the two planes by two sets of 2 cm long quadrupoles placed with half the periodicity of the horizontal and vertical betatron oscillations every $\lambda_x/2 = 2\lambda$ and $\lambda_y/2 = \lambda$ along the channel. The horizontal and vertical resonance driving lenses were positioned at the $\lambda_x/8$ and $\lambda_y/8$ distances in front of the focal point at the absorber for the x and y resonances, respectively. Each set consisted of alternating positive and negative polarity quadrupoles to compensate their betatron tune shift. In order to further reduce the energy modulation caused by the absorbers and energy recovery, each absorber was closely surrounded by two RF cavities. We also reduced the absorber thickness to 2 mm to first better understand the resonant dynamics. The horizontal resonance driving lenses included an octupole field harmonic for the study of non-linear effect compensation. The resulting system configuration is illustrated in Fig. 1.

Study without Induced Parametric Resonance

We used the GEANT-based G4beamline program [7] to track 10^3 200 MeV/c muons through 500 helix periods of the cooling channel containing the wedge absorbers and static electric field regions. The resulting phase-space diagrams at different distances along the channel are shown in Fig. 2. Note that introduction of the absorbers and energy recovery changes the periodic orbit and periodic momentum. This leads to a mismatch between the initial beam and the new periodic trajectory causing the initial increase of the horizontal phase space in Fig. 2 due to filamentation.

We next tuned the periodic momentum to correspond to the correlated optics value. Both with the static field and RF and at both 200 MeV/c and 250 MeV/c, we observed stable oscillations with two rather than one attractor points in the horizontal phase space. Our interpretation of this effect is that it is a manifestation of a parasitic parametric resonance caused by energy kicks from the absorbers and electric field every $\lambda_x/2$.

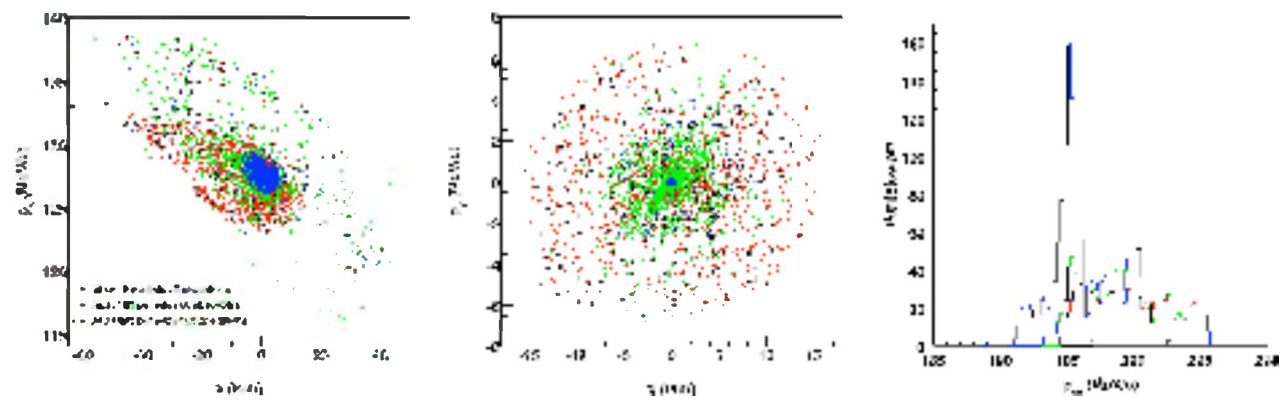

Figure 2: Horizontal (left) and vertical (middle) phase-space distributions and momentum distribution histogram (right) at different distances along the cooling channel containing the wedge absorbers and static electric field regions. The initial beam had uniform spatial $\sigma_x = \sigma_y = \pm 2\ mm$, angular $\theta_x = \theta_y = \pm 50\ mrad$ and momentum $\Delta p/p = \pm 2.7\%$ distributions and was launched along the reference orbit. The stochastic processes and muon decay were off.

Copyright © 2011 by PAC'11 OC/IEEE — cc Creative Commons Attribution 3.0 (CC BY 3.0)

Study with Induced Parametric Resonance

We induced a parametric resonance in the horizontal plane using the resonance driving quadrupole lenses discussed above. Figure 3 illustrates the particle horizontal phase-space trajectory at the absorber. The trajectory demonstrates the expected hyperbolic behavior corresponding to a half-integer resonance where the angle increases as the amplitude shrinks. The hyperbolic dependence becomes distorted for large amplitudes and angles due to aberrations. We introduced an octupole magnetic field harmonic in the horizontal resonance driving lenses to study its effect on the non-linear dynamics as shown in Fig. 3.

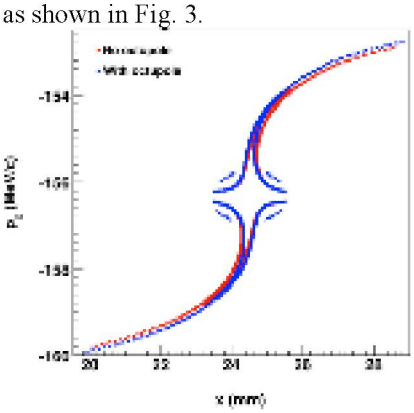

Figure 3: G4beamline simulations of half-integer parametric resonant dynamics in horizontal phase space without absorbers and RF. A first attempt to adjust the distortion of the separatrix using octupoles is shown.

Note that introduction of the parametric resonance in the horizontal plane causes an instability in the vertical plane because the resonance driving quadrupoles are placed with the periodicity of the vertical betatron oscillations. We believe that it can be either compensated by appropriate optics or the parametric lens system can be modified so that a single quadrupole set drives the required parametric resonances in both planes taking advantage of the correlated optics design.

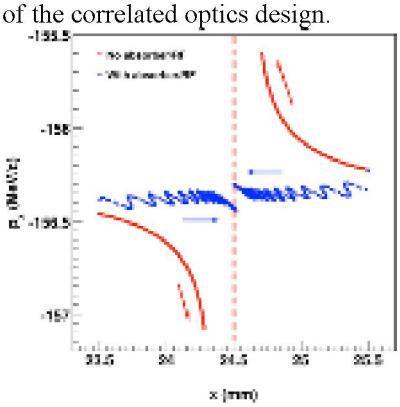

Figure 4: G4beamline simulations of half-integer parametric resonant dynamics in horizontal phase space without and with absorbers and RF. Ionization cooling limits the angular spread while the resonance reduces the beam size. Stochastic processes are not included.

Thin 2 mm absorber plates closely surrounded by two energy-restoring RF cavities were then installed at the focal points. The RF cavities were synchronized using an unperturbed reference particle, which ignored ionization energy loss and electric fields. The synchronous phase was set at 30°. The average beam energy in this case is determined by the timing of the RF cavities rather than their voltage gradient and is equal to the reference particle energy. The stabilizing effect of the absorbers and RF is illustrated in Fig. 4. The absorbers and RF prevent the angle from growing while the size shrinks.

We next tracked a beam of fifty 250 MeV/c muons in the horizontal plane under the parametric resonant condition through 1000 helix periods of the cooling channel containing absorber plates and RF cavities. Figure 5 shows the resulting phase-space diagrams at the absorbers at different distances along the channel. Note that the beam evolves into a state with a large angular spread and a small size, which is consistent with the parametric resonant picture.

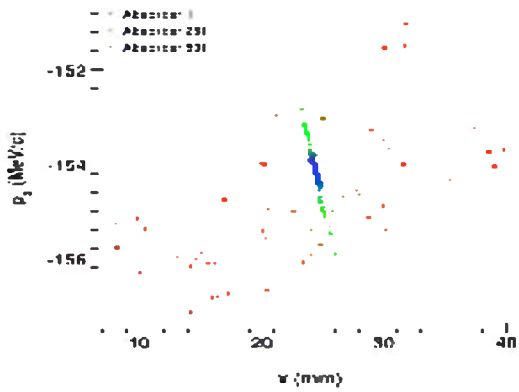

Figure 5: Horizontal phase-space distribution in the middle of the absorbers at different distances along the cooling channel with parametric resonance. The stochastic processes and muon decay were off.

REFERENCES

[1] Y.S. Derbenev and R.P. Johnson, "Parametric-resonance Ionization Cooling and Reverse Emittance Exchange for Muon Colliders" in COOL'05, AIP Conf. Proc. 821, 2006, p. 420.
[2] Y.S. Derbenev and R.P. Johnson, "Parametric-resonance ionization cooling", in preparation.
[3] V.S. Morozov et al., "Epicyclic twin-helix magnetic structure for parametric-resonance ionization cooling", in Proc. IPAC'10, Kyoto, Japan.
[4] V.S. Morozov et al., "Twin-helix channel for parametric-resonance ionization cooling", in Proc. 2010 Adv. Acc. Conc. Workshop, Annapolis, MD.
[5] Y.S. Derbenev and R.P. Johnson, PRST-AB 8, 041002 (2005).
[6] T. Tominaka et al., NIM A 459, 398 (2001).
[7] G4beamline, http://g4beamline.muonsinc.com

Copyright © 2011 by PAC'11 OC/IEEE — cc Creative Commons Attribution 3.0 (CC BY 3.0)

EPIC MUON COOLING SIMULATIONS USING COSY INFINITY*

James Anthony Maloney, Bela Erdelyi (Northern Illinois University, DeKalb, Illinois), Alex Bogacz, Yaroslav Serg Derbenev (JLAB, Newport News, Virginia), Andrei Afanasev, Rolland Paul Johnson (Muons, Inc, Batavia), Vasiliy Morozov (ODU, Norfolk, Virginia).

Abstract

Next generation magnet systems needed for cooling channels in both neutrino factories and muon colliders will be innovative and complicated. Designing, simulating and optimizing these systems is a challenge. Using COSY INFINITY, a differential algebra-based code, to simulate complicated elements can allow the computation and correction of a variety of higher order effects, such as spherical and chromatic aberrations, that are difficult to address with other simulation tools. As an example, a helical dipole magnet has been implemented and simulated, and the performance of an epicyclic parametric ionization cooling system for muons is studied and compared to simulations made using G4Beamline, a GEANT4 toolkit.

INTRODUCTION

One of the key technical challenges to proposed neutrino factories and muon colliders is the design and implementation of an effective beam cooling system [1, 2]. Muons produced for such machines have an extremely large phase space volume requiring cooling and transporting within a relatively short decay time. The specifications for a high-luminosity muon collider, in particular, are challenging. A variety of competing schemes have been proposed to address this challenge [2], often involving complicated magnetic fields which are not easily simulated. Furthermore, these systems are often more sensitive to the effects of fringe fields and higher order aberrations within the beam. The complicated geometries of the next-generation magnet systems used in these cooling channels make it difficult to address these effects using conventional methods. COSY INFINITY [3] can be used to compute and help correct the higher order effects in these next-generation magnet systems.

SIMULATION OF THE EPICYCLIC TWIN HELIX CHANNEL IN COSY INFINITY

The twin helix channel model [4] for Epicyclic Parametric Resonance Ionization Cooling (EPIC) [5] presents a promising proposal for the cooling challenges of a muon collider. Such a channel can be simulated and studied with COSY INFINITY (COSY).

Epicyclic Parametric Resonance Ionization Cooling

Epicyclic Parametric Resonance Ionization Cooling (EPIC) theory uses a combination of induced parametric resonances to cause periodic beam size reductions. Ionization cooling is then achieved with absorbing wedges. Emittance exchange allows for longitudinal cooling while energy restoring RF is used to maintain particle momentum. The fundamentals for such a design are illustrated in Figure 1. A varying dispersion function (in blue) necessary for aberration correction is related to the superimposed harmonic magnetic fields (horizontal plane in red and two fields for the vertical plane in green) via correlated optics.

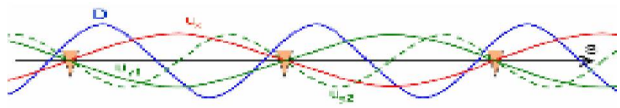

Figure 1: Example of EPIC layout.

The Twin Helix Channel

One interesting case for trying to implement the EPIC theory is the twin helix channel [4]. This channel utilizes two helical harmonics with equal scalar field components and equal but opposite wave numbers.

The helical harmonics, in the horizontal plane, are given by:

$$B_x = -\left(\frac{2}{nk}\right)^{n-1} b_n[I_{n-1}(nkx) + I_{n+1}(nkx)]sin(nkz) \quad (1)$$

$$B_y = \left(\frac{2}{nk}\right)^{n-1} b_n[I_{n-1}(nkx) - I_{n+1}(nkx)]cos(nkz) \quad (2)$$

$$B_z = -2\left(\frac{2}{nk}\right)^{n-1} b_n I_n(nkx)cos(nkz) \quad (3)$$

Where n = 1, and 2 represent the dipole and quadrupole terms, b_n is the n-1 order derivative of the vertical field component, and I_n are modified Bessel functions of the 1st kind. When the two helical harmonics with identical moments ($b_{n1}=b_{n2}$), and equal but opposite wave numbers ($k_1=-k_2$) are superimposed, the resulting compound field leaves only a vertical field component in the horizontal plane:

$$B_x = 0 \quad (4)$$

$$B_y = 2\left(\frac{2}{nk}\right)^{n-1} b_n[I_{n-1}(nkx) - I_{n+1}(nkx)]cos(nkz) \quad (5)$$

$$B_z = 0 \quad (6)$$

The result is to create a periodic orbit in the horizontal plane, and regions of stable transverse motion in both planes. Absorbing wedges followed by energy recovering cells are inserted at points of low dispersion to create effective 6D ionization cooling.

Implementation of the Twin Helix in COSY INFINITY

COSY INFINITY (COSY) is a DA based simulation code that allows the calculation of transfer maps of beam systems to arbitrary order. [3] For systems where a

*Work supported by in part by DOE STTR Grant DE-SC00005589
#physics_maloney@yahoo.com

Copyright © 2011 by PAC'11 OC/IEEE — cc Creative Commons Attribution 3.0 (CC BY 3.0)

reference particle that orbits in a plane, such as involved in the twin helix channel previously mentioned, implementation in COSY can be accomplished by modifying the existing base code to include a new helical magnet element. The new magnetic element is defined by specifying the magnetic field in the x-z plane, and allowing COSY to calculate the potential in all space from Maxwell's equation. The element allows the user to specify parameters for the length of the cell, the wave number for the harmonic fields, the half gap of the magnet, and the dipole and quadrupole field component at the center of the field.

COSY includes a customizable absorbing wedge element that is parameterized by the Bethe-Bloch formula. This element is placed inside the helix along with a DC electric field for energy recovery. Ultimately, the DC field can be replaced with an RF cell once a time structure has been fixed. The result is a complete simulation of a twin helix with both dipole and quadrupole moments, absorbing wedge and energy recovering cell.

COSY can now be used to calculate the transfer and aberration maps for the element for any number of orbital periods. This allows for statistical studies to tune system performance, examination of optical aberrations, and error analysis of the system.

EMITTANCE STUDIES OF THE TWIN HELIX IN COSY INFINITY

Using studies of the twin helix in a modified version of G4Beamline (a GEANT4 toolkit) [6] as a baseline for comparison, the COSY simulation examine the performance of the basic twin helix cell. Table 1 summarizes the parameters utilized in the standard cell. In this configuration the standard cell is twice the helix period and the absorber wedge is placed where the value of the dispersion function is 3cm, and immediately followed by the energy restoring DC electric field.

Table 1: Twin Helix Parameters

Parameter	Value
Reference momentum	200 MeV/c
Helix period	1 m
Dipole Strength	1.3031406 T
Quadrupole Strength	0.57640625 T/m
Absorber Material	Beryllium
Absorber Thickness	2 cm
Absorber Gradient	.3 (symmetric at surfaces)
DC Field Length	2 cm
DC Field Strength	322.806156 MV/m

As a consistency check, a sample distribution of particles was sent through a single cell without either the absorbing wedge or DC field included. Figure 2 demonstrates how the cell manipulates horizontal phase space. The transfer matrix, extracted using COSY, has a determinant of 1, verifying that there is no change in emittance, as expected in absence of any wedge absorber.

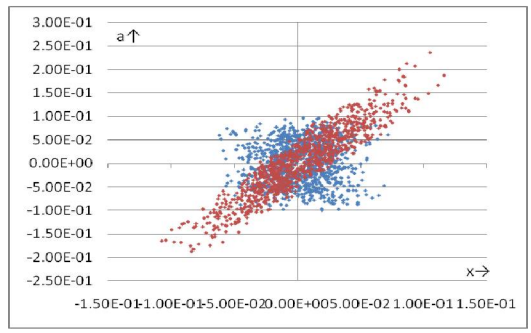

Figure 2: Initial (blue) and final (red) distribution in horizontal phase space for single Twin Helix cell without absorbing wedge.

Study of Emittance Change from Transfer Matrices in Twin Helix Systems

COSY generates an array containing an initial distribution of particles, represented as vectors with particle optical coordinates of the form:

$$\{r_k\} = (x_k, a_k, y_k, b_k, t_k, \delta_k) \tag{7}$$

Where a and b are the dimensionless horizontal and vertical momentum, t is time of flight and δ is the change in total energy of the particle. COSY calculates the function, M, known the transfer map (or taylor map) for the system, which described the evolution of particles in the system. The linear terms of the transfer map function comprise the matrix (transfer matrix) of the system. [7]

$$\{\vec{r_f}\} = M\{\vec{r_i}\} = \begin{pmatrix} (x|x) & \cdots & (x|\delta) \\ \vdots & \ddots & \vdots \\ (\delta|x) & \cdots & \{\delta|\delta\} \end{pmatrix} \{\vec{r_i}\} \tag{8}$$

Using the transfer matrix of the system and a randomly generated array of particles, emittance of the twin helix system can also be evaluated. The transverse (4D) and 6D emittance can be calculated from the determinant of the covariance matrix derived from a distribution of particles. [8]

$$\epsilon^{4D} = \sqrt[4]{det(\mathcal{M}_{ij})_{4D}} \qquad \epsilon^{6D} = \sqrt[6]{det(\mathcal{M}_{ij})_{6D}} \tag{9}$$

The covariance matrix is a function of the particle distribution, and the transfer matrix relates changes in the initial and final beam emittance by the following relation:

$$\epsilon_f = \int_{beam} dx_f dp_{x_f} \tag{10}$$

$$\epsilon_f = \int_{beam} |\det M| dx_i dp_{x_i} = |detM| \epsilon_i \tag{11}$$

$$|detM| = \frac{\epsilon_f}{\epsilon_i} \tag{12}$$

The determinants of the 4D and 6D components for this matrix, and the transfer matrices of systems with 10 and 50 continuous cells with wedges and absorbers, is provided in Table 2.

Copyright © 2011 by PAC'11 OC/IEEE — cc Creative Commons Attribution 3.0 (CC BY 3.0)

Table 2: Transfer Matrix Emittance Calculations

System	4D	6D
1 cell	0.10056	0.0432475
10 cells	0.04156	0.00281985
50 cells	4.69456E-05	6.75281E-07

Study of Particle Distributions in Twin Helix Systems

An array containing the vectors of an initial particle distribution was composed with the 3rd order transfer map of the twin helix system. The emittance of the distribution is given as

$$\varepsilon_{tr,rms} = \sqrt{\langle x^2\rangle\langle a^2\rangle - \langle xa\rangle^2}\sqrt{\langle y^2\rangle\langle b^2\rangle - \langle yb\rangle^2} \quad (12)$$

The emittance calculations for both the initial and final vector arrays are summarized in Table 3, and can be analyzed to see change as the beam is transported through the twin helix channel. Figures 3, 4 and 5 show the horizontal phase space of the initial and final distributions.

Table 3: Particle Distribution Emittance Calculations

System	ϵ(4D)
Initial	9.96835E-07
1cell	1.00325E-07
10 cells	1.8326E-08
50 cells	9.62192E-10

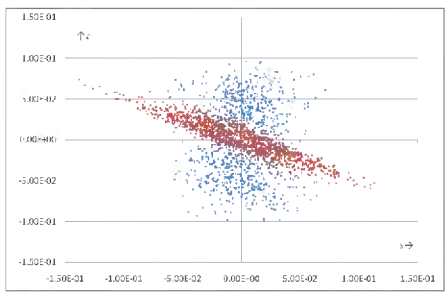

Figure 3 Initial (blue) and final (red) distribution in horizontal phase space for 1 Twin Helix cell.

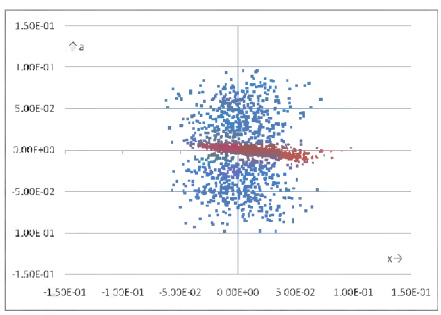

Figure 4: Initial (blue) and final (red) distribution in horizontal phase space for a series of 10 Twin Helix cells.

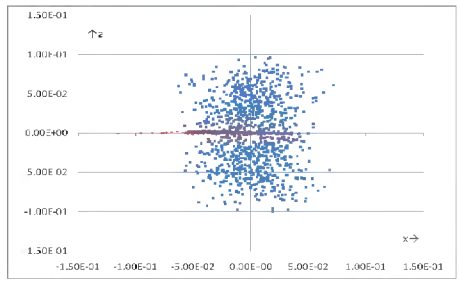

Figure 5: Initial (blue) and final (red) distribution in horizontal phase space for a series of 50 Twin Helix cells.

CONCLUSION

The twin helix channel model for an EPIC muon cooling system has been implemented in COSY, and preliminary studies offer supporting evidence of cooling. Using the same structure, higher order harmonic multipoles (e.g. sextupole and octupole) will need to be added to correct existing chromatic and spherical aberrations in the system. Using the transfer and aberration map output from COSY will aid in the design of such corrective optical systems. Furthermore, the methods developed in implementing this innovative magnet system can be used to simulate similarly novel magnet systems in other proposed muon cooling channels being developed for a next generation neutrino factory or muon collider.

REFERENCES

[1] R. Johnson, "Ionization Cooling and Muon Colliders", EPAC'08, Genoa, June 2008, THYG03, p. 2917 (2008); http://www.JACoW.org.
[2] Muon Collider Task Force R&D Draft Proposal; https://mctf.fnal.gov
[3] M. Berz & K. Makino, COSY Infinity Version 9, *Nuclear Instruments and Methods* A558 (2005) 346-350; http://www.bt.pa.msu/edu/index_files/cpsy.htm.
[4] V. Morozov et al., "Ionization Cooling Simulations in Epicyclic Twin-Helix Channel", this conf.
[5] A. Afanasev et al., "Epicyclic Helical Channels for Parametric Resonance Ionization Cooling", PAC09, Vancouver, May 2009, FR5RFP012, p. 4554 (2009); http://www.JACoW.org.
[6] G4Beamline access: http://www.muonsinc.com/tiki-index.php?page=Computer+Programs
[7] M. Berz, Advances in Imaging and Electron Physics, Vol. 108, p. 145-6 (1999).
[8] D. Kaplan & T. Hart, "Emittance Measurements in MICE", 34th Int. Conf. On HEP, Philadelphia, Oct 2008, arXiv:0809.4796v2 [physics.acc-ph].

Copyright © 2011 by PAC'11 OC/IEEE — cc Creative Commons Attribution 3.0 (CC BY 3.0)

CORRECTING ABERRATIONS IN COMPLEX MAGNET SYSTEMS FOR MUON COOLING CHANNELS*

James Anthony Maloney, Bela Erdelyi, Northern Illinois University, DeKalb, Illinois, U.S.A.
Yaroslav Serg Derbenev, JLAB, Newport News, Virginia, U.S.A.
Andrei Afanasev, Rolland Paul Johnson, Muons, Inc, Batavia, Illinois, U.S.A.
Vasiliy Morozov, ODU, Norfolk, Virginia, U.S.A.

Abstract

Designing and simulating complex magnet systems needed for cooling channels in both neutrino factories and muon colliders requires innovative techniques to correct for both chromatic and spherical aberrations. Optimizing complex systems, such as helical magnets for example, is also difficult but essential. By using COSY INFINITY, a differential algebra based code, the transfer and aberration maps can be examined to discover what critical terms have the greatest influence on these aberrations.

INTRODUCTION

The challenging emittance size needed to implement a neutrino factory or muon collider has motiviates searches for innovating techniques in beam cooling [1, 2]. For example, the use of Parametric-resonance Ionization Cooling (PIC) has been proposed for the final stage of 6D cooling of a high-luminosity muon collider [3]. In this system, an induced resonance is used to cause periodic beam size reductions, and ionization cooling is then achieved via wedges of absorbing materials. An epicyclic twin helical channel offers to achieve the goals of PIC, correlating the dispersion and betatron functions of the beam [4]. The critical challenges of this system include correcting chromatic and spherical aberrations induced in the channel.

USING COSY INFINITY TO STUDY ABERRATIONS IN A SYSTEM

COSY INFINITY (COSY) is a DA-based code allowing simulation of beam transfer and aberration maps to arbitrary order [5]. With modification of the base code, the twin helix channel was implemented and simulated in COSY [6]. In these simulations, COSY takes a reference particle defined as:

$$\{r_k\} = (x_k, a_k, y_k, b_k, t_k, \delta_k) \quad (1)$$

Where a and b are the dimensionless horizontal and vertical momentum, t is time of flight and δ is the change in total energy of the particle. COSY calculates the function, $\mathcal{M}$, known the transfer map (or taylor map) for the system, which described the evolution of particles in the system. The linear terms of the transfer map function comprise the matrix M, often referred to as the linear map or transfer matrix of the system [5], that satisfies the relation:

$$\{r_f\} = M\{r_i\} = \begin{pmatrix} (x|x) & \cdots & (x|\delta) \\ \vdots & \ddots & \vdots \\ (\delta|x) & \cdots & (\delta|\delta) \end{pmatrix} \{r_i\} \quad (2)$$

The non-linear terms, N, remaining in the transfer map can be expressed separately:

$$\mathcal{M} = \mathrm{M} + \mathrm{N} \quad (3)$$

In terms of the component of the transfer map, each of the final vector components for a particle can be expressed in form:

$$x_f = \sum \left(x \mid x^{i_x} a^{i_a} y^{i_y} b^{i_b} t^{i_t} \delta^{i_\delta}\right) x^{i_x} a^{i_a} y^{i_y} b^{i_b} t^{i_t} \delta^{i_\delta} \quad (4)$$

Where the terms are summed over $(i_x,i_a,i_y,i_b,i_t,i_\delta)$ for each component. The terms in the transfer map of 2nd or higher order are commonly referred to as aberrations. COSY calculated these aberrations and generates output, referred to as an aberration map. The aberration map is in a format similar to the transfer map.

Examination of the transfer and aberration maps provides important clues in improving a beam system. If, for example, the input suffers from large variation in initial angle and final horizontal position needs minimization to fit a particular aperture in the beamline, then aberrations in (x_f) dependent on initial angle (a_i) may be particularly important to minimize. We would want to pay particular attention to terms in the aberration map involving higher orders of a, such as (x|aa) or (x|aaa). If those terms are not minimized, variations in initial angle threaten to blow up the horizontal position of the final beam. Similarly, if we know that initial position is small, we can put less emphasis on minimizing aberrations that depend on (x_i), particularly higher order terms involving 2 or more powers of x, such as (x|axx), where initial position may dominate initial angular spread.

To minimize these aberrations, it is also important to recognize how magnetic systems contribute to the transfer map. The linear terms of the transfer map are determined by the dipole and quadrupole moments of magnetic elements. Correction for higher order aberrations requires use of higher order multipoles. Thus, sextupoles are used to correct 2nd order aberrations, and octupoles are used for 3rd order aberrations.

Using various symmetries of the beam system can also be an effective technique for aberration correction [7].

*Work supported in part by DOE STTR Grant DE-SC00005589.
#physics_maloney@yahoo.com.

Copyright © 2011 by PAC'11 OC/IEEE — cc Creative Commons Attribution 3.0 (CC BY 3.0)

For example, systems are described as having midplane symmetry if particle motion is symmetric on each side of plane (called the miplane). If we let:

$$r_f = (x_f, a_f, y_f, b_f, t_f, \delta_f) = \mathcal{M}(x_i, a_i, y_i, b_i, t_i, \delta_i) \quad (5)$$

then as a result of midplane symmetry,

$$(x_f, a_f, -y_f, -b_f, t_f, \delta_f) = \mathcal{M}(x_i, a_i, -y_i, -b_i, t_i, \delta_i) \quad (6)$$

From this relation, the following coefficients of the transfer map can be determined to be zero:

$$(x \mid x^{i_x} a^{i_a} y^{i_y} b^{i_b} t^{i_t} \delta^{i_\delta}) = 0 \quad \text{if } i_y+i_b \text{ is odd} \quad (7)$$

$$(a \mid x^{i_x} a^{i_a} y^{i_y} b^{i_b} t^{i_t} \delta^{i_\delta}) = 0 \quad \text{if } i_y+i_b \text{ is odd} \quad (8)$$

$$(y \mid x^{i_x} a^{i_a} y^{i_y} b^{i_b} t^{i_t} \delta^{i_\delta}) = 0 \quad \text{if } i_y+i_b \text{ is even} \quad (9)$$

$$(b \mid x^{i_x} a^{i_a} y^{i_y} b^{i_b} t^{i_t} \delta^{i_\delta}) = 0 \quad \text{if } i_y+i_b \text{ is even} \quad (10)$$

$$(t \mid x^{i_x} a^{i_a} y^{i_y} b^{i_b} t^{i_t} \delta^{i_\delta}) = 0 \quad \text{if } i_y+i_b \text{ is odd} \quad (11)$$

$$(\delta \mid x^{i_x} a^{i_a} y^{i_y} b^{i_b} t^{i_t} \delta^{i_\delta}) = 0 \quad \text{if } i_y+i_b \text{ is odd} \quad (12)$$

This has the effect of eliminating nearly half of the terms, and allows us to substantially simplify the transfer map. For example, the linear evolution of the system reduces to:

$$\begin{pmatrix} x_f \\ a_f \\ y_f \\ b_f \\ t_f \\ \delta_f \end{pmatrix} = \begin{bmatrix} (x \mid x) & (x \mid a) & 0 & 0 & (x \mid t) & (x \mid \delta) \\ (a \mid x) & (a \mid a) & 0 & 0 & (a \mid t) & (a \mid \delta) \\ 0 & 0 & (y \mid y) & (y \mid b) & 0 & 0 \\ 0 & 0 & (b \mid y) & (b \mid b) & 0 & 0 \\ (t \mid x) & (t \mid a) & 0 & 0 & (t \mid t) & (t \mid \delta) \\ (\delta \mid x) & (\delta \mid a) & 0 & 0 & (\delta \mid t) & (\delta \mid \delta) \end{bmatrix} \begin{pmatrix} x_i \\ a_i \\ y_i \\ b_i \\ t_i \\ \delta_i \end{pmatrix}$$

ABERRATIONS IN THE TWIN HELIX

In the twin helix channel, several key factors contribute to aberrations in the system. The entire channel's dipole harmonic fields will create a continual dispersive effect. As a result, energy dependent (chromatic) aberrations have the potential to become a dominant problem in the channel. Figures 1 shows the evolution of the phase space of the beam in the horizontal planes, and strong skewing due to chromaticity in a twin helix cell without any absorbing wedge. These effects are increased after introduction of the absorbing wedge as shown in Figure 2.

Examination of the aberration map from of a single twin helix harmonic magnet cell shows that the only non-zero terms effecting the x and a vector components are the energy dependent aberrations. At second order, the (a|xδ) and (a|δδ) components are an order of magnitude greater than the other aberrations effecting horizontal phase space. A sampling of the aberration map terms effecting horizontal phase space is contained in Table 1. These show the all the aberrations effecting x_f and a_f at 2nd and the largest ones at 3rd order. Given their magnitude, the 3rd order aberrations look to pose the more challenging problem to solve.

Table 1: Selected Components for the Aberration Map for the Single Twin Helix Cell

Map Term	Value
2nd Order Horizontal Aberations	
(x|xδ)	.9189890 E-04
(x|aδ)	.7036055 E-05
(x|δδ)	.1887682 E-04
(a|xδ)	-.3331598 E-02
(a|aδ)	-.2550771 E-03
(a|δδ)	-.6843386 E-02
3rd Order Horizontal Aberrations	
(x|xxx)	.3781061 E-02
(x|xyy)	.1877792 E-02
(x|xxδ)	.2329986 E-02
(a|xxx)	.1526752 E-01
(a|xyy)	.7582325 E-02
(a|xxδ)	.9408237 E-02

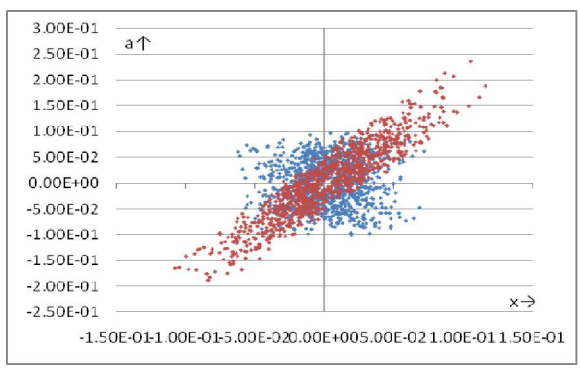

Figure 1: Initial (blue) and final (red) distribution in horizontal phase space for single Twin Helix cell without absorbing wedge.

Copyright © 2011 by PAC'11 OC/IEEE — cc Creative Commons Attribution 3.0 (CC BY 3.0)

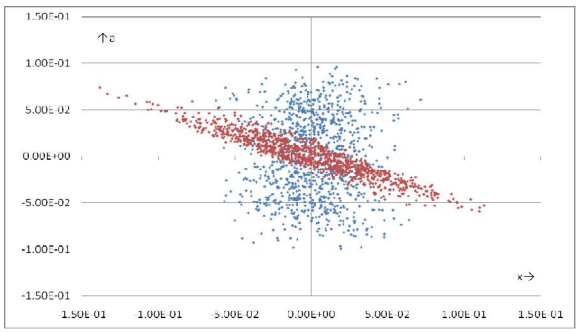

Figure 2: Initial (blue) and final (red) distribution in horizontal phase space for single Twin Helix cell with absorbing wedge.

Also, terms involving initial position (xi) are of concern. For beams that begin at a "point-like source," these aberrations tend to vanish, but in the case of a muon cooling channel, the large initial beam size can cause these terms to dominate in the evolution of the beam thru the channel.

METHODS FOR MINIMIZING ABERRATIONS

COSY's internal tools allow a user to optimize parameters in their simulations to meet particular objective functions. For example, helical sextupole harmonics can be added to the twin helix cell to attempt to minimize a second order aberration such as (x|δδ). These higher order magnetic moments will not alter the linear terms in the transfer map, since such terms are fixed by the dipole and quadrupole moments. Free parameters for the sextupole harmonic (such as field strength or phase) may be varied in a simulation in an attempt to minimize functions based upon specific terms in the transfer or aberration maps.

Due to the continuous dispersion occurring from the dipole harmonic in the helical channel, chromatic aberrations pose a considerable challenge. As an added complication, planar orbit of the reference particle will need to be maintained. One method is thru adjustment of the poletip field strength and the phase of the sextupole helical harmonic. It is also possible to introduce a series of sextupole harmonics with independent parameters to achieve the corrective effects of sextupole doublets utilized in linear beamlines.

The challenge in using these method is understanding the interdependence of the aberration and transfer map components. Attempts to minimize certain terms can easily create problems by increasing different aberrations in the system. COSY provides an excellent tool to help study beam aberrations and evaluate efforts to correct their effects.

CONCLUSIONS AND FUTURE WORK

With the twin helix channel simulated in COSY INFINITY, extensive testing can be done to study chromatic and spherical aberrations of the proposed system. Chromaticity poses a challenge in this channel that merits further study. Utilizing the aberration map, and understanding the symmetries in the beam line will be helpful in testing and optimizing aberrations. Further testing will include higher order magnet elements, including the sextupole helical harmonic field that has already been implemented in COSY.

REFERENCES

[1] R. Johnson, "Ionization Cooling and Muon Colliders", EPAC'08, Genoa, June 2008, THYG03, p. 2917 (2008); http://www.JACoW.org.
[2] Muon Collider Task Force R&D Draft Proposal; https://mctf.fnal.gov.
[3] A. Afanasev et al., "Epicyclic Helical Channels for Parametric Resonance Ionization Cooling", PAC09, Vancouver, May 2009, FR5RFP012, p. 4554 (2009); http://www.JACoW.org.
[4] V. Morozov et al., "Ionization Cooling Simulations in Epicyclic Twin-Helix Channel", this conference.
[5] M. Berz & K. Makino, COSY Infinity Version 9, *Nuclear Instruments and Methods* A558 (2005) 346-350; http://www.bt.pa.msu/edu/index_files/cpsy.htm.
[6] J. Maloney et al., "EPIC Simulations using COSY INFINITY", MOP050, this conference.
[7] M. Berz, Advances in Imaging and Electron Physics, Vol. 108, p. 145-6 (1999).

Copyright © 2011 by PAC'11 OC/IEEE — cc Creative Commons Attribution 3.0 (CC BY 3.0)

HELICAL COOLING CHANNEL DEVELOPMENTS*

R. P. Johnson#, C. Yoshikawa, Muons, Inc., Batavia, IL, U.S.A.
Y. S. Derbenev, V. S. Morozov, JLab, Newport News, VA, USA

Abstract

Several beam phase space manipulation and cooling stages are required to provide the extraordinary reduction of emittances required for an energy-frontier muon collider. From the pion production target, the pions and their decay muons must be collected into RF bunches, rotated in phase space to reduce momentum spread, cooled in 6 dimensions by 6 orders of magnitude, cooled in each transverse plane by another order of magnitude, and accelerated and matched to the RF system used to accelerate the muons to the final collider energy. Many of these stages have Helical Cooling Channel (HCC) [1] solutions based on superimposed solenoid, helical dipole, and helical quadrupole magnetic fields. The HCC was invented to achieve efficient ionization cooling with continuous emittance exchange. We first describe the essential HCC equations and describe how they can be applied for longitudinal and transverse emittance matching. We then describe simulations of HCC segments with a continuous gaseous hydrogen energy absorber suitable for basic 6d cooling as well as new results of related pressurized RF cavity beam tests. We then describe a new and creative application of the theory and use of the HCC that has been developed for Parametric-resonance Ionization Cooling (PIC), and the phase space matching needed for transitions between various cooling channel subsystems

INTRODUCTION

Considerable progress has been made in developing promising subsystems for muon beam cooling channels to provide the extraordinary reduction of emittances required for an energy-frontier muon collider. A high-performance front end from the target to the cooling systems has been designed and simulated [2], and many advances in theory, simulation codes, and hardware development have been achieved, especially regarding the 6d HCC described below. However, the HCC theory is not necessarily restricted to channels having solenoid fields. For example, the Twin Helix [3], which is also described below, does not possess a solenoid field component. The HCC theory and its extensions can describe a wide variety of beam dynamics and is thus well suited to provide the platform from which matching sections can be designed. We now review the theory of the HCC and examine how it can be used for emittance matching between cooling segments that have been independently developed.

Basic Helical Cooling Channel

In the HCC, a solenoid field is augmented with a transverse helical field that provides a constant dispersion along the channel as necessary for the emittance exchange that allows longitudinal cooling. The Hamiltonian that describes motion in this magnetic configuration is easily solved by a transform into the frame of the rotating helical magnet, where it is seen that the addition of a helical quadrupole field provides beam stability over a very large acceptance.

The helical dipole magnet creates an outward radial force due to the longitudinal momentum of the particle while the solenoid magnet creates an inward radial force due to the transverse momentum of the particle:

$$F_{h-dipole} \approx p_z \times b; \quad b \equiv B_\perp; \qquad F_{solenoid} \approx -p_\perp \times B; \quad B \equiv B_z,$$

where B is the field of the solenoid, the axis of which defines the z axis and b is the field of the transverse helical dipole. By moving to the rotating frame of the helical fields, a time- and z-independent Hamiltonian can be formed to derive the beam stability and cooling behaviour [1]. The motion of particles around the equilibrium orbit is shown schematically in Figure 1.

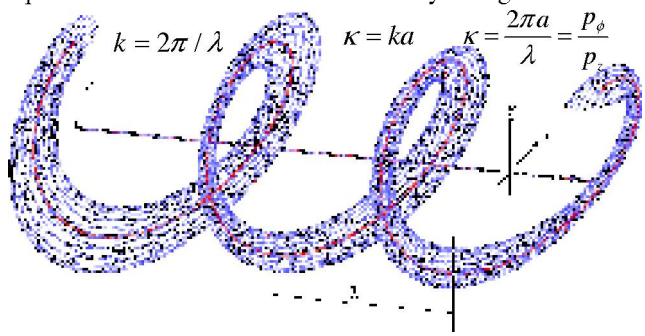

Figure 1: Schematic of beam motion in a HCC.

The equilibrium orbit shown in red follows the equation that is the Hamiltonian solution:

$$p(a) = \frac{\sqrt{1+\kappa^2}}{k}\left[B - \frac{1+\kappa^2}{\kappa} b\right] \qquad (1)$$

The dispersion factor $\hat{D}$ can be expressed in terms of the field components B, b, and the transverse magnetic field radial gradient $\partial b/\partial a$ on the particle's orbit:

$$\hat{D} = \frac{p}{a}\frac{da}{dp} = \left(\frac{a}{p}\frac{dp}{da}\right)^{-1}; \qquad \hat{D}^{-1} = \frac{\kappa^2 + (1-\kappa^2)q}{1+\kappa^2} + g; \qquad g \equiv \frac{-(1+\kappa^2)^{3/2}}{pk^2}\frac{\partial b}{\partial a},$$

where g is the effective field index at the periodic orbit.

The magnetic field ratio on the equilibrium trajectory satisfies the condition

$$\frac{b}{B} = \frac{\kappa}{1+\kappa^2}\left(1 - \frac{k}{k_c}\right) = \frac{\kappa}{1+\kappa^2}\left(\frac{q}{q+1}\right), \text{ where } q \equiv \frac{k_c}{k} - 1.$$

For stability, the following condition has to be satisfied

$$0 \;<\; G \equiv (q-g)\hat{D}^{-1} \;<\; R^2 \equiv \frac{1}{4}\left(1 + \frac{q^2}{1+\kappa^2}\right)^2. \qquad (2)$$

Use of a continuous homogeneous absorber takes advantage of a positive dispersion along the entire cooling

*Work supported in part by DOE HEP STTR Grant DE-SC00005589.
rol@muonsinc.com

path, a condition that has been shown to exist for an appropriately designed helical dipole channel. We have also shown that this condition is compatible with stable periodic orbits.

HCC LONGITUDINAL TRANSITIONS

Longitudinal emittance matching in transition sections can be facilitated, subject to simultaneously satisfying stability criterion (2), by continuously varying the RF bucket area to match RF parameters from one cooling section to the next. The RF bucket area is given by:

$$A_{bucket} \cong \frac{16}{w_{rf}}\sqrt{\frac{eV'_{\max}\lambda_{RF}m_\mu c^2}{2\pi|\eta_H|}}\left[\frac{1-\sin(\varphi_s)}{1+\sin(\phi_s)}\right] \quad (3)$$

Where the term in brackets is an approximation for the moving-bucket factor, w_{rf} is the RF frequency in radians/second, V'max is the maximum E-field voltage gradient, λ_{rf} is the RF wavelength, m_μ is the mass of the muon, φ_s is the synchronous particle RF phase, and η_H is the translational mobility or slip factor, derived in [1] for the HCC as:

$$\eta_H = \frac{\sqrt{1+\kappa^2}}{\gamma\beta^3}\left(\frac{\kappa^2}{1+\kappa^2}\hat{D} - \frac{1}{\gamma^2}\right) \quad (4)$$

where $1/\gamma_T^2 = \left(\kappa^2/\left(1+\kappa^2\right)\right)\hat{D}$ and the dispersion factor $\hat{D}$ relates to apparatus quantities and design momentum via:

$$\hat{D}^{-1} = \frac{a}{p}\frac{dp}{da} = \frac{\kappa^2+(1-\kappa^2)[(B\sqrt{1+\kappa^2}/pk)-1]}{1+\kappa^2} - \frac{(1+\kappa^2)^{3/2}}{pk^2}\frac{\partial b}{\partial a} \quad (5)$$

where p is the reference momentum; a reference radius, $\kappa = p_t/p_z$ = helix pitch, B the solenoid B_z, $k = 2\pi/\lambda$; λ is the helix period, and $\partial b/\partial a$ the quadrupole component.

Thus, in matching between sections with different longitudinal dynamics, the RF bucket area can be continually manipulated by varying any of the following: the gradient of the dipole field ($\partial b/\partial a$), the reference momentum (p), the accelerating phase (φ_s), the transition energy γ_t, or the maximum gradient (V'_{max}).

HCC TRANSVERSE TRANSITIONS

In the case of transverse matching, equation (1) would be used to compute the evolution of the solenoid B and helical dipole b fields between cooling segments, where $\partial b/\partial a$ is subject to constraint (2).

G4beamline HCC 6d Cooling Simulations

The analytic relationships above have been used to guide GEANT [4] simulations using G4beamline [5] and ICOOL [6]. Simulation results [7] show a 190,000-fold 6d emittance reduction for a series of eight 250 MeV/c HCC segments, where the reference orbit radii are decreased and fields are increased as the beam cools. Longitudinal and transverse emittances at the end of each HCC segment are shown in Table 1 and are also plotted as red dots in Figure 2. The peak RF field is 27 MV/m and 60 μm Be windows make the cavities true pillboxes. The hydrogen gas pressure is 160 atm at 300 K. Forty per cent of the beam is lost in the 303 m long channel. About 22% of the beam is lost due to muon decay while the rest of the loss is due to emittance mismatches, which can be improved. A new Helical Solenoid (HS) magnet design [8] that uses simple offset coils to generate the required solenoid, dipole and quadrupole field components, was invented and superconducting prototypes are being tested.

Table 1: The parameters of the 8 HCC cooling channel segments used by Yonehara [7].

#	Z	b	b'	b_z	λ	ν	ε_T	ε_L	ε_{6D}	ε
	m	T	T/m	T	m	GHz	μm	mm	mm^3	
1	0	1.3	-0.5	-4.2	1.0	0.325	20.4	42.8	12900	1.0
2	40	1.3	-0.5	-4.2	1.0	0.325	5.97	19.7	415.9	0.92
3	49	1.4	-0.6	-4.8	0.9	0.325	4.01	15.0	10.8	0.86
4	129	1.7	-0.8	-5.2	0.8	0.325	1.02	4.8	2.0	0.73
5	219	2.6	-2.0	-8.5	0.5	0.65	0.58	2.1	3.2	0.66
6	243	3.2	-3.1	-9.8	0.4	0.65	0.42	1.3	0.14	0.64
7	273	4.3	-5.6	-14.1	0.3	0.65	0.32	1.0	0.08	0.62
8	303	4.3	-5.6	-14.1	0.3	1.3	0.32	1.0	0.07	0.60

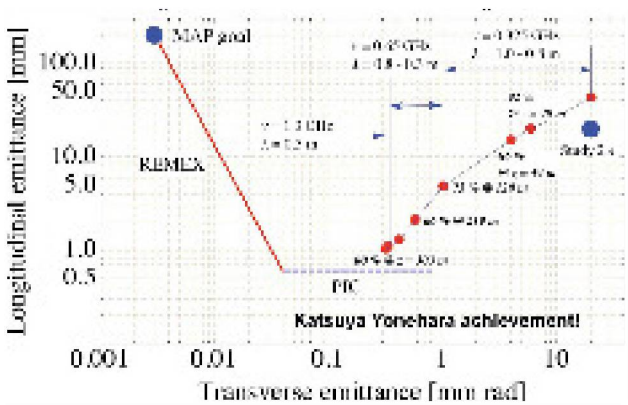

Figure 2: Fernow-Neuffer plot of the G4beamline simulated emittance evolution shown in Table 1.

RF BEAM TESTS

The simple idea that emittance exchange can occur in a practical homogeneous absorber without shaped edges followed from the observation that RF cavities pressurized with a low Z gas are possible [9]. Recent experiments with the proton beam at the Fermilab MuCool Test Area have verified that such cavities will not suffer RF breakdown in a beam. Other parameters have been measured that verify many features of models of the cavities as well. The recombination rate of the ionized electrons produced by the beam is fast enough that the RF amplitude is likely to be adequate for the muon beam that will be less than 100 ns long. Figure 3 shows the first tests of a pressurized RF cavity being hit by a charged particle beam. The voltage drops due to the absorption of energy by the ionized electrons and to the change in impedance of the cavity due to the plasma causing the power from the klystron to be reflected.

The use of a 1 part in 10,000 SF_6 dopant has been shown to largely mitigate the drop in RF voltage caused by the motion of ionized electrons in the RF field that

heat the gas. Namely, the electrons attach to the SF_6 and the large mass of the resulting ion inhibits its motion in the RF field and its energy transfer to the hydrogen gas. Figure 3 shows the influence of a proton beam in a high pressure gas filled cavity without the aid of SF_6 to inhibit the effect of electrons, while Figure 4 illustrates the improvement by addition of the SF_6 dopant. Preliminary models indicate that for short bunch trains (< 100 ns), the doped RF cavity stability allows HCC use as in Figure 2.

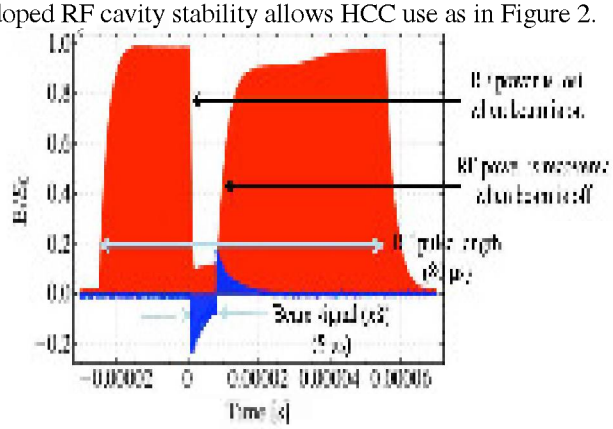

Figure 3: Beam influence on 950 psi hydrogen-filled RF test cell. Red is the 802 MHz RF envelope which rises to E_0~20 MV/m. Blue is the toroid signal from the beam from the 400 MeV H- Linac to the MTA.

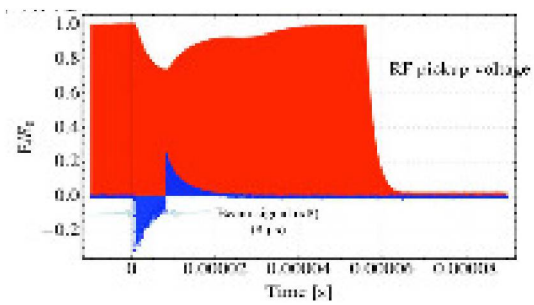

Figure 4: Beam influence on 950 psi hydrogen-filled RF test cell with a 0.01% dopant addition of SF_6. The gradient drops by about 30% during the 8 μs beam pulse, where some of that is due to the impedance mismatch caused by the plasma that in turn causes most of the klystron power to be reflected.

OTHER HCC SEGMENT EXAMPLES

In all cases we can imagine, the pions are produced in a strong solenoid that becomes weaker along the channel so that transverse momenta are folded forward. The decay muon phase space must be matched to the acceptance of the HCC for 6d cooling, a matching that goes from solenoid with no helical dipole to an HCC.

At the end of a 6d HCC segment as shown in Figure 2, you could either match into a strong field solenoid channel for extreme cooling or to a PIC channel. While the former is an example of HCC to solenoid transition, the PIC channel being discussed is even more of a challenge in that it is made up of two helical magnets with no solenoid field component.

PIC and the Twin-Helix Example

Parametric-resonance Ionization Cooling (PIC) requires a half integer resonance to be induced in a ring or beam-line such that the normal elliptical motion of particles in *x-x'* phase space becomes hyperbolic, with particles moving to smaller *x* and larger *x'* as they pass down the beamline. (This is almost identical to the technique used for half integer extraction from a synchrotron where the hyperbolic trajectories go to small *x'* and larger *x* to pass the wires of an extraction septum.) Thin absorbers placed at the focal points of the channel then cool the angular divergence of the beam by the usual ionization cooling mechanism, where each absorber is followed by RF cavities. Thus, in PIC the phase space area is reduced in *x* due to the dynamics of the parametric resonance and *x'* is reduced or constrained by ionization cooling.

The main constraint in parametric-resonance ionization cooling channel design is the requirement to combine low dispersion at the wedge absorber plates (for emittance exchange to compensate energy straggling) with large dispersion in the space between plates (where sextupoles can be placed to compensate for chromatic aberration). The desired large angular divergence of + 200 mr at the absorber plates also implies significant corrections for spherical aberrations and the next step in the development of this channel is to compensate for aberrations. The horizontal and vertical optics also have to be correlated such that there must be places where each plane has a focus at the absorber plates.

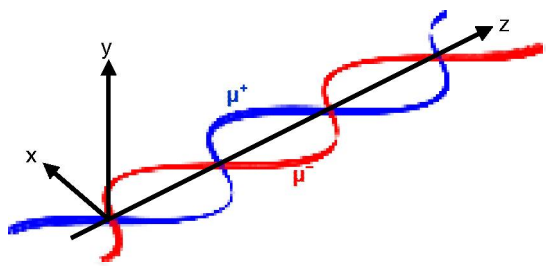

Figure 5: G4beamline display of planar trajectories of muons of both signs in the Twin Helix magnet system.

Perhaps one of the more interesting recent cooling channel developments follows from the realization that two helical dipole magnetic fields of opposite helicity can be superimposed to create a purely vertical magnetic field that varies sinusoidally in amplitude along the magnet axis. This magnet system, called the Twin-Helix [10], produces muon orbits as shown in Figure 5, with a possible coil configuration shown in Figure 6. Here the horizontal and vertical betatron wavelengths differ by a factor of two so energy loss wedge absorbers are placed at every focal point in one plane where the same position corresponds to every other focal point in the other plane. The dispersion is also correlated in that it is small but not zero at the focal points and RF cavities, but large between absorbers where aberration correction magnets can be located.

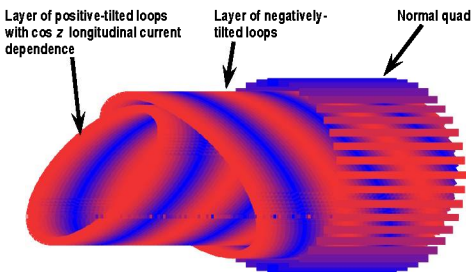

Figure 6: Possible coil configuration for the Twin Helix magnet system.

Space Charge

At some points in the muon cooling channel, the bunching could be extreme, where some estimates are as high as 10^{13} muons in an RF bucket, and the energy low enough to anticipate that space charge effects can be problematic. Through a project supported by the SBIR-STTR program, space charge calculation capability has been added to G4beamline. The transitions between cooling channel segments will incorporate the appropriate criteria to manage any space charge tune shifts.

Gas, Vacuum, and Liquid transitions

Transitions between cooling channel segments may also involve windows or pressure barriers to separate vacuum, pressurized gas, or liquid hydrogen regions. It is quite likely that the beam sizes or beta functions at the window locations will have to be included in the constraints for the matching regions in order to reduce emittance growth from multiple scattering or to help solve engineering problems.

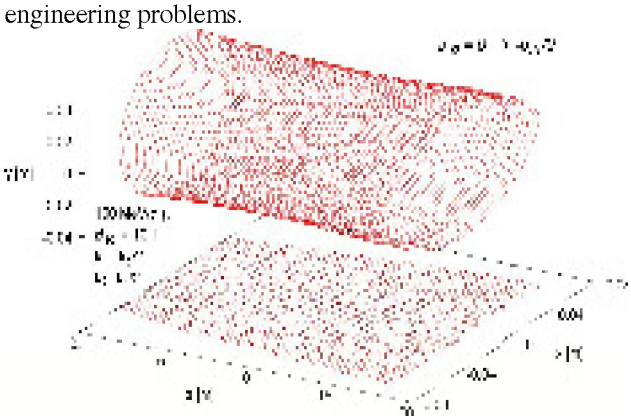

Figure 7: Adiabatic turn-on of the secondary helical dipole. The cyclotron wave number is $k_c = qB/cp_z$. The wave numbers k_1 and k_2 refer to the primary and secondary dipole fields, respectively.

As for creating the matching sections, one approach is an adiabatic turn-on of various components of an HCC. A demonstration of this is shown in Figure 7, where a particle is initially in an HCC that consists of a single helical dipole component. The desire here is to match into another HCC that consists of two helical dipoles, the second of which has a magnetic strength of -1/9 of the primary dipole, and what is shown is an adiabatic turn on of that second helical dipole component. Note how the initially circular orbit transforms into an elliptical trajectory.

Since a solenoid may be thought of as a special case of an HCC with the dipole component turned off, this adiabatic approach seems promising to match between a solenoid and any type of helical channel. Furthermore, the HCC theory may be extended to segments without solenoid field components such as the Twin-Helix.

CONCLUSIONS

The HCC theory and its extensions can be used to solve a wide variety of emittance manipulation and beam cooling problems that are needed to create intense muon beams suitable for a collider. A new use under development is to provide the emittance matching sections between cooling section segments which have very different parameters. Helical solenoid engineering solutions for HCC fields and recent proof of principle hydrogen pressurized RF cavity experiments with intense beams give confidence that practical, complete muon cooling designs will enable an energy frontier collider.

REFERENCES

[1] Y. S. Derbenev and R. P. Johnson, Phys. Rev. ST – Accelerators and Beams 8 (2005) 041002
[2] D. Neuffer, C. Ankenbrandt, R. P. Johnson, C. Yoshikawa, "Muon Capture, Phase Rotation, and Precooling in Pressurized RF Cavities," PAC09, WE6PFP089
[3] V. S. Morozov, Y. S. Derbenev, A. Afanasev, R. P. Johnson, "Epicyclic Twin-Helix Ionization Cooling Simulations." IPAC11, WEPZ009
[4] http://wwwasd.web.cern.ch/wwwasd/geant4/geant4
[5] T. J. Roberts et al., "G4BL Simulation Program for Matter-dominated Beamlines", Proc. PAC07, Albuquerque, NM, pp. 3468-3470 (2007)
[6] R. Fernow, ICOOL, http://pubweb.bnl.gov/users/fernow/www/icool/readme.html
[7] K. Yonehara, R. P. Johnson, M. Neubauer, Y. S. Derbenev, "A helical cooling channel system for muon colliders" , IPAC10, MOPD076 http://epaper.kek.jp/IPAC10/papers/mopd076.pdf
[8] V. Kashikhin et al., "Design Studies of Magnet Systems for Muon Helical Cooling Channels", Proc. EPAC 08, Genoa, Italy, 23-27 Jun 2008, pp. 2437-2439.
[9] R. P. Johnson et al., "High Pressure, High Gradient RF Cavities for Muon Beam Cooling", Proc. LINAC 2004, Lubeck, Germany, p.266 (2004)
[10] V. S. Morozov, Y. S. Derbenev, A. Afanasev, R. P. Johnson, B. Erdelyi, J. A. Maloney, PAC11 WEPZ009

STUDIES OF THE TWIN HELIX PARAMETRIC-RESONANCE IONIZATION COOLING CHANNEL WITH COSY INFINITY*

J.A. Maloney#, B. Erdelyi (Northern Illinois University, DeKalb, IL, USA), S.A. Bogacz, Y. S. Derbenev, V.S. Morozov (JLAB, Newport News, VA, USA), A. Afanasev (George Washington University, Washington, D.C., USA) K.B. Beard, R. P. Johnson (Muons, Inc., Batavia, IL, USA)

Abstract

A primary technical challenge to the design of a high luminosity muon collider is an effective beam cooling system. An epicyclic twin-helix channel utilizing parametric-resonance ionization cooling (EPIC) has been proposed for the final 6D cooling stage. A proposed design of this twin-helix channel is presented that utilizes correlated optics between the horizontal and vertical betatron periods to simultaneously focus transverse motion of the beam in both planes. Parametric resonance is induced in both planes via a system of helical quadrupole harmonics. Ionization cooling is achieved via periodically placed wedges of absorbing material, with bi-periodic rf cavities restoring longitudinal momentum necessary to maintain stable orbit of the beam. COSY INFINITY is utilized to simulate the theory at first order. The motion of particles around a hyperbolic fixed point is tracked. Comparison is made between the EPIC cooling channel and standard ionization cooling effects. Cooling effects are measured, after including stochastic effects, for both a single particle and a distribution of particles.

INTRODUCTION

A proposed next-generation muon collider will require major technical advances to achieve the rapid beam cooling requirements [1]. A twin-helix cooling channel design has been proposed for the final 6-D cooling stage [2]. This channel utilized pairs of helical harmonic magnetic fields with matching field strengths and phase shifts, but equal and opposite helicities. Continuous multipole fields are also superimposed on the channel. This channel maintains a condition of correlated optics where the horizontal and vertical betatron tunes are integer multiples of each other and of the dispersion function [3]. Using the correlated optics condition, wedge absorbers are placed at locations of small, but nonzero, dispersion. RF cavities are also used to maintain the momentum of the reference particle [4]. Using additional pairs of helical harmonic magnets, a parametric resonance is induced inside the channel's absorbers to achieve parametric resonance ionization cooling (PIC) [5]. PIC offers the potential to increase cooling by a factor of 10 over standard ionization cooling [6]. The twin helix channel is simulated using COSY Infinity, a DA-based code that allows for calculation of non-linear effects to arbitrary order [7]. This paper details a linear simulation of this channel, with and without stochastic effects, and studies cooling efficiency with and without the effects of PIC. The linear simulation provides a baseline for ideal cooling in the channel if nonlinear aberrations in the channel have been fully corrected.

SIMULATION PARAMETERS

Table 1 details the parameters used in this linear simulation. The basic cell consists of a continuous straight quadrupole field superimposed upon a pair of helical harmonic dipole fields to establish the correlated optics condition. Wedge absorbers, made of beryllium with a central thickness of 2 cm and a gradient of 30%, are placed every 4 meters in the channel at a location of small but non-zero dispersion. Idealized RF cavities are placed 3 cm after the center of each wedge. COSY INFINITY calculates the transfer map for a 4-meter long cell (from the center of a wedge absorber through the center of the next wedge absorber). Figure 1 illustrates the geometry of this cell.

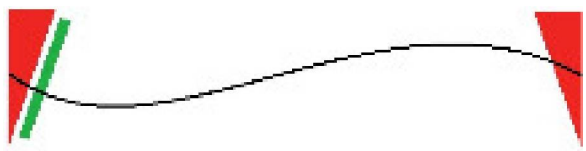

Figure 1. Schematic of single twin helix cell.

The total transfer map for the twin helix channel is obtained by composing the maps for each of the cells that make up the channel upon one another. The orbit of the reference particle (a 250 MeV/c muon) is periodic from the beginning to end of each cell.

Table 1: Four Meter Cell Parameters

H. Dipole Field	1.63 T
H. Dipole wavelength	1 meter
Continuous Quadrupole Field	.72 T/m
H. Quadrupole Field (Horizontal Lenses)	.02 T/m
H. Quadrupole wavelength	2 meters
H. Quadrupole Field (Vertical Lenses)	.04 T/m
H. Quadrupole wavelength	1 meter
RF Voltage	-12.5 MeV
RF Frequency	201.25 MHz
RF Phase	30 Degrees

* Work supported by in part by DOE STTR Grant DE-SC00005589
# physics_maloney@yahoo.com

Copyright © 2012 by IEEE – cc Creative Commons Attribution 3.0 (CC BY 3.0) — cc Creative Commons Attribution 3.0 (CC BY 3.0)

SIMULATION OF THE PARAMETRIC RESONANCE CONDITION IN THE TWIN HELIX CHANNEL

To induce the resonance condition for PIC in the twin helix channel, two independent pairs of helical harmonic quadrupole fields (parametric lenses) are used; one pair induces resonance in the horizontal plane, the other in the vertical plane. The resonances induced by these fields create a hyperbolic fixed point; i.e., motion of particles relative to the reference orbit at the center of the wedge absorber becomes hyperbolic rather than elliptical. Figures 2a-b show this condition in the basic cell (without wedge absorber or RF) when a test particle that is offset both horizontally and vertically in both position and angle relative to the reference orbit by 2 cm and 130 mrads respectively. With the parametric lenses, the position offset is quickly minimized at the expense of a rapid blowup in the angle offset.

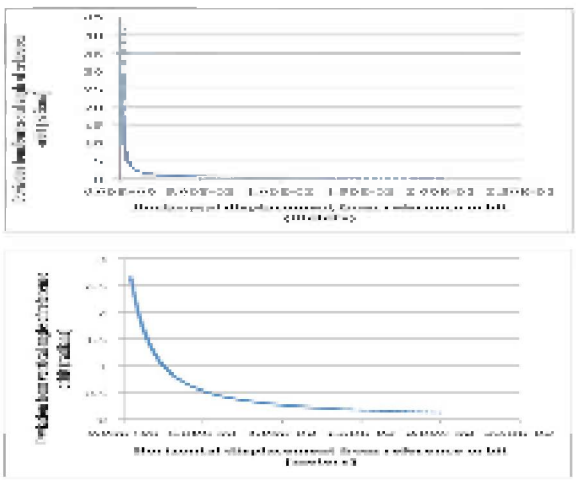

Figures 2a-b. Single particle launched with a horizontal and vertical offsets of 2 cm and .130 radians from the reference orbit and tracked for 200 cells.

SIMULATION OF IONIZATION COOLING IN THE TWIN HELIX CHANNEL

The next stage in the simulations adds wedge absorbers and RF every 4 meters. Figures 3a-b show simulations with and without the parametric lenses to demonstrate the effects of ionization cooling with and without the PIC condition. The simulations demonstrate the expected results. With only ionization cooling, initial cooling effects are primarily to angle, and only later to the positional offset. With PIC the cooling effects are primarily to position offset, i.e., spot size of the beam. The increase in angle offset is minimized thru the ionization cooling effects of the wedge absorber.

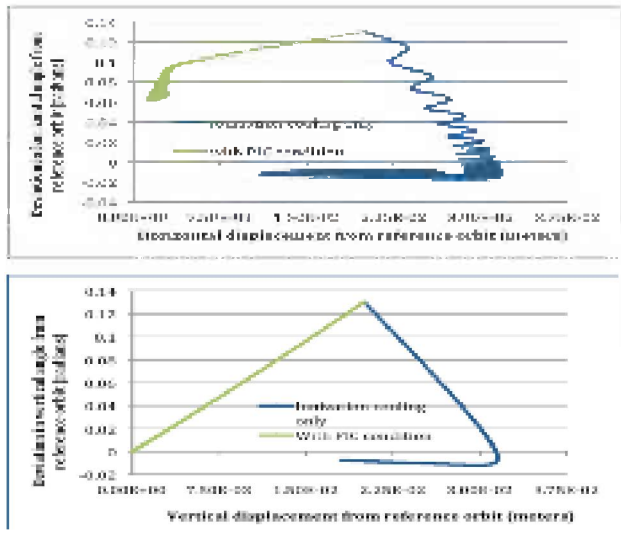

Figures 3a-b. Single particle tracked thru 1000 cells with PIC condition and with ionization cooling only.

SIMULATION OF STOCHASTIC EFFECTS IN THE TWIN HELIX CHANNEL

Stochastic effects of multiple scattering and energy straggling within the wedge absorber were then added to the simulations. Figures 4a-b show the results of combining ionization cooling with stochastic effects on a single particle initially offset both horizontally and vertically in both position and angle relative to the reference orbit by 2 cm and 130 mrads respectively.

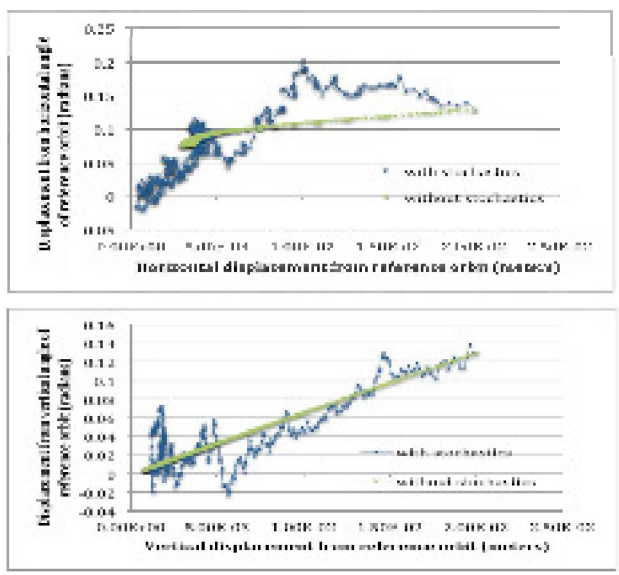

Figures 4a-b. Single particle tracked showing cooling thru 350 cells with and without stochastic effects.

As expected, the test particle is cooled until equilibrium is reached when cooling has been balanced with the effects of multiple scattering and energy straggling [8].

Copyright © 2012 by IEEE – cc Creative Commons Attribution 3.0 (CC BY 3.0) — cc Creative Commons Attribution 3.0 (CC BY 3.0)

A distribution of test particles was also used to test cooling effects in the full simulation of the linear channel. The initial distribution uses a sigma of 2 cm in positions, 130 mrad in angles, and 1% spread in energy from the reference particle. The distribution is also spread over a bunch length of ± 3 cms relative to the reference particle. Figure 5 shows the 2D emittance change in the system calculated from the distribution. The horizontal and vertical 2D emittances are both reduced until equilibrium is reached. Longitudinal emittance is determined from deviation in path length and energy from the reference particle. Once the transverse emittance has reached equilibrium, the increases in longitudinal emittance contribute to heating in the beam distribution. Total 6D emittance for the distribution is plotted in Figure 6 with and without parametric lenses to induce the PIC condition. Figure 7 shows the cooling factor for the channel with and without the PIC condition.

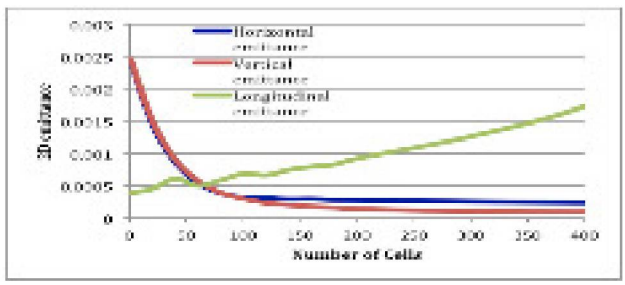

Figure 5: Emittance reduction for a distribution of 1000 particles tracked thru the twin-helix channel with the PIC condition and stochastic effects.

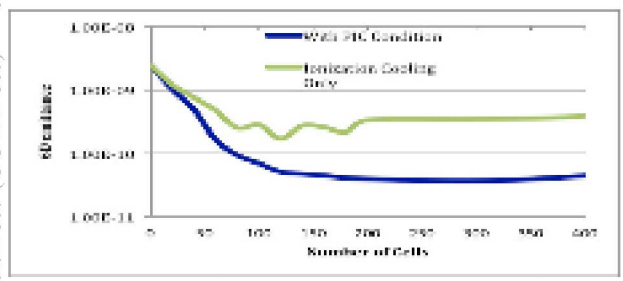

Figure 6: Comparison of 6D emittance reduction with and without the PIC condition.

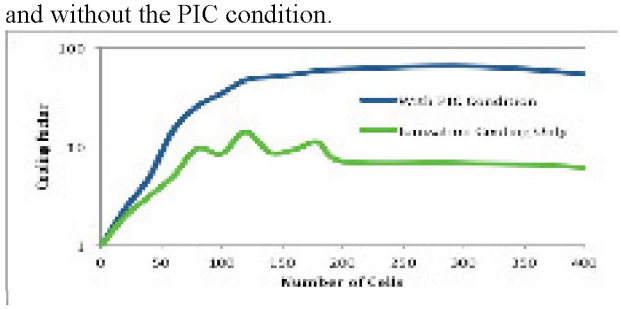

Figure 7: Comparison of cooling factor (ratio of initial to final 6D emittance) with and without the PIC condition.

The determinant of the transfer map for the cell, a 6x6 matrix in the linear case, can also be used to show transverse and 6D cooling in the system [9]. The determinant for the transfer matrix for this test channel is 0.945372. The determinant of the transverse 4x4 quadrant of the transfer matrix is 0.986054.

CONCLUSIONS AND FUTURE WORK

Current simulations in COSY INFINITY have demonstrated that the linear model with stochastic effects of the twin helix channel achieves the resonance condition for PIC, as well as 6D cooling. Future simulations will determine the optimal parameters for this linear model, including cell length, magnet strengths, helicity and phase shifts for the helical harmonic magnets. Wedge gradients and thickness, as well as RF placement and parameters, will also be optimized. Next, studies will determine the largest nonlinear aberrations affecting this optimized twin-helix channel and the dependence these aberrations have on higher order helical harmonic and continuous multipole fields of differing strength, helicity and phase. The cooling efficiency of a system with corrected higher order effects can then be measured and compared with competing 6D cooling methods.

REFERENCES

[1] Muon Collider Task Force R&D Draft Proposal; https://mctf.fnal.gov.
[2] R.P. Johnson, "Ionization Cooling and Muon Colliders", EPAC'08, Genoa, June 2008, THYG03, p. 2917 (2008); http://www.JACoW.org.
[3] A. Afanasev, et al., "Epicyclic Helical Channels for Parametric Resonance Ionization Cooling", PAC'09, Vancouver, May 2009, FRSRFP012, p. 4554 (2009); http://www.JACoW.org.
[4] V.S. Morozov, et al., "Epicyclic Twin-Helix Ionization Cooling Simulations", PAC'11, New York, March 2011, MOP036, p. 163 (2011); http://www.JACoW.org.
[5] V.S. Morozov, et al., "Parametric-Resonance Ionization Cooling in the Twin-Helix", IPAC'11, San Sebastián 2011, WEPZ009, p. 2784 (2011); http://www.JACoW.org.
[6] Y.S. Derbenev and R.P. Johnson, "Parametric-resonance Ionization Cooling", in preparation.
[7] M. Berz & K. Makino, COSY Infinity Version 9, *Nuclear Instruments and Methods* A558 (2005) pp. 346-50.
[8] Y.S. Derbenev and R.P. Johnson, Phys. Rev. ST-AB 8 (2005) 41002.
[9] J.A. Maloney, et al., "EPIC Muon Cooling Simulations Using COSY Infinity", PAC'11, New York, March 2011, MOP050, p. 190 (2011); http://www.JACoW.org.

Copyright © 2012 by IEEE – cc Creative Commons Attribution 3.0 (CC BY 3.0) — cc Creative Commons Attribution 3.0 (CC BY 3.0)

PROGRESS ON MUON PARAMETRIC-RESONANCE IONIZATION COOLING CHANNEL DEVELOPMENT*

V.S. Morozov#, Ya.S. Derbenev, Jefferson Lab, Newport News, VA, USA
A. Afanasev, George Washington University, Washington, DC, USA
K.B. Beard, R.P. Johnson, Muons, Inc., Batavia, IL, USA
B. Erdelyi, J.A. Maloney, Northern Illinois University, DeKalb, IL, USA

Abstract

Parametric-resonance Ionization Cooling (PIC) is intended as the final 6D cooling stage of a high-luminosity muon collider. To implement PIC, a continuous-field twin-helix magnetic channel with a correlated behavior of the horizontal and vertical betatron motions and dispersion was developed. A 6D cooling with stochastic effects off is demonstrated in a GEANT4/ G4beamline model of a system where wedge-shaped Be absorbers are placed at the appropriate dispersion points in the twin-helix channel and are followed by short rf cavities. To proceed to cooling simulations with stochastics on, compensation of the beam aberrations from one absorber to another is required. Initial results on aberration compensation using a set of various-order continuous multipole fields are presented. As another avenue to mitigate the aberration effect, we optimize the cooling channel's period length. We observe a parasitic parametric resonance naturally occurring in the channel's horizontal plane due to the periodic beam energy modulation caused by the absorbers and rf. We discuss options for compensating this resonance and/or properly combining it with the induced half-integer parametric resonance needed for PIC.

INTRODUCTION

Combining muon ionization cooling with parametric resonant dynamics should allow much smaller final transverse muon beam sizes than conventional ionization cooling alone [1, 2]. In the PIC concept, a half-integer parametric resonance is induced in a muon cooling channel. The beam is then naturally focused with the period of the channel's free oscillations. The horizontal and vertical betatron periods must be correlated in such a channel so that, at certain locations, focusing occurs in both planes simultaneously. Absorber plates for ionization cooling are placed at the focal points and are followed by energy-restoring RF cavities. At the absorbers, ionization cooling limits the angular spread while the parametric resonance causes a strong reduction of the beam spot size. The final equilibrium transverse emittances in this scheme should be at least an order of magnitude smaller than those achievable with conventional ionization cooling [2]. An emittance exchange to maintain the longitudinal emittance is introduced by tapering the absorber and having a proper dispersion at its location.

SIMULATIONS IN A TWIN HELIX

A continuous-field twin-helix magnetic channel was proposed for the implementation of PIC [3-8]. The channel is a combination of two helical dipole harmonics pitched in opposite directions but otherwise identical. Additionally, a continuous straight quadrupole is superimposed on top of the helical fields [3]. Such a system is adjusted to meet the correlated optics requirements. Half-integer parametric resonances are induced in both planes using a pair of opposite-helicity but otherwise matching continuous helical quadrupole harmonics per plane [7]. Locations of the focal points are set by the phases of the helical quadrupole pairs.

Figure 1 shows 250 MeV/c muon tracks in a twin-helix channel with 1 m helix period. 2 cm thick Be absorbers with 0.3 thickness gradient are placed every two helix periods where the beam can be simultaneously focused in both the horizontal and vertical planes. The absorber location within a period is chosen at a point with 3 cm dispersion providing the necessary emittance exchange.

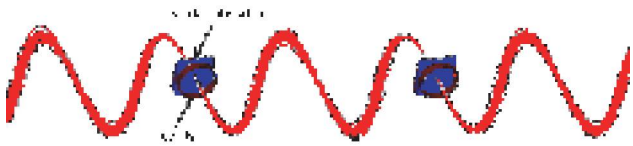

Figure 1: 250 MeV/c muon tracks in a 1 m period twin helix with wedge absorbers and rf cavities.

We used the system shown in Fig. 1 to demonstrate 6D cooling without parametric resonances and with stochastic effects switched off. The simulation was done using a GEANT4-based G4beamline code [9]. The obtained evolution of the three 2D emittances along the channel is shown in Fig. 2. We intentionally chose relatively small initial emittance values to stay close to the linear regime to be able to compare this result to the first-order simulations in [8]. The initial emittance oscillations are caused by a phase-space mismatch because the initial bunch was generated using independent Gaussian distributions for the 6D phase-space coordinates without taking into account proper correlations between them. The later oscillations are probably due to a finite number (only 1000) of particles in the bunch. Since the stochastic effects are off, the emittances cool virtually to zero. This confirms that our basic system is setup correctly.

* Supported in part by DOE SBIR grant DE-SC0005589.
Notice: Authored by Jefferson Science Associates, LLC under U.S. DOE Contract No. DE-AC05-06OR23177. The U.S. Government retains a non-exclusive, paid-up, irrevocable, world-wide license to publish or reproduce this manuscript for U.S. Government purposes.
morozov@jlab.org

Copyright © 2012 by IEEE – cc Creative Commons Attribution 3.0 (CC BY 3.0) — cc Creative Commons Attribution 3.0 (CC BY 3.0)

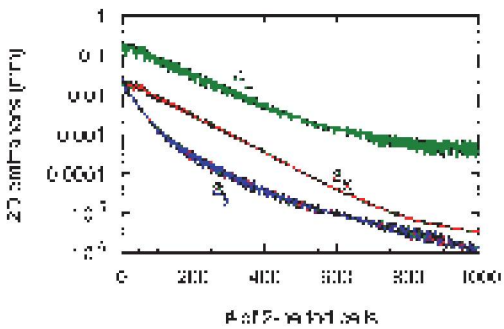

Figure 2: Horizontal ε_x, vertical ε_y, and longitudinal ε_z emittances along the cooling channel plotted vs. the number of 2-period cells (equal to the number of passed absorbers).

To proceed to cooling simulations with stochastics on, compensation of beam aberrations is required. This was verified by running a first-order simulation with stochastics on [8]. One approach to aberration compensation [7] is the following. Since in PIC regime the beam has a small size and a large angular spread at the absorber, a set of particles with systematically-arranged initial angles is started from a focal point on the reference trajectory and tracked to the next focal point to determine the aberration-induced beam smear at that location. A general optimization procedure is used to minimize the beam smear by introducing various-order continuous multipole fields.

Figure 3 shows an example of such optimization. The particles' initial angles were distributed on a grid of azimuthal angles from 0 to 2π in $\pi/4$ steps and polar angles from 20 to 220 mrad in 40 mrad steps. Straight sextupole and octupole harmonics as well as helical quadrupole and decapole pairs were added to the system. The aberrations were minimized by varying the strengths of the straight field components and both strengths and phases of the helical harmonic pairs.

A more systematic approach to aberration compensation is to use COSY Infinity [10], a matrix-based code, which works by expanding a particle's trajectory around a reference orbit to an arbitrary order in the 6D phase-space coordinates. Therefore, it can be used to unfold and analyze individual aberrations [5].

Another avenue to mitigate the aberration effect is to optimize the cooling channel's period length. The helix period is an important parameter for a number of reasons. From the engineering point of view, it determines the channel's total length and sets the requirements on the magnet and rf cavity parameters. From the performance point of view, it determines the cooling rate per unit length and muon loss due to decay. It also determines the channel's optical properties, such as its focusing strength, periodic orbit amplitude, and values of the beta functions and dispersion.

The helix period was optimized by minimizing the particle loss after an initially zero-emittance muon beam passed through a large number of 1 mm absorbers and short rf cavities in a twin-helix channel. For long helix periods, the particles were getting lost due to large absolute aberration sizes. For short helix periods, the loss was apparently due to reduction of the dynamic aperture. A balance between these effects seemed to be established for a helix period of about 20 cm, which is also reasonable from a practical point of view.

We also determined that the main mechanism for the particle loss is apparently the longitudinal dynamics. Figure 4 shows the beam's longitudinal phase space after 900 absorbers. Shown in red are the particles that are lost after 100 more absorbers. There is a clear loss pattern in the longitudinal phase space, which is not observed in the other dimensions.

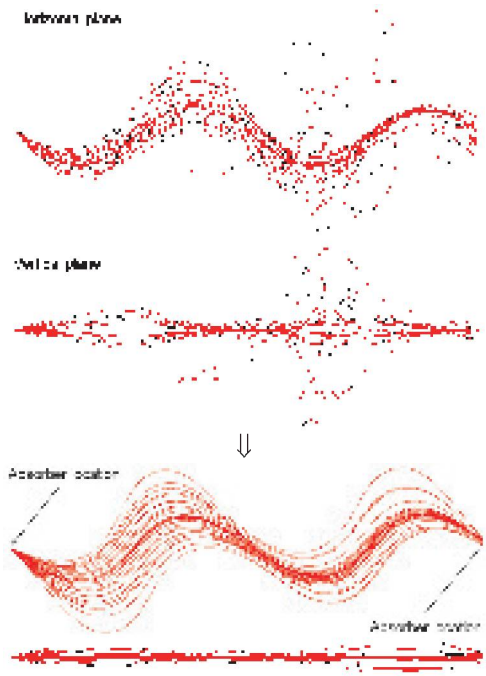

Figure 3: 250 MeV/c muon tracks from one focal point to the next before (top) and after (bottom) aberration compensation using field harmonics up to decapole.

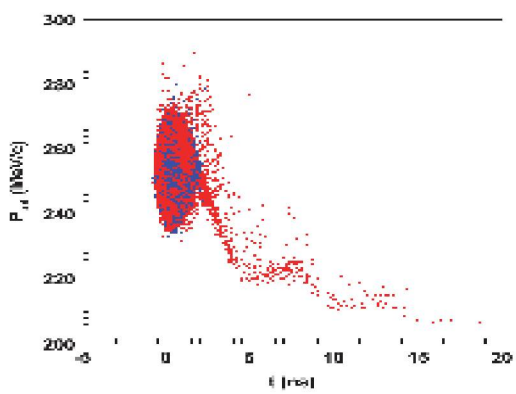

Figure 4: Longitudinal phase space after an initially zero-emittance bunch passes through 900 thin absorbers. Shown in red are the particles that are lost after 100 more absorbers.

Copyright © 2012 by IEEE – cc Creative Commons Attribution 3.0 (CC BY 3.0) — cc Creative Commons Attribution 3.0 (CC BY 3.0)



Figure 5: Muon tracks in a 0.2 m period twin helix.

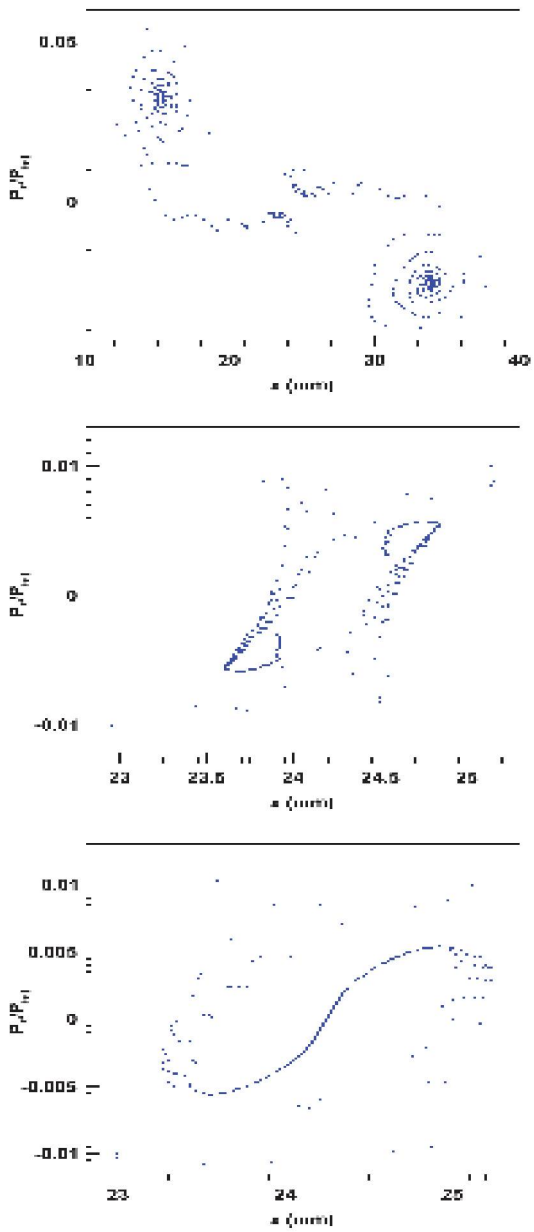

Figure 6: Horizontal phase space trajectory of a single muon at the absorber locations in a 0.2 m period twin helix without induced parametric resonances (top), with horizontal and vertical resonances induced with the nominal phases (middle), and with the phase of the induced horizontal resonance shifted by 200 mrad (bottom).

To address this issue, we introduced more longitudinal cooling. We again used high thickness-gradient 2 cm absorbers as in Fig. 1. Since the dispersion scales together with the helix period, we accounted for its reduction in the now 20 cm period twin helix by moving the absorbers to the maximum dispersion points corresponding to the points of maximum reference orbit offset as illustrated in Fig. 5.

Tracking in the shorter-period system showed a strong parasitic parametric resonance [6]. The resonance is excited in the horizontal plane due to the periodic beam energy modulation caused by the absorbers and rf, which happens at twice the frequency of the horizontal betatron oscillations. Its effect is more pronounced for shorter helix periods because relative impact of the absorbers and rf cavities is greater. This effect is now well understood. Symmetric positioning of the rf cavities should help correct the parasitic resonance. One can also account for the parasitic resonance by adjusting the phase of the induced horizontal resonance so that the net effect of the two resonances is what is needed for PIC.

Figure 6 (top) shows a muon's horizontal phase space trajectory at the absorber locations in a system without induced parametric resonances. The two stability islands in the phase space are an indication of a half-integer resonance. Figure 6 (middle) is the phase space trajectory of the same particle when horizontal and vertical parametric resonances are induced in the twin helix with their nominal phases. The parasitic and induced horizontal resonances interfere together resulting in a change of the stability island locations; however, their orientation is not suitable for PIC. Adjusting the phase of the induced horizontal resonance by 200 mrad gives the picture shown in Fig. 6 (bottom). The particle cools to a single point in the phase space. These results are preliminary but they demonstrate the general approach to treating the parasitic resonance when setting up PIC.

REFERENCES

[1] Ya.S. Derbenev and R.P. Johnson, AIP Conf. Proc. 821 (AIP, Melville, NY, 2006), p. 420.
[2] Ya.S. Derbenev et al., arXiv:1205.3476v1 [physics. acc-ph].
[3] V.S. Morozov et al., AIP Conf. Proc. 1299 (AIP, Melville, NY, 2010), p. 664.
[4] J.A. Maloney et al., in Proc. PAC'11, MOP050.
[5] J.A. Maloney et al., in Proc. PAC'11, WEP074.
[6] V.S. Morozov et al., in Proc. PAC'11, MOP036.
[7] V.S. Morozov et al., in Proc. IPAC'11, WEPZ009.
[8] J.A. Maloney et al., "Studies of the twin-helix parametric-resonance ionization cooling channel with COSY Infinity", this conference, TUPPD011.
[9] G4beamline, http://g4beamline.muonsinc.com
[10] K. Makino and M. Berz, NIM A558, 346 (2005).

Copyright © 2012 by IEEE – cc Creative Commons Attribution 3.0 (CC BY 3.0) — cc Creative Commons Attribution 3.0 (CC BY 3.0)

Parametric-Resonance Ionization Cooling of Muon Beams

V.S. Morozov[a], Ya.S. Derbenev[a], A. Afanasev[b,c], R.P. Johnson[b], B. Erdelyi[d], and J.A. Maloney[d]

[a]*Thomas Jefferson National Accelerator Facility, Newport News, Virginia 23606, USA*
[b]*Muons, Inc., Batavia, Illinois 60510, USA*
[c]*The George Washington University, Washington, D.C. 20052, USA*
[d]*Northern Illinois University, DeKalb, Illinois 60115, USA*

Abstract. Parametric-resonance Ionization Cooling (PIC) is proposed as the final 6D cooling stage of a high-luminosity muon collider. Combining muon ionization cooling with parametric resonant dynamics should allow an order of magnitude smaller final equilibrium transverse beam emittances than conventional ionization cooling alone. In this scheme, a half-integer parametric resonance is induced in a cooling channel causing the beam to be naturally focused with the period of the channel's free oscillations. Thin absorbers placed at the focal points then cool the beam's angular divergence through the usual ionization cooling mechanism where each absorber is followed by RF cavities. A special continuous-field twin-helix magnetic channel with correlated behavior of the horizontal and vertical betatron motions and dispersion was developed for PIC. We present the results of modeling PIC in such a channel using GEANT4/ G4beamline. We discuss the challenge of precise beam aberration control from one absorber to another over a wide angular spread.

Keywords: parametric resonance ionization cooling.
PACS: 29.27.-a, 29.20.-c, 14.60.Ef, 41.85.Lc

INTRODUCTION

The principle of ionization cooling is well known [1]: as a particle passes through an energy-absorbing material, its momentum components are reduced in all three dimensions and only the longitudinal component is restored by RF fields. The angular divergence x' of the particle is thereby diminished until it reaches equilibrium with multiple Coulomb scattering in the material. Employing a parametric resonance at twice the betatron oscillation frequency in a periodic magnetic channel overcomes this equilibrium in the following way [2]. The resonant perturbation changes the particles' phase-space trajectories at periodic locations along the channel from their normal elliptical shapes to hyperbolic as shown in Fig. 1(a). At certain periodic focal positions, the beam becomes progressively narrower in x and wider in x' as it passes down the channel. Without damping, the beam dynamics is not stable because the beam envelope grows with every period as illustrated in Fig. 1(b). Placing energy absorbers at the focal points stabilizes the beam motion by limiting the beam's angular divergence at those points through the usual ionization cooling mechanism. The resonant dynamics then causes a strong reduction of the beam spot size at the absorber locations leading to transverse beam emittances that are an order of magnitude smaller than without the resonance. The longitudinal emittance is maintained constant using emittance exchange introduced by tapering the absorbers and placing them at points with appropriate dispersion. Another way to interpret the PIC mechanism is that a parametric resonance focuses the beam with the period of the channel's free oscillations. Being a resonant process, this focusing can effectively be very strong without involving large magnetic fields.

The normalized equilibrium transverse emittance achievable in PIC is given by [2, 3]

$$\varepsilon_{\perp}^{n} = \frac{\sqrt{3}}{4\beta}(Z+1)\frac{m_e}{m_\mu}w \qquad (1)$$

Advanced Accelerator Concepts
AIP Conf. Proc. 1507, 843-848 (2012); doi: 10.1063/1.4773808
© 2012 American Institute of Physics 978-0-7354-1125-8/$30.00

TABLE 1. Expected PIC parameters.

Parameter	Unit	Initial	Final
Muon beam momentum, p	MeV/c	250	250
Number of particles per bunch, N_b	10^{10}	1	1
Be ($Z = 4$) absorber thickness, w	mm	20	2
Normalized transverse emittance (rms), $\varepsilon_x = \varepsilon_y$	μm	230	23
Beam size at absorbers (rms), $\sigma_a = \sigma_x = \sigma_y$	mm	0.7	0.1
Angular spread at absorbers (rms), $\theta_a = \theta_x = \theta_y$	mrad	130	130
Momentum spread (rms), $\Delta p/p$	%	2	2
Bunch length (rms), σ_z	mm	10	10

where $\beta = v/c$ is the relativistic factor, Z is the absorber material's atomic number, m_e and m_μ are the electron and muon masses, respectively, and w is the average absorber thickness in the beam direction. The equilibrium beam size σ_a and angular spread θ_a at the absorber and the equilibrium momentum spread $\Delta p/p$ are given by [3]

$$\sigma_a^2 = \frac{1}{8}\frac{(Z+1)}{\gamma\beta^2}\frac{m_e}{m_\mu}w^2, \qquad \theta_a^2 = \frac{3}{2}\frac{(Z+1)}{\gamma\beta^2}\frac{m_e}{m_\mu}, \qquad (\Delta p/p)^2 = \frac{3}{8}\frac{(\gamma^2+1)}{\gamma\beta^2}\frac{m_e}{m_\mu}\frac{1}{\log}. \tag{2}$$

where γ is the muon relativistic energy factor and log is the Coulomb logarithm of ionization energy loss for fast particles. The expected PIC parameters following from Eqs. (1) and (2) for a 250 MeV/c muon beam are summarized in Table 1. Note that the absorbers are thicker at the beginning of the channel in order to produce a higher cooling rate of an initially large-emittance beam. As the beam cools propagating down the channel, the absorber thickness is gradually reduced in order to reach the minimum practical transverse emittance. Since the cooling rate gets lower for thinner absorbers, the minimum practical absorber thickness is determined by the practically acceptable beam loss due to muon decay.

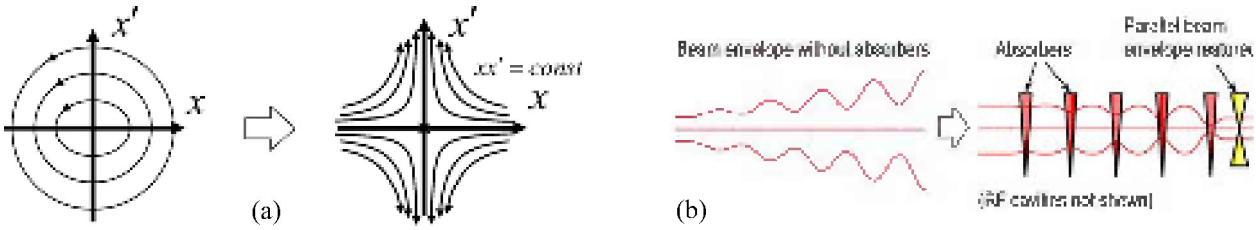

FIGURE 1. (a) Transformation of a particle's phase space motion by a half-integer parametric resonance: elliptical phase-space trajectories become hyperbolic. The trajectories are illustrated at the focal points. (b) Stabilizing effect of ionization cooling energy absorbers in a channel with a half-integer resonance.

PIC CHANNEL

To provide focusing of the beam in both horizontal and vertical planes simultaneously, the horizontal oscillation period λ_x must be equal to or be a low-integer multiple of the vertical oscillation period λ_y. The PIC scheme also requires alternating dispersion D such that it is

- small at the beam focal points to minimize energy straggling in the absorber,
- non-zero at the absorber for emittance exchange to maintain constant longitudinal emittance,
- relatively large between the focal points to allow for correction of momentum-dependent aberrations.

From the above dispersion requirements, it follows that λ_x and λ_y must also be low integer multiples of the dispersion period λ_D. Note that λ_x and λ_D should not be equal to each other in order to avoid an unwanted resonance. Thus, the cooling channel optics must have correlated values of λ_x, λ_y and λ_D:

$$\lambda_x = n\lambda_y = m\lambda_D, \tag{3}$$

where n and m are integers. An optics example satisfying Eq. (3) with $\lambda_x = 2\lambda_y = \mathbf{4}\lambda_D$ is illustrated in Fig. 2.

The same type of cooling channel with correlated optics can be used for Reverse EMittance EXchange (REMEX). The only difference is that in REMEX the angles of the wedge absorbers are reversed to provide

cooling of the transverse emittance by another factor of ten at the expense of the longitudinal emittance. The bunch length during this process is maintained constant by adiabatic damping due to acceleration.

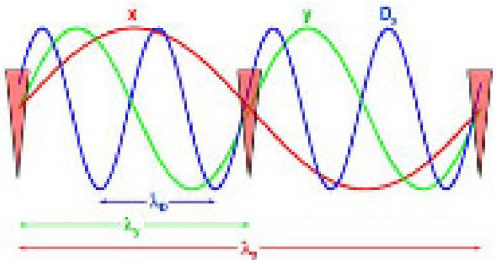

FIGURE 2. Particle's horizontal x and vertical y betatron trajectories and horizontal dispersion D_x for the $\lambda_x = 2\lambda_y = 4\lambda_D$ case of correlated optics.

The PIC dynamics is very sensitive to magnetic fringe fields, which produce numerous beam aberrations. One approach to finding a practical fringe-field-free solution is to use helical harmonics [4, 5]. In order to create alternating dispersion required for PIC, two equal-strength helical dipole harmonics with equal periods but opposite helicities are superimposed leading to the name "twin helix" channel. Analogously to how combining two circularly-polarized waves produces a linearly-polarized one, the magnetic field in the midplane of this configuration is transverse to the plane. This means that the periodic orbit is flat and lies in the midplane. The horizontal and vertical motions are stable and uncoupled. A continuous straight quadrupole is added to the system in order to redistribute focusing between the horizontal and vertical dimensions. The resulting field configuration is continuous and free of fringe fields as desired for PIC. It was demonstrated [6] that a twin-helix channel can be adjusted to meet all of the above correlated optics requirements while offering large dynamic aperture and momentum acceptance.

The magnetic field strength at the center of each dipole harmonic B_d and the quadrupole field gradient $\partial B_y/\partial x$ corresponding to the correlated optics shown in Fig. 2 are given by [6, 7] (4)

$$B_d = 6.515\cdot 10^{-3}[\mathrm{Tm/(MeV/c)}]\, p/\lambda, \qquad \partial B_y/\partial x = 2.883\cdot 10^{-3}[\mathrm{Tm/(MeV/c)}]\, p/\lambda^2,$$

where p is the muon momentum and λ is the helix period. The optical properties of the twin-helix channel are well-understood [6]. The periodic orbit amplitude x_{max}, dispersion amplitude $D_{x\,max}$ and horizontal and vertical chromaticities ξ_x and ξ_y corresponding to the correlated optics are given by [6, 7]

$$x_{\max} = 0.121\,\lambda, \qquad D_{x\,\max} = 0.196\,\lambda, \qquad \xi_x = -0.646, \qquad \xi_y = -0.798. \tag{5}$$

Equations (4) and (5) are used to obtain the twin helix correlated optics parameters for a given muon momentum and helix period.

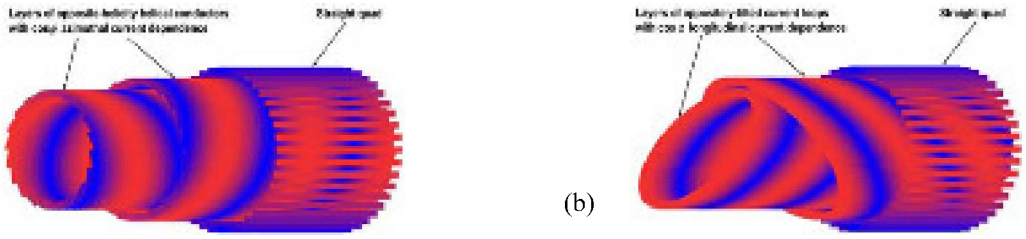

FIGURE 3. Conceptual diagrams of possible practical implementations of the twin-helix channel. The color represents current variation in the conductors.

Conceptually, the required magnetic field configuration can be obtained by winding two separate coaxial layers of helical conductors and coaxially superimposing a straight quadrupole as shown in Fig. 3(a). The helical conductors constituting the two layers have the same special periods and opposite helicities. Within each layer, the currents in the helical conductors vary azimuthally as cos(ϕ). Note that the two layers do not have to have the same radius. The difference in the radii can be accounted for by adjusting the layers' currents. Another approach

to producing the desired magnetic field is to combine two coaxial layers consisting of a series of tilted current loops overlaid with a coaxial straight quadrupole as shown in Fig. 3(b). The inclined loops comprising the two different layers are tilted in opposite directions. The current in the loops of each layer varies longitudinally as cos(kz). Such a technology, without longitudinal current variation, is used to make constant-field dipoles [8]. Perhaps, a more practical approach to the channel's engineering design is to develop a conductor configuration that is centered on and follows the beam's periodic orbit similarly to [9].

PIC SIMULATIONS

We used GEANT4-based G4beamline code [10] to simulate PIC in a twin-helix channel. The simulation setup is shown in Fig. 4. An important simulation parameter is the helix period. From the engineering point of view, it determines the channel's total length and sets the requirements on the magnet and rf cavity parameters. From the performance point of view, it determines the cooling rate per unit length and muon loss due to decay. It also determines the channel's optical properties, such as its focusing strength, periodic orbit amplitude, and values of the beta functions and dispersion. Simulations suggest [11] that a helix period of about 20 cm provides an optimal balance between the channel's focusing strength and the magnitude of its non-linear effects. Such a channel length is perhaps also reasonable from the practical point of view.

Be wedge absorbers with an average thickness of 2 cm and a thickness gradient of 0.3 are placed every two periods of the twin helix, which is the shortest possible separation corresponding to a half period of the horizontal betatron oscillations and a full period of the vertical betatron oscillations. The absorbers are centered on the reference trajectory and their axes are aligned with the reference momentum. In order to provide the necessary emittance exchange, the absorbers are placed at the maximum dispersion points corresponding to the points of maximum reference orbit offset as shown in Fig. 4.

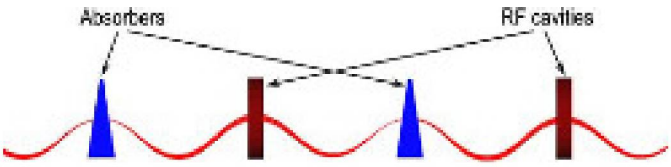

FIGURE 4. Simulation setup of the twin-helix channel in G4beamline.

Short 201 MHz RF cavities are placed half way between the absorbers. Such a symmetric arrangement of the absorbers and RF cavities allows one to easily compensate a parasitic parametric resonance caused by period energy modulation as discussed below. The RF cavities were modeled as unrealistically short in order to initially decouple from the transit time effect. However, a 250 MeV/c muon energy loss in 2 cm of Be can be compensated by a realistic RF cavity.

A pair of opposite-helicity but otherwise identical helical quadrupoles is used to excite a parametric resonance in each plane [12]. The periodicity of the helical quadrupole pair has to be half the respective betatron period [7]. Locations of the parametric-resonance focal points are set to coincide with the absorber locations by adjusting the parametric quadrupole phases using the fact that the focal point is located 1/8 of the respective betatron period from the maximum of the quadrupole field [7]. Using this approach, we are able to independently induce a parametric resonance in each plane.

Figure 5 shows the horizontal phase-space trajectories of a sample particle for a few different strengths of the parametric-resonance-inducing quadrupoles. The simulation in Fig. 5(a) with zero strength of the induced resonance indicates that there is a parasitic parametric resonance. This can be seen from the two fixed points in the upper left and lower right quadrants of the phase space. This parasitic resonance is excited in the horizontal plane due to the periodic beam energy modulation caused by the absorbers and RF, which happens at twice the frequency of the horizontal betatron oscillations [7]. This effect is well understood. Symmetric positioning of the absorbers and RF cavities puts the parasitic resonance exactly out of phase with the induced resonance, which makes it easy to compensate the parasitic resonance by simply increasing the strength of the induced resonance. Such compensation is illustrated in Fig. 5. As the induced resonance's strength is increased, the fixed points first become closer, then a balance is established between the resonant excitation and ionization cooling, i.e. PIC. Finally, the induced resonance overcomes the cooling process, and two fixed points appear in the upper right and lower left quadrants of the phase space. Based on these studies, a quadrupole strength of 1 T/m is chosen to generate a parametric resonance in each of the horizontal and vertical planes.

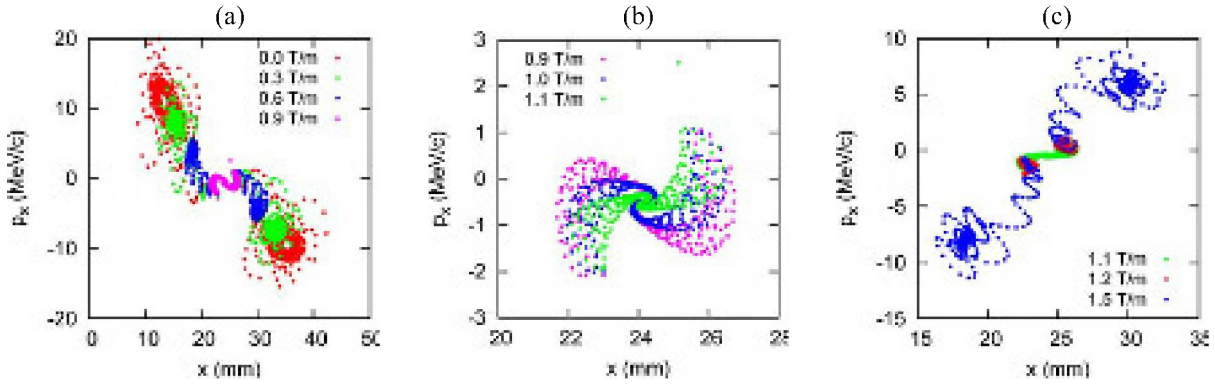

FIGURE 5. Horizontal phase-space trajectories of a sample particle for different strengths of an induced half-integer parametric resonance. The indicated field gradient is the strength amplitude of each quadrupole in the resonance-inducing pair.

Figure 6 shows evolution of the three 2D emittances along a twin-helix channel obtained in a PIC simulation using the above setup. The initial emittance values were intentionally chosen relatively small in order to stay close to the linear regime to allow comparisons with the first-order simulations in [13]. The initial emittance oscillations are caused by a phase-space mismatch due to the initial bunch being generated using independent Gaussian distributions for the 6D phase-space coordinates without taking into account proper correlations between them. The later oscillations are probably due to a finite number (only 1000) of particles in the bunch. Since the stochastic effects are off, the emittances cool virtually to zero. This confirms that our basic system is setup correctly.

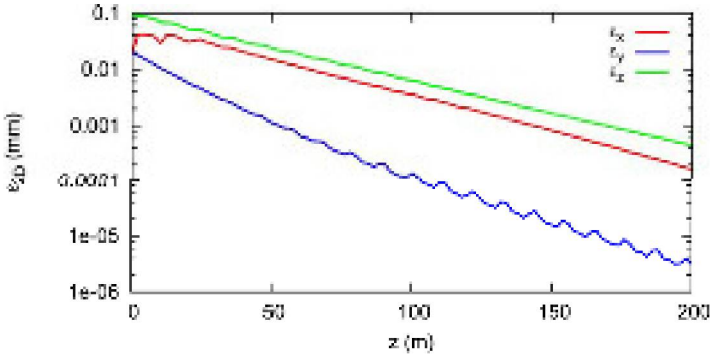

FIGURE 6. Evolution of the horizontal ε_x, vertical ε_y, and longitudinal ε_z 2D emittances along a twin-helix channel ignoring stochastic effects.

To proceed to cooling simulations including stochastic effects, compensation of beam aberrations is required. This was verified by running a first-order simulation with stochastics on [13]. Aberrations from one absorber to another must be compensated to a degree where they are small compared to the beam size at the absorber. Since the equilibrium angular spread in Table 1 is on the order of a hundred milliradians, the angle-dependent aberrations must be precisely compensated over the angular range of a few hundred milliradians. This is a challenging task. However, some of the intrinsic symmetries of the correlated optics reduce the number of aberration compensation conditions. The number of conditions can be further reduced by using a coupling resonance [3].

Here we demonstrate one approach to aberration compensation [11, 12]. Since in PIC regime the beam has a small size and a large angular spread at the absorber, a set of particles with systematically-arranged initial angles is started from a focal point on the reference trajectory and tracked to the next focal point to determine the aberration-induced beam smear at that location. A general optimization procedure is used to minimize the beam smear by introducing various-order continuous multipole fields.

Figure 7 shows an example of such optimization. The particles' initial angles were distributed on a grid of azimuthal angles from 0 to 2π in $\pi/4$ steps and polar angles from 20 to 220 mrad in 40 mrad steps. Straight sextupole and octupole harmonics as well as helical quadrupole and decapole pairs were added to the system. The aberrations were minimized by varying the strengths of the straight field components and both strengths and phases of the helical harmonic pairs.

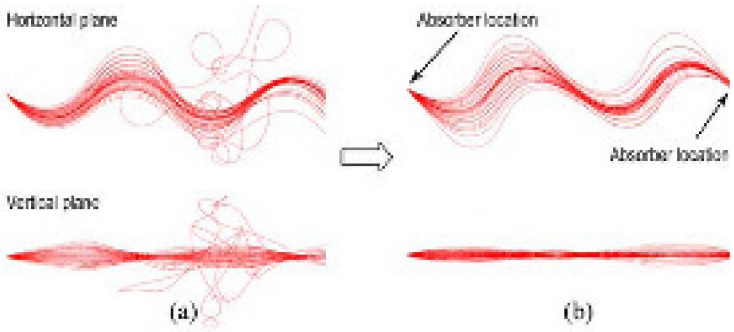

FIGURE 7. Demonstration of aberration compensation in a twin helix up to a polar angle of 220 mrad: 250 MeV/c muon tracks are shown from one focal point to the next before (a) and after (b) aberration compensation using field harmonics up to decapole.

A more systematic approach to aberration compensation is to use COSY Infinity [14], a matrix-based code, which works by expanding a particle's trajectory around a reference orbit to an arbitrary order in the 6D phase-space coordinates. Therefore, it can be used to unfold and analyze individual aberrations, which is well-suited for our purpose. COSY Infinity has been extended to include helical harmonics and to calculate the reference orbit in a twin helix [13]. Work on compensating aberration using COSY Infinity is in progress with promising results [15].

CONCLUSIONS AND FUTURE PLANS

PIC combines muon ionization cooling with parametric resonant dynamics to allow final equilibrium transverse beam emittances that are an order of magnitude smaller than those achievable with conventional ionization cooling alone. Applying the same dynamics for REMEX should reduce the transverse emittances by another factor of ten. Thus, PIC and REMEX together can provide two orders of magnitude luminosity increase of a muon collider.

A special continuous-field twin-helix magnetic channel with correlated behavior of the horizontal and vertical betatron motions and dispersion was developed for PIC. A basic model of a PIC channel with absorbers and RF cavities was setup in G4beamline. The model's validity was confirmed by PIC simulations with stochastic effects off. Compensation of beam aberrations is required for a complete demonstration of PIC with stochastic effects on. A lot of progress has been made on this problem already, and it is going to remain a focus of our near-future studies.

ACKNOWLEDGMENTS

This work was supported in part by U.S. DOE OHEP STTR Grant DE-SC0005589. This manuscript has been authored by Jefferson Science Associates, LLC under U.S. DOE Contract No. DE-AC05-06OR23177. The U.S. Government retains a non-exclusive, paid-up, irrevocable, world-wide license to publish or reproduce this manuscript for U.S. Government purposes.

REFERENCES

1. D. M. Kaplan, Introduction to Muon Cooling, http://www.slac.stanford.edu/econf/C010630/papers/M102.PDF
2. Ya.S. Derbenev and R.P. Johnson, in Proc. PAC05, Knoxville, TN (IEEE, Knoxville, Tennessee, 2005), p. 1374.
3. Ya. S. Derbenev et al., arXiv:1205.3476v1 [physics. acc-ph].
4. T. Tominaka et al., Nucl. Instrum. Meth. A 459, 398 (2001).
5. Y.S. Derbenev and R.P. Johnson, Phys. Rev. ST Accel. Beams 8, 041002 (2005).
6. V.S. Morozov et al., AIP Conf. Proc. 1299 (AIP, Melville, NY, 2010), p. 664.
7. V.S. Morozov et al., in Proc. PAC'11, New York, NY (IEEE, New York, 2011), MOP036, p. 163.
8. R.B. Meinke et al., in Proc. PAC'09, Vancouver, BC, Canada (IEEE, Piscataway, NJ, 2009), MO6PFP041, p. 229.
9. V. S. Kashikhin, et. al., IEEE Trans. on Applied Superconductivity 18, 252 (2008).
10. G4beamline, http://g4beamline.muonsinc.com
11. V.S. Morozov et al., in Proc. IPAC'12, New Orleans, LA, WEPPP005, p. 2729.
12. V.S. Morozov et al., in Proc. IPAC'11, San Sebastian, Spain, WEPZ009, p. 2784.
13. J.A. Maloney et al., in Proc. IPAC'12, New Orleans, LA, TUPPD011, p. 1428.
14. K. Makino and M. Berz, Nucl. Instrum. Meth. A 558, 346 (2005).
15. J.A. Maloney et al., to be published in Proc. NuFact'12, Williamsburg, VA.

Progress Towards Parametric-Resonance Ionization Cooling in the Twin-Helix Channel*

J.A. Maloney[a#], B. Erdelyi[a], V.A. Morozov[b], Y.A. Derbenev[b], R.P. Johnson[c], and A. Afanasev[d]

[a]*Northern Illinois University, DeKalb, Illinois 60115, USA*
[b]*Thomas Jefferson National Accelerator Facility, Newport News, Virginia 23606, USA*
[c]*Muons, Inc., Batavia, Illinois 60510, USA*
[d]*The George Washington University, Washington, D.C. 20052, USA*

Abstract. Parametric-resonance Ionization Cooling (PIC) is proposed as the final 6D cooling stage of a high-luminosity muon collider. Combining muon ionization cooling with parametric resonant dynamics could allow an order of magnitude smaller final equilibrium transverse emittance than conventional ionization cooling alone. The same type of cooling channel can be used for Reverse EMittance EXchange (REMEX) to reduce the transverse emittance by another factor of ten. Together, PIC and REMEX can provide two orders of magnitude luminosity increase for a muon collider.

Keywords: parametric resonance ionization cooling.
PACS: 29.27.-a, 29.20.-c, 14.60.Ef, 41.85.Lc

OVERVIEW OF PARAMETRIC-RESONANCE IONIZATION COOLING

Cooling presents a key challenge for the successful development of both a Higgs factory and muon collider. Because muons are produced as tertiary particles, a beam of a statistically acceptable number of muons will be produced with a large phase space volume. Cooling is required for acceptance into acceleration and storage structures in the machine, and reducing emittance improves luminosity from collisions. Longitudinal cooling is particular important for a Higgs factory. The need for muon cooling is complicated by the short lifetime of the muons, and non-linear effects from the complex magnetic fields of the cooling and transport channels. Ionization cooling techniques offer the best way to accomplish the substantial cooling needed within the limited muon lifetime. Parametric-resonance Ionization Cooling (PIC) is a proposed method for final stage 6D muon cooling that leverages resonance-driven strong focusing with ionization cooling to minimize angular divergence of muons in the beam.

Ionization cooling [1] is achieved by passing a particle through an energy-absorbing material, reducing the particle's momentum in all dimensions while RF fields restore longitudinal momentum. The angular divergence and energy spread are reduced until they reach equilibrium with the stochastic effects of multiple Coulomb scattering and energy straggling. In PIC, a resonance is introduced in a period magnetic channel based on multiples of the betatron oscillation frequency. This allows the channel to reach a new equilibrium [2, 3]. The resonance perturbs the phase-space trajectories of particles at periodic locations along the channel changing their normal elliptical shapes to hyperbolic. At certain periodic focal points, muons in the beam become progressively narrower in position while diverging in angle as they pass down the channel. Without damping, the beam dynamics are not stable and the angular divergence of particles in the beam grows with every period. Placing energy absorbers followed by RF cavities at these focal points allows ionization cooling to limit the growth in angular divergence while maintaining total particle momentum and this stabilizes the beam motion. This resonance also causes a strong reduction of the beam spot size at the absorber locations leading to transverse beam emittance that is about an order of magnitude smaller than without the resonance. The longitudinal emittance is maintained through emittance exchange and shaped wedge absorbers. The absorber locations must be at points of small, but non-zero dispersion. A magnetic channel meeting the requirements for PIC could also be used for Reverse EMittance EXchange (REMEX) [4] by reversing the orientation of the wedge absorbers. This offers the potential of an additional reduction in transverse emittance by about another factor of 10 at the expense of longitudinal emittance.

* Supported in part by U.S. DOE SBIR Grant DE-SC0005589.
# physics_maloney@yahoo.com

One of the key points for the PIC is the correlated optics condition. Under this condition a stable orbit for a finite emittance is maintained with beta functions in both the horizontal (β_x) and vertical (β_y) planes being low-integer multiples of the second of the dispersion functions (λ_{xy}) for the system. The PIC also requires dispersion D such that is small or near-zero at the absorber to minimize energy straggling while allowing for emittance exchange to maintain constant longitudinal emittance. Thus the correlated optics values such that $\beta_x = b\beta_y = a\lambda_{xy}$ where a, b are integers.

Because the PIC dynamics are very sensitive to non-linear aberrations from magnetic hinge fields a toroidal helical harmonics [5, 6, 7] has been proposed. To create dispersion in the channel two helical dipole harmonics having equal field strengths and equal periods but opposite helicities are superimposed onto each other. Under this configuration, a reference orbit maintains a stable orbit within the x-z midplane. A continuous straight quadrupole is superimposed to establish the correlated optics condition. It was demonstrated [6, 7] that a solenoid channel could meet the correlated optics requirements while offering large dynamic aperture and momentum acceptance.

Beryllium wedge absorbers are added at every other periodic focal point in the channel for emittance cooling, followed shortly by RF cavities to restore the reference particle momentum. To induce resonances, two uncoupled pairs of helical quadrupole harmonics with equal low field strength perturb the orbit at the focal points. For each pair of harmonics like the primary helical dipole pair, the field strengths and periods are the same but the harmonics in each pair have opposite helicities. One such pair is used to induce the resonance in the horizontal plane while a second pair induces the resonance in the vertical plane.

LINEAR MODELING IN COSY

Simulations for PIC have been performed with two different simulation codes [6, 7]. One set of simulations was performed using G4Beamline [8] (G4BL) a beam-line toolkit. The other used COSY Infinity [9] (COSY), a differential algebra tool code that allow calculation of transfer and aberration maps for particles in the channel to arbitrary order. Because of its ability to sum up non-linear effects of various orders one of the primary COSY offers particular advantages for optimization and aberration correction. Additions to the six beam physics package used with COSY had to be made to facilitate these simulations. These modifications included:

- Implementation of the magnetic field elements for a helical harmonic pair of arbitrary harmonic order with provisions for superposition of multiples straight alignment multipoles of arbitrary order.
- Implementation of a tuning routine to determine the stable reference orbit for a beam of a particular energy within the channel.
- Implementation of the stochastic processes of multiple scattering and energy straggling in material.
- Implementation of a particle tracking method for single particles and basic particle distributions.

Benchmarking was performed with G4BL to verify consistency of results between the two codes despite differences in the simulation methods [10]. With these modifications, simulation of the linear (first order) model of the channel was performed to verify that the simulation results were consistent with theory. The preliminary simulations were done without stochastic effects. A 251 with momentum of 291 MeV/c was chosen as the reference particle. The period of the helical dipole harmonics was 1 meter and set at 1 meter and the field strengths for the harmonics and the straight quadrupole were tuned to achieve the correlated optics condition. Resonances were induced with the final quadruple harmonic pair (quintuplet) lenses for each plane that satisfied the correlated optics conditions of $\lambda_{xy} = 4\lambda_{xy}$. Simulation shown in Fig. 1 verified that a test particle offset from the reference orbit in initial position and angle follows a sinusoidal trajectory and recloses on the reference

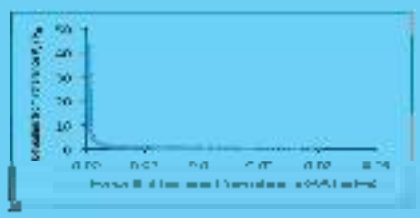

FIGURE 1. The horizontal (x) plane simulated in COSY with parameters: Momentum of 250 MeV/c, 1 mm offset and 50 mrad is tracked every 2 meters through 8 periods of the harmonics.

Next, beryllium wedge absorbers with a central thickness of 2 cm and a 30% thickness gradient were placed at every other focal point. An idealized RF cavity was placed 3 cm after each absorber and tuned to restore momentum for the reference particle to maintain its stable orbit. Simulations for the same test particle, Fig. 3, show the effects of emittance cooling with and without using harmonics to induce the PIC resonance condition. With PIC resonances induced, strong cooling occurs with more reduction in the position

offset and a much greater reduction in beta at first step the same number of wedge absorbers.

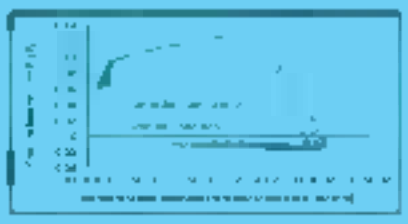

FIGURE 3. The full 6-dimensional simulated cooling of COSY vertical survivor PIC transmission. The primary and 2nd vertical survivor PIC transmission. The primary and 2nd vertical survivor PIC transmission. The primary and 2nd vertical survivor PIC transmission.

The stochastic effects of multiple scattering and energy straggling were added to the simulations by varying the equilibrium emittance and improved reduction in spot size predicted by theory. To implement multiple scattering, COSY calculates the path length each individual particle takes through the wedge absorber. This parameter, as well as the other characteristics for that same particle and the absorber, are used to determine standard deviation for the Gaussian angle straggle PDF for muons RMS95 [...] modeling method [1]. A random number generated from Gaussian distribution is used to determine the exact kick to the particle, and the result is split via polar angle between the horizontal and vertical plane. Particle trajectories are then modified in momentum coordinates in the tracking subroutine. For energy straggling, a similar approach is used with the Bohr approximation [2] for determining standard deviation for the change in energy [12].

$$\theta_{rms} = \frac{z\,(0.0\ldots)}{\beta c p}\sqrt{\frac{L_{\ldots}}{|X_0|}}\left[1 + 0.038\ln\left|\frac{L_{\ldots}}{X_0}\right|\right] \quad (1)$$

$$\Omega_{\ldots} = \left[\ldots\right] - 2\ldots \quad (2)$$

Where X_0 represents the radiation length of the absorber material, $Z_{\ldots}$ is the absorber material's atomic number, N_A is Avogadro's number, and ρ is the density of the absorber. Both processes are repeated for each individual particle every time the particle encounters an absorber in the channel. The results of these calculations for the horizontal plane are shown in Fig. – with and without the stochastic effects being included in the simulation. Even with the inclusion of these two important stochastic effects, cooling as predicted by the theory is observed [3–7].

Simulations were also performed using an uncorrelated distribution of 1000 muons with the following standard deviations from the reference orbit: 1 cm offset in each plane, 1 cm beta offset in each plane, 13 mrad (2) energy spread, 1% and (4) bunch length. The 6D emittance of final distribution was tracked as it traveled through the channel with and without running the PIC resonance correction. Fig. 5 shows the cooling factor, a figure of merit determined by dividing the final 6D emittance of the surviving particles in the beam by their initial emittance.

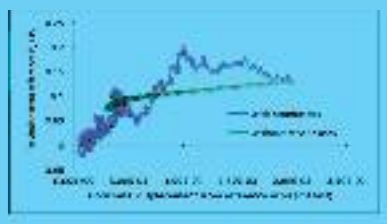

FIGURE 4. The full 6-dimensional simulated cooling of COSY vertical survivor PIC transmission. The primary and 2nd vertical survivor PIC transmission. The primary and 2nd vertical survivor PIC transmission. The primary and 2nd vertical survivor PIC transmission.

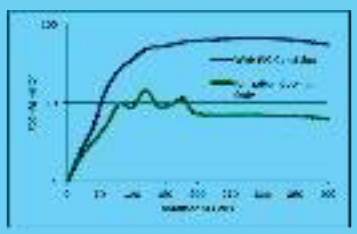

FIGURE 5. Comparison of cooling factor as a function of distance traveled in 6D emittance, with and without PIC resonance.

As predicted by theory, the cooling with the PIC resonance correction reaches an equilibrium state that is significantly better than ionization cooling alone by about a factor of 10.

PROGRESS TOWARDS ABERRATION CORRECTION AND OPTIMIZATION

The baseline simulations described above provide an important tool for optimizing the PIC cooling channel. This linear model simulates the efficiency of the cooling channel where the aberrations have been effectively corrected. Since muon beams can have a very large initial angular and energy spread, aberrations in the system dependent on these parameters can dramatically impact the final spot size of the beam.

To illustrate this, consider the progress toward aberration correction and optimization of the solenoid channel. Through separate simulations a reference helical path in the harmonic period (z_0) of 20 cm was chosen for a reference momentum of 250 MeV/c and the magnetic field strengths of the 3 helical dipole

...structed quadrupole components scaled accordingly [4]. With COSY the largest nonlinear aberrations in the system can be identified order by order, as well as their effects given a specified range in initial particle coordinates. This allows correction of a sensitivity of a system's optics to a range of initial beam parameters. For the helical channel, Table I lists the largest 2nd and 3rd order aberrations affecting final size at the period focal points in the channel. The aberration (x,ax) for example shows how final horizontal position of the particle changes as a function of the square of its initial angle (p_x/p_z)^2 in the horizontal plane. Similarly b_x|x^2 refers to initial angle (p_x/p_z)^2 in the vertical plane.

TABLE I Largest 2nd and 3rd order aberrations affecting spot size for a 250 cm waveguide

Aberration	Magnitude [cm]
x|aa|	1.5
(x|ac)	5.1
x|aaa|	-17.5
(x|abb)	6.1
(x|aab)	1.1
x|bbb|	1.2

Studies are currently ongoing to correct these and other significant higher order aberrations in the Parabolic channel using solenoidal magnetic fields including higher order helical harmonic pairs and straight multipole fields. In all cases the correlated momentum condition must also be maintained, and the reference orbit must be recalculated since these higher order magnetic fields can modify the orbit of the reference particle. Field strength, phase offset, helicity and mode number provide a number of variable parameters for the system.

One such correction scheme minimizing 1st, 2nd and 3rd order aberrations, but contributing to deviations in the final position of the particle at each wedge absorber uses a straight octopole field, two pairs of helical sextupole harmonics and two pairs of helical octupole harmonics. Two pairs of helical quadrupole harmonics are also required to maintain the correlated optics in the channel. Fig. 6 shows a 2nd order simulation in this system after 20 cells.

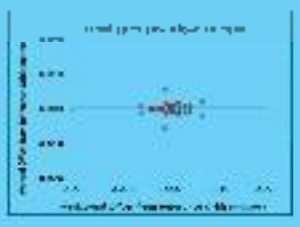

FIGURE 6. Tracking of concentric circles with angular components of up to 150 mrads of 200 MeV/c muons launched on the closed orbit in COSY with nonlinear fields through 3rd order and solenoid fringe effects.

For this system in this section of the channel without corrections, while those shown in red show effects of the correction magnetic fields. Survivability of muons has dramatically increased as well as focusing of the beam. Aberrations beyond 3rd order still need to be corrected.

CONCLUSIONS AND FUTURE WORK

PIC combines muon ionization cooling with parametric-resonance dynamics to allow final emittances in transverse beam emittance that are order of magnitude smaller than those achievable with conventional ionization cooling alone. Linear simulations including space charge effects have verified the predictions of PIC theory. Using the same magnetic channel, RLMLX could allow reduction in transverse emittance by another factor of ten. Thus PIC and RLMLX together promise the potential to increase luminosity by two orders of magnitude.

A four-helix magnetic channel with correlated optics has been developed for PIC. A basic model of a PIC channel with absorbers and RF cavities has been simulated in G4BL and COSY. Results in simulations in COSY have confirmed the model's validity with stochastic effects included. Compensation of beam aberrations in the ring-type helical channel will be returned for a proof-of-principle demonstration of PIC. Progress has been made on the problem and ongoing efforts continue.

REFERENCES

1. D. M. Kaplan et al., Proc. Snowmass 2013 (Minneapolis, MN, 2013) MOM12.
2. Y. S. Derbenev and R. P. Johnson, Phys. Rev. ST Accel. Beams 8, 041002 (2005).
3. Y. S. Derbenev et al., arXiv:1205.3761 [physics.acc-ph].
4. V. S. Morozov et al., Phys. Rev. AB 15, 024001 (2012).
5. V. S. Morozov et al., AIP Conf. Proc. 1299, 651 (2010); Knoxville, TN, 2010, p. 651.
6. V. S. Morozov et al., Proc. of PAC'11, New York, NY, USA, MOP085, p. 779 (2011).
7. J. A. Maloney et al., Proc. of PAC'11, New York, NY, USA, THP211, p. 1128 (2011).
8. G. Penn et al., Phys. Rev. ST Accel. Beams 9, 064002 (2006).
9. K. Makino and M. Berz, Nucl. Instrum. Meth. A 558, 346 (2006).
10. V. S. Morozov et al., in Proc. IPAC'11, San Sebastián, Spain, WEPS026, p. 2484 (2011).
11. H. Bichsel et al., Particle Data Group, Chin. Phys. C 38, 090001 (2014).
12. S. Boscolo et al., Nucl. Instrum. Meth. Phys. Res. A 571, 479 (2007).

SKEW-QUAD PARAMETRIC-RESONANCE IONIZATION COOLING: THEORY AND MODELING*

A. Afanasev#, George Washington University, Washington, DC 20052, USA
Y. Derbenev, V.S. Morozov, A. Sy, Jefferson Lab, Newport News, VA 23606, USA
R.P. Johnson, Muons, Inc., Batavia, IL, USA

Abstract

Muon beam ionization cooling is a key component for the next generation of high-luminosity muon colliders. To reach adequately high luminosity without excessively large muon intensities, it was proposed previously to combine ionization cooling with techniques using a parametric resonance (PIC). Practical implementation of PIC proposal is a subject of this report. We show that an addition of skew quadrupoles to a planar PIC channel gives enough flexibility in the design to avoid unwanted resonances, while meeting the requirements of radially-periodic beam focusing at ionization-cooling plates, large dynamic aperture and an oscillating dispersion needed for aberration corrections. Theoretical arguments are corroborated with models and a detailed numerical analysis, providing step-by-step guidance for the design of Skew-quad PIC (SPIC) beamline.

INTRODUCTION

Experiments at energy-frontier colliders require high luminosities, of order 10^{34} cm^{-2} sec^{-1} or more, in order to obtain reasonable rates for events having point-like cross sections. High luminosities require intense beams, small transverse emittances, and a small beta function at the collision point. For muon colliders, high beam intensities and small emittances are difficult and expensive to achieve because muons are produced diffusely and must be cooled drastically within their short lifetimes. Ionization cooling is a major first step toward providing adequate luminosity without large muon intensities, and its 6D-implementation with a helical cooling channel was described in Ref. [1]. Further reduction of emittances requires anomalously large magnetic fields in ionization-cooling channels, but the use of parametric resonance allows relaxing this requirement, while providing significant beam cooling effects [2].

PIC CONCEPT

In the PIC technique the resonant approach to particle focusing can achieve equilibrium transverse emittances that are at least an order of magnitude smaller than in conventional ionization cooling. The main principle is similar to half-integer parametric resonant extraction from a synchrotron, except for targeting different variables of the phase space [2]. Briefly speaking, parametric resonance provides focusing of the muon beam at periodic locations down the beamline; the beam angular spread is naturally maximized at these locations, therefore unw anted angular smearing (or "heating") due to multiple Coulomb scattering in ionization-cooling plates has the least effect.

While the concept of PIC has been around for a few years, its practical implementation faced several difficulties that were addressed by an Epicyclic PIC proposal [3] and proposed epicyclic twin-helix magnetic structure [4]. The latter uses a superposition of two opposite-helicity equal-period equal-strength helical dipole harmonics and a straight normal quadrupole. Here we propose and develop a technique that will help to avoid (integer) resonances in such a system that requires periodic focusing, making the important step toward its engineering design.

COUPLING RESONANCE IN PIC

Our proposal is based on inducing a linear betatron coupling resonance in PIC transport line between the horizontal (x) and vertical (y) planes. Previously developed (and described in Ref. [4]) twin-helix magnetic system is supplemented with skew quads that generate coupling between horizontal and vertical betatron motion.

Let us consider the effect of such coupling, first in a simplified model. The equations for coupled betatron oscillations are

$$x_b'' + k_x^2 x_b + g y_b = 0$$
$$y_b'' + k_y^2 y_b + g x_b = 0$$

where $k_x^2 = K^2 - n$, $k_y^2 = n$, with K^2 and n denoting the curvature function and quad strength, respectively. Coupling g is provided by 45°-skewed quadrupoles.

In the case of constant coefficients, the above system has an analytic solution described by superposition of two normal-mode oscillations with wave vectors $k_{1,2}^2 = \frac{1}{2}(k_x^2 + k_y^2 \pm \sqrt{(k_x^2 - k_y^2)^2 + 4g^2})$.

$$x_b(s) = C_1 \cos(k_1 s) + C_1' \sin(k_1 s) + G \cdot (C_2 \cos(k_2 s) + C_2' \sin(k_2 s))$$
$$y_b(s) = -G \cdot (C_1 \cos(k_1 s) + C_1' \sin(k_1 s)) + C_2 \cos(k_2 s) + C_2' \sin(k_2 s),$$

where $G = (k_2^2 - k_y^2)/g = -(k_1^2 - k_x^2)/g$, and s is the path length along the reference trajectory. The constants are obtained from initial conditions at s=0:

*Work supported in part by DOE STTR Grants DE-SC0005589 and DE-SC0007634, and and DOE Contract No. DE-AC05-06OR23177
#E-mail: afanas@gwu.edu

$$C_1 = \frac{x_0 - Gy_0}{1+G^2},\ C_1' = \frac{(x_0' - Gy_0')/k_1}{1+G^2}$$
$$C_2 = \frac{Gx_0 + y_0}{1+G^2},\ C_2' = \frac{(Gx_0' + y_0')/k_2}{1+G^2}$$

Note that $k_x^2 + k_y^2 = k_1^2 + k_2^2 = K^2$. Inverse relation between the oscillation wave vectors with and without coupling has a form:

$$k_{x,y}^2 = \left(k_1^2 + k_2^2 \pm \sqrt{(k_1^2 - k_2^2)^2 - 4g^2}\right)/2.$$

This expression is useful for finding parameters K^2 and n for the desired wavelengths of normal modes. It also sets an upper limit for $|g|$ for given values of $k_{1,2}$:

$$(k_1^2 - k_2^2)^2 \geq 4g^2$$

In the limit $g \to 0$, we also have $G \to 0$ and the solution is separated into two plane waves with wave vectors k_x and k_y, respectively. For any nonzero value of g the solution for x and y is a superposition of two plane waves with wave vectors k_1 and k_2. One can identify normal modes, each described by the wave vector k_1 or k_2, by constructing linear combinations: $x_b - Gy_b$ and $y_b + Gx_b$. Introducing a parameter θ defined as G=tan(θ), transformation into normal coordinates (X_b,Y_b) may be represented as rotation by an angle θ:

$$X_b = x_b \cos\theta - y_b \sin\theta = X_b(0)\cos(k_1 s) + X_b'(0)\sin(k_1 s)$$
$$Y_b = x_b \sin\theta + y_b \cos\theta = Y_b(0)\cos(k_2 s) + Y_b'(0)\sin(k_2 s)$$

For each normal mode X_b, Y_b, the oscillation is described by a single wave vector k_1 and k_2, respectively.

The following relation relates the rotation angle θ and the coupling strength:

$$g = -\frac{1}{2}(k_1^2 - k_2^2)\sin(2\theta)$$

If coupling g is piece-wise constant, we can still use the above solutions for x_b and y_b, but with re-defined coefficients $C_{1,2}$ and $C_{1,2}'$ for the corresponding intervals of s.

Example 1: $k_1 = 2\pi, k_2 = \pi$, and g(s) a periodic step-like function with a period $\lambda_g = 2$, as shown in Fig. 1.

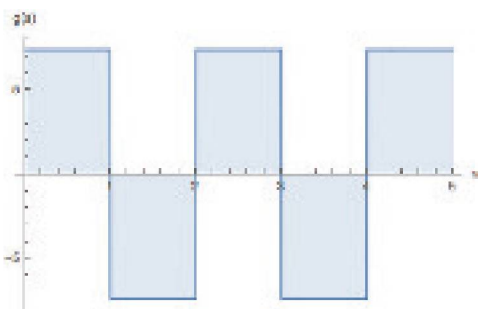

Figure 1: Step-like periodic coupling function g(s).

Prior to constructing a general solution, we obtain an expression for R-matrix that transforms the state vector (x_b,y_b,x_b',y_b') over a period $\lambda_g = 2$: $R(s = 0 \to 2)$.

The matrix is a product of two matrices, each for the corresponding section of constant g:

$$R(s = 0 \to 2) = R(s = 1 \to 2)R(s = 0 \to 1)$$

To find the matrix elements of R-matrix we use the above analytic solution for xb, yb to get:

$$x_b(s=1) = \frac{1-G^2}{1+G^2}x_0 - \frac{2G}{1+G^2}y_0$$
$$y_b(s=1) = -\frac{1-G^2}{1+G^2}y_0 - \frac{2G}{1+G^2}x_0$$
$$x'_b(s=1) = \frac{1-G^2}{1+G^2}x'_0 - \frac{2G}{1+G^2}y'_0$$
$$y'_b(s=1) = -\frac{1-G^2}{1+G^2}y'_0 - \frac{2G}{1+G^2}x'_0$$

Using the previously introduced parameterization G=tan(θ) we find:

$$\frac{1-G^2}{1+G^2} = \cos 2\theta, \qquad \frac{2G}{1+G^2} = \sin 2\theta$$

with R-matrix taking the form:

$$R(s = 0 \to 1) = \begin{pmatrix} M_1 & 0 \\ 0 & N_1 \end{pmatrix},$$
$$M_1 = N_1 = \begin{pmatrix} \cos 2\theta & -\sin 2\theta \\ -\sin 2\theta & -\cos 2\theta \end{pmatrix}$$

We see that for both the coordinates (x_b, y_b) and the derivatives (x_b',y_b') the corresponding transformation corresponds to rotation by angle θ in xy-plane and reflection with respect to xz-plane. Such a transformation is known as an *improper rotation* or *rotary reflection*, with detM_1=detN_1=-1.

The matrix $R(s = 1 \to 2)$ is obtained from $R(s = 0 \to 1)$ by a replacement $\theta \to -\theta$:

$$R(s = 1 \to 2) = \begin{pmatrix} M_2 & 0 \\ 0 & N_2 \end{pmatrix},$$
$$M_2 = N_2 = \begin{pmatrix} \cos 2\theta & \sin 2\theta \\ \sin 2\theta & -\cos 2\theta \end{pmatrix}$$

and the resulting R-matrix per period is obtained from their product:

$$R(s = 0 \to 2) = \begin{pmatrix} M & 0 \\ 0 & N \end{pmatrix},$$
$$M = N = \begin{pmatrix} \cos 4\theta & -\sin 4\theta \\ \sin 4\theta & \cos 4\theta \end{pmatrix}$$

We recognize that R-matrix describes rotation by an angle 4θ for both the coordinates and derivatives per one period of function g. Note that R(s=1→3) is obtained from R(s=0→2) by switching the sign of $\theta \to -\theta$.

The conventional transfer matrix M_T that maps the state vector (x_b, x_b', y_b, y_b') over a period $\lambda_g = 2$ has a form:

$$M_T = \begin{pmatrix} \cos 4\theta & 0 & \sin 4\theta & 0 \\ 0 & \cos 4\theta & 0 & \sin 4\theta \\ -\sin 4\theta & 0 & \cos 4\theta & 0 \\ 0 & -\sin 4\theta & 0 & \cos 4\theta \end{pmatrix}$$

with two non-identical eigenvalues equal $e^{-i4\theta}$ and $e^{i4\theta}$, where one may recognize a betatron tune that equals 4θ. This is the main result we achieved: skewed quads induce coupling that results in radially-periodic beam motion, while the betatron tune is controlled by the coupling strength and allows to avoid integer resonances in such a transport channel.

NUMERICAL ANALYSIS

The results of the above calculations are illustrated in Fig. 2, where the value of g was chosen arbitrarily such that $\theta = 1/4$ radian.

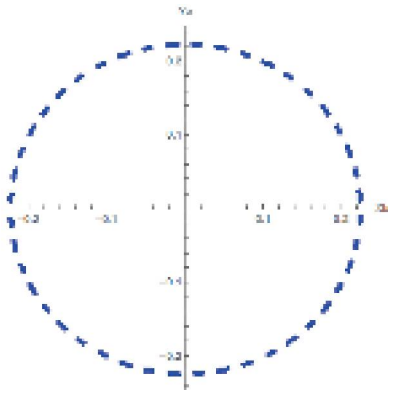

Figure 2: Particle positions calculated at the end of each period of function g (s=0, 2, 4,...) for 300 periods. One dot corresponds to one position. The magnitude of g is such that θ=1/4 rad (value chosen for illustration only). For other choices of initial position s the (x,y) locations follow an ellipse.

For small values of rotation angle 4θ that correspond to weak coupling g we can see from above analysis that after each period particle positions in (x,y) plane undergoes rotation, defining piece-wise constant coefficients of the solution for $x_b(s)$, $y_b(s)$. As a result, the magnitude of the oscillations effectively becomes modulated with factors $\cos(2\theta s)$ and $\sin(2\theta s)$, making an appearance of "beating" coming from a coupling resonance in the oscillator. This is illustrated in Fig. 3.

Formally the effect may be viewed as superposition of two oscillations with close frequencies, but actually it originates from beam rotation induced by the alternating-sign coupling function. Other functional forms for the periodic coupling have been studied and showed similar effects, with the difference that circular beam rotation becomes elliptic. We also obtained required alternating-sign behavior of the dispersion function in both planes.

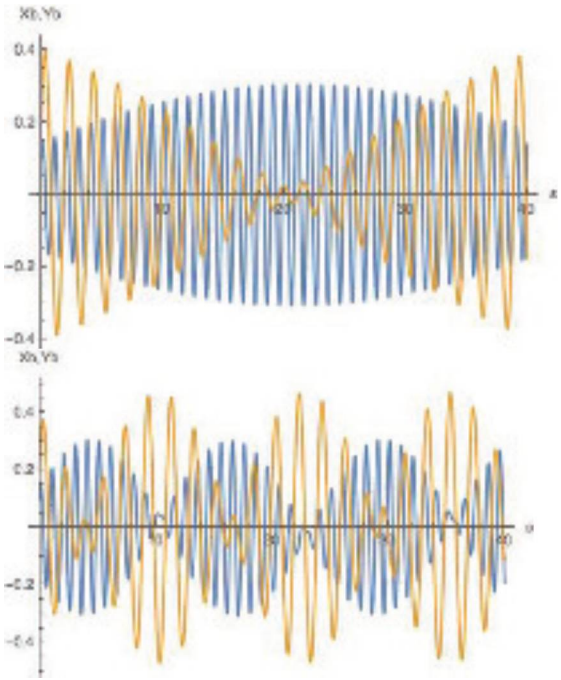

Figure 3: Beating effect in the coupled betatron oscillations. (a) 4θ=0.1rad, (b) 4θ=0.5rad.

SUMMARY

We have demonstrated that inducing a linear betatron coupling resonance in PIC transport line between the horizontal (x) and vertical (y) planes results in a transport line suitable for PIC implementation that allows to avoid integer resonances. Further simulations aimed at engineering design of this system are being performed using MAD-X software, as reported in Ref. [5].

REFERENCES

[1] Y.S. Derbenev and R.P. Johnson, Phys. Rev. ST Accel. Beams **8**, 041002 (2005).

[2] Y.S. Derbenev, V.S. Morozov, A. Afanasev et al., "Parametric-resonance Ionization Cooling of Muon Beams", arXiv:1205.3476 (May 2012).

[3] Y.S. Derbenev and R. P. Johnson, Proc. EPAC2008, Genoa, Italy, pp.2838-2840; A. Afanasev, Y.S. Derbenev and R.P. Johnson, "Aberration-free Muon Transport Line for Extreme Ionization Cooling: a Study of Epicyclic Helical Channel", WEPP147, Proc. EPAC2008, http://jacow.org

[4] V.S. Morozov, A. Afanasev, V.S. Derbenev, and R.P.Johnson, "Epicyclic Twin-Helix Magnetic Structure for Parametric-Resonance Ionization Cooling", MOPEA042, Proc. IPAC2010, Kyoto, Japan.

[5] A. Sy et al., WEPJE015, Proc. IPAC2015, http://jacow.org

MUON TRACKING STUDIES IN A SKEW PARAMETRIC RESONANCE IONIZATION COOLING CHANNEL

A. Sy#, Y. Derbenev, V.S. Morozov, Jefferson Lab, Newport News, VA 23606, U.S.A.
A. Afanasev, George Washington University, Washington, DC 20052, U.S.A.
R. P. Johnson, Muons, Inc., Batavia, IL 60510, U.S.A.

Abstract

Skew Parametric-resonance Ionization Cooling (SPIC) is an extension of the Parametric-resonance Ionization Cooling (PIC) framework that has previously been explored as the final 6D cooling stage of a high-luminosity muon collider. The addition of skew quadrupoles to the PIC magnetic focusing channel induces coupled dynamic behavior of the beam that is radially periodic. The periodicity of the radial motion allows for the avoidance of unwanted resonances in the horizontal and vertical transverse planes, while still providing periodic locations at which ionization cooling components can be implemented. A first practical implementation of the magnetic field components required in the SPIC channel is modeled in MADX. Dynamic features of the coupled correlated optics with and without induced parametric resonance are presented and discussed.

INTRODUCTION

The limit on the minimum achievable emittance in muon ionization cooling comes from the equilibrium between the cooling process and multiple Coulomb scattering in the absorber material. The concept of Parametric-resonance Ionization Cooling (PIC) is to push this limit by an order of magnitude in each transverse dimension by focusing the muon beam very strongly in both planes at thin absorber plates. This creates a large angular spread of the beam at the absorber locations, which is then cooled to its equilibrium value resulting in greatly reduced transverse emittances. Achieving adequately strong focusing using conventional magnetic optics would require unrealistically strong magnetic fields. Instead, PIC relies on a resonant process to provide the necessary focusing. A parametric resonance is induced in a cooling channel, causing focusing of the beam with the period of the channel's free oscillations. To attain simultaneous focusing in both planes at regular locations, the horizontal and vertical betatron oscillation periods must be commensurate with each other and with the channel's period. A magnetic channel possessing such optical properties, called a Twin helix channel, has been successfully developed and simulated [1].

Another important condition necessary for implementation of PIC is compensation of the beam smear from one focal point to another, to a degree where it is small compared to the focused beam size. Since the angular spread at the focal point is on the order of 100 mrad rms while the beam size is a fraction of a mm, this can be quite challenging. To mitigate this problem, the Twin helix channel was designed using continuous helical fields eliminating fringe-field effects. Significant progress has been made on compensation of aberrations using helical multipole fields [1]. However, multipole fields in combination with correlated optics introduce another serious problem, namely, non-linear resonances causing loss of dynamical stability.

To illustrate this problem, consider the Hamiltonian term of a continuous harmonically-varying octupole field $H_{oct} = n_{oct}(6x^2y^2 - x^4 - y^4)/4$ where $n_{oct} \sim \cos(2\pi mz/L)$ is the normalized octupole strength, m is an integer, z is the longitudinal coordinate, L is the channel period length, $x \sim \cos(2\pi\nu_x z/L)$ and $y \sim \cos(2\pi\nu_y z/L)$ are the horizontal and vertical transverse betatron coordinates, respectively, and ν_x and ν_y are the horizontal and vertical betatron tunes, respectively. Multiple octupole harmonics are needed in a cooling channel to compensate spherical aberrations. However, as can be clearly seen from the Hamiltonian, with our choice of betatron tunes of $\nu_x = 0.25$ and $\nu_y = 0.5$, any octupole harmonic m causes resonances in both planes. Dispersion further complicates the resonance structure. Selecting different betatron tunes does not help; as long as the betatron periods are integer multiples of the channel period as required by PIC, multipole fields will tend to cause non-linear resonance. This makes it difficult to find a set of multipoles sufficient for aberration compensation that does not cause beam instabilities.

To overcome this problem, we developed the concept of Skew PIC (SPIC). We introduce coupling in a cooling channel in such a way that the point to point focusing needed for PIC is preserved but the canonical betatron tunes are shifted from their resonant values, i.e. the canonical phase advances in the two planes are shifted from $m\pi$ values. A simple way to think of it is that the beam is azimuthally rotated between consecutive focal points. This moves the dispersion and betatron motion away from non-linear resonances. It also offers a number of other benefits: (a) it allows for control of the dispersion size for chromatic compensation; (b) it reduces the dimensionality of the aberration compensation problem to just the radial dimension and therefore reduces the number of required compensating multipoles; (c) it equates the parametric resonance rates in the two planes, and therefore only one resonance harmonic is needed; (d) it equates the two cooling decrements in the two transverse dimensions. In this paper, we present a design of a SPIC channel and first results of dynamics studies in this channel.

#amysy@jlab.org

SKEW PIC IMPLEMENTATION IN MADX

A cooling channel compatible with SPIC is initially implemented using a lumped elements approach in MADX [2] for ease of simulation and to provide a direct analog to the numerical simulations studied [3]. A step-like alternating curvature function K(s) is implemented using thin dipoles of equal strength but opposite curvature. A straight quadrupole extends over the length of the channel. A step-like alternating coupling function g(s) with relative wavelength $\lambda_g=2\lambda_K$ is implemented using zero-length skew quadrupoles inserted between each thin dipole. Figure 1 demonstrates the phasing and periodicity of the curvature and coupling functions implemented in the SPIC channel. The horizontal and vertical tunes are set to 0.5 and 1.0, respectively, by optimizing the dipole strength and straight quadrupole strength in the absence of coupling. Coupling is then introduced, and the dipole and straight quadrupole strengths are readjusted to reach the SPIC solution. The nonzero coupling shifts the tunes away from their initial integer and half-integer values. The SPIC solution is obtained by constraining particular values in the transfer matrix from one periodic absorber position to the next. Figure 2 shows the reference orbit geometry for one period of a SPIC-compatible channel.

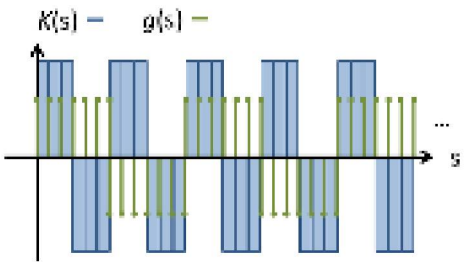

Figure 1: Schematic demonstrating periodicity and phasing of curvature and coupling functions.

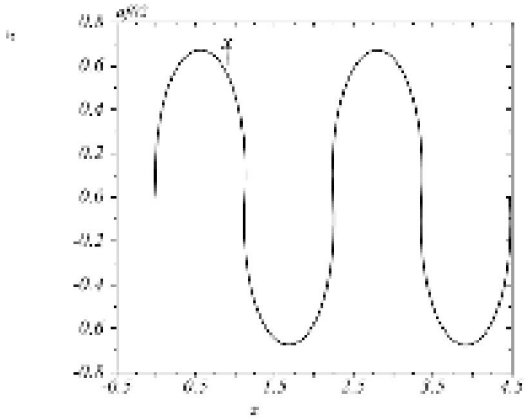

Figure 2: Reference orbit geometry of a SPIC channel.

Single particles are tracked through the SPIC channel to verify the dynamic features of the coupled correlated optics induced in the SPIC channel.

SKEW PIC DYNAMIC FEATURES

Periodic Rotational Behavior

The correlated optics of the previously studied PIC solution naturally defines periodic positions for the absorbers used for ionization cooling due to the periodic nature of the x and y transverse motion. The introduction of coupling in the SPIC channel results in x and y transverse motion that is no longer periodic in each respective plane; the transverse motion instead becomes radially periodic. At these periodic positions, the particle rotates in x-y phase space as shown in Figure 3. Because the SPIC solution enforces little to no coupling between particle coordinates and angles, the angular component also rotates in p_x-p_y phase space, also shown in Figure 3.

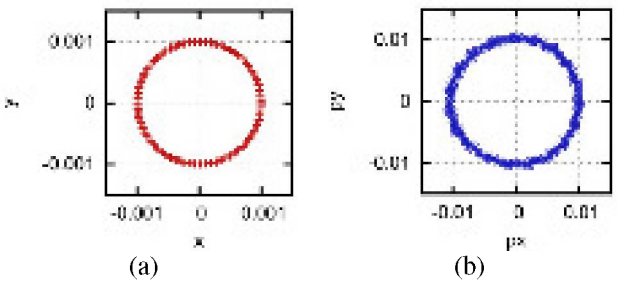

Figure 3: (a) Particle rotation in x-y phase space at periodic points in SPIC channel. (b) Particle rotation in p_x-p_y phase space at same periodic points in SPIC channel. Note that these plots were generated using two separate particles.

Periodic Alternating Dispersion

The introduction of coupling with skew quadrupoles into the PIC channel induces a vertical dispersion component that oscillates with a period equal to the period of the coupling function. The magnitude of the vertical dispersion function is proportional to the coupling strength. SPIC requires small dispersion at the periodic absorber locations to minimize the energy straggle within the absorber, and thus the relative phase shift between the curvature function K(s) and the coupling function g(s) is adjusted to meet these conditions. We note that the vertical dispersion function generally has maxima at the intended absorber positions where the horizontal dispersion function has negative-going zero crossings, and thus the condition of small dispersion at the absorber positions can be met with small coupling strength. Figure 4 illustrates the horizontal and vertical dispersion functions in the SPIC channel.

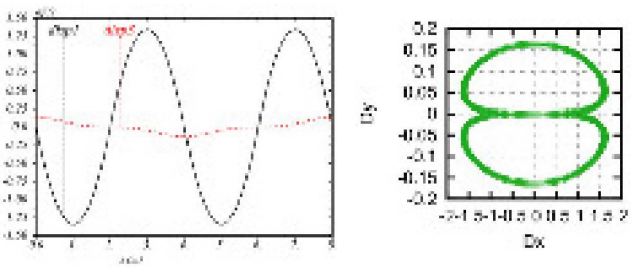

(a) (b)

Figure 4: (a) Horizontal (black) and vertical (red) dispersion functions in one periodic cell of SPIC channel. (b) Horizontal and vertical dispersion components parameterized in s. The vertical dispersion has maxima at zeros of the horizontal dispersion.

INDUCING PARAMETRIC RESONANCE

Parametric resonant behavior was induced in the SPIC channel with quadrupoles of sinusoidally-varying strength. As in [1], the resonance focal point was made to coincide with the periodic absorber position by adjusting the period and phase of the parametric resonance quadrupoles. We note here that while two separate sets of quadrupoles were necessary to induce a half-integer parametric resonance in each of the transverse planes of the PIC channel, only one set is required for the SPIC channel due to the coupling between the planes. These quadrupoles were implemented in the SPIC channel by adding a normal quadrupole component of appropriate strength to each of the existing zero-length skew quadrupoles. Figure 5 demonstrates the phasing and periodicity of the parametric resonance inducing quadrupoles.

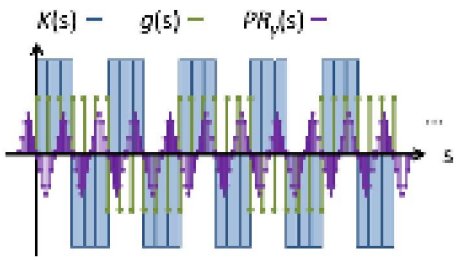

Figure 5: Schematic demonstrating periodicity and phasing of parametric resonance inducing quadrupoles with respect to curvature and coupling functions.

A distinctive feature of the parametric resonance is the periodic transformation of the transverse phase space motion from elliptical orbits to hyperbolic motion. The particle amplitudes are damped over successive periods; the corresponding angular growth eventually leads to instability and loss in the absence of the intended ionization cooling. This hyperbolic transformation is demonstrated in Figure 6.

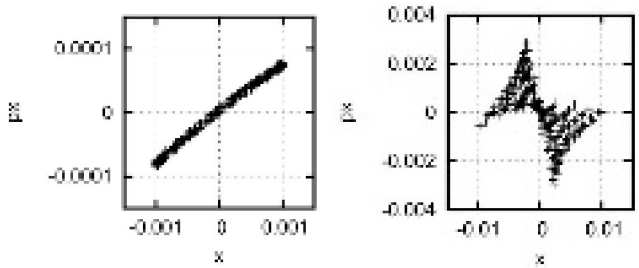

(a) (b)

Figure 6: (a) Elliptical x-p_x phase space at periodic locations in SPIC channel. (b) Hyperbolic x-p_x phase space at same periodic locations in SPIC channel due to parametric resonance.

The amplitude damping/angular growth rate varies with the strength of the induced parametric resonance. A strong parametric resonance is ideal for fast damping and fast ionization cooling, but the motion can become unstable quickly and must be controlled.

SUMMARY

A first pass at implementation of a channel compatible with Skew Parametric-resonance Ionization Cooling (SPIC) has been performed using a lumped elements approach in MADX. The coupled correlated optics of the channel results in particle motion that is radially periodic at positions intended for ionization cooling. Particle tracking simulations have demonstrated this dynamic behavior as well as the expected phase space transformation in the presence of a parametric resonance. These initial results are promising and form the basis for further SPIC simulation studies.

ACKNOWLEDGMENTS

Authored by Jefferson Science Associates, LLC under U.S. DOE Contract No. DE-AC05-06OR23177 and supported by U.S. DOE STTR Grant DE-SC0007634. The U.S. Government retains a non-exclusive, paid-up, irrevocable, world-wide license to publish or reproduce this manuscript for U.S. Government purposes.

REFERENCES

[1] V.S. Morozov, et al., "Parametric-Resonance Ionization Cooling of Muon Beams," AIP Conf. Proc. 1507, 843-848 (2012).
[2] MAD-X. http://madx.web.cern.ch/madx
[3] A. Afanasev, et al., "Skew-Quad Parametric-Resonance Ionization Cooling: Theory and Modeling," IPAC15, TUPHA013 (2015).

PARAMETRIC-RESONANCE IONIZATION COOLING OF MUON BEAMS

Ya.S. Derbenev, V.S. Morozov
Jefferson Lab, Newport News, VA 23606, USA
A. Afanasev
The George Washington University, Washington, DC 20052, USA
K.B. Beard, R.P. Johnson
Muons, Inc., Batavia, IL 60610, USA
B. Erdelyi, J.A. Maloney
Northern Illinois University, DeKalb, IL 60115, USA

Abstract

Cooling of muon beams for the next-generation lepton collider is necessary to achieve its higher luminosity with fewer muons. In this paper we present an idea to combine ionization cooling with parametric resonances that is expected to lead to muon beams with much smaller transverse sizes. We describe a linear magnetic transport channel where a half integer resonance is induced such that the normal elliptical motion of particles in x-x' phase space becomes hyperbolic, with particles moving to smaller x and larger x' at the channel focal points. Thin absorbers placed at the focal points of the channel then cool the angular divergence of the beam by the usual ionization cooling mechanism where each absorber is followed by RF cavities. We present a theory of Parametric-resonance Ionization Cooling (PIC), starting with the basic principles in the context of a simple quadrupole-focused beam line. Then we discuss detuning caused by chromatic, spherical, and non-linear field aberrations and the techniques needed to reduce the detuning. We discuss the requirement that PIC be accompanied by emittance exchange in order to keep the momentum spread sufficiently small. Examples of PIC channel are presented, along with computer simulations aimed at practical implementation of the described theoretical concept.

I. INTRODUCTION

Experiments at energy-frontier colliders require high luminosities, of order 10^{34} cm^{-2} sec^{-1} or more, in order to obtain reasonable rates for events having point-like cross sections. High luminosities require intense beams, small transverse emittances, and a small beta function at the collision point. For muon colliders, high beam intensities and small emittances are difficult and expensive to achieve because muons are produced diffusely and must be cooled drastically within their short lifetimes. Ionization cooling as it is presently envisioned will not cool the beam sizes sufficiently well to provide adequate luminosity without large muon intensities. However, to the extent that the transverse emittances can be reduced further than with conventional ionization cooling, several problems can be alleviated.

Lower transverse emittance allows a reduced muon current for a given luminosity, which implies:
1) a proton driver with reduced demands to produce enough proton power to create the muons;
2) reduced site boundary radiation limits from circulating muons that decay into neutrinos that interact in the earth;
3) reduced detector background from the electrons from the decay of circulating muons;
4) reduced proton target heat deposition and radiation levels;
5) reduced heating of the ionization cooling energy absorber;
6) less beam loading and wake field effects in the accelerating RF cavities.

Smaller transverse emittance has virtues beyond reducing the required beam currents, namely:
1) smaller, higher-frequency RF cavities with higher gradient can be used for acceleration;
2) beam transport is easier, with smaller aperture magnetic and vacuum systems;
3) stronger collider interaction point focusing can be used, since that is limited by beam extension in the IP quadrupoles.

Ionization cooling of a muon beam involves passing a magnetically focused beam through an energy absorber, where the muon transverse and longitudinal momentum components are reduced, and through RF cavities, where only the longitudinal component is regenerated. After some distance, the transverse components shrink to the point where they come into equilibrium with the heating caused by multiple coulomb scattering. The equation describing the rate of cooling is a balance between these cooling (first term) and heating (second term) effects:

$$\frac{d\varepsilon_n}{ds} = -\frac{1}{v^2}\frac{dE_\mu}{ds}\frac{\varepsilon_n}{E_\mu} + \frac{1}{v^3}\frac{\beta(0.014)^2}{2E_\mu m_\mu X_0}.$$

Here ε_n is the normalized emittance, E_μ is the muon energy in GeV, dE_μ/ds and X_0 are the energy loss and radiation length of the absorber medium, $\beta = \lambda/2\pi$ is the transverse beta-function of the magnetic channel, and v is the particle velocity normalized to light velocity.

Setting the heating and cooling terms equal defines the equilibrium emittance, the very smallest possible with the given parameters:

$$\varepsilon_n^{(equ.)} = \frac{\beta(0.014)^2}{2vm_\mu \frac{dE_\mu}{ds} X_0}.$$

One can see that the figure of merit for a cooling absorber material is the product of the energy loss rate times the scattering length. Up to now, liquid hydrogen has been the energy-absorbing medium of choice, with dE/ds= 60 MeV/m and X_0 = 8.7 m. Superconducting solenoidal focusing is used to give a small value of β : 10 cm, corresponding to a 100 MeV/c muon in a 6 T field.

In the PIC technique described below, the resonant approach to particle focusing can achieve equilibrium transverse emittances that are at least an order of magnitude smaller than in conventional ionization cooling. That is, the beam cooling in a conventional ionization cooling channel would require an unrealistically high magnetic field for an equilibrium transverse emittance as small as PIC can achieve. Another advantage to PIC is that a beryllium energy absorber is more effective than hydrogen, since the ratio of the absorber thickness to the betatron wavelength is a measure of its effectiveness. That is, the density of beryllium relative to hydrogen is more important than the product of energy loss rate times Coulomb scattering length in a channel that is required to be as short as possible to reduce losses by muon decay. The practical advantage of beryllium is that the required energy absorber geometry and refrigeration have straightforward engineering solutions.

II. BASIC PIC CONCEPTS

A. Hyperbolic dynamics of PIC

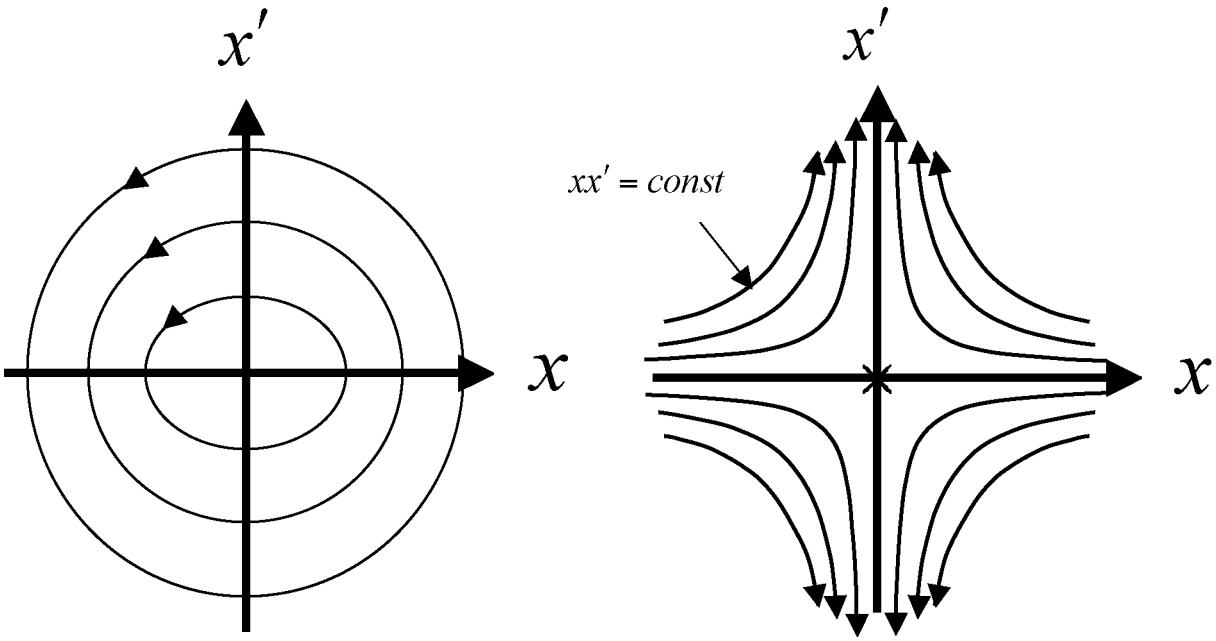

Figure 1: Comparison of particle motion at periodic locations along the beam trajectory in transverse phase space for: LEFT ordinary oscillations and RIGHT hyperbolic motion induced by perturbations at a harmonic of the betatron frequency.

In general, a parametric resonance is induced in an oscillating system by using a perturbing frequency that is the same as or a harmonic of a parameter of the system. Physicists are often first introduced to this phenomenon in the study of a rigid pendulum, where a periodic perturbation of the pivot point can lead to stable motion with the pendulum upside down. Half-integer resonant extraction from a synchrotron is another example familiar to accelerator physicists, where larger and larger radial excursions of particle orbits at successive turns are induced by properly placed quadrupole magnets that perturb the beam at a harmonic of the betatron frequency. In this case, the normal elliptical motion of a particle's horizontal coordinate in phase space at the extraction septum

position becomes hyperbolic, $xx' = const$, leading to a beam emittance which has a wide spread in x and narrow spread in x'.

In PIC, the same principle is used but the perturbation generates hyperbolic motion such that the emittance becomes narrow in x and wide in x' at certain positions as the beam passes down a line or circulates in a ring. Ionization cooling is then used to damp the angular spread of the beam. Figure 1 shows how the motion is altered by the perturbation. The principle of ionization cooling [1] is well known, where a particle loses momentum in all three coordinates as it passes through some energy absorbing material and only the longitudinal component is replaced by RF fields. The angular divergence x' of the particle is thereby reduced until it reaches equilibrium with multiple Coulomb scattering in the material. The concept of ionization cooling is shown in Figure 2.

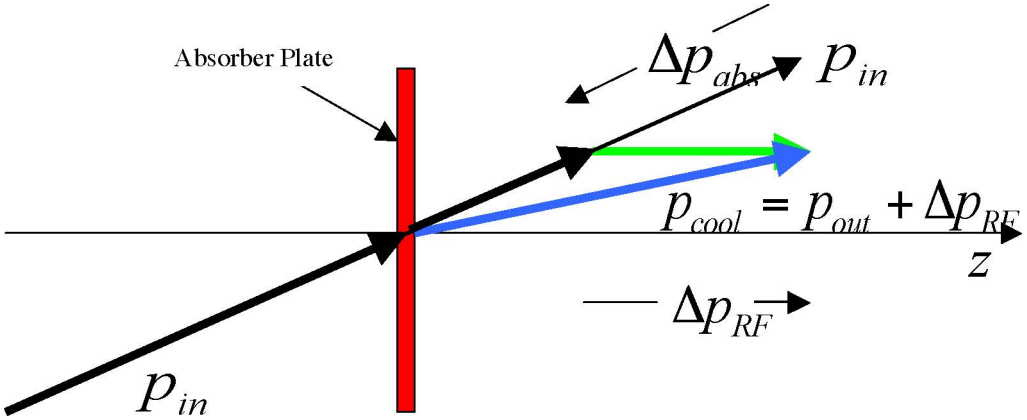

Figure 2: Principle of transverse ionization cooling. A particle loses momentum in all three coordinates as it passes through an energy absorbing plate. Only the longitudinal component is replaced by RF fields, thereby reducing the angular divergence of the particle, $\vartheta = x'$.

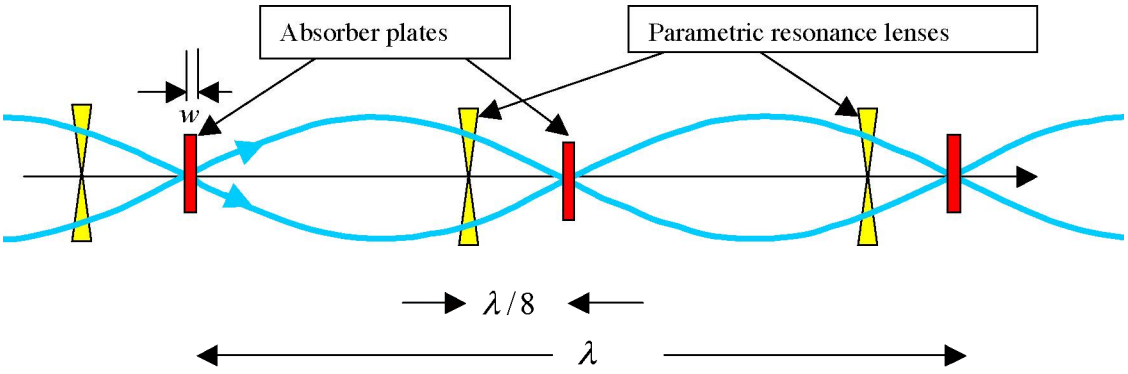

Figure 3: Conceptual diagram of a beam cooling channel in which hyperbolic trajectories are generated in transverse phase space by perturbing the beam at the betatron frequency, a parameter of the beam oscillatory behavior. Neither the focusing magnets that generate the betatron oscillations nor the RF cavities that replace the energy lost in the absorbers are shown in the diagram. The blue trajectories indicate the betatron motion of particles that define the beam envelope.

Thus in PIC the phase space area is reduced in x due to the dynamics of the parametric resonance and x' is reduced or constrained by ionization cooling. For PIC to work, however, the beam must be cooled first by other means. For this analysis the initial conditions for PIC are assumed to be those as might be attained using a helical cooling channel [2] as shown in the table below.

Parameter	Unit	equilibrium rms value
Beam momentum, p	MeV/c	100
Synchrotron emittance, ε_s	μm	300
Relative momentum spread	%	2
Beam width due to $\Delta p / p$	mm	1.5
Bunch length	mm	11
Transverse emittances, $\varepsilon_+ / \varepsilon_-$	mm-mr	100/300
Beam widths, σ_1 / σ_2	mm	4.5/2.8

Table1: Beam parameters at the output of a proposed 6D helical cooling channel [2].

Let there be a periodic focusing lattice of period λ along the beam path with coordinate z. Particle tracking or mapping is based on a single period transformation matrix, M (between two selected points, z_0 and $z_0 + \lambda$), for particle transverse coordinate and angle,

$$\begin{pmatrix} x \\ x' \end{pmatrix}_{z_0+\lambda} = M_x \begin{pmatrix} x \\ x' \end{pmatrix}_{z_0},$$

with a similar expression for the y coordinate.

The matrices M_x and M_y are symplectic or canonical, which means each has determinant equal to one. Otherwise, the matrix elements are arbitrary in general. Thus, each can be represented in a general form convenient for later discussions as follows:

$$M = \begin{pmatrix} e^{-\lambda\Lambda_d}\cos\psi & g\sin\psi \\ -\frac{1}{g}\sin\psi & e^{\lambda\Lambda_d}\cos\psi \end{pmatrix} \quad (1)$$

In particular, the optical period can be designed such that, for $\sin\psi = 0$ (i.e. $\psi = \pi$ or $\psi = 2\pi$), the evolving particle coordinate and angle (or momentum) appear uncoupled:

$$(x)_{z_0+\lambda} = \pm e^{-\lambda\Lambda_d}(x)_{z_0} \text{ and } (x')_{z_0+\lambda} = \pm e^{\lambda\Lambda_d}(x')_{z_0}.$$

Thus, if the particle angle at point z_0 grows ($\Lambda_d > 0$), then the transverse position experiences damping, and vice versa. Liouville's theorem is not violated, but particle trajectories in phase space are hyperbolic ($xx' = const$); this is an example of a parametric resonance. Exactly between the two resonance focal points the opposite situation occurs where the transverse particle position grows from period to period, while the angle damps.

B. Stabilizing absorber effect

If we now introduce an energy absorber plate of thickness w at each of the resonance focal points as shown in Figure 3, ionization cooling damps the angle spread with a rate Λ_c. Here we assume

balanced 6D ionization cooling, where the three partial cooling decrements have been equalized using emittance exchange techniques as described in reference [2]:

$$\Lambda_c = \frac{1}{3}\Lambda, \quad \Lambda = 2\frac{\langle \gamma'_{abs} \rangle}{\gamma} = 2\frac{\gamma'_{acc}}{\gamma}, \quad \langle \gamma'_{abs} \rangle = \gamma'_{abs} 2w/\lambda,$$

where γ'_{abs} and γ'_{acc} are the intrinsic absorber energy loss and the RF acceleration rates, respectively. If $\Lambda_d = \Lambda_c / 2$ then the angle spread and beam size are damped with decrement $\Lambda_c / 2$:

$$\begin{pmatrix} x \\ x' \end{pmatrix}_{z_0+\lambda} = e^{-\lambda\Lambda_c/2} \begin{pmatrix} x \\ x' \end{pmatrix}_{z_0}.$$

C. Reduction of phase diffusion and equilibrium emittance

The rms angular spread is increased by scattering and decreased by cooling,

$$\frac{d}{dz}\overline{(x')^2} = \frac{(Z+1)}{2\gamma v^2}\frac{m_e}{m_\mu}\Lambda - \Lambda_c\overline{(x')^2},$$

which leads to the equilibrium angular spread at the focal point:

$$\overline{(x')^2_{eq}} = \frac{1}{\Lambda_c}\frac{d}{dz}\overline{(x')^2_{z_0}} = \frac{3}{2}\frac{(Z+1)}{\gamma v^2}\frac{m_e}{m_\mu}. \tag{2}$$

The rms product $\left[\overline{(x^2)}\cdot\overline{(x')^2}\right]^{\frac{1}{2}}_{z_0}$ determines the effective 2D beam phase space volume, or emittance.

Taking into account the continuity of x in collisions, the diffusion rate of particle position at the focus is a function of $s = z - z_0$, the local position of the beam within the absorber:

$$\delta(x)_{z_0} = -s\delta x', \quad -\frac{w}{2} \le s \le \frac{w}{2},$$
$$\frac{d}{dz}\overline{(\delta x)^2_{z_0}} = \frac{w^2}{12}\frac{d}{dz}\overline{(\delta x')^2}. \tag{3}$$

Thus, in our cooling channel with resonance optics and correlated absorber plates, the equilibrium beam size at the plates is determined not by the characteristic focal parameter of the optics, $\lambda/2\pi$, but by the thickness of absorber plates, w. Hence, the equilibrium emittance is equal to

$$(\varepsilon_x)_{eq} = \gamma v\left[\overline{(x^2)}\cdot\overline{(x')^2}\right]^{\frac{1}{2}}_{z_0} = \gamma v\frac{w}{2\sqrt{3}}\overline{(x')^2_{z_0}} = \frac{\sqrt{3}}{4v}(Z+1)\frac{m_e}{m_\mu}w.$$

The emittance reduction by PIC is improved compared to a conventional cooling channel by a factor

$$\frac{\pi}{\sqrt{3}}\frac{w}{\lambda} = \frac{\pi}{2\sqrt{3}}\frac{\gamma'_{acc}}{\gamma'_{abs}}.$$

Using the well-known formula for the instantaneous energy loss rate in an absorber, we find an explicit expression for the transverse equilibrium emittance that can be achieved using PIC:

$$\varepsilon_x = \frac{\sqrt{3}}{16}v\left(1+\frac{1}{Z}\right)\frac{(\lambda/2\pi)}{nr_e^2\log}\gamma'_{acc}.$$

Here Z and n are the absorber atomic number and concentration, r_e the classical electron radius, and v is the muon velocity. Here log is a symbol for the Coulomb logarithm of ionization energy loss for fast particles:

$$\log \equiv \ln\left(\frac{2p^2}{I\!v\, m_\mu}\right) - v^2,$$

with m_μ the muon mass and $I\!v$ the effective ionization potential [3]. A typical magnitude of the log is about 12 for our conditions. The equilibrium emittance in the resonance channel is primarily determined by the absorber atomic concentration, and it decreases with beam energy in the non-relativistic region.

III. COMBINING PIC WITH EMITTANCE EXCHANGE

Longitudinal cooling must be used with PIC in order to maintain the energy spread at the level achieved by the basic 6D cooling from the helical cooling channel. Emittance exchange must therefore be used for longitudinal cooling, which requires the introduction of bends and dispersion. Since the beam has already undergone basic 6D cooling, its transverse sizes are so small that the absorber plates can have a large wedge angle to provide balanced 6D cooling even with small dispersion. Since the beam size at the absorber plates decreases as it cools, the wedge angle can increase along the beam path while the dispersion decreases. In this way, longitudinal cooling is maintained while the straggling impact on transverse emittance is negligible. Thus there is no conceptual contradiction to have simultaneous maximum transverse PIC with optimum longitudinal cooling.

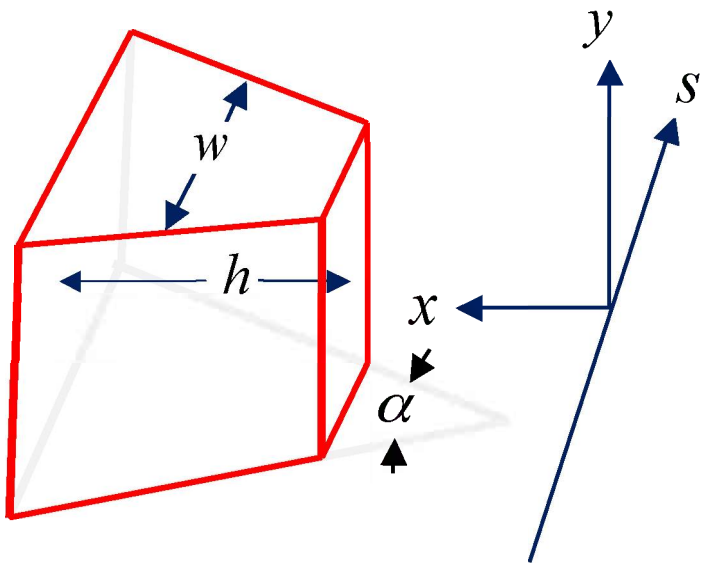

Figure 4: Geometry of a wedge-shaped absorber. The average thickness of the absorber in the beam (s) direction is w. In this diagram, the magnetic field of the dipoles of the channel is along the y axis such that the dispersion is in the x direction, where h is the horizontal size of the absorber in the x direction. The wedge angle α is determined by the requirement that emittance exchange and longitudinal cooling must accompany PIC to keep the energy spread small to control chromatic detuning.

A. Emittance exchange using wedge absorbers

In order to prevent energy spread growth in the beam due to energy straggling in the absorber, one can use wedge absorber plates and introduce dispersion, i.e. make the beam orbit energy-dependent. Such dependence results from a beam bend by a dipole field (alternating along the beam line). As usual, the particle coordinate relative to a reference orbit can be represented as a superposition

$$x = D\frac{\Delta\gamma}{\gamma v^2} + x_b \tag{4}$$

where the dispersion D and x_b do not interfere on the particle trajectory. The absorber wedge orientation (i.e. the gradient of the plate width) must alternate coherently with the D oscillation. Considering only the effects of energy loss in the wedge absorber plates, we find a systematic change of particle energy and position x_b at the plates:

$$\Delta\gamma' = \frac{\partial\gamma'}{\partial\gamma}\Delta\gamma + \frac{\partial\gamma'}{\partial x}x = \frac{\Lambda}{2v^2}\left(\frac{2}{\gamma^2} - \frac{D_a}{h}\Delta\gamma\right)$$

$$(x_{0b}^2)' = -2\left(\Lambda_d - \frac{\Lambda}{2v^2}\frac{D_a}{h}\right)x_{0b}^2.$$

Here we introduced the parameter h as an effective height of the absorber wedge as indicated in figure 4:

$$h^{-1} = \frac{1}{\gamma'}\frac{\partial\gamma'}{\partial x},$$

and D_a, the dispersion at the absorber plates. Thus, if the ratio D_a/h is positive, there is damping of the energy spread while the phase cooling decrement decreases. Let us assume an arrangement that makes the decrements of the three emittances equal to $\Lambda/3$ yet leaves equal the damping decrements of beam size and angle spread at the absorber plates. This assumption leads to the following relationships:

$$D_a = 2h\left(1 - \frac{2}{3}v^2\right) \equiv D_o. \tag{5}$$

IV. PIC FOR AN IDEALLY TUNED BEAM

A. Transverse equilibrium

The dispersion introduced for longitudinal cooling will also cause transverse emittance growth because of straggling, the stochastic change of particle energy due to scattering off of electrons in the absorber [4]. The related change of the particle 'free' coordinate x_b after scattering in a plate can be found simply taking again into account the continuity of the total coordinate x:

$$D_0\frac{\delta\gamma}{\gamma v^2} + \delta x_b = 0.$$

Thus we find the betatron coordinate diffusion rate due to energy straggling:

$$\frac{d}{ds}\overline{(\delta x_b)^2_{str}} = \frac{1}{2}\overline{\frac{D^2}{\gamma^2 v^4}\frac{d}{ds}(\delta\gamma)^2} = \frac{\Lambda}{8}\frac{\gamma^2+1}{\gamma v^2}\frac{m_e}{\log m_\mu}D_a{}^2.$$

Combining this with the angle scattering in equation (3), we obtain the total rate of betatron coordinate diffusion and the associated beam size at the absorber plate and the emittance:

$$\overline{(x_b^2)'} = \frac{\Lambda}{8\gamma\beta^2}\frac{m_e}{m_\mu}\left[\frac{Z+1}{3}w^2 + \frac{\gamma^2+1}{\log}4h^2(1-\frac{2}{3}v^2)^2\right]$$
$$\sigma_b^2 = \frac{1}{8\gamma v^2}\frac{m_e}{m_\mu}[(Z+1)w^2 + 12\frac{\gamma^2+1}{\log}h^2(1-\frac{2}{3}v^2)^2] \quad (6)$$
$$\varepsilon_{eq} = \varepsilon_0 \equiv \gamma v \vartheta_0 \sigma_0$$

The contribution of straggling to transverse emittance growth can be minimized by reducing the wedge absorber horizontal size h. However h must be large compared to σ_b. Let us introduce $\chi_h = \sigma_b / h$, then equation (6) can be written:

$$\sigma_b^2 = \frac{Z+1}{8\gamma v^2}\frac{m_e}{m_\mu}w^2 \frac{1}{1-\frac{3}{2\chi^2 v^2}\frac{m_e}{m_\mu}\frac{\gamma^2+1}{\gamma\log}(1-\frac{2}{3}v^2)^2}$$

The condition for straggling not to be important is

$$1 >> \chi >> (1-\frac{2}{3}v^2)[\frac{3}{2v^2}\frac{\gamma^2+1}{\gamma\log}\frac{m_e}{m_\mu}]^{1/2}$$

B. Optimum cooling and PIC equilibrium

We define optimum cooling by equating the three emittance cooling rates (thus, making each of them equal to $\Lambda/3$) to obtain the following relationships:

$$\frac{D}{h} = 2-\frac{4}{3}v^2; \quad \frac{\Lambda_d}{\Lambda} = \frac{1}{2v^2} - \frac{1}{6} \quad (7)$$

Then the balance equations lead to equilibrium as follows:

$$\theta^2 = \frac{3m_e}{2\gamma v^2 m_\mu}(Z+1+\frac{\gamma^2+1}{4\log}D'^2) \quad (8)$$

$$\sigma^2 = \frac{3m_e}{2\gamma v^2 m_\mu}(\frac{Z+1}{12}w^2 + \frac{\gamma^2+1}{4\log}D^2) \quad (9)$$

$$(\frac{\Delta p}{p})^2 = \frac{3m_e}{8\gamma v^2 m_\mu}\cdot\frac{\gamma^2+1}{\log}.$$

For the conditions that follow from equations (8) and (9),

$$D' << 2\left(\frac{Z+1}{\gamma^2+1}\log\right)^{1/2} \text{ and } h = \frac{w}{(1-\frac{2}{3}v^2)}\left[\frac{(Z+1)\log}{12(\gamma^2+1)}\right]^{1/2},$$

the equilibrium normalized transverse emittance and beam size σ will be close to minimum values:

$$\varepsilon_\perp \Rightarrow \varepsilon_{\perp 0} = \frac{\sqrt{3}}{4v}(Z+1)\frac{m_e}{m_\mu}w, \ \sigma = \frac{\theta w}{2\sqrt{3}} \qquad (10)$$

C. PIC potential

The equilibrium emittance (5) can be expressed as function of the intrinsic energy loss in the absorber, E_i' and the average energy loss or accelerating field using the relationships $(2w/\lambda)E_i' =< E_i' >=< E_{acc}' >$:

$$\varepsilon_{\perp 0} = \frac{\sqrt{3}}{8v}\frac{m_e}{m_\mu}\lambda\frac{< E_i' >}{E_i'}(Z+1).$$

The emittance that can be achieved after an "ordinary" (non-resonance) 6D cooling [1] in hydrogen absorber is $\varepsilon_{ord} = (3\lambda m_e / 2\pi v m_\mu)$; so PIC results in the reduction of transverse emittance by a factor $\frac{\pi}{4\sqrt{3}}\frac{< E_i' >}{E_i'}(Z+1)$. As a function of Z, the factor $E_i'/(Z+1)$ is about $(60/v^2)$ MeV/m in case of beryllium (compare with $(15/v^2)$ MeV/m in case of liquid hydrogen) and does not change significantly with Z for heavier elements. Note that use of absorbers with large atomic number is disadvantageous because of the small thickness of the plates, which makes it difficult to tune to resonance. Note also that the equilibrium emittance can be decreased by decreasing the plate thickness and lowering the accelerating field, which makes the beam line longer. Thus the cooling rate and equilibrium emittance are limited by beam loss due to muon decay. For an optimal PIC design, the plate thickness w should diminish along the cooling channel, starting from a maximum determined by the available accelerating voltage. Table 2 illustrates the PIC effect.

Table 2: Potential PIC effect

Parameter	*Unit*	*Initial*	*Final*
Beam momentum, p	MeV/c	100	100
Distance between plates, $\lambda/2$	cm	19	19
Plate thickness, w	mm	6.4	1.6
Intrinsic energy loss rate (Be)	MeV/m	600	600
Average energy loss	MeV/m	20	5
Angle spread at plates, rms, $\theta_x = \theta_y$,	mr	150	200
Beam transverse size at plates, rms, $\sigma_x = \sigma_y$	mm	2.0	0.1
Transverse rms emittance, norm. $\varepsilon_x = \varepsilon_y$	μm	300	20
Momentum spread , $\Delta p/p$, rms	%	2.7	2.7
Bunch length σ_z, rms	cm	1	1
Longitudinal emittance $\sigma_z \Delta p/mc$	cm	$2.7\text{x}10^{-2}$	$2.7\text{x}10^{-2}$
PIC channel length	m	100	
Integrated energy loss	GeV	0.7	
Beam loss due to muon decay	%	15	
Number of particles/bunch		10^{11}	
Tune spread due to space charge*, $\Delta\lambda/\lambda$	.001	0.75	

*To overcome the space charge impact on tuning, one can implement a beam recombining scheme, namely, generate a low charge/bunch beam and recombine bunches after cooling and acceleration to sufficiently relativistic energy (under investigation).

V. TUNING DEMANDS OF PIC

For PIC to work at all, the relative spread in betatron function must be much smaller than the ratio of the betatron function to the cooling length, $l_c = \gamma mc^2/\langle E' \rangle$:

$$\frac{\Delta\beta}{\beta} << \frac{\beta}{l_c}.$$

The phase advance accumulated along a single cooling decrement length must be smaller than the absorber thickness divided by the beta function in order for PIC to work with full efficiency:

$$\delta\psi = \int_{l_c} \frac{\delta\beta(s)}{\beta^2} ds << \frac{w}{\beta}.,$$

i.e.

$$\frac{\Delta\beta}{\beta} \ll \frac{w}{L_c}$$

The precision required to control elements for compensating tune spread $\frac{\Delta\beta}{\beta}$ is

$$\frac{\nu}{i}\frac{\beta}{\Delta\beta}.$$

Random linear optics errors lead to a requirement for beta function control

$$\frac{\Delta\beta}{\beta} \ll \frac{n}{i_-}\sqrt{\frac{i_-}{\beta}}$$

VI. PIC IN A SNAKE CHANNEL

A. Alternating dispersion and linear optics design

The main constraint of parametric resonance ionization cooling channel design is to combine low dispersion at the wedge absorber plates (for emittance exchange to compensate energy straggling) with large dispersion in the space between plates (where sextupoles can be placed to compensate for chromatic aberration). This constraint can be achieved in a channel created by an alternating dipole field as indicated in figure 5.

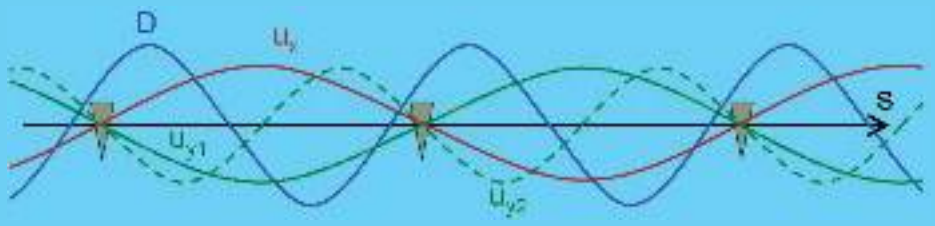

Figure 5: Lattice functions of a beam cooling channel suitable for PIC showing D, the dispersion (blue), the horizontal betatron amplitude u_x (red), and two possible solutions for the vertical betatron amplitude, u_{y1} and u_{y2} (green). The triangles represent the wedge absorbers. The dipoles and quadrupoles are not shown.

In such a channel, the dispersion alternates with the orbit displacement. The absorber plates then are positioned near zero dispersion points. Obviously, the betatron (i.e. focusing) wave length in horizontal plane must not be the same as the bend and dispersion periods, but it should be two times longer. Thus one should design the alternating bend, non-coupled linear optics channel such that the dispersion and wedges maintain the minimum momentum spread ($\sim 2.5\%$) and that the dispersion is small enough at the absorbers to prevent a *straggling impact* on the horizontal emittance, but large in between to compensate for *chromatic detuning*.

The notation for the following discussion follows the normal conventions:

$$x'' + (K^2 - n)x = Kq$$

$$y'' + ny = 0$$

$$x = Dq + \bar{x}$$
$$x' = D'q + \bar{x}'$$

$$D'' + (K^2 - n)D = K$$
$$\bar{x}'' + (K^2 - n)\bar{x} = 0$$

$$\bar{x} = a_x u_x + b_x v_x$$
$$\bar{x}' = a_x u_x' + b_x v_x'$$

$$y = a_y u_y + b_y v_y$$
$$y' = a_y u_y' + b_y v_y'$$

$$u_{x,y}(-s) = u_{x,y}(s)$$
$$v_{x,y}(-s) = -v_{x,y}(s)$$

Three possible cases suitable for PIC are:

$$\lambda_x = \lambda_y \qquad (K^2 - n \approx n)$$

$$\lambda_y = 2\lambda_x \qquad (K^2 - n = 4n)$$

$$\lambda_x = 2\lambda_y \qquad (K^2 - n \approx \frac{n}{4})$$

To avoid resonance between the dispersion and horizontal betatron motion, the dispersion period λ_0 must be half or one quarter of λ_x. The third option seems preferred due to large horizontal aperture.

It is convenient to use a symmetric lattice to simplify the linear optics design and the addition of aberration correction elements. The symmetry relative to the absorbers can be chosen naturally with K and D antisymmetric and K^2 and n symmetric. Note that D is not exactly antisymmetric since some small dispersion is needed at the absorbers in order to create the emittance exchange required for longitudinal cooling.

Since the lattice we need is designed with correlated dispersion and betatron motion, we are sensitive to unwanted strong linear structure parametric resonances that must be avoided.
The desired driving parametric resonance can be arranged in two planes by modulation of B and n, but preferably by specific weak lenses.

B. Parametric resonance in a horizontal plane

Here we derive the equations for a perfectly tune snake channel with no tune spread. Consider motion in two planes:

$$x'' + k^2(1 + \Delta_x)^2 x - 4\zeta k^2 x \sin 2ks = Kq$$

$$y'' + 4k^2(1 + \Delta_y)^2 y + 4\zeta k^2 y \sin 2ks = 0$$

where $(\Delta_y, \Delta_x) \ll 1$ are constant detunes in two planes from exact correlated optics, while $\zeta = const \ll 1$ is frequency modulation parameter due to introduced alternated quadrupole field.

Let us represent the oscillator motion in terms of "slow" variables $a(z), b(z)$ that would be constant at detunes and modulation

$$x = Dq + x_b = Dq + a_x \cos ks + b_x \sin k\, s$$
$$x' = D'q + x'_b = D'q + k(-a_x \sin k\, s + b_x \cos ks)$$

$$y = a_y \cos 2ks + b_y \sin 2ks$$
$$y' = 2k(-a_y \sin 2ks + b_y \cos 2ks)$$

Here, a and kb represent particle coordinate and angle in the x-plane, respectively, at points of the beam orbit where $\sin kz = 0$, while at points where $\cos kz = 0$ the coordinate and angle are correspondently represented by b and ka. Let us rewrite above relationships using the variables a and b as functions of x and x':

$$a_x = (x - Dq)\cos ks - \frac{1}{k}(x' - D'q)\sin ks$$
$$b_x = (x - Dq)\sin ks + \frac{1}{k}(x' - D'q)\cos ks$$

$$a_y = y\cos 2ks - \frac{1}{2k}y'\sin 2ks$$
$$b_y = y\sin 2k\, s + \frac{1}{2k}y'\cos 2ks$$

$$x'' + k^2(1 + \Delta_x)^2 x - 4\zeta k^2 x \sin 2ks = Kq$$

$$y'' + 4k^2(1 + \Delta_y)^2 y + 4\zeta k^2\, y \sin 2ks = 0$$

Then, we can easily find the derivatives a' and b' by taking into account the equation of motion:

$$a'_x = 2k\Delta_x x \sin ks - 4\zeta kx \sin ks \cdot \sin 2ks$$
$$b'_x = -2k\Delta_x x\, \cos ks + 4\zeta kx \cos ks \cdot \sin 2ks$$

$$a'_y = 4k\Delta_y y \sin 2ks + 2k\zeta\, y \sin^2 2ks$$
$$b'_y = -4k\Delta_y y \cos 2ks - k\zeta\, y \sin 4ks$$

Thus, we derived the equations of motion in terms of slow variables a and b. The coefficients of these equations are periodic with period π / k. Assuming that both parameters ζ and ν are small, we can approximate the change of a and b during a single period by simply integrating the equations over one period at a =const, b = const on the right side of the equations. Then we find:

$$a'_x \Longrightarrow \Delta_x k b_x - \zeta k a_x$$
$$b'_x \Longrightarrow -\Delta_x k a_x + \zeta k b_x$$

$$a'_y \Longrightarrow 2\Delta_y k b_y$$
$$b'_y \Longrightarrow -2\Delta_y k a_y$$

At ideal tuning $\Delta_x = 0$

$$a_y' = -\zeta k a_x$$
$$b_x' = \zeta k b_x$$

$$a_y = a_y(0)\exp(-\zeta k s)$$
$$b = b_x(0)\exp(\zeta k s)$$

Let us assume $\zeta > 0$. According to these equations the beam experiences an exponential shrinkage at points where $\sin kz = 0$, where we can put absorbers. The angle spread would grow exponentially if it were not constrained by the ionization cooling due to the absorber. Correspondently, the beam size grows while angle spread damps at points $\cos kz = 0$. Thus, at the exact parametric resonance we observe the hyperbolic dynamics identical to that described in section II above.

At a finite detune,

$$\begin{vmatrix} \kappa + \zeta, & \Delta_x \\ -\Delta_x, & \kappa - \zeta \end{vmatrix} = 0$$

$$\kappa = \pm\sqrt{\zeta^2 - \Delta_x^2}$$

By complementing the lattice with skew quadrupole harmonic $\propto \sin 4ks$, it is possible to have the parametric resonance condition also in the vertical plane, to reach the beam focused simultaneously at the same point in both planes.

C. Two-dimensional parametric resonance by introducing a coupling resonance

Another possibility that could be more convenient would be to introduce a coupling resonance as a way to equalize the cooling rates in each transverse plane and to simplify the parametric resonance design by using skew-quads.

Other important attribute of the coupling resonance is that it also can be effectively used to reduce the number of compensation conditions for detuning due to numerous chromatic, geometrical, and non-linear aberrations in the optics of the PIC channel. This reduction becomes critical while approaching equilibrium at the end of the PIC process.

Coupling resonance in correlated optics channel

It is critically important to design the two betatron periods to be different by a factor of 2 so that the coupling resonance causes beam rotation in space at the absorber, while keeping the horizontal and vertical beam sizes small and maintaining the PIC condition. The skew gradient field should alternate with a frequency equal to the difference of the two betatron frequencies.

$$x'' + k^2 x = Kq + 4gk^2 y \sin ks$$

$$y'' + 4k^2 y = 4gk^2 x \sin ks$$

$$x_b'' + k^2 x_b = -4gk^2 y \sin ks$$

$$y'' + 4k^2 y = -4gk^2 (Dq + x_b) \sin ks$$

$$a'_x = 4gky \sin ks \cdot \sin ks$$

$$b'_x = -4gky \sin ks \cdot \cos ks$$

$$a'_y = 2gk \sin 2ks \cdot (Dq + x_b) \sin ks$$
$$b'_y = -2\, gk \cos 2ks \cdot (Dq + x_b) \sin ks$$

By applying the averaging method to the equations of *x* and *y* motion in terms of slow variables *a* and *b* as above used in the case of the parametric resonance, we obtain the coupled x-y dynamics with equations as follows:

$$a'_x = -gka_y; \qquad a'_y = \tfrac{1}{2} gka_x$$

$$b'_x = -gkb_y; \qquad b'_y = \frac{1}{2} gk\, b_x$$

$$a''_x + \tfrac{1}{2}(gk)^2 a_x; \qquad a''_y + \tfrac{1}{2}(gk)^2 a_y;$$

$$b''_x + \tfrac{1}{2}(gk)^2 b_x; \qquad b''_y + \tfrac{1}{2}(gk)^2 b_y;$$

$$\Omega = gk/\sqrt{2}$$

$$a_x + i\sqrt{2}a_y = Aexp(i\Omega s)$$
$$b_x + i\sqrt{2}b_y = Bexp(i\Omega s)$$

$$a_x = |A| \cos \Phi_a; \quad a_y = \tfrac{1}{\sqrt{2}} |A| \sin \Phi_a;$$
$$b_x = |B| \cos \Phi_b; \quad b_y = \tfrac{1}{\sqrt{2}} |B| \sin \Phi_b;$$
$$\Phi'_a = \Phi'_b = \Omega$$

The equations show that the coupling resonance causes beam rotation at the absorbers (where the beam is focused by the parametric resonance), while it does not change the sum of the Courant-Snyder actions.

$$a_x^2 + 2a_y^2 = |A|^2 = const$$
$$b_x^2 + 2b_y^2 = |B|^2 = const$$

PIC channel with parametric and coupling resonance

$$a'_x = \Delta_x k b_x - \zeta k a_x - gka_y$$
$$a'_y = 2\Delta_y k b_y + \frac{1}{2} gka_x$$

$$b'_x \Longrightarrow -\Delta_x k a_x + \zeta k b_x - gkb_y;$$
$$b'_y \Longrightarrow -2\Delta_y k a_y + \frac{1}{2} gk\, b_x$$

$$A = (a_x + i\sqrt{2}a_y)exp(-i\Omega s)$$
$$B = (b_x + i\sqrt{2}b_y)exp(-i\Omega s)$$

$$A' = (a_x + i\sqrt{2}a_y)'\exp(-i\Omega s) - i\Omega A$$
$$B' = (b_x + i\sqrt{2}b_y)'\exp(-i\Omega s) - i\Omega B$$

$$A' == k(\Delta_x b_y + 2i\sqrt{2}\Delta_y b_y - \zeta a_x)\exp(-i\Omega s)$$
$$B' = k(-\Delta_x a_x - 2i\sqrt{2}\Delta_y a_y + \zeta b_x)\exp(-i\Omega s)$$

If the coupling parameter *g* is large enough compared to the rates of the parametric resonance and ionization cooling, the coupling resonance will effectively equalize the PIC dynamics and cooling rates of the two planes.

$$A' \Longrightarrow -\frac{\zeta}{2}kA + (\frac{1}{2}\Delta_x + \Delta_y)kB$$

$$B' \Longrightarrow \frac{\zeta}{2}kB - (\frac{1}{2}\Delta_x + \Delta_y)kA$$

D. 2d PIC in snake channel with coupling resonance

$$A' = k[\Delta_x b_y + 2i\sqrt{2}\Delta_y b_y - \zeta a_x + (a_x + i\sqrt{2}a_y)_i']\exp(-i\Omega s)$$

$$B' = k[-\Delta_x a_x - 2i\sqrt{2}\Delta_y a_y + \zeta b_x + (b_x + i\sqrt{2}b_y)_i']\exp(-i\Omega s)$$

$$(a_y')_i = -(y'')_i\frac{\sin 2ks}{2k}$$

$$(b_y')_i = (y'')_i\frac{\cos 2ks}{2k}$$

$$(a_x')_i = -(x'')_i\frac{\sin ks}{k} - \frac{(\gamma')_i}{\gamma v^2}(D\cos ks - D'\frac{\sin ks}{k})$$

$$(b_x')_i = (x'')_i\frac{\cos ks}{k} - \frac{(\gamma')_i}{\gamma v^2}(D\sin ks + D'\frac{\cos ks}{k})$$

$$(\gamma')_i = \overline{(\gamma')_i} + (\gamma')_{sc}$$

$$(x'')_i = \frac{\overline{(\gamma')_i}}{\gamma v^2}x' + (x'')_{sc}$$

$$(y'')_i = \frac{\overline{(\gamma')_i}}{\gamma v^2} y' + (y'')_{sc}$$

$$\delta|A|^2 = A^*\delta A + A\delta A^* + |\delta A|^2$$

$$\delta|B|^2 = B^*\delta B + B\delta B^* + |\delta B|^2$$

$$< |A|^2 >' = A^* < A' > + A < A'^* > + < |\delta A|^2 >'$$

$$< |B|^2 >' = B^* < B' > + B < B'^* > + < |\delta B|^2 >'$$

$$D_a' = 0$$

$$A' = [k(\Delta_x b_x + 2i\sqrt{2}\Delta_y b_y - \zeta a_x) + (a_x + i\sqrt{2}a_y)_i'] \exp(-i\Omega s)$$

$$B' = [-k(\Delta_x a_x + 2i\sqrt{2}\Delta_y a_y - \zeta b_x) + (b_x + i\sqrt{2}b_y)_i'] \exp(-i\Omega s)$$

$$< A' > = \left(\frac{\Delta_x}{2} + \Delta_y\right) kB + \frac{1}{2}\left(-k\zeta + \frac{\Lambda_6}{v^2}\frac{D_a}{h}\right) A \equiv \left(\frac{\Delta_x}{2} + \Delta_y\right) kB - \Lambda_A A$$

$$< B' > = -\left(\frac{\Delta_x}{2} + \Delta_y\right) kA + \frac{1}{2}\left(k\zeta - \frac{\Lambda_6}{v^2}\right) B \equiv -\left(\frac{\Delta_x}{2} + \Delta_y\right) kA - \Lambda_B B$$

$$< \Delta\gamma' > = \frac{\Lambda_6}{v^2}\left(\frac{1}{\gamma^2} - \frac{D_a}{2h}\right)\Delta\gamma \equiv -\Lambda_\gamma \Delta\gamma$$

$$\Lambda_6 \equiv -2\frac{< (\gamma')_i >}{\gamma}$$

$$2(\Lambda_A + \Lambda_B) + \Lambda_\gamma = \Lambda_6$$

$$2\Lambda_A = 2\Lambda_B = \Lambda_\gamma = \frac{1}{3}\Lambda_6$$

$$\Lambda_\gamma = \tfrac{1}{3}\Lambda_6 \rightarrow D_a = 2h(1 - \tfrac{2}{3}v^2)$$

$$\zeta = \frac{\Lambda_6}{2kv^2}(3 - \frac{4}{3}v^2)$$

$$< |\delta A|^2 >' = < (\delta a_x)^2 + 2(\delta a_y)^2 >'$$

$$< |\delta B|^2 >' = < (\delta b_x)^2 + 2(\delta b_y)^2 >'$$

$$\delta a_y = -\delta y' \frac{\sin 2ks}{2k}; \quad \delta a_x = -\delta x' \frac{\sin ks}{k} - \frac{\delta p}{p} D_a \cos ks$$

$$\delta b_y = \delta y' \frac{\cos 2ks}{2k}; \quad \delta b_x = \delta x' \frac{\cos ks}{k} - \frac{\delta p}{p} D_a \sin ks$$

$$< |\delta A|^2 >' = < 2(\delta y' \frac{\sin 2ks}{2k})^2 >' + < (\delta x' \frac{\sin ks}{k})^2 >' + < (\frac{\delta p}{p} D_a \cos ks)^2 >'$$

$$< |\delta B|^2 >' = = < 2(\delta y' \frac{\cos 2ks}{2k})^2 >' + (\delta x' \frac{\cos ks}{k})^2 >' < (\frac{\delta p}{p} D_a \sin ks)^2 >'$$

$$< |\delta A|^2 >' = \frac{m_e}{m_\mu \gamma^2 v^2} < |\gamma_i'|| [\frac{Z+1}{k^2} (\frac{1}{2} \sin^2 2ks + \sin^2 ks) + \frac{\gamma^2 + 1}{2log} (D_a \cos ks)^2] >$$

$$< |\delta B|^2 >' = \frac{m_e}{m_\mu \gamma^2 v^2} < |\gamma_i'|| [\frac{Z+1}{k^2} (\frac{1}{2} \cos^2 2ks + \cos^2 ks) + \frac{\gamma^2 + 1}{2log} (D_a \sin ks)^2] >$$

$$< |\delta A|^2 >' \Rightarrow \Lambda_6 \frac{m_e}{4 m_\mu \gamma v^2} (\frac{Z+1}{2} w^2 + \frac{\gamma^2 + 1}{log} D_a^2)$$

$$< |\delta B|^2 >' \Rightarrow \Lambda_6 \frac{3 m_e}{4 m_\mu \gamma v^2} \frac{Z+1}{k^2}$$

$$< |A|^2 >' = -\frac{\Lambda_6}{3} < |A|^2 > + < |\delta A|^2 >'$$

$$< |B|^2 >' = -\frac{\Lambda_6}{3} < |B|^2 > + < |\delta B|^2 >'$$

$$< |A|^2 > \Rightarrow < |A|^2 >_{eq} = \frac{3 m_e}{4 m_\mu \gamma v^2} (\frac{Z+1}{2} w^2 + \frac{\gamma^2 + 1}{log} D_a^2)$$

$$< |B|^2 > \Rightarrow < |B|^2 >_{eq} = \frac{9 m_e}{8 m_\mu \gamma v^2} \frac{Z+1}{k^2}$$

$$< a_x^2 > = 2 < a_y^2 > = \frac{1}{2} < |A|^2 >$$

$$< \theta_x^2 > = k^2 < b_x^2 > = 2k^2 < b_y^2 > = \frac{1}{2} < \theta_y^2 > = \frac{k^2}{2} < |B|^2 >$$

$$\epsilon_x = \sqrt{< a_x^2 >< \theta_x^2 >} = \frac{k}{2} \sqrt{< |A|^2 >< |B|^2 >}$$

$$\epsilon_y = \epsilon_x$$

$$\epsilon_n = \gamma v c \Rightarrow \frac{3\sqrt{3}(Z+1)}{16v}\frac{m_e}{m_\mu} w \sqrt{(1+\frac{2}{log}\frac{\gamma^2+1}{Z+1}\frac{D_a^2}{w^2})}$$

$$< |A|^2 >' = \left(\frac{\Delta_x}{2}+\Delta_y\right) k < (A^*B + AB^*) > -\frac{\Lambda_6}{3} < |A|^2 > + < |\delta A|^2 >'$$

$$< |B|^2 >' = -Ck < (A^*B + AB^*) > -\frac{\Lambda_6}{3} < |B|^2 > + < |\delta B|^2 >'$$

$$< A' > = +\frac{1}{2}\left(-k\zeta + \frac{\Lambda_6}{v^2}\frac{D_a}{h}\right)A \equiv \left(\frac{\Delta_x}{2}+\Delta_y\right)kB - \Lambda_A A$$

$$< B' > = -\left(\frac{\Delta_x}{2}+\Delta_y\right)kA + \frac{1}{2}\left(k\zeta - \frac{\Lambda_6}{v^2}\right)B \equiv -\left(\frac{\Delta_x}{2}+\Delta_y\right)kA - \Lambda_B B$$

$$< (A^*B + AB^*) >' = -2k\left(\frac{\Delta_x}{2}+\Delta_y\right)(< |B|^2 - |A|^2 >) - \frac{\Lambda_6}{3} < (A^*B + AB^*) >$$

$$< (A^*B + AB^*) > = -\frac{6k}{\Lambda_6}\left(\frac{\Delta_x}{2}+\Delta_y\right)(< |B|^2 - |A|^2 >)$$

at

$$k\left(\frac{\Delta_x}{2}+\Delta_y\right) \ll \frac{\Lambda_6}{6},$$

$$< |A|^2 > \approx < |A|^2 >_0 + < |B|^2 > \frac{1}{2}\left[\frac{6k}{\Lambda_6}\left(\frac{\Delta_x}{2}+\Delta_y\right)\right]^2$$

so, it should be:

$$\left(\frac{\Delta_x}{2}+\Delta_y\right) \ll \frac{\Lambda_6}{6} w$$

An example of a particular implementation of the snake channel is presented in Appendix B.

VII. COMPENSATION FOR ABERRATIONS IN SNAKE CHANNEL

The realization of Parametric-resonance Ionization Cooling requires compensation for tunes spreads caused by numerous aberrations: chromatic, spherical, and non-linear field effects. Our analysis of the compensation is based on the expansion of Hamiltonian function for a plane snake type beam transport derived in the Appendix A.

A. Compensation for the chromatic effects

The 3d power Hamiltonian terms

The 3d order terms to be compensated are seen in the expansion of the Hamiltonian presented in

Appendix:

$$H_3 = -\frac{1}{2}(p_x^2 + p_y^2)(q - Kx) - \frac{1}{2}K[(K^2 + n)x^3 - nxy^2]$$
$$- \alpha_3(x^3 + 3xy^2) - K'xyp_y - \frac{1}{3}n_{sext}(x^3 - 3xy^2)$$
$$\alpha_3 \equiv \frac{1}{12}(K'' - 3K^3 - Kn)$$

where the parameter n_{sext} is the field index of the introduced sextupole components.

Chromatic Hamiltonian

The chromatic terms in the initial general form are defined as linear on particle momentum deviation from the reference particle:
$H_3 \Longrightarrow -q\mathfrak{H}_3$;
here

$$\mathfrak{H}_3 = a_x^2 U_x + b_x^2 V_x + a_x b_x W_x + a_y^2 U_y + b_y^2 V_y + a_y b_y W_y$$

$$U_x \equiv \frac{1}{2}(1 - KD)u'^2_x + \left[\frac{3}{2}K(K^2 + n) + 3\alpha_3 + n_{sext}\right]Du_x^2 - KD'u_x u'_x$$

$$V_x \equiv \frac{1}{2}(1 - KD)v'^2_x + \left[\frac{3}{2}K(K^2 + n) + 3\alpha_3 + n_{sext}\right]Dv_x^2 - KD'v_x v'_x$$

$$U_y \equiv \frac{1}{2}(1 - KD)u'^2_y + \left(3\alpha_3 - \frac{1}{2}Kn - n_{sext}\right)Du_y^2 + K'Du_y u'_y$$

$$V_y \equiv \frac{1}{2}(1 - KD)v'^2_y + \left(3\alpha_3 - \frac{1}{2}Kn - n_{sext}\right)Dv_y^2 + K'Dv_y v'_y$$

$$W_x \equiv (1 - KD)u'_x v'_x - KD'(u_x v_x)' + [3K(K^2 + n) + 6\alpha_3 + 2n_{sext}]Du_x v_x$$

$$W_y \equiv (1 - KD)u'_y v'_y + (6\alpha_3 - Kn - 2n_{sext})Du_y v_y + K'D(u_y v_y)'$$

Rate of change of amplitudes a and b is given by the canonical equations:

$$b'_x = \frac{\partial H_3}{\partial a_x} = (2U_x a_x + W_x b_x)q\ ;$$

$$a'_x = -\frac{\partial H_3}{\partial b_x} = -(2V_x b_x + W_x a_x)q\ ;$$

and similar for the y plane.

In our *correlated optics* PIC channel, all the coefficient functions of the Hamiltonian are periodic on the longitudinal coordinate s with period of lattice or twice of it. Therefore, compensation for aberrations due to chromatic and non-linear effects are equivalent to demand that change of

amplitudes a and b over a period should be equal to zero or small enough in order not to disturb significantly the ionization cooling process compared to the case of an ideal linear optics tuned to the parametric resonance. Change for a period can be found by integration of equations for the amplitudes a and b over a single period, using the iteration method. In the first order approximation, the change is given by integration of the right sides over a period at constant amplitudes a and b; so the compensation requirement can be express in terms of averaging over a period:

$$H_3 \Longrightarrow < H_3 >=< q\mathfrak{H}_3 > \Longrightarrow 0.$$

Compensation for chromatic tune spread

Let us first consider the dynamics in absence of absorber and RF field, i.e. $q = const$.

$q = const$

$< H_3 > \Longrightarrow q < \mathfrak{H}_3 >;$

$$< \mathfrak{H}_3 >= a_x^2 < U_x > + b_x^2 < V_x > + a_y^2 < U_y > + b_y^2 < V_y > + a_x b_x < W_x > + a_y b_y < W_y >$$

The compensation for chromaticity problem is simplified for a lattice which is symmetric about the mid-point between absorbers; this conditioning can be naturally arranged. Taking this symmetry into account, we find:

$$U_x(s) = U_x(-s), \qquad V_x(s) = V_x(-s),$$

and similar for U_y and V_y, while:

$$W_x(s) = -W_x(-s), \qquad W_y(s) = -W_y(-s).$$

So we have
$< W_x >= 0, \qquad < W_y >= 0.$

Then, the averaged Hamiltonian function $< H_3 >$ is reduced to the following expression:

$$< \mathfrak{H}_3 >= a_x^2 < U_x > + b_x^2 < V_x > + a_y^2 < U_y > + b_y^2 < V_y >;$$

and the correspondent averaged equations for the amplitudes are as follows:

$b_x' = -2qa_x < U_x >$

$a_x' = 2qb_x < V_x >$

Complete compensation for the linear chromaticity

There are four equations for complete linear compensation of chromatic tunes :

$$< U_x >=< V_x >=< U_y >=< V_y >= 0$$

Sufficient compensation

In practice, it might be enough to satisfy only two requirements

$$< U_x >=< U_y >= 0,$$

thus removing excitation of the v-modes of particle trajectories by the chromatic detunes. In this way, the introduced parametric resonance will provide beam focusing at the absorbers, consequently reducing the scattering effect. Estimates for typical momentum spreads show that, perturbation of the u-modes according to equation for the amplitude a (i.e. increase of angle spread at absorbers) is relatively small.

Design of compensating sextupoles

To satisfy compensation conditions, the compensating sextupole field should be designed for case $\lambda_x = 2\lambda_y = 4\lambda_0$ reflecting the field behavior along the beam path by two harmonics as follows:

$$n_s(s) \propto n_{s1} \sin k_0 s + n_{s2} \sin 2k_0 s \; ; \qquad k_0 = 2\pi/\lambda_0$$

Parasitic parametric resonance and its compensation

With absorbers and RF field in the channel, particle energy in a single period varies with coordinate s. Considering integration of equations for the amplitudes inside a single cell, one can represent variable q as

$$q = \bar{q} + \tilde{q}\,; \quad \tilde{q}(s) = -\tilde{q}(-s); \quad < \tilde{q} >= 0$$

where $\bar{q}$ is constant inside a period, but is experiences a change ("jump") over every period with particle synchrotron phase φ (in linear approximation):

$$\Delta\bar{q} = V_a\varphi\,.$$

The alternate part $\tilde{q}$ is phase dependent together with $\Delta\bar{q}$:

$$\tilde{q}(s,\varphi) = \tilde{q}_0(s) + \tilde{q}_1(s)\varphi.$$

The average Hamilton function now has a "parasitic" parametric resonance addition, due to that $\tilde{q}$ oscillates with a period twice (and four times) shorter compared to the periods of the y and x betatron oscillation, respectively:

$$H_{par} = -< \tilde{q}\mathfrak{H}_1 >= -< \tilde{q}W_x > a_x b_x - < \tilde{q}W_y > a_y b_y.$$

Note that,

$$< \tilde{q}U_x >=< \tilde{q}V_x >=< \tilde{q}U_y >=< \tilde{q}V_y > = 0$$

due to the odd symmetry of $\tilde{q}(s)$.

The change in rates of b and a are given by the canonical equations:

$$b_x' = \frac{\partial H_{pr}}{\partial a_x} = -< qW_x > b_x ;$$

$$a_x' = -\frac{\partial H_{pr}}{\partial b_x} = < qW_x > a_x ;$$

here

$$< qW_x > = < q_0 W_x > + < q_1 W_x > \varphi .$$

Strength of this parasitic resonance is of the order of value of cooling decrement, hence about same strength as of the induced, the driving parametric resonance. The phase independent part of the parasitic resonance can be compensated by a simple correction of the resonance driving force. Effect of the phase dependent part is relatively small due to the two factors. One is that phases φ particles are small. Other is that φ are experiencing the synchrotron oscillations, frequency of which is large compared to the cooling and parametric resonance decrements. After all, phase dependent part can also be compensated by a specific RF arrangement, if needed; however, such sophistication seems not required.

B. Compensation for spherical and other 4th order aberrations

The 4th order Hamiltonian terms

The spherical and some other geometrical terms to be compensated are seen in the fourth power terms of the expansion of the Hamiltonian:

$$H_4 = \frac{1}{8}(p_x^2 + p_y^2)^2 + \frac{1}{2}(K'xy)^2 - \alpha_3 K(x^4 + 3x^2y^2) - \alpha_4(x^4 - y^4)$$
$$- \beta_4 x^2y^2 - \frac{1}{3}Kn_{sext}(x^4 - 3x^2y^2) - \frac{1}{4}n_{oct}(x^4 + y^4 - 6x^2y^2)$$

Here we use the following notation:

$$\alpha_3 \equiv \frac{1}{12}(K'' - 3K^3 - Kn)$$
$$\alpha_4 = \frac{1}{24}(K^2 n - n'' + \delta)$$
$$\beta_4 = -\frac{3}{2}K\alpha_3 + \frac{1}{4}\delta$$
$$\delta = \frac{9}{2}K^4 + K^2 n - 2K'^2 - 3KK'',$$

and n_{oct} is the field index of the introduced octupole components.

Compensation for the 4th order effects

The main compensation conditions that are connected to the 4th power of oscillation mode are antisymmetric about the absorber points of the snake orbit. (Note that the symmetric oscillation components damp!) These conditions are:

$$8 < (K\alpha_3 + \alpha_4 + \frac{1}{3}Kn_{sext} + \frac{1}{4}n_{oct})u_x^4 >=< u_x'^4 >$$

$$8 < (\frac{1}{4}n_{oct} - \alpha_4)u_y^4 >=< u_y'^4 >$$

$$4 < (3K\alpha_3 + \beta_4 - Kn_{sext} - \frac{3}{2}n_{oct})(u_x u_y)^2 >=< (u_x' u_y')^2 >$$

The compensating octupole field design for the case that $\lambda_x = 2\lambda_y = 4\lambda_0$ should include a constant component and the two lowest harmonics of the lattice period:

$$n_{oct} = n_{0oct} + n_{1ont}\cos k_0 s + n_{2oct}\cos 2k_0 s.$$

- Typical magnitudes of the spherical and non-linear detunes
- Coupling resonance and non-linear instabilities in a channel with correlated optics
- Required precision control of the compensating magnets

Compensation for Higher Order Aberrations

Other 4th power terms result from the second order effect of the 3d power Hamiltonian as shown in the Appendix. Finally, there are several higher power terms in the expansion of the Hamiltonian function which may also require compensation. Compensation for all these terms can be greatly simplified by the use of a coupling resonance, as discussed above. The relevant compensation tools (related multipole field components, beam simulations, and experimental diagnostics) are subject of further study. One example involves simulation software COSY INFINITY [9] that is a highly efficient tool for aberration corrections (Appendix C).

VIII. TUNE SPREAD DUE TO MUON SPACE CHARGE IN THE PIC CHANNEL

The tune spread due to the space charge of muon bunch under PIC can be estimated from first principles based on:

$$x'' + k^2 x = f_x \qquad (11)$$

$$k^2 \equiv \frac{1}{\beta^2}$$

with space charge transverse force, f_x. The maximum tune shift is produced for particles near the beam center, while for large amplitude particles (beam tails) the shift tends to zero. Therefore, the absolute tune spread value can be found by calculating the tune shift for the center particles. Here, assuming bunch longitudinal size large compared to the transverse beam size (round beam), the transverse space charge force can be approximated by linear behavior as follows:

$$f_x \Rightarrow f_0 \equiv \frac{2\pi n_0(s) r_\mu}{\gamma^3 v^2} x,$$

where the density factor $n_0(s)$ is controlled by the beam envelope developed in the PIC process. For a Gaussian charge distribution in the bunch, the density factor is found equal to

$$n_0(s) = \frac{N}{(2\pi)^{3/2}\sigma_\perp^2(s)\sigma_s}$$

with $\sigma_\perp(s)$ and $\sigma_s = const$ for beam rms size in transverse and longitudinal direction, respectively. Since the tune spread due to space charge is supposed to be small (as for any source of tune spread), the effect can be calculated by the perturbation method. For this, we transform the description of transverse dynamics to variables a and ψ, according to the representation

$$x = a\sin\psi \tag{12}$$

$$x' = ka\cos\psi \tag{13}$$

For unperturbed motion in a focusing lattice, we have $a = const$ and $\psi = ks + const$. Our aim is to calculate the average change of phase advance per betatron period due to the space charge force. For this, we express the phase ψ as a function of x and x' using equations (12) and (13):

$$tg\psi = \frac{kx}{x'}.$$

By taking the derivative of this equation along "time" s, we find a relationship

$$\frac{\psi'}{\cos^2\psi} = k - \frac{kxx''}{x'^2};$$

By substituting $\cos\psi$ according to equation (11) and x'' according to equation (13) we find:

$$\psi' = k - \frac{fx}{ka^2}.$$

Now, we will integrate this equation along the unperturbed oscillation trajectory $a = const$, $\psi = ks$, for a particle near the beam center:

$$(\delta\psi')_0 = -\frac{f_0 x}{ka^2} = -\frac{2\pi n_0 r_\mu}{\gamma^3 v^2 k}\frac{x^2}{a^2}$$

or

$$(\delta\psi')_0 = -\frac{Nr_\mu\beta}{\gamma^3 v^2\sqrt{2\pi}\sigma_z}\frac{\sin^2\psi}{\sigma_\perp^2(s)}.$$

In the PIC process, particle trajectories tend to focus at absorber points, then there is a full spread in amplitudes $\Delta a = \sigma_0 \Rightarrow \beta\theta^*$ determined by the angle spread at the absorbers

$$\theta^{*2} = \frac{3(Z+1)m_e}{2\gamma v^2 m_\mu} \tag{14}$$

Thus, the beam envelope at the end of the PIC process is described by

$$\sigma_\perp^2(s) \Rightarrow \sigma_0^2\sin^2 ks + \sigma^{*2},\ \sigma_0^2 >> \sigma^{*2}\ .$$

Then,

$$-(\delta\psi')_0 \Rightarrow \frac{Nr_\mu\beta}{\gamma^3 v^2\sigma_z\sqrt{2\pi}}\frac{\sin^2 ks}{\sigma_0^2\sin^2 ks + \sigma^{*2}} < \frac{Nr_\mu\beta}{\sigma_z\sqrt{2\pi}\gamma^3 v^2\sigma_0^2}$$

Note, that the moment of crossing the minimum transverse size (at the absorber) does not bring a dominating contribution to the space charge phase advance. In fact, the instantaneous tune shift is almost constant along the beam envelope. Then we find an accurate estimation for phase advance per period of betatron oscillation and tune shift for center particles, and tune spread:

$$(\delta\psi)_0 = \oint (\delta\psi')\,ds \approx 2\pi\beta(\delta\psi')_0$$

$$\Delta\nu = -\delta\nu_0 \equiv -\frac{(\delta\psi)_0}{2\pi} \approx \frac{Nr_\mu}{\gamma^3 v^2 \sigma_z\sqrt{2\pi}}\frac{\beta^2}{\sigma_0^2} = \frac{Nr_\mu}{\gamma^3 v^2 \theta^{*2}\sigma_z\sqrt{2\pi}}$$

Finally, by taking into account relationship (14), we find:

$$\Delta\nu = \frac{2Nr_e}{3(Z+1)\gamma^2\sigma_z\sqrt{2\pi}}.$$

This formula was used for the numerical estimate of tune spread due to the space charge at PIC equilibrium shown in Table 2.

It should be noted that the tune spread due to space charge is determined in PIC not by the beam transverse phase space (true emittance reduced by PIC), but by the beam characteristic size between absorbers and beam optics along the PIC channel. Remarkably, the tune spread is determined, in fact, simply by the angle spread at the absorbers, which is not function of beam optics at all. Finally, the resulting expression for tune spread depends only on the absorber atomic number Z. The beam transverse phase space (true emittance) after PIC will be transformed by matching optics to a conventionally defined beam emittance.

IX. AN OPTIMIZED PIC DESIGN

In order to approach a practical PIC design, the cooling channel parameters can be modified as the beam is cooled.

First of all and in general, PIC may start with reasonably thick absorbers in order to minimize the beam path while developing the parametric resonance beam envelope.

The maximum initial cooling rate may be limited by the available accelerating RF power. To alleviate this limitation, the initial cooling sections can be effectively isochronous, without RF, where the lattice magnet strengths scale with the decreasing beam momentum. The beam energy could then be restored by RF cavities installed between cooling sections.

Also note that at the beginning and during the middle PIC stages, high precision compensation for aberrations is not required since the beam is not so well focused. Thus the design of the PIC channel for the initial stages can be relatively easy compared to the final stage.

X. CONCLUSIONS

In this paper we have introduced the basic theory of ionization cooling using parametric resonances and discussed the requirements that must be satisfied to achieve significant beam cooling using this technique. We have derived the effects of chromatic, spherical, and non-linear field aberrations and described how these aberrations can be compensated. That PIC must be accompanied by emittance exchange and that these two techniques are compatible has been demonstrated. We have suggested a particular transport scheme using alternating bends to achieve the two requirements of small dispersion at absorbers and large dispersion where aberrations can be compensated. In addition, the use of a conservative coupling resonance is proposed with the

purpose of providing equal parametric resonance and cooling rates in the two planes of the beam transport line, and of simplifying the aberration compensation design and control.

We are developing RF schemes to provide regeneration of the energy lost in the absorbers and to use synchrotron motion as an additional correction to chromatic effects [5], to include wedge engineering limitations, and to use realistic aberration correction magnets to provide guidance for simulations.

APPENDIX A: HAMILTONIAN FRAMEWORK FOR PLANE BEAM BEND

Hamilton's method in dynamics provides a convenient and effective analytical technique of formulating, reducing and solving the equation of particle motion in an external field. A particular feature of this method is that it allows one to immediately recognize and utilize the dynamical invariants and canonical relationships between the invariants and some important characteristics of particle motion, such as orbital tunes, dispersions and others. The method is based on introduction of the Hamilton function of particle coordinates and canonical momenta in a chosen coordinate frame.

In classical dynamic theory, a conventional way of Hamilton's formulation is based on transformation from Lagrange-Euler equations to Hamilton's equations, either explicitly or through Hamilton-Jacobi method. Meanwhile, there exists a possibility to obtain the classical Hamilton function and canonical equations, starting with the Schrödinger or Klein-Gordon equation of quantum mechanics. In this way, the Hamilton formulation appears immediately as an initial or fundamental in classical mechanics (viewed as an asymptotic limit of the quantum description); the Lagrange-Euler formulation then is not inquired.

An ordinary Hamilton form is the energy function

$$H_t(\vec{P},\vec{r}) = \sqrt{p^2+m^2} + A_t = \sqrt{(\vec{P}-\vec{A})^2+m^2} + A_t,$$

with equations of motion

$$\frac{d}{dt}\vec{P} = -\frac{\partial}{\partial \vec{r}} H_t; \qquad \frac{d\vec{r}}{dt} = \frac{\partial}{\partial \vec{P}} H_t$$

A. Hamilton function in s-representation of the reference orbit

In the case of a particle beam transported along a curved but plane reference orbit, it is convenient to consider beam path coordinate s as a time argument, while the time can be treated as one of three independent coordinates x, y, t. As usual, we introduce *Frenet frame* with variables x, y, s, t :

$$\vec{r} = \vec{r}_0(s) + x\vec{e}_x + y\vec{e}_y; \quad \vec{r}_0' = \vec{e}_s; \quad \vec{e}_x' = K\vec{e}_s; \quad \vec{e}_s' = -K\vec{e}_x$$

$$Kp_0 = B_0$$

The Hamiltonian function and equations of motion in this representation can be quickly derived using the covariant equation for the wave function $\Psi(\vec{r},t)$, or the relativistic Schrödinger equation

$$[(\hat{P}_t - A_t)^2 - (\vec{P}-\vec{A})^2 - m^2]\Psi(\vec{r},t) = 0$$

where $\hat{H}_t \equiv i\hbar\frac{\partial}{\partial t}$ and $\hat{\vec{P}} \equiv -i\hbar\frac{\partial}{\partial \vec{r}} \equiv \vec{\nabla}$

are the time and space components of four-vector momentum as a quantum operator. In Frenet frame differential operator $\vec{\partial}$ is written as

$$\vec{\nabla} = \vec{e}_x\frac{\partial}{\partial x} + \frac{\vec{e}_s}{1+Kx}\frac{\partial}{\partial s} + \vec{e}_y\frac{\partial}{\partial y}$$

In the quasi-classical limit, the Schrödinger equation can be rewritten, optionally, in two equivalent forms:

A)

$$i\hbar\frac{\partial}{\partial t}\Psi = [\sqrt{(\hat{\vec{P}} - \vec{A})^2 + m^2} + A_t]\Psi \equiv \hat{H}_t\Psi,$$

with corresponding classical equations of motion

$$\frac{d\hat{\vec{P}}}{dt} = -\frac{1}{i\hbar}[\hat{H}_t, \hat{\vec{P}}] \to \frac{d\vec{P}}{dt} = \{H_t, \vec{P}\} = -\frac{\partial}{\partial \vec{r}}H_t$$

$$\frac{d\vec{r}}{dt} = -\frac{1}{i\hbar}[\hat{H}_t, \vec{r}] \to \frac{d\vec{r}}{dt} = \{H_t, \vec{r}\} = \frac{\partial}{\partial \vec{P}}H_t$$

where H_t is the conventional form of the Hamilton function (*t-representation*):

$$H_t \equiv \sqrt{(\hat{\vec{P}} - \vec{A})^2 + m^2} + A_t;$$

B)

$$i\hbar\frac{\partial}{\partial s}\Psi = -(1+Kx)[\sqrt{(\hat{H}_t - A_t)^2 - (\hat{\vec{P}}_\perp - \vec{A}_\perp)^2 - m^2} + A_s]\Psi \Rightarrow H_s\Psi,$$

with equations of motion (in a classical limit)

$$P_x' = -\frac{\partial}{\partial x}H_s; \quad x' = \frac{\partial}{\partial P_x}H_s; \quad P_y' = -\frac{\partial}{\partial y}H_s; \quad y' = \frac{\partial}{\partial P_y}H_s$$

$$H_t' = \frac{\partial}{\partial t}H_s; \qquad t' = \frac{\partial}{\partial s}H_s$$

where H_s is the Hamilton function in *s-representation*:

$$H_s \equiv -(1+Kx)[\sqrt{(H_t - A_t)^2 - (\vec{P}_\perp - \vec{A}_\perp)^2 - m^2} + A_s]$$
$$= -(1+Kx)(\sqrt{p^2 - p_\perp^2} + A_s)$$

Thus, in s-representation the Hamiltonian coincides with the canonical momentum (with a reversed sign)

$$P_s = (1+Kx)(p_s + A_s)$$

taken as a function of energy and transverse momentum according to the covariant equation $E^2 - p^2 = m^2$:

$$H_s = -(1+Kx)(p_s + A_s) = -(1+Kx)(\sqrt{p^2 - p_\perp^2} + A_s);$$

$$\vec{p}_\perp = \vec{P}_\perp - \vec{A}_\perp; \qquad p_x = P_x - A_x; \quad p_y = P_y - A_y$$

$$H_t = E + A_t \qquad p^2 = E^2 - m^2$$

$$H_s = -(1+Kx)[\sqrt{(H_t - A_t)^2 - m^2 - (P_x - A_x)^2 - (P_y - A_y)^2} + A_s]$$

B. Equations for vector potential of the magnetic field

We use the standard definition of vector potential of static magnetic field in vacuum:

$$\vec{B} = \vec{\nabla} \times \vec{A}$$

$$\vec{A} = A_s\vec{e}_s + A_x\vec{e}_x + A_y\vec{e}_y$$

$$\vec{\nabla}\vec{A} = 0, \vec{\nabla}^2\vec{A} = 0$$

In Frenet frame we have the following equations:

$$\vec{\nabla}^2\vec{A} = [\frac{1}{1+Kx}\frac{\partial}{\partial x}(1+Kx)\frac{\partial}{\partial x} + \frac{\partial^2}{\partial y^2} + \frac{1}{1+Kx}\frac{\partial}{\partial s}\frac{1}{1+Kx}\frac{\partial}{\partial s}]\vec{A} = 0$$

$$\frac{\partial A_s}{\partial s} + \frac{\partial}{\partial x}(1+Kx)A_x + (1+Kx)\frac{\partial}{\partial y}A_y = 0$$

Let us introduce the transverse part of the Laplace operator as

$$\Delta_\perp \equiv \frac{\partial^2}{\partial y^2} + \frac{1}{1+Kx}\frac{\partial}{\partial x}(1+Kx)\frac{\partial}{\partial x};$$

Then we rewrite equations for vector components as follows:

$$\Delta_\perp A_s + \frac{1}{(1+Kx)^2}[(1+Kx)\frac{\partial}{\partial s}\frac{1}{1+Kx}(\frac{\partial A_s}{\partial s} + KA_x) + K(\frac{\partial A_x}{\partial s} - KA_s)] = 0$$

$$\Delta_\perp A_x + \frac{1}{(1+Kx)^2}[(1+Kx)\frac{\partial}{\partial s}\frac{1}{1+Kx}(\frac{\partial A_x}{\partial s} - KA_s) - K(\frac{\partial A_s}{\partial s} + KA_x)] = 0$$

$$\Delta_\perp A_y + \frac{1}{1+Kx}\frac{\partial}{\partial s}\frac{1}{1+Kx}\frac{\partial}{\partial s}A_y = 0$$

C. Expansion of the s-Hamiltonian

Below we will expand the vector potential and s-Hamiltonian in powers of deviations of particle momentum and transverse coordinates relatively the reference trajectory, in terms of the Frenet frame, including all terms up to the 4th power.

Expansion of s-Hamiltonian on momentum vector

$$H_s \approx -(1+Kx)\{p_0 + \Delta p - \frac{p_\perp^2}{2p_0}[1 - \frac{\Delta p}{p_0} + (\frac{\Delta p}{p_0})^2] - \frac{p_\perp^4}{8p_0^3} + A_s\}$$

$$\vec{p}_\perp = \vec{P}_\perp - \vec{A}_\perp$$

Expansion of the vector potential of magnetic field

$$A_s \approx A_{s1} + A_{s2} + A_{s3} + A_{s4};$$

$$\vec{A}_\perp \approx \vec{A}_{\perp 1} + \vec{A}_{\perp 2} + \vec{A}_{\perp 3}$$

The first and second order terms of vector potential

Longitudinal component:

$$A_{s1} = -B_0(s)x$$

$$A_{s2} = -\frac{1}{2}(\alpha x^2 + ny^2);$$

$$\Delta_\perp (A_{s1} + A_{s2})_0 \Rightarrow 0 \rightarrow \alpha = -n - K^2$$

$$A_{s2} = \frac{1}{2}[(K^2 + n)x^2 - ny^2]$$

Transverse components:

$$\vec{A}_{\perp 1} = 0$$

$$A_{x2} = 0; \qquad A_{y2} = \gamma_{y2} xy$$

$$\gamma_{y2} x - K'x = 0 \rightarrow \gamma_{y2} = K' \rightarrow A_{y2} = K'xy$$

The third order terms of vector potential

Longitudinal component:

$$\Delta_{\perp}(A_{s1}+A_{s2}+A_{s3}) = -\frac{\partial^2 A_{s1}}{\partial s^2} + K^2 A_{s1} = (K'' - K^3)x$$

$$(\frac{\partial^2}{\partial x^2} + \frac{\partial^2}{\partial y^2})A_{s3} + K\frac{\partial}{\partial x}A_{s2} - K^2 A_{s1} = (K'' - K^3)x$$

$$A_{s3} = \alpha_{s3}(x^3 - 3xy^2) + \hat{\alpha}_{s3}(x^3 + 3xy^2)$$

$$\hat{\alpha}_{s3} = \frac{1}{12}(K'' - 3K^3 - Kn)$$

Transverse components of the third order:

$$(\frac{\partial^2}{\partial x^2} + \frac{\partial^2}{\partial y^2})A_{x3} = \frac{\partial}{\partial s}KA_{s1} + K\frac{\partial}{\partial s}A_{s1}$$

$$\frac{\partial}{\partial x}A_{x3} + \frac{\partial}{\partial y}A_{y3} + Kx\frac{\partial}{\partial y}A_{y2} + \frac{\partial}{\partial s}A_{s2} = 0$$

$$(\frac{\partial^2}{\partial x^2} + \frac{\partial^2}{\partial y^2})A_{y3} + K\frac{\partial}{\partial x}A_{y2} = 0$$

$$A_{x3} = \alpha_{x3}(x^3 - 3xy^2) + \hat{\alpha}_{x3}(x^3 + 3xy^2)$$

$$A_{y3} = \hat{\beta}_{y3}(y^3 + 3x^2 y)$$

$$\alpha_{x3} = -\frac{1}{3}(KK' + \frac{1}{2}n')$$

$$A_{x3} = -\frac{1}{6}(2KK' + n')(x^3 - 3xy^2) - \frac{1}{4}KK'(x^3 + 3xy^2)$$

$$A_{y3} = K'xy - \frac{1}{12}KK'(y^3 + 3x^2 y)$$

The fourth order terms of vector potential (longitudinal component only)

$$(\frac{\partial^2}{\partial x^2} + \frac{\partial^2}{\partial y^2})A_{s4} = -K\frac{\partial A_{s3}}{\partial x} + K^2 x\frac{\partial A_{s2}}{\partial x} - K^3 x^2\frac{\partial A_{s1}}{\partial x} - (\frac{\partial^2}{\partial s^2} - K^2)A_{s2} +$$

$$2Kx(\frac{\partial^2}{\partial s^2} - K^2)A_{s1} + K'x\frac{\partial A_{s1}}{\partial s}$$

$$A_{s4} = \alpha_{s4}(x^4 + y^4 - 6x^2 y^2) + \beta_{s4}(x^4 - y^4) + \gamma_{s4}x^2 y^2$$

$$\gamma_{s4} = -\frac{3}{2}K\hat{\alpha}_{s3} + \frac{1}{4}a$$

$$\beta_{s4} = -\frac{1}{4}K\alpha_{s3} + \frac{1}{24}(K^2 n - n'') + \frac{1}{24}a$$
$$a \equiv \frac{9}{2}K^4 + K^2 n - 2K'^2 - 3KK''$$

Expansion of the s-Hamiltonian on vector potential

$$H_1 = -(Kp_0 - B_0)x - \Delta p \Rightarrow -\Delta p;$$

$$H_2 = -Kx\Delta p + \frac{P_\perp^2}{2p_0} - KxA_{s1} - A_{s2}$$

$$H_3 = \frac{P_\perp^2}{2p_0}(Kx - \frac{\Delta p}{p_0}) - KxA_{s2} - A_{s3} - \frac{\vec{P}_\perp \vec{A}_{\perp 2}}{p_0}$$

$$H_4 = -Kx(\frac{\vec{P}_\perp \vec{A}_{\perp 2}}{p_0} + \frac{P_\perp^2}{2p_0^2}\Delta p + A_{s3}) + \frac{\vec{A}_{\perp 2}^2}{2p_0} + \frac{P_\perp^4}{8p_0^3} - \frac{\vec{P}_\perp \vec{A}_{\perp 3}}{p_0} + \frac{P_\perp^2 (\Delta p)^2}{2p_0^3} - A_{s4}$$

D. Second order Hamilton function for the linear optic design

$$H_2 = -Kx\Delta p + \frac{P_x^2 + P_y^2}{2} + \frac{1}{2}[(K^2 - n)x^2 + ny^2]$$

Linear equations:

$$x'' + (K^2 - n)x = K\Delta p; \qquad y'' + ny = 0$$
$$x = D\frac{\Delta p}{p} + x_b; \qquad D'' + (K^2 - n)D = K$$
$$K(s) = K(s + \lambda_0); \qquad n(s) = n(s + \lambda_0)$$

E. The third power Hamiltonian terms

Combining all the 3d power terms of the above expansions of the Hamiltonian and vector potential, we obtain the 3d power Hamiltonian part as follows:

$$H_3 = -\frac{1}{2}(p_x^2 + p_y^2)(q - Kx) - \frac{1}{2}K[(K^2 + n)x^3 - nxy^2]$$
$$-\alpha_3(x^3 + 3xy^2) - K'xyp_y - \frac{1}{3}n_{sext}(x^3 - 3xy^2) \quad ,$$
$$\alpha_3 \equiv \frac{1}{12}(K'' - 3K^3 - Kn)$$

where the parameter n_{sext} is the field index of the introduced sextupole components.

F. The fourth power terms

Combining all the 4th power terms of the above expansions of the Hamiltonian and vector potential, we obtain the 4th power Hamiltonian part as follows:

$$H_4 = \frac{1}{8}(p_x^2 + p_y^2)^2 + \frac{1}{2}(K'xy)^2 - \alpha_3 K(x^4 + 3x^2y^2) - \alpha_4(x^4 - y^4)$$
$$- \beta_4 x^2y^2 - \frac{1}{3}Kn_{sext}(x^4 - 3x^2y^2) - \frac{1}{4}n_{oct}(x^4 + y^4 - 6x^2y^2)$$

Here we use the following notation:

$$\alpha_4 = \frac{1}{24}(K^2 n - n'' + \delta)$$
$$\beta_4 = -\frac{3}{2}K\alpha_3 + \frac{1}{4}\delta$$
$$\delta = \frac{9}{2}K^4 + K^2 n - 2K'^2 - 3KK'',$$

and n_{oct} is the field index of the introduced octupole components.

More terms of the 4th power on transverse variables arrive as secondary effects from the 3d order Hamiltonian. They are generally formulated as resulting from a Poisson bracket as follows:

$$H_4^{(3)} = \frac{1}{2}\{H_3, \hat{H}_3\}$$

where

$$\hat{H}_3 \equiv \int H_3(s)ds,$$

with the Hamiltonian term H_3 considered as a function of time s with constant particle trajectory parameters a and b.

APPENDIX B: TWIN-HELIX IMPLEMENTATION OF THE SNAKE CHANNEL

A. Correlated Optics Condition

To ensure the beam's simultaneous focusing in both horizontal and vertical planes, the horizontal oscillation period λ_x must be equal to or be a low-integer multiple of the vertical oscillation period λ_y. The PIC scheme also requires alternating dispersion D such that D is

- small at the beam focal points to minimize energy straggling in the absorber,
- non-zero at the absorber for emittance exchange to maintain constant longitudinal emittance,
- relatively large between the focal points to allow for aberration correction to keep the beam size small at the absorbers.

Given the above dispersion requirements, it is clear that λ_x and λ_y must also be low integer multiples of the dispersion period λ_D. Note that λ_x and λ_D should not be equal to avoid an unwanted resonance. Thus, the cooling channel optics must have correlated values of λ_x, λ_y and λ_D:

$$\lambda_x = n\lambda_y = m\lambda_D \qquad 1.$$

e.g. $\lambda_x = 2\lambda_y = 4\lambda_D$ or $\lambda_x = 2\lambda_y = 2\lambda_D$.

B. Orbital Dynamics

The PIC dynamics is very sensitive to magnetic fringe fields. One approach to finding a practical fringe-field-free solution is to use helical harmonics [2, 7]:

$$B_\varphi^n = \left(\frac{2}{nk}\right)^{n-1} \left.\frac{\partial^{n-1} B_\varphi^n}{\partial \rho^{n-1}}\right|_0 \cos(n[\varphi - kz + \varphi_0^n])\,[I_{n-1}(nk\rho) - I_{n+1}(nk\rho)],$$

$$B_\rho^n = \left(\frac{2}{nk}\right)^{n-1} \left.\frac{\partial^{n-1} B_\varphi^n}{\partial \rho^{n-1}}\right|_0 \sin(n[\varphi - kz + \varphi_0^n])\,[I_{n-1}(nk\rho) + I_{n+1}(nk\rho)],$$

$$B_z^n = -2\left(\frac{2}{nk}\right)^{n-1} \left.\frac{\partial^{n-1} B_\varphi^n}{\partial \rho^{n-1}}\right|_0 \cos(n[\varphi - kz + \varphi_0^n])\, I_n(nk\rho),$$

where B_φ, B_ρ, and B_z are the azimuthal, radial, and longitudinal helical magnetic field components, respectively, n is the harmonic number (e.g. $n = 1$ is the dipole harmonic), and $k = 2\pi / \lambda_h$ is the helix wave number while λ_h is the helix period.

One extensively-studied system based on helical field is the Helical Cooling Channel (HCC) [2]. However, the HCC is not suitable for PIC because it has constant dispersion magnitude. It was suggested [6] that alternating dispersion could be created by superimposing the HCC with an opposite-helicity helical dipole field with a commensurate characteristic period. However, with this approach, the periodic orbit solution is somewhat complicated and producing sufficiently large acceptance seems problematic.

Here we study a somewhat different configuration of magnetic fields, however, retaining the principle of Ref. [6] of creating an alternating dispersion by superimposing two helical-dipole fields with commensurate periods. We use a superposition of two equal-strength helical dipole harmonics with equal periods and opposite helicities ($k_1 = -k_2$) as a basis for our PIC channel design. Analogously to how combining two circularly-polarized waves produces a linearly-polarized one, the magnetic field in the mid-(horizontal)-plane of this configuration is transverse to the plane. This means that the periodic orbit is flat and lies in the mid-plane. The horizontal and vertical motions are uncoupled. This is a more conventional orbital dynamics problem than the one with a 3D reference orbit and coupled transverse motion.

Figure B1(a) shows an example of the periodic orbit solutions for 100 MeV/c μ^+ and μ^- in a twin-helix channel with 1 m period and 0.741 T magnetic field strength of each helical dipole harmonic. The periodic orbit was determined numerically by locating the fixed point in the phase space. For this procedure, one only needed to consider the x-x' horizontal phase space and the procedure was further simplified by selecting a longitudinal position where x' was zero. Figure B1(b) shows the dispersion as a function of the longitudinal position for the μ^+ solution shown in Fig. B1(a). Note that the dispersion has oscillatory behavior required for PIC. Note also that the dispersion period is equal to the helix period, i.e. $\lambda_D = \lambda_h$.

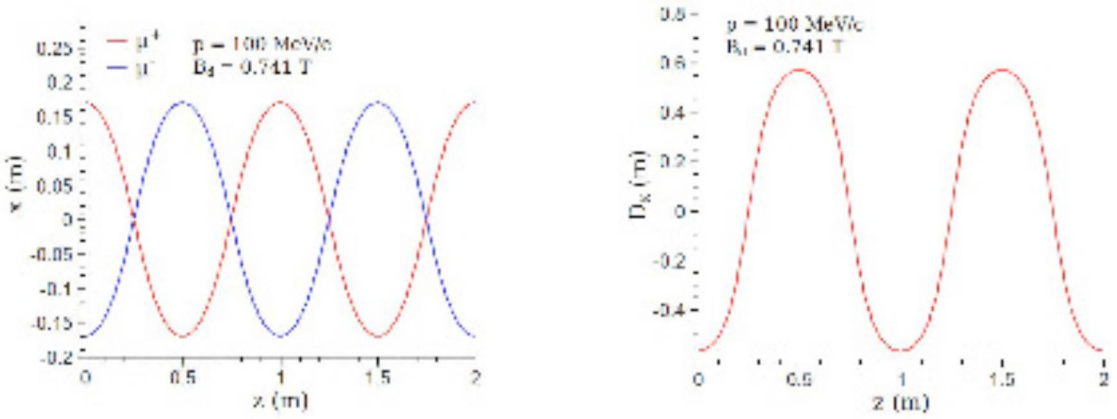

(a) (b)

FIGURE B1. (a) Periodic orbits of 100 MeV/c μ^+ and μ^- in a twin-helix channel with 1 m period and 0.741 T magnetic field strength of each helical dipole harmonic. (b) Dispersion behavior as a function of the longitudinal position for the μ^+ solution in (a).

The transverse motion in a twin-helix consisting of two helical dipole harmonics only is stable around the periodic orbit in both dimensions as long as the helical dipole strength does not exceed a certain limiting value. Figures B2(a) and B2(b) show the periodic orbit amplitude and the betatron tunes, respectively, vs. the helical dipole strength B_d for three different values of the helix period. In the calculations shown in Figs. B2(a) and B2(b), the strength B_d was changed in small steps. On each step, the new periodic orbit was obtained as described above using the previous step's solution as the initial guess. The betatron tunes were extracted from a single-period linear transfer matrix, which was obtained numerically in terms of canonical coordinates. The canonical coordinates were calculated using an analytic expression for the helical magnetic field vector potential [7].

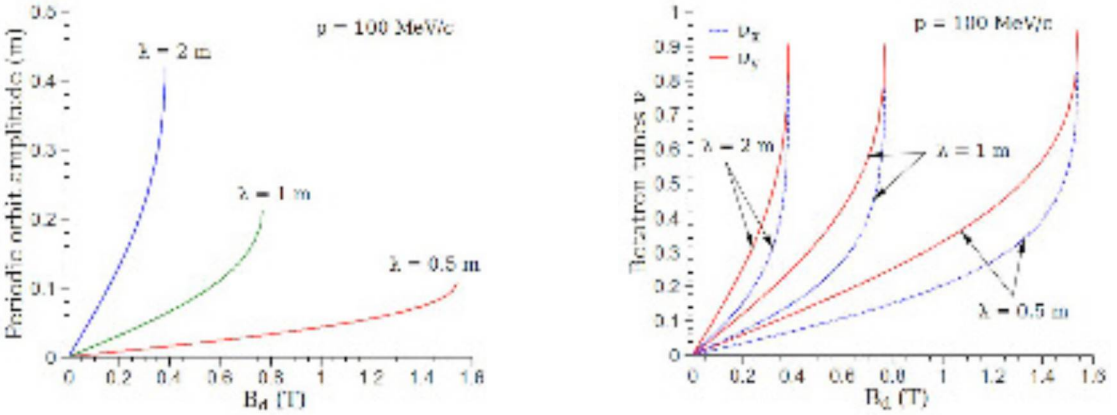

(a) (b)

FIGURE B2. Periodic orbit amplitude (a) and horizontal and vertical betatron tunes (b) vs. the helical dipole strength.

Since the dispersion period is determined by the helix period $\lambda_D = \lambda_h$, the correlated optics condition of Eq. (i) imposes the following conditions on the betatron tunes: $\nu_x = \lambda_h/\lambda_x = \lambda_h/(m\lambda_D) = 1/m$ and $\nu_y = \lambda_h/\lambda_y = \lambda_h/(m\lambda_D/n) = n/m$, e.g. $\nu_x = 0.5$, $\nu_y = 1$ or $\nu_x = 0.25$, $\nu_y = 0.5$. Examining Fig. 3(b) shows that it is not possible to satisfy these conditions by adjusting λ_h and B_d. Thus, we introduced a straight normal quadrupole to redistribute focusing between the horizontal and vertical dimensions. One subtlety is that, in addition to changing the focusing properties of the lattice, the

quadrupole also changes the periodic reference orbit. The helical dipole strength B_d and the quadrupole gradient $\partial B_y/\partial x$ were iteratively adjusted until, at $B_d = 1.303$ T and $\partial B_y/\partial x = 1.153$ T/m, we achieved the correlated optics condition with $\nu_x = 0.25$ and $\nu_y = 0.5$. Having $\nu_x = 0.5$ and $\nu_y = 1$ would be more beneficial by allowing shorter spacing between the absorbers but it was not possible to adjust these tune values because of a strong parametric resonance at $\nu_y = 1$. We also attempted tuning the correlated optics condition by using a helical quadrupole pair instead of a straight quadrupole but that configuration did not seem compatible with the correlated optics requirements. Figures 4(a) and 4(b) show the dependence of the betatron tunes on B_d at $\partial B_y/\partial x = 1.153$ T/m and on $\partial B_y/\partial x$ at $B_d = 1.303$ T, respectively. The crossing lines indicate the correlated optics condition. Note that the straight quadrupole introduces an asymmetry into the magnetic field so that the correlated optics condition is satisfied for one muon charge only.

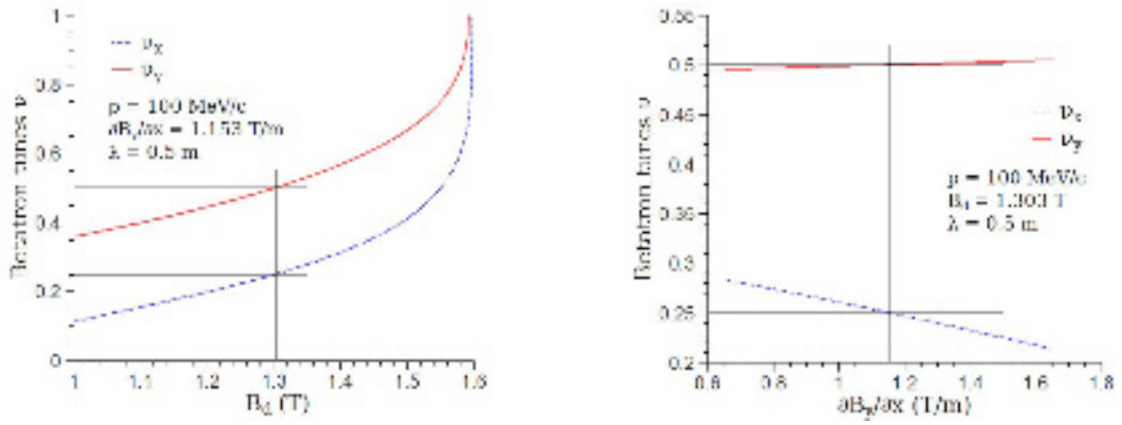

FIGURE B3. Horizontal and vertical betatron tunes vs. the helical dipole strength B_d at $\partial B_y/\partial x = 1.153$ T/m (a) and the straight quadrupole gradient $\partial B_y/\partial x$ at $B_d = 1.303$ T (b).

We next studied the dependence of the periodic orbit and of the betatron tunes on the muon momentum as shown in Figs. B4(a) and B5(b). These studies demonstrated large momentum acceptance of the twin-helix channel. We found that, with correlated optics, the dispersion amplitude $D_{x\,max} = p\ \partial x_{max}/\partial p$ was 0.098 m and the horizontal and vertical chromaticities were $\xi_x = p\ \partial\nu_x/\partial p = -0.646$ and $\xi_y = -0.798$, respectively. The correlated optics parameters scale with the muon momentum and helix period in the following way:

$$B_d \propto p/\lambda; \quad \partial B_y/\partial x \propto p/\lambda^2; \quad x_{max}, D_x \propto \lambda; \quad \xi_x, \xi_y \propto \text{const.} \qquad 2.$$

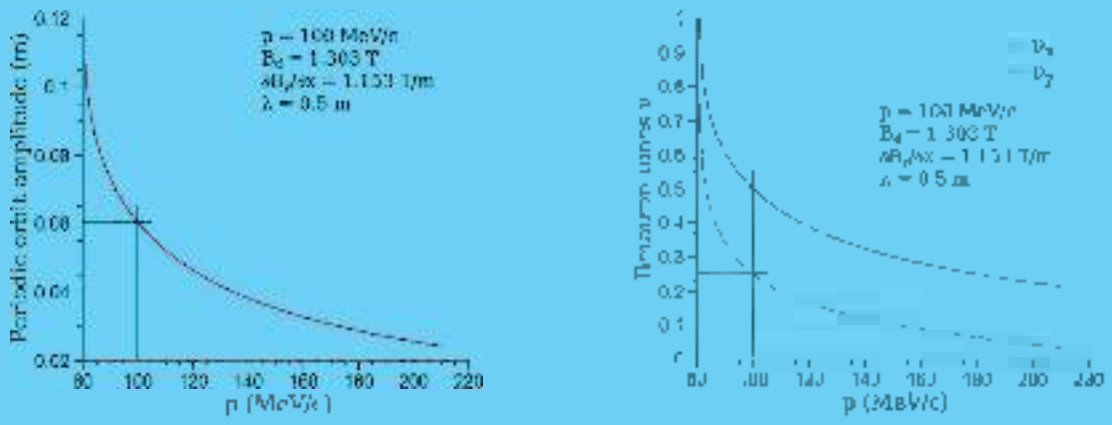

FIGURE B4. Periodic orbit amplitude (a) and betatron tunes (b) vs. the muon momentum with correlated optics.

C. G4beamline Simulation

To estimate the dynamic aperture of the correlated optics channel, we tracked 10^5 100 MeV/c muons through 100 periods of the channel using the GEANT4-based G4beamline program [8]. The initial muon beam was monochromatic, parallel and uniformly distributed within a 10 cm × 10 cm square. Figures B5(a) and B5(b) show the initial and final transverse muon distributions, respectively. The initial positions of the particles that were not lost after 100 periods are shown in Fig. B5(a) in blue. Figures B5(a) and B5(b) suggest a very large dynamic aperture and therefore high transmission efficiency of the twin-helix channel.

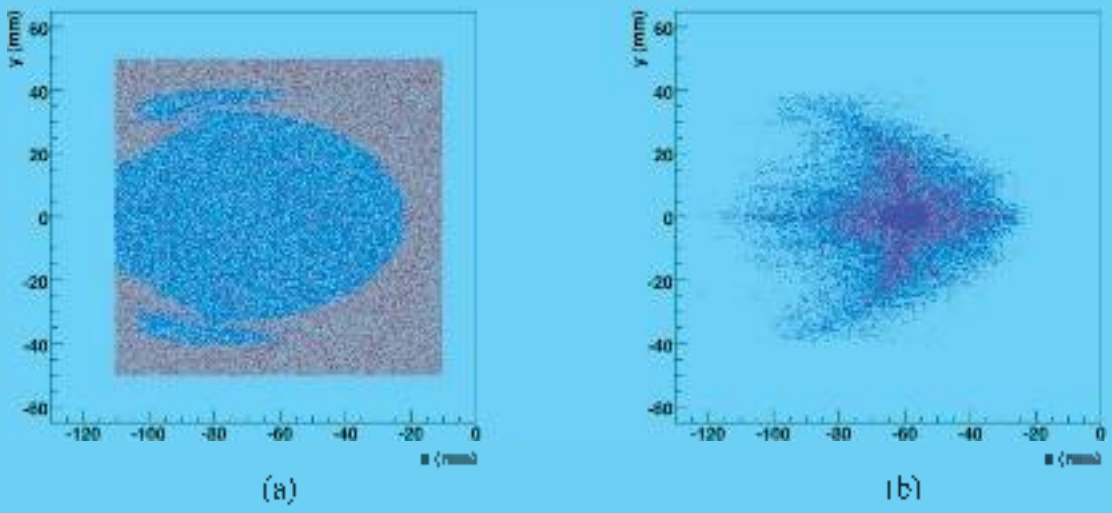

FIGURE B5. Initial (a) and final (b) transverse muon beam distributions in a G4beamline tracking study.

D. Possible Practical Implementation

In practice, the required magnetic field configuration can be obtained by winding two separate coaxial layers of helical conductors and coaxially superimposing a straight quadrupole as shown in Fig. B6(a). The helical conductors constituting the two layers have the same spatial periods and opposite helicities. Within each layer, the currents in the helical conductors vary azimuthally as $\cos(\varphi)$. Note that the two layers do not have to have the same radius. The difference in the radii can

be accounted for by adjusting the layers' currents. Another approach to producing the desired magnetic field is to combine two coaxial layers consisting of series of tilted current loops and overlay a coaxial straight quadrupole as shown in Fig. B6(b). The inclined loops comprising the two different layers are tilted in opposite directions. The current in the loops of each layer varies longitudinally as $\cos(kz)$. Such a technology, without longitudinal current variation, is used for making constant-field dipoles.

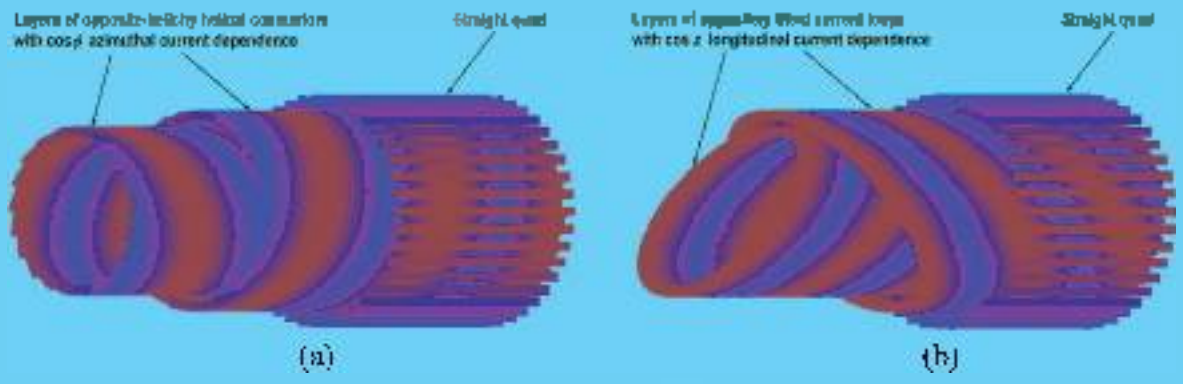

FIGURE B6. Conceptual diagrams of possible practical implementations of a twin helix channel featuring a combination of two helical conductor layers and a straight quadrupole and featuring a combination of two layers of tilted current loops and a straight quadrupole. The colors represent current variation in the conductors.

APPENDIX C: STUDIES OF THE TWIN HELIX PARAMETRIC RESONANCE IONIZATION COOLING CHANNEL WITH COSY INFINITY

The twin helix channel is simulated using COSY Infinity, a DA-based code that allows for calculation of non-linear effects to arbitrary order [7]. This paper details a linear simulation of this channel, with and without stochastic effects, and studies cooling efficiency with and without the effects of PIC. The linear simulation provides a baseline for ideal cooling in the channel if nonlinear aberrations in the channel have been fully corrected.

A. Simulation Parameters

Table C1 details the parameters used in this linear simulation. The basic cell consists of a continuous straight quadrupole field superimposed upon a pair of helical harmonic dipole fields to establish the correlated optics condition. Wedge absorbers, made of beryllium with a central thickness of 2 cm and a gradient of 30%, are placed every 4 meters in the channel at a location of small but non-zero dispersion. Idealized RF cavities are placed 3 cm after the center of each wedge. COSY INFINITY calculates the transfer map for a 4-meter long cell (from the center of a wedge absorber through the center of the next wedge absorber). Figure 1 illustrates the geometry of this cell.



Figure C1. Schematic of Single Twin Helix Cell

The total transfer map for the twin helix channel is obtained by composing the maps for each of the cells that make up the channel upon one another. The orbit of the reference particle (250 MeV/c muon) is periodic from the beginning to the end of each cell.

Table C1: 4-meter Cell Parameters

H. Dipole Field	1.63 T
H. Dipole wavelength	1 meter
Continuous Quadrupole Field	.72 T/m
H. Quadrupole Field (Horizontal Lenses)	.02 T/m
H. Quadrupole wavelength	2 meters
H. Quadrupole Field (Vertical Lenses)	.04 T/m
H. Quadrupole wavelength	1 meter
RF Voltage	-12.5 MeV
RF Frequency	201.25 MHz
RF Phase	30 Degrees

B. Simulation of the Parametric Resonance Condition in the Twin Helix Channel

To induce the resonance condition for PIC in the twin helix channel, two independent pairs of helical harmonic quadrupole fields (parametric lenses) are used; one pair induces resonance in the horizontal plane, the other in the vertical plane. The resonances induced by these fields create a hyperbolic fixed point; i.e., motion of particles relative to the reference orbit at the center of the wedge absorber becomes hyperbolic rather than elliptical. Figures C2a-b show this condition in the basic cell (without wedge absorber or RF) when a test particle that is offset both horizontally and vertically in both position and angle relative to the reference orbit by 2 cm and 130 mrads respectively. With the parametric lenses, the position offset is quickly minimized at the expense of a rapid blowup in the angle offset.

C. Simulation of Ionization Cooling in the Twin Helix Channel

The next stage in the simulations adds wedge absorbers and RF every 4 meters. Figures C3a-b show simulations with and without the parametric lenses to demonstrate the effects of ionization cooling with and without the PIC condition. The simulations demonstrate the expected results. With only ionization cooling, initial cooling effects are primarily to angle, and only later to the positional offset. With PIC the cooling effects are primarily to position offset, i.e., spot size of the beam. The increase in angle offset is minimized thru the ionization cooling effects of the wedge absorber.

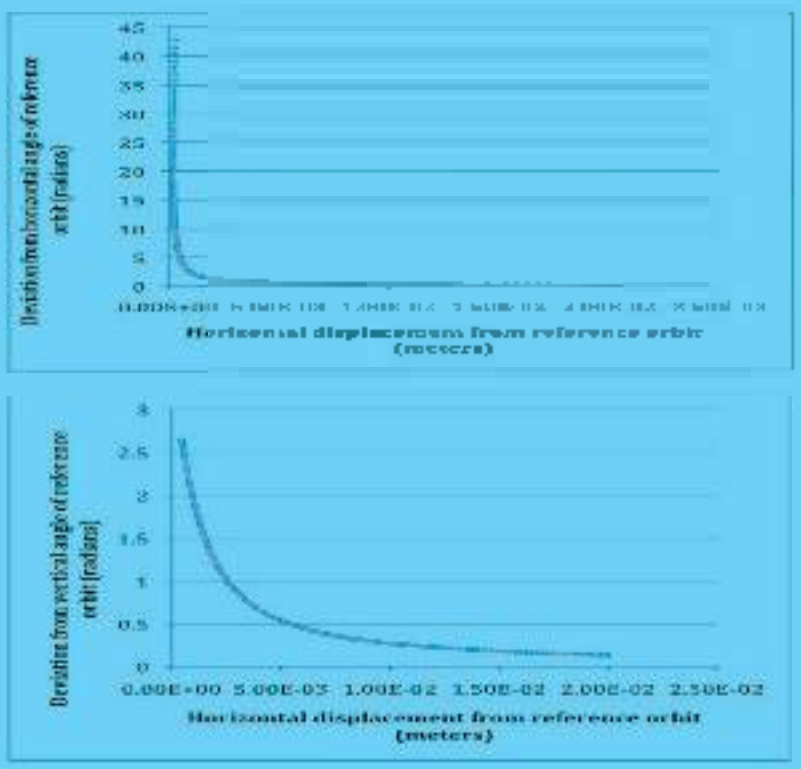

Figure C2a-b. Single particle launched with a horizontal and vertical offsets of 2 cm and -.30 radians from the reference orbit and tracked for 200 cells

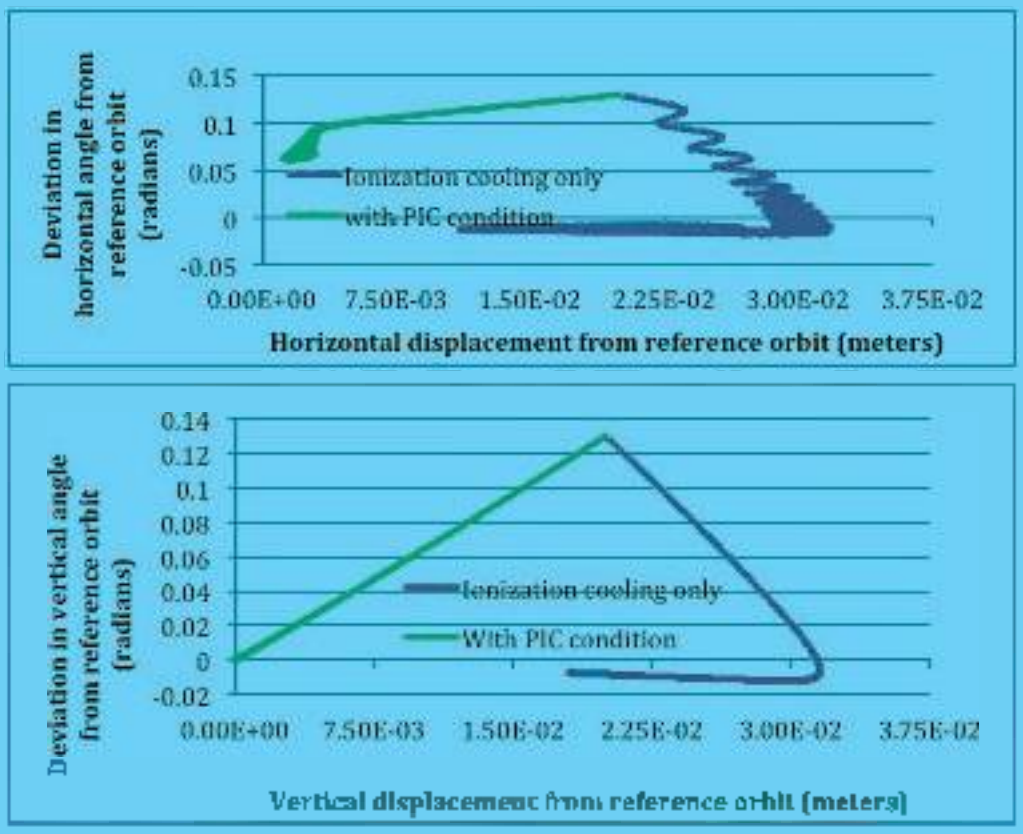

Figures C3a-b. Single particle tracked through 1000 cells with PIC condition and with ionization cooling only

D. Simulation of Stochastic Effects in the Twin Helix Channel

Stochastic effects of multiple scattering and energy straggling within the wedge absorber were then added to the simulations. Figures C4a-b show the results of combining ionization cooling with stochastic effects on a single particle initially offset both horizontally and vertically in both position and angle relative to the reference orbit by 2 cm and 130 mrad respectively.

As expected, the test particle is cooled until equilibrium is reached when cooling has been balanced with the effects of multiple scattering and energy straggling [6].

A distribution of test particles was also used to test cooling effects in the full simulation of the linear channel. The initial distribution uses a sigma of 2 cm in positions, 130 mrad in angles, and 1% spread in energy from the reference particle. The distribution is also spread over a bunch length of $\sigma_z = 3$ cms relative to the reference particle. Figure C5 shows the 2D emittance change in the system calculated from the distribution. The horizontal and vertical 2D emittances are both reduced until equilibrium is reached. Longitudinal emittance is determined from deviation in path length and energy from the reference particle. Once the transverse emittance has reached equilibrium, the increases in longitudinal emittance contribute to heating in the beam distribution. Total 6D emittance for the distribution is plotted in Figure 6 with and without parametric lenses to induce the PIC condition. Figure C 7 shows the cooling factor for the channel with and without the PIC condition.

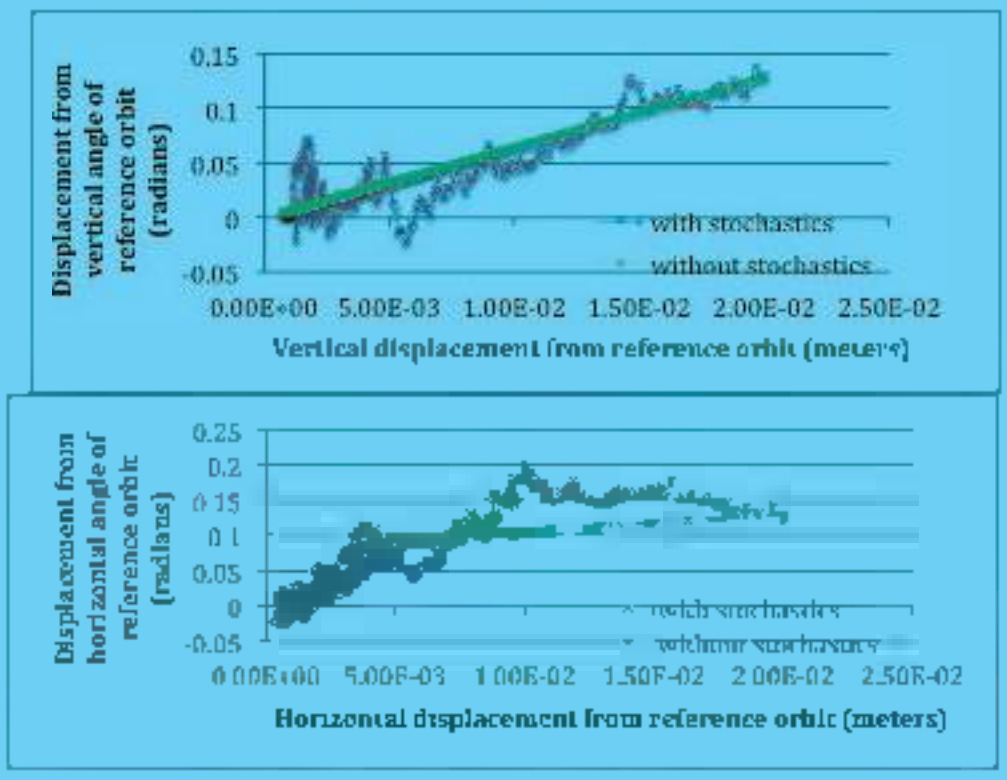

Figure C4a-b. Single particle tracked showing cooling thru 350 cells with and without stochastic effects

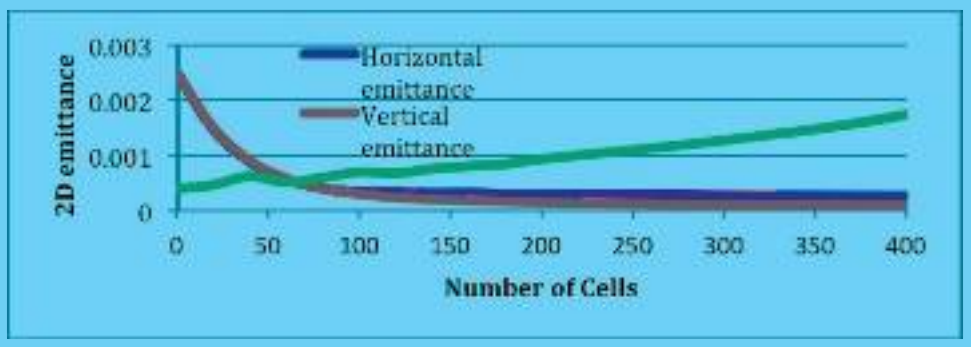

Figure C5. 3cm lattice reduction for a distribution of 1000 particles tracked through the twin-helix channel with the PIC condition and stochastic effects

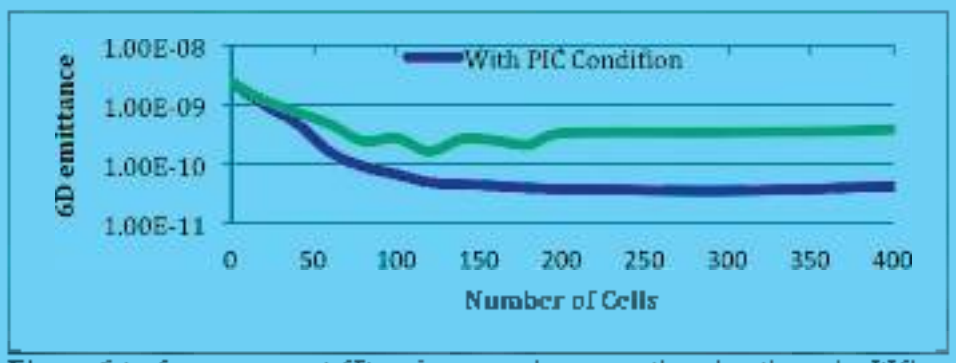

Figure C6. Comparison of 6D emittance reduction with and without the PIC condition

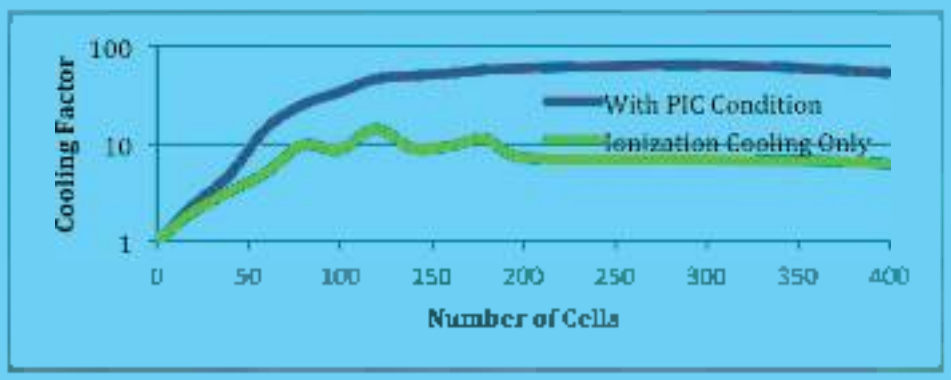

Figure C7. Comparison of cooling factor (ratio of initial to final 6D emittance) with and without the PIC condition

The determinant of the transfer map for the cell, a 6x6 matrix in the linear case, can also be used to show transverse and 6D cooling in the system [10]. The determinant for the transfer matrix for this test channel is 0.915372. The determinant of the transverse 4x4 quadrant of the transfer matrix is 0.986054.

C. Conclusions and Future Work

Current simulations in COSY INFINITY have demonstrated that the linear model with stochastic effects on the twin helix channel achieves the resonance condition for PIC, as well as 6D cooling. Future simulations will determine the optimal parameters for this linear model, including cell length, magnet strengths, helicity and phase shifts for the helical harmonic magnets. Wedge

gradients and thickness, as well as RF placement and parameters, will also be optimized. Next, studies will determine the largest nonlinear aberrations affecting this optimized twin-helix channel and the dependence these aberrations have on higher order helical harmonic and continuous multipole fields of differing strength, helicity and phase. The cooling efficiency of a system with corrected higher order effects can then be measured and compared with competing 6D cooling methods.

REFERENCES

[1] D. M. Kaplan, *Introduction to Muon Cooling*, http://www.slac.stanford.edu/econf/C010630/papers/M102.PDF

[2] Y. Derbenev and R. P. Johnson, Phys. Rev. Special Topics Accel. and Beams 8, 041002 (2005). http://www.muonsinc.com/reports/PRSTAB-HCCtheory.pdf

[3] L. D. Landau and E. M. Lifshits, Theoretical Physics v. 8, Electrodynamics of continuous media 1960 QC 518.L23.

[4] Y. Derbenev and R. P. Johnson, op. cit.

[5] K. Beard et al., SIMULATIONS OF PARAMETRIC RESONANCE IONIZATION COOLING OF MUON BEAMS, http://accelconf.web.cern.ch/AccelConf/p05/PAPERS/TPPP013.PDF

[6] Y.S. Derbenev and R.P. Johnson, "Advances in Parametric-resonance Ionization Cooling" in Proceedings of *EPAC 08*, Genoa, Italy, 2008, pp. 2838-2840; A. Afanasev, Y.S. Derbenev and R.P. Johnson, "Aberration-free Muon Transport Line for Extreme Ionization Cooling: a Study of Epicyclic Helical Channel", *ibid.*, p. WEPP147.

[7] T. Tominaka *et al.*, *Nucl. Instrum. Meth.* A **459**, 398 (2001).

[8] G4beamline, http://g4beamline.muonsinc.com

[9] M. Berz & K. Makino, COSY Infinity Version 9, *Nuclear Instruments and Methods* A558 (2005) pp. 346-50.

[10] J.A. Maloney, et al., "EPIC Muon Cooling Simulations Using COSY Infinity", Proc. PAC'11, New York, March 2011, MOP050, p. 190 (2011); http://www.JACoW.org.

Numerical Studies of Optimization and Aberration Correction Methods for the Preliminary Demonstration of the Parametric Ionization Cooling (PIC) Principle in the Twin Helix Muon Cooling Channel

J.A. Maloney[a,c,f], V.S. Morozov[b], Ya. S. Derbenev[b], A. Afanasev[c,d], R.P. Johnson[c], C.A. Ankenbrandt[c], C. Yoshikawa[c], K. Yonehara[e], D. Neuffer[e], B. Erdelyi[f],

[a]Triumf, Vancouver, B.C., V6T2A3, CANADA
[b]Thomas Jefferson National Accelerator Facility, Newport News, Virginia 23606, USA
[c]Muons, Inc., Batavia, Illinois 60510, USA
[d]The George Washington University, Washington, D.C. 20052, USA
[e]Fermi National Accelerator Laboratory, Batavia, Illinois 60510, USA
[f]Northern Illinois University, DeKalb, Illinois 60115, USA
(Received 31 January 2014)

PACS Numbers: 41.75.-i; 41.85.-p; 1460.Ef; 29.27.-a

Muon colliders have been proposed for the next generation of particle accelerators that study high-energy physics at the energy and intensity frontiers. In this paper we study a possible implementation of muon ionization cooling, Parametric-resonance Ionization Cooling (PIC), in the twin helix channel. The resonant cooling method of PIC offers the potential to reduce emittance beyond that achievable with ionization cooling with ordinary magnetic focusing. We examine optimization of a variety of parameters, study the nonlinear dynamics in the twin helix channel and consider possible methods of aberration correction.

I. INTRODUCTION

Muon colliders have been proposed for the next generation of particle accelerators that study high-energy physics at both the energy and intensity frontiers. One of the principal technical challenges in designing a next generation muon collider is muon beam cooling. Muons are produced as tertiary particles, and a muon beam will occupy a very large volume of phase space. Muon cooling reduces the emittance of the beam, a measure of the phase space volume of the beam. This can improve both the luminosity and the physics reach of the collider. A muon collider will need to reduce beam emittance by approximately 6 orders of magnitude to fit within the dynamic aperture of accelerating structures and meet collider luminosity goals [1]. The need for precise energy resolution also makes muon cooling essential for a muon-based Higgs factory operating at the intensity frontier [2]. Additional transverse beam cooling as supplied by the PIC

method described here allows other benefits such as even higher luminosity, reduced detector backgrounds and reduced demands on the proton driver and accelerating systems. [3]

To achieve a collider in the luminosity range from 10^{34}-10^{35} cm^{-2} s^{-1}, the transverse emittance for the muon beams must be reduced to about 10 π mm-mr. Conventional beam cooling techniques are not useful for cooling such muon beams. The cooling timescales for laser cooling (~10^{-4} s), stochastic cooling (many seconds) and electron cooling (~10^{-2} s), for example, are too long compared to the short muon lifetime of 2.2 μs. The large muon mass also means that synchrotron radiation cooling, an effective technique for electron/positron beams, cannot be used in a muon collider. Instead, muon cooling channels reduce emittance through ionization cooling. One proposal for the final stage of 6D muon cooling is a channel that utilizes the principle of parametric-resonance ionization cooling (PIC) and is based on a twin helix [4]. This channel couples ionization cooling with induced ½ integer resonances to achieve strong focusing in the beam. The potential of PIC is a reduction in equilibrium emittance in each transverse plane by about a factor of 10, which would increase luminosity by a factor of 10 beyond the level of non-resonant ionization cooling using the same magnetic field strengths. Control of nonlinear dynamics is needed to achieve the cooling potential of PIC because uncorrected aberrations in the beam optics can overcome the strong focusing effects of the induced resonances.

This paper studies how a variety of parameters of the twin helix channel may be optimized. This paper also details studies, using COSY INFINITY, of the nonlinear dynamics in the twin helix channel and considers possible methods of aberration correction.

II. PARAMETRIC-RESONANCE IONIZATION COOLING AND THE TWIN HELIX CHANNEL

The principle of parametric-resonance ionization cooling (PIC) can be implemented in a channel where the muon beam is transported in a periodic magnetic structure. The ordinary phase space trajectory for particles in a stable orbit in this channel is elliptical. The magnetic fields in

the channel are perturbed to induce a half-integer resonance that alters the phase space trajectories of particles at periodic fixed points in the channel from parabolic to hyperbolic orbits. This results in strong focusing in position at the expense of growth in angular divergence of the beam [5]. A key aspect of PIC is correlated optics where this strong focusing occurs simultaneously in both the horizontal and vertical planes at a location with small, but non-zero dispersion to allow for 6D cooling through emittance exchange [6]. Wedge absorbers are placed at these points to stabilize the growth in angular divergence and enable emittance exchange. RF cavities are interspersed between the absorbers to maintain the reference momentum of the beam.

One proposed implementation of the PIC principle is the twin helix channel [7]. The basic twin helix channel utilizes a pair of superimposed helical magnetic dipole harmonics. These helical harmonics have equal field strength, and equal but opposite helicity. This creates a channel with alternating dispersion that is practically fringe-field-free. The magnetic fields for helical harmonics can be analytically expressed in cylindrical coordinates as:

$$B_\phi^n(\phi,\rho,z) = B_n[I_{n-1}(nk\rho) - I_{n+1}(nk\rho)]\cos(n[\phi - kz + \phi_0^n]) \quad (1)$$

$$B_\rho^n(\phi,\rho,z) = B_n[I_{n-1}(nk\rho) + I_{n+1}(nk\rho)]\sin(n[\phi - kz + \phi_0^n]) \quad (2)$$

$$B_z^n(\phi,\rho,z) = -2B_n I_n(nk\rho)\cos(n[\phi - kz + \phi_0^n]) \quad (3)$$

$$\text{where} \quad B_n = \left(\frac{2}{nk}\right)^{n-1} \left.\frac{\partial^{n-1} B_\phi^n}{\partial \rho^{n-1}}\right|_{\substack{\phi+\phi_0^n=0 \\ \rho=0 \\ z=0}} \quad (4)$$

B_n is the appropriate derivative of the magnetic field strength, and $I_n(x)$ is the modified Bessel function of the first kind. The order of the Bessel functions and the harmonic multipole are determined by the parameter, n ($n = 1$ for dipole, $n = 2$ for quadrupole, etc.).

When two helical harmonics with equal field strength and equal but opposite helicity are superimposed, the total horizontal (x) and longitudinal (z) components of the magnetic field vanish and the resulting magnetic field in the x-z mid-plane simplifies to:

$$\vec{B} = 2B_n[I_{n-1}(nkx) - I_{n+1}(nkx)]\cos(n[kz + \phi_0^n])\,\hat{y} \quad (5)$$

This channel enables a beam of particles to have a stable reference orbit in the x-z mid-plane [8]. Additional pairs of similarly matched helical harmonics, as well as continuous "straight" magnetic multipoles, may be superimposed while maintaining this planar reference orbit. By using combinations of continuous magnetic fields and helical harmonic pairs, the optics of the channel can be adjusted without complications caused by fringe fields from a series of lumped elements with discrete length.

In addition to the helical dipole harmonic pair, a continuous straight quadrupole magnetic field is superimposed onto the basic twin helix channel to redistribute focusing between the horizontal and vertical planes. This basic channel is designed to satisfy the PIC requirement of correlated optics: the horizontal and vertical betatron tunes are both integer multiples of the dispersion function [9]. The parameters of this basic twin helix channel also can be easily rescaled. The scaling relationships in 6-9 are given for arbitrary values of the momentum of the reference particle (p) and the period length of the helical dipole harmonic (λ) as:

$$B_d = 6.515 \cdot 10^{-3}\ [T \cdot m/MeV/c]\ p/\lambda \tag{6}$$

$$\partial B_y/\partial x = 2.883 \cdot 10^{-3}\ [T \cdot m/MeV/c]\ p/\lambda^2 \tag{7}$$

$$x_{max} = 0.121\ \lambda\ [m] \tag{8}$$

$$D_x = 0.196\ \lambda\ [m] \tag{9}$$

where B_d is the field strength of each helical dipole harmonic, $\partial B_y/\partial x$ is the gradient of the continuous quadrupole, x_{max} is the maximum amplitude of the periodic orbit in the horizontal mid-plane and D_x is the maximum dispersion amplitude [10].

Two additional pairs of helical quadrupole harmonics are superimposed onto this basic channel to perturb the magnetic fields to induce the PIC ½-integer resonance condition [11]. One pair induces the resonance in the vertical plane while the other induces the resonance in the horizontal plane. These additional harmonics alter each particle trajectory within the beam so that strong focusing reduces spot size at regular intervals throughout the channel at the expense of

increased angular divergence. To avoid beam instability caused by these resonances, wedge absorbers are placed at every other point of strong focusing to stabilize the beam and enable ionization cooling and emittance exchange [12]. An RF cavity is placed after each absorber to restore and maintain the beam's reference momentum.

A linear model of this channel has been previously simulated using COSY INFINITY (COSY) [13]. COSY uses differential algebraic techniques to allow computation of Taylor maps for arbitrary order, allowing the user to disentangle linear and non-linear effects [14]. Additional coding was added to modify the COSY beam physics package and include the stochastic effects of multiple Coulomb scattering and energy straggling in these simulations [15]. Beam cooling has been demonstrated with this non-optimized model [16]. A comparison was made of the cooling effects of the channel with and without inducing the PIC resonance. These simulations verified the analytic theory, showing improved cooling with PIC [17].

III. OPTIMIZATION OF THE TWIN HELIX CHANNEL

Optimization of the channel design began with consideration of the period length for the helical dipole harmonics. The final stage of 6D cooling in a muon collider or Higgs factory needs to reduce emittance by about 2 orders of magnitude beyond the reduction achieved through initial 6D cooling methods. The drift space between wedges should be minimized to maximize ionization cooling per channel length. Additionally, the total length of this final stage of 6D cooling should be as short as possible to minimize losses due to muon decays. Consideration must also be given, however, to allow sufficient space for energy-restoring RF cavities.

Using the scaling relationships for the twin helix, eqns. 6-9, the parameters for the basic twin helix channel can be adjusted for different helical dipole period lengths. The maximum amplitude and maximum dispersion can also be determined. For a variety of helical dipole period lengths, G4Beamline (G4BL) [18], was used to track particle distributions and the transmission rate was measured after 1000 absorbers. The simulations tracked a distribution of 1000 muons with momentum of 250 MeV/c. These simulations indicate that choosing a helical dipole period

of approximately 20 cm was optimal for improved transmission while minimizing the drift space between absorbers. Table I shows the scaling relations among the helical dipole period, magnetic field strengths, maximum offset, dispersion, and the resulting transmission rate.

TABLE I. Comparison of parameters for various twin helix configurations.

λ_D	B_D	$\partial B_y/\partial x$	x_{max}	$D_{x\,max}$	% transmission
.05 cm	48.84 T	76.08 T/m	0.006 cm	0.010 m	03.0
.10 cm	24.42 T	38.04 T/m	0.012 cm	0.020 m	26.1
.20 cm	16.28 T	18.02 T/m	0.024 cm	0.039 m	37.3
.30 cm	08.14 T	09.01 T/m	0.036 cm	0.059 m	35.9

This choice of 20 cm for the period of the helical dipole harmonics has additional advantages. The maximum dispersion is just under 4 cm, which is approximately the same small, but non-zero, value at the location chosen for the wedge absorber in the prior simulations with a helical dipole period of one meter [19]. For a twin helix channel with a 20 cm dipole period, wedge absorbers would be ideally placed at the points of maximum dispersion. As illustrated in Fig. 1, this allows RF cavities to be symmetrically placed between the absorbers.

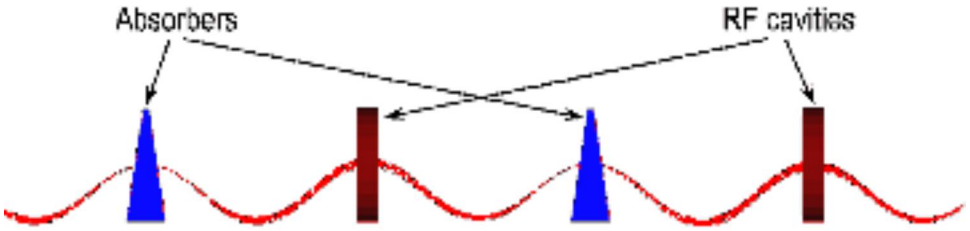

FIG. 1. (Color) Schematic of symmetric twin helix layout.

In addition to improving transmission, shortening the helical dipole period also reduces some beam aberrations. One major drawback, however, is the increase in the strengths of the

magnetic fields as the helical dipole period is reduced. For a 20 cm helical dipole period, the combined field from the pair of helical dipole harmonics scales to 16.3 T. With a 20 cm period for the helical dipole harmonic in the basic twin helix channel, wedge absorbers placed every other period allow less than 40 cm for the RF cavities. The result is a set of parameters that are challenging but within the levels contemplated for an energy frontier muon collider. The 20 cm period maximizes transmission while minimizing unnecessary length between the wedge absorbers, providing a good balance between cooling efficiency and channel length. The dipole period can be rescaled, if necessary, to an increased length to reduce these magnetic field strengths.

After selecting the period length for the helical dipole harmonics, the simulations of the linear model of the channel were repeated using COSY. For a 20 cm period, the field strength of each helical dipole harmonic was 8.14375 T, with a superimposed continuous quadrupole field of 18.01875 T/m. A test particle was tracked every 40 cm (2 helical dipole periods) as it traveled in this channel. Relative to the reference orbit, the particle follows an elliptical trajectory as shown in Fig. 2.

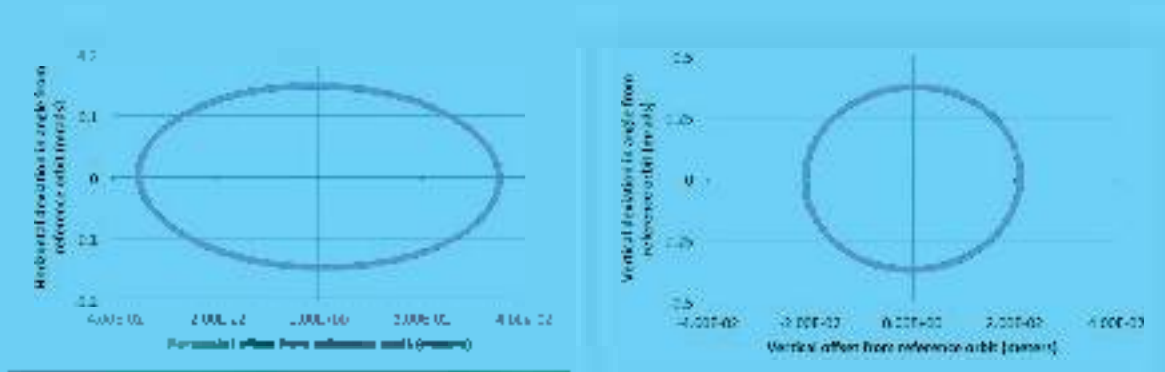

FIG. 2(a)-(b) of (c) The 20 cm basic twin helix channel simulated in COSY without wedge absorbers or energy restoring RF cavities. The trajectory of 250 MeV/c p was launched off set in both planes from the reference orbit by 2 cm and 130 mr and tracked and plotted every two dipole periods in (a) the horizontal plane and (b) vertical planes.

To induce the horizontal ½ integer resonance, a pair of helical quadrupole harmonic fields was added to the basic channel. Each harmonic in this pair had a field strength of 0.063662 T/m, a period of 80 cm and a phase advance that shifted the location of the maximum field amplitude by 30 cm relative to maximum field for the underlying helical dipole harmonic pair. The vertical resonance was induced by an additional pair of helical quadrupole harmonics, which each had a field strength of 0.127324 T/m, a period of 80 cm and a ≈ 4 cm phase shift. Fig. 3 shows the change in trajectory for the test particle once the PIC resonances have been introduced.

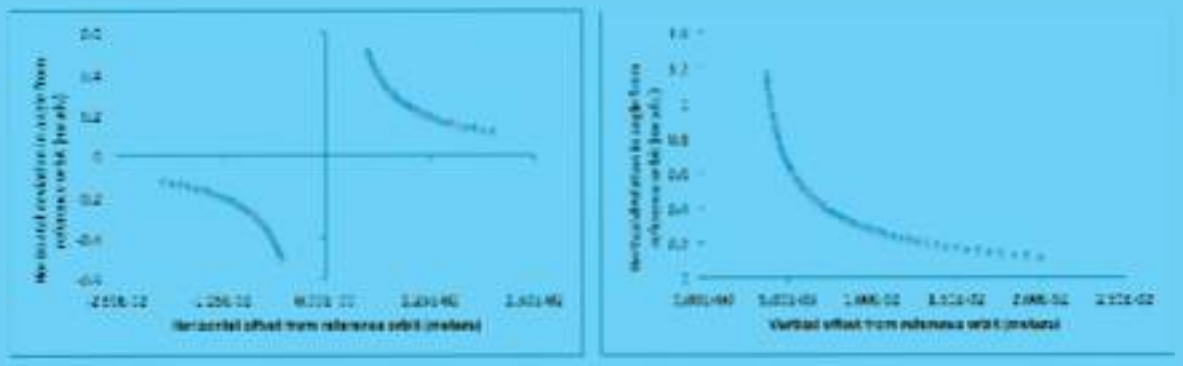

FIG. 3(a) (b) (Color) The λ_0=20 cm basic twin helix channel with induced ½ integer parametric resonance simulated in COSY without wedge absorbers or energy restoring RF cavities. The trajectory of a 250 MeV/c μ was launched offset in both planes from the reference orbit by 2 cm and 130 mm and tracked and plotted every two dipole periods in (a) the horizontal plane and (b) vertical planes.

The resonance can also be seen in the linear transfer matrix for one cell in this channel. Under this approach, the horizontal and vertical magnification matrix elements (x,x) and (y,y) should be less than one, while (x,a) and (y,b) should approach zero, where a = p_x/p_0 and b = p_y/p_0. In the present model, for example, the values for these matrix elements are presented in Table II.

TABLE II. The 4x4 s-matrix for the λ_0=20 cm basic twin helix cell with induced parametric resonance

	(x)	(a)	(y)	(b)
(x)	-0.971	-6.26×10^{-6}	0	0
(a)	5.70×10^{-7}	1.05	0	0
(y)	0	0	0.958	1.01×10
(b)	0	0	8.26×10^{-4}	1.04

Wedge absorbers were added at every other periodic focal point, with RF cavities symmetrically placed in between them. The central thickness of the wedge absorbers was arbitrarily set at 2 cm. The frequency and phase of the RF cavities were chosen as 201.5 MHz and 30 degrees. This is similar to cavities used in simulations for a helical cooling channel (HCC) [20] that could be upstream of a twin helix final cooling channel.

Optimization of the wedge thickness and RF parameters are not being studied at this time. In the final channel design, wedge thickness will be decreased as the beam travels through the channel to maintain cooling efficiency [21]. Parameters for the RF cavities will also need to be adjusted to maintain the reference momentum and match the time structure of the beam. Optimization of these parameters is left for consideration until after the exact structure of the upstream beam being delivered to the PIC channel and the beam acceptance parameters for the downstream accelerating structures have been determined.

The effects of varying the horizontal wedge gradient (dx/dz) were studied without a resonance (no helical quadrupole harmonic pairs). Fig. 4 shows some examples with (a) a flat absorber, (b) 0.10 wedge gradient, (c) 0.20 wedge gradient, and (d) 0.30 wedge gradient with the wedge orientation reversed. Increasing the gradient increases the rate of longitudinal cooling but also reduces horizontal transverse cooling by the same rate [22]. The final example demonstrates the principle of reverse emittance exchange (REMEX) used to gain extra reduction in transverse emittance at the expense of an increase in longitudinal emittance [23]. A wedge gradient of 0.10 was chosen to balance transverse cooling with longitudinal cooling through emittance exchange.

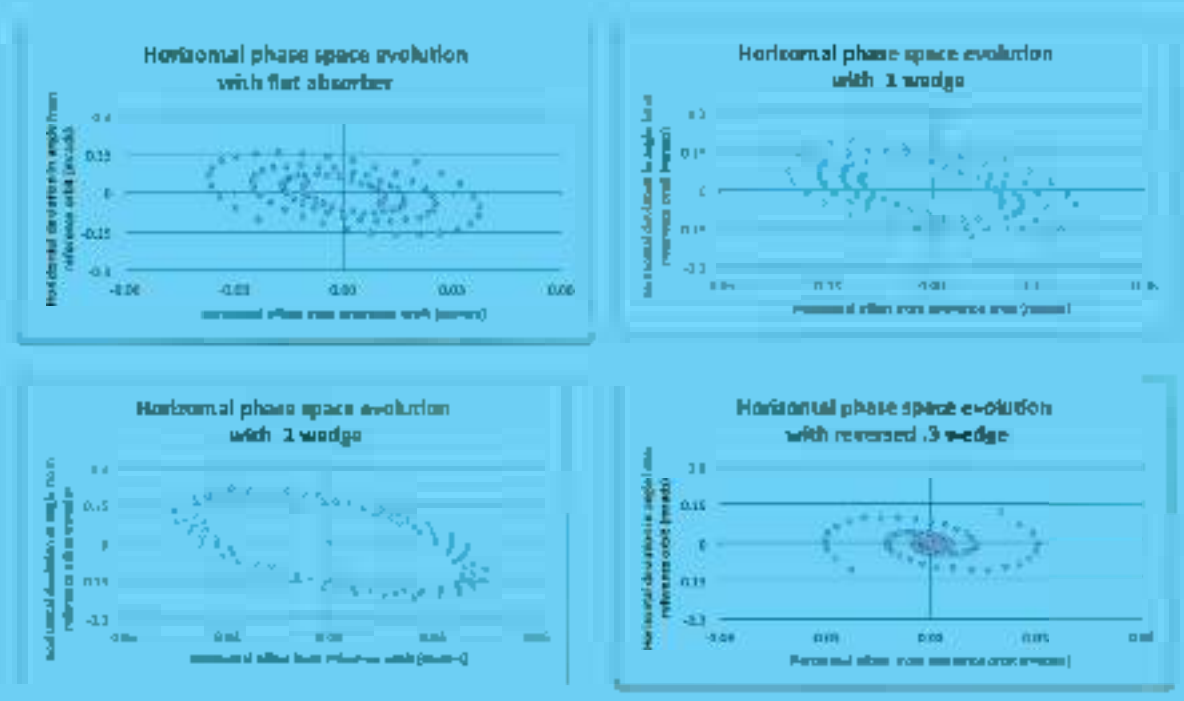

FIG. 4(a)-(c) (Color). The λ_H=20 cm twin helix channel simulated in COSY with wedge absorbers and energy resolving RF cavities. The trajectory of a 250 MeV/c μ was launched offset in both planes from the reference orbit by 2 cm and 130 mr and tracked and plotted every two dipole periods in the horizontal plane for (a) flat absorber, (b) 0.10 wedge gradient, (c) 0.20 wedge gradient, and (d) 0.30 wedge gradient with reverse wedge orientation (REMEX).

Next, the helical quadrupole harmonic pairs were added to induce the PIC resonance for the chosen wedge gradient. The effects of varying the field strength of the resonance harmonic pairs were studied. The same field strength of 0.127324 T/m used to induce the resonance in the vertical plane, shown in Fig. 3(b), was maintained. Fig. 5 shows the trajectory of the test muon in the vertical plane with this resonance induced.

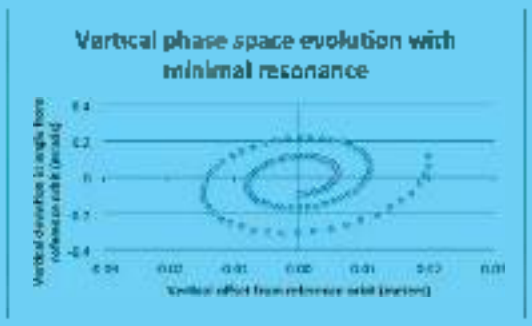

FIG. 5. (Color) The λ_c =20 cm full twin helix channel with induced vertical resonance simulation in COSY. The trajectory of a 250 MeV/c μ was launched offset in both planes from the reference orbit by 2 cm and 30 mr and tracked and plotted every two dipole periods in the vertical plane.

The field strength of the helical quadrupole harmonic pair used to induce horizontal phase space resonance in the basic channel, as shown in Fig. 3(a), was not strong enough once the wedge and RF cavities were added. As a result, the magnification term in the linear transfer matrix, $f(\lambda)$, was greater than 1. This effect is caused by a parasitic resonance that has been previously identified [24]. To induce the resonance, the strength of this helical harmonic pair was doubled. Cooling simulations showed that increasing the field strength further distorted the beam and reduced the cooling efficiency of the channel. Fig. 6 shows the effects on the trajectory of a test particle in horizontal phase space with (a) no resonance, (b) below resonance (0.063662 T/m), (c) resonance minimally triggered (0.127324 T/m), and (d) resonance strongly triggered (0.31831 T/m).

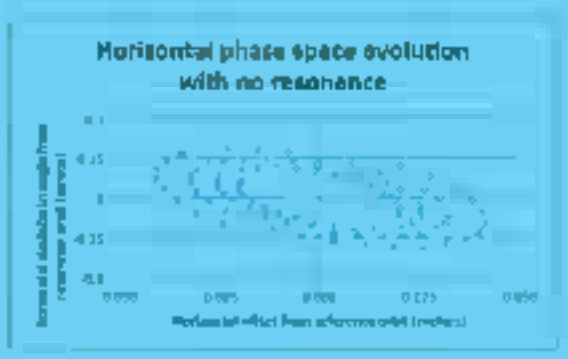



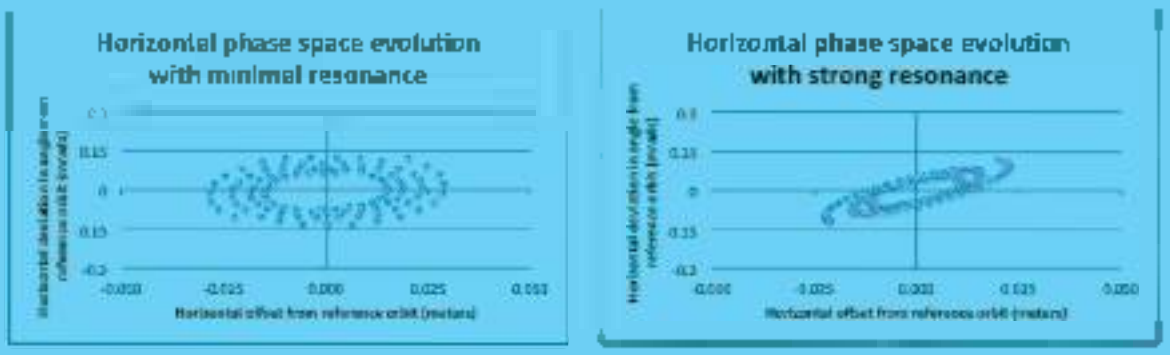

HCC muon (0) ; (Color) The x_p–$2x$ emittance in the channel with induced horizontal resonance simulated in COSY. The trajectory of a 250 MeV/c μ was launched offset in both planes from the reference orbit by 2 cm and 140 mr and tracked ~ 10 plotted every two dipole periods in the horizontal plane with (a) no resonance induced and (b) (d) various strengths for resonance inducing harmonic fields

After linear simulations of cooling without stochastic effects for a distribution of particles it was determined that using the parameters listed in Table III provided the best cooling efficiency after 200 cells. The initial distribution has a 6D emittance of 1.27×10^{-4} m^3 rad^3. Without inducing the parametric resonance after 200 cells 6D emittance was reduced to 7.9×10^{-6} m^3 rad^3. With the induced resonance, 6D emittance was reduced to 4.39×10^{-14} m^3 rad^3 after the same number of cells. Additional optimization of the wedge thickness and RF cavity parameters is expected to improve this result and improve cooling by more than merely a factor of 2.

TABLE III. Parameters for optimized twin helix cell

PARAMETER	VALUE
Reference particle	250 MeV/c μ
H. Dipole field	8.14375 T
H. Dipole wavelength	20 cm
Straight Quadrupole field	18.91875 T/m
H. Quadrupole field (horizontal resonance part)	4 pT/m
H. Quadrupole wavelength	80 cm
H. Quadrupole phase advance	90 cm
H Quadrupole field (vertical resonance part)	4 pT/m
H. Quadrupole wavelength	40 cm
H. Quadrupole phase advance	14 cm
Beryllium wedge vertical thickness	2 cm
Wedge angle gradient	10
RF cavity voltage	-12.546 MV
RF frequency	201.25 MHz
RF phase	30 degrees

Next stochastic effects were added to the simulations. This was done through modification of the COSY language to calculate and apply a unique stochastic map for each particle interacting with any absorber, following the same methodology used to verify PIC theory for the linear model [25]. Fig. 7(a) and (b) shows the results of the tracking of the trajectory for an individual test muon in the horizontal and vertical phase space for 200 cells with the addition of stochastic effects of multiple Coulomb scattering and energy straggling.

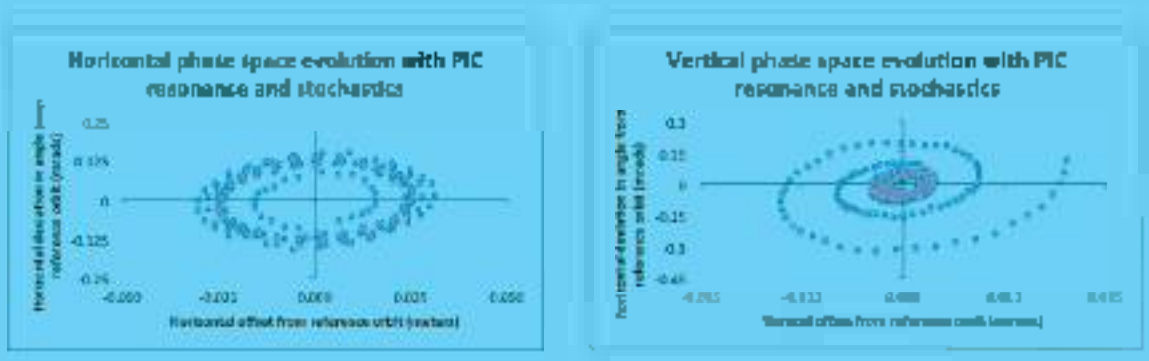

FIG. 7(a-b). (Color) The optimized rotating helix channel simulated in COSY with the stochastic effects of multiple Coulomb scattering and energy straggling. The trajectory of a 250 MeV/c muon was simulated first in both planes of the reference orbit by 2 cm and 130 mr and tracked at the center of each wedge absorber in the (a) the horizontal and (b) vertical planes.

The parameters given in Table III were used for a distribution of 1000 test muons with stochastic effects of multiple Coulomb scattering and energy straggling. For this distribution, the initial coordinates were calculated using a Gaussian distribution with the following sigma ray deviations from the reference orbit: (1) offset in each plane 2 mm; (2) offset in angle in each plane 130 mr; (3) energy spread 1%; and (4) longitudinal bunch length 2 cm. These beam parameters were chosen based on the expected output from an upstream initial 6D helical cooling channel. The results are shown in Fig. 8-(1). With an optimizing wedge thickness of the RF

parameters equilibrium is reached after about 300 cells. The channel's target of a reduction of 6D emittance by 3 orders of magnitude is accomplished after only about 100 cells, equating to a channel length of approximately 10 meters.

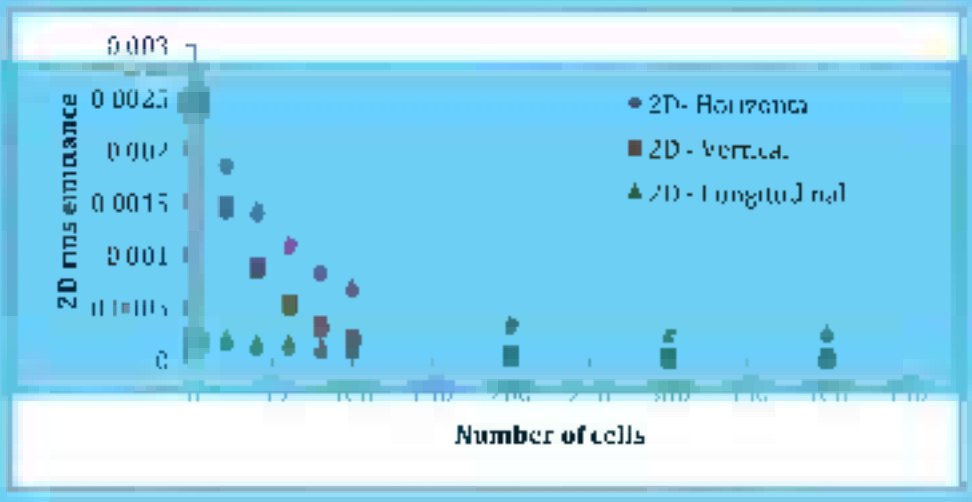

FIG. 8. (Color) Reduction in 2D emittance as a function of channel length.

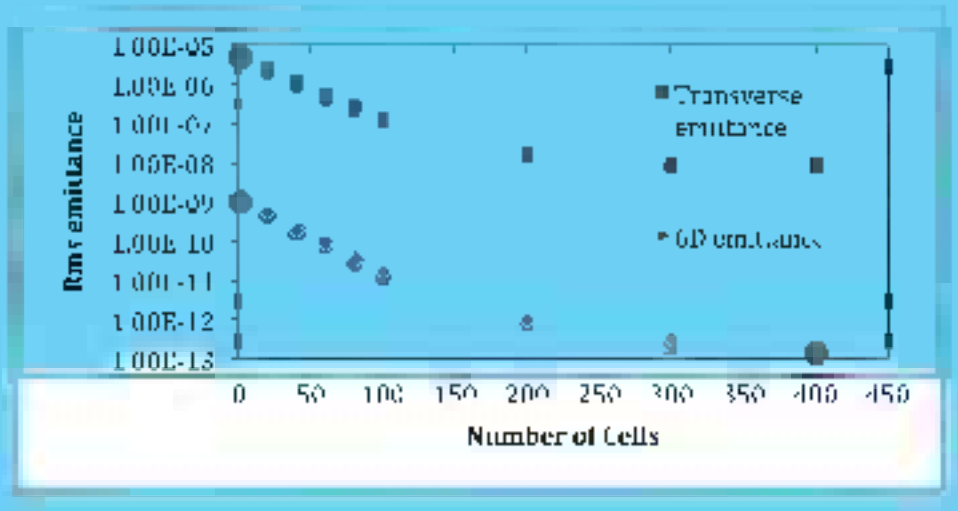

FIG. 9. (Color) Changes in transverse and 6D rms emittance as a function of channel length.

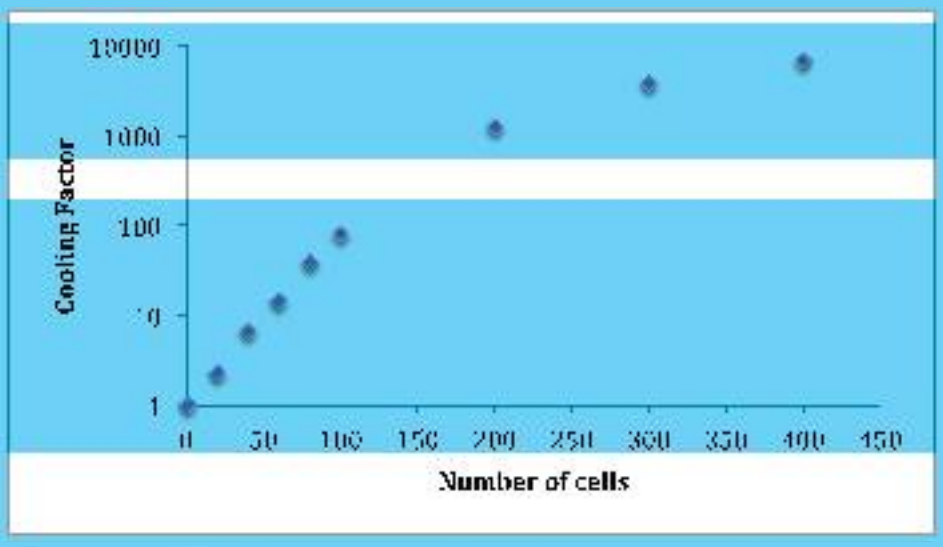

FIG. 10. Cooling Factor (ratio 6D emittance final 6D emittance) as a function of channel length

IV. EVALUATION OF ABERRATIONS IN THE TWIN HELIX CHANNEL

Having studied methods to optimize various parameters for the twin helix channel and simulated cooling with a linear model, the effects of aberrations in the channel need to be evaluated. The linear model described above provides an important tool for optimizing the PIC cooling channel design. This linear model simulates the efficiency of the cooling channel if all non-linear aberrations in the system are perfectly corrected [26]. Since muon beams can have a very large initial angular and energy spread, non-linear effects (aberrations) in the system dependent on these parameters can dramatically change the final spot size of the beam. The efficiency of aberration correction can be determined by comparing the corrected system including non-linear effects, against the linear model.

The optimized PIC channel was simulated to determine how aberrations impacted performance of the cooling channel. The transfer and aberration maps are calculated by COSY from a point on the reference particle orbit at the center of one wedge absorber to the point on the reference orbit that is the center of the next wedge absorber based on the maximum beam size parameters. The optimized twin helix parameters from Table III and a reference momentum of

250 MeV/c were used. Aberrations were determined for: (1) a horizontal and/or vertical deviation from the reference orbit of up to 2 mm in position; (2) a horizontal and/or vertical deviation from the reference orbit in angle of up to 130 mr; (3) a bunch length of up to 3 cm; and (4) a deviation in momentum ($\Delta p/p$) of up to 2%.

Table IV lists the largest 2nd and 3rd order aberrations affecting the final spot size at the periodic focal points in the channel. The maximum effect on final spot size for all other 2nd and 3rd order aberrations is less than 1 mm. The aberration (x|aa), for example, shows the variation (in meters) in final horizontal position of the particle as a function of the square of its initial angle (p_x/p_0) in the horizontal plane.

TABLE IV. Largest 2nd and 3rd order aberrations affecting final spot size for the optimized basic and full twin helix channel with λ_p=20 cm and a 250 MeV/c reference muon.

Aberration	Full Cell Parameter (meters)	Basic Cell Parameter (meters)
(x|aa)	0.00235	0.00173
(x|aδ)	0.00218	0.00208
(x|aaa)	-0.01760	-0.01920
(x|abb)	-0.00599	-0.00640
(y|aab)	0.00598	0.00650
(y|bbb)	0.00111	0.00122

The data in Table IV is noteworthy in that the aberrations for the basic channel are identical in nature and nearly identical in size to those for the full twin helix channel, with resonance inducing helical harmonic pairs, wedge absorbers and RF cavities. Since the aberrations are due primarily to the optics of the basic channel's helical dipole pair and straight quadrupole components, and not the additional elements in the full channel, aberration correction efforts can focus initially on correcting aberrations without the complications of the induced resonances, wedges and RF components.

The aberration maps calculated with COSY show that angular-based aberrations have the greatest effect on the final position of particles in the channel. Because the angular spread in the muon beam can be large, correcting these aberrations is critical to a successful cooling channel

design. In addition to the 2nd and 3rd order aberrations previously noted, angular aberrations of 5th and 7th order were also non-trivial. In particular (planned) and (chromatic), the aberrations to the final horizontal offset from reference orbit based on 5th and 7th powers of the initial horizontal angular deviation from the reference orbit (px/pz), caused substantial instability and particle loss.

Correction efforts focused on superimposing a variety of continuous magnetic fields on the channel. A series of simulations were performed to study the effects of various parameters on the largest 2nd and 3rd order aberrations as well as other aberrations increased by adding correcting magnetic fields.

The basic twin helix channel was simulated with continuous sextupole, octupole and decapole fields superimposed one or one at a time. The effects on the identified aberrations were studied as the pole tip field strengths of these multipoles were varied. Fig. 11 shows an example of this evaluation for the continuous octupole field. The effects of aberrations are plotted in Fig. 11 as functions of the field strength parameter.

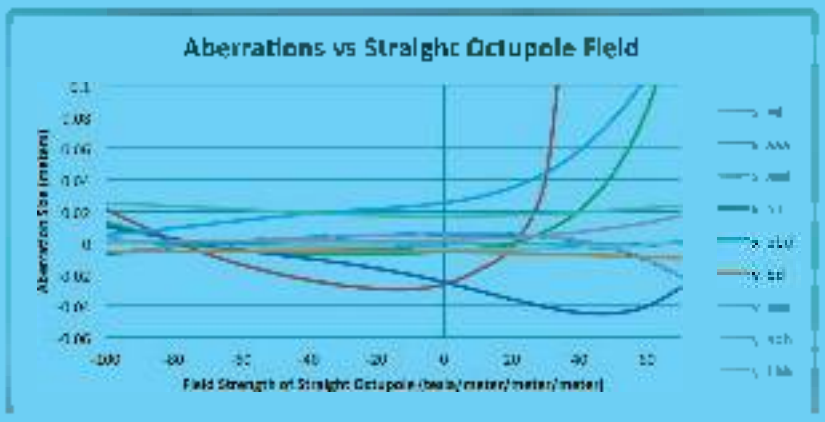

FIG. 11. Effect Dependence of twin helix aberrations on the continuous octupole magnetic field

The effect of superimposing various pairs of helical harmonic magnetic fields was also assessed. These included pairs of helical quadrupole, sextupole, octupole, and decapole harmonics. The effects of each pair were studied independently. Like the helical dipole harmonic pair in the basic 6-D helix channel, each harmonic in these higher order pairs had equal field strengths, phase offsets and equal but opposite helicities. For each superimposed harmonic pair, the effects of varying field strength, wave number, and phase offset on the target aberrations were independently assessed. Figs. 12-14 show examples of this study plotted for the helical sextupole harmonic pairs. Variations in field strength are plotted in a manner similar to that used for the continuous correcting fields. Wavelength variation is plotted as a function of n/k, where n is the number of periods in the given wavelength and k is the wave number ($2\pi/\lambda$).

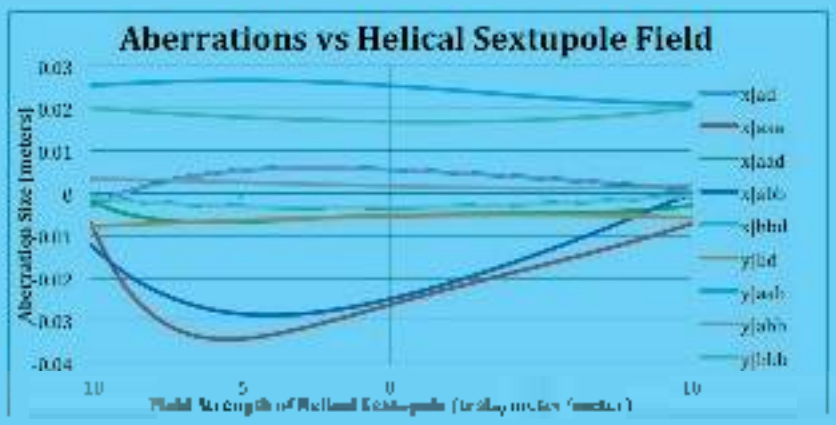

Fig. 12. (Color) Dependence of 6-D helix aberrations on the helical sextupole harmonic magnetic field. Phase offset from helical dipole pair = 0 and $n/k = 1$.

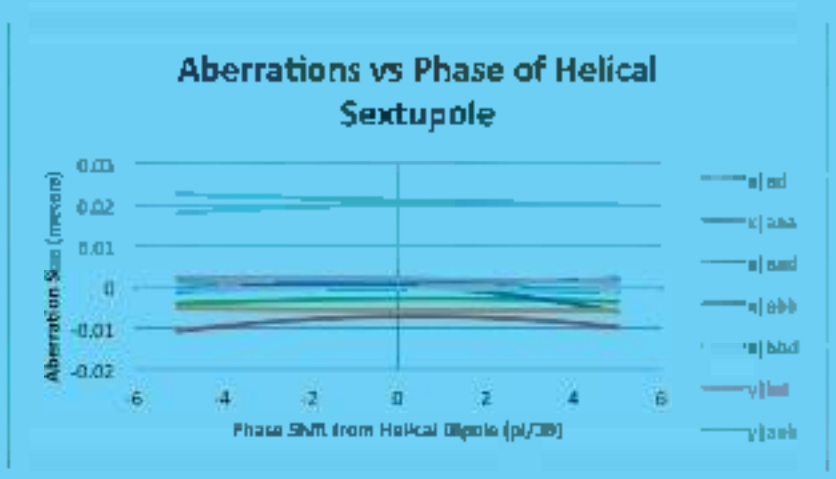

FIG. 13. (Color) Dependence of twin helix aberrations on the helical sextupole harmonic phase offset. Field strength = 10 kG/m², and nk = 3.

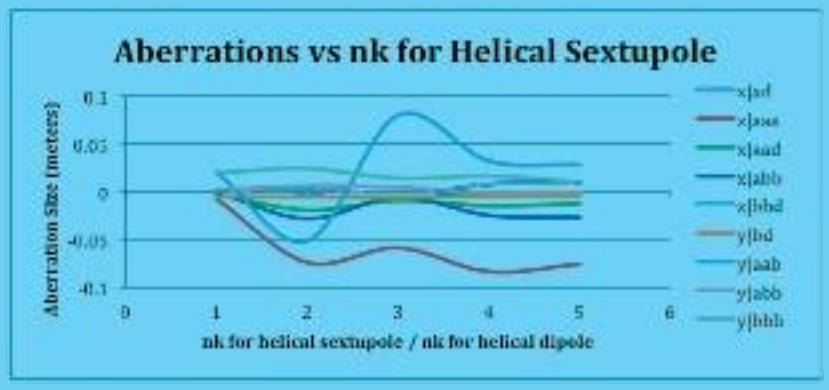

FIG. 14. (Color) Dependence of twin helix aberrations on the helical sextupole harmonic wave number. Field strength = 10 kG/m², helical phase offset from helical dipole part = 0.

These studies identified potential methods for correcting higher order aberrations as well as which aberrations were least sensitive to correction. Based on what was learned, various combinations of correcting magnetic fields were used in an attempt to minimize aberrations in the basic twin helix channel.

In all cases, the correlated optics condition was maintained, and this means that the reference orbit had to be recalculated since these higher order magnetic fields have a "feed-down" effect that modifies the original orbit of the reference particle. For example, as the reference particle oscillates around the channel's optical axis in the x-z mid-plane, it experiences a dipole-

like and quadrupole fo rield from a sextupole field that has been superimposed to correct aberrations. Field strength, phase offset, period and harmonic number provide a number of variable parameters for correcting the system.

A correction model was developed after attempts to simultaneously minimize all three aberrations. This design superimposed two additional pairs of helical quadrupole harmonics, one pair of helical sextupole harmonics, and three pairs of helical octupole harmonics onto the basic twin helix channel. Figs. 15 and 16 show that even after one cell, the sensitivity to large initial angle can be seen. In these simulations, four concentric cones of muons are launched from the same location along the reference orbit with the same momentum, 250 MeV/c. These cones deviate from the reference orbit by an angle of ±30, 60, 90 and 120 mr. The simulations included all non-linear effects up to 9th order, which was sufficient for numerical convergence.

After one cell, as shown in Fig. 15, there is strong focusing for some of the particles, but substantial deviation in final position of others. The muons showing deviation are the ones from the two cones with the largest initial angular deviations from the reference orbit. After 20 cells, as shown in Fig. 16, the surviving muons have the strong focusing characteristic of the PIC resonance effect. Unfortunately, only muons in the cones with angular deviations from the reference orbit of ±30 and 60 mr have survived.

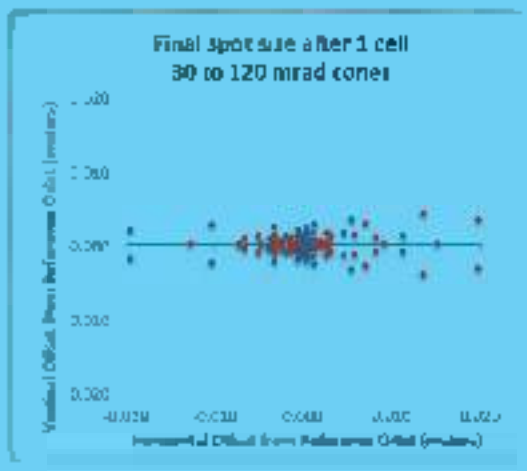

FIG. 15. (Color) Tracking of concentric cones with angular deviation of 30, 60, 90 and 120 mr, of 250 MeV/c muons launched on the reference orbit in COSY with non-linear effects through 9th order for the uncorrected (red) and corrected (blue) gym helix channel

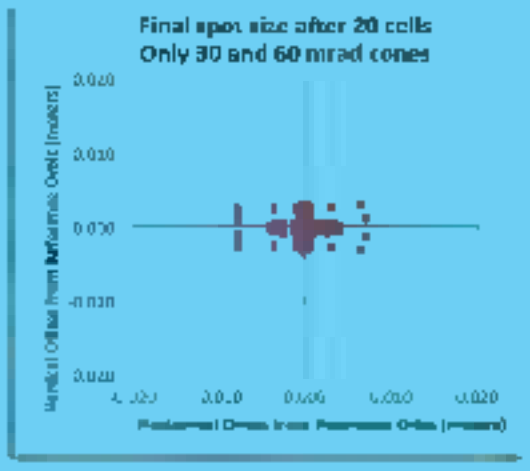

FIG. 16. (Color) Tracking of two concentric cones with angular deviation of 60 and 120 mr, of 250 MeV/c muons launched on the reference orbit in COSY with non-linear effects through 9th order for the uncorrected (red) and corrected (blue) gym helix channel

Fig. 7 displays results of a GEBL simulation of the same channel tracking muons with initial angular spread of up to ± 70 mr through two helix periods. Although these results are promising for this small angle distribution it represents only about half of the equilibrium rms angle expected for a muon with momentum of 250 MeV/c. Muons with an initial angular deviation greater than about 40 mr are eventually lost.

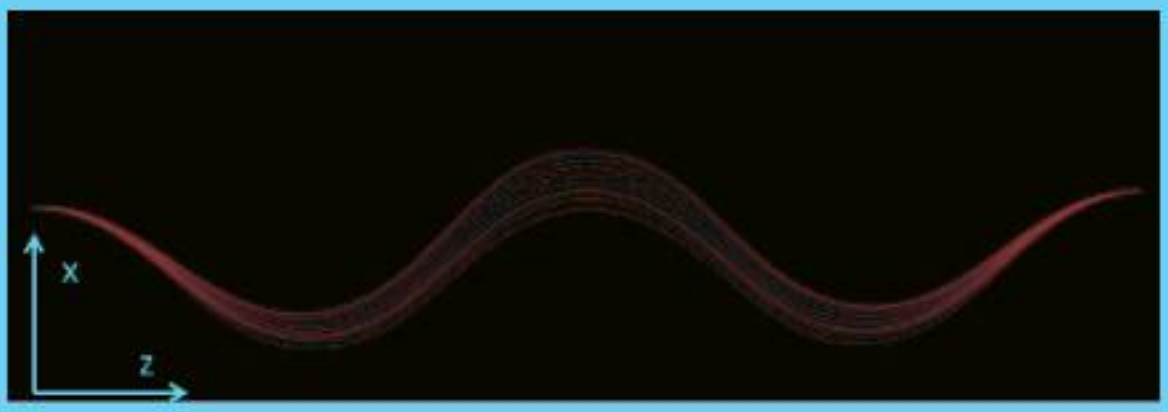

FIG. 17. Cyclic G4Beamline simulation of horizontal motion in the x-z mid-plane through Level 12 dipole periods for a distribution of 250 MeV/c muons launched from the reference orbit with horizontal angular deviations from the reference orbit of up to ±70 mr.

Under the analytic linear model for PIC, the equilibrium beam conditions can be determined as a function of key parameters. The equilibrium rms beam size σ_x and angular spread θ at the absorber and the equilibrium rms momentum spread $\Delta p/p$ are given by eqns. 10 [27]

$$\sigma_x^2 = \frac{1}{8}\frac{(2\gamma^2-1)}{\gamma\beta^2}\frac{m_e}{m_\mu}w^2, \quad \theta_x^2 = \frac{3}{2}\frac{(2\gamma^2-1)}{\gamma\beta^2}\frac{m_e}{m_\mu}, \quad \left(\Delta p/p\right)^2 = \frac{3}{8}\frac{(2\gamma^2-1)}{\gamma\beta^2}\frac{m_e}{m_\mu}\frac{1}{\log} \tag{10}$$

where γ and β are the usual relativistic factors, w is the wedge absorber central thickness, m_e and m_μ are the electron and muon masses, respectively, and $\log$ is the Coulomb logarithm of ionization energy loss for fast particles. Based on these relations, the equilibrium angular and momentum spreads are determined by the reference energy of the muon beam, and the thickness of the wedge absorbers, w, can be used to scale the equilibrium beam size.

The dynamic aperture of the corrected system was still smaller than the equilibrium angular spread for a 250 MeV/c muon beam. Since equilibrium angle spread is inversely proportional to the square root of energy, increasing the reference momentum to 1 GeV/c, lowers the equilibrium angle spread from 130 mr to 65 mr. This is within the acceptance shown in Fig. 17. This would mean accelerating the beam after initial 6D cooling and before a final 6D PIC cooling channel. To verify this, the magnet strength and other parameters were scaled and refit

for a beam with a 1 GeV/c reference momentum. Fig. 18 shows the results of this higher momentum model with aberration correction. In this model, concentric cones of 1 GeV/c muons deviating in angle from the reference orbit by +20, 40, 60 and 80 mr are launched from reference orbit and their final positions are tracked after 40 helical dipole periods. Due to the increase in the reference momentum, this model's dynamic aperture exceeds the equilibrium value for angular spread in the beam. Fig. 9 shows transmission for the same set of concentric cones of 1 GeV/c muons to a final 2 mm spot size after 40 dipole periods. In the uncorrected system, the transmission of muons to a final 2 mm spot size was less than 23%, but in the corrected system this is increased to 60%.

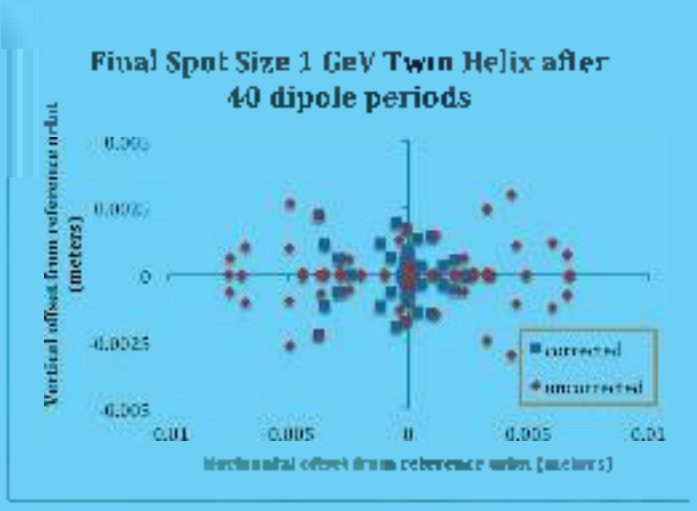

FIG. 18. (Color) Tracking of concentric cones with initial angular deviation of 20, 40, 60, and 80 mr of 1 GeV/c muons launched on the reference orbit in COSY with non-linear effects through 5th order for the uncorrected (red) and corrected (blue) twin helix channel.

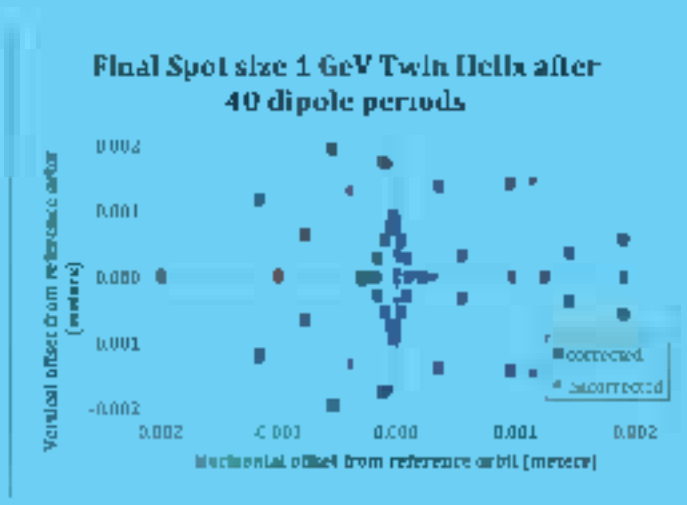

FIG. 9. (Color) Surviving particles within a spot size deviating up to 1 mm from the reference orbit after 40 helical dipole periods for concentric cones, with initial angular deviations of 20, 40, 60 and 80 mr, of 1 GeV/c muons launched on the reference orbit in COSY with non-linear effects through 5th order for the uncorrected (red) and corrected (blue) twin helix channel.

Additional simulations added wedge absorbers to attempt to evaluate cooling in the corrected 1 GeV/c model. Unfortunately, the higher beam energy increased stochastic heating in the beam since energy straggling scales with v^2, and this effect overcame the ionization cooling provided by the thin wedge absorbers. Alternative beamline configurations that implement the PIC principle are being investigated to find a cooling channel lattice with less susceptibility to nonlinear effects.

V. CONCLUSIONS

Muon cooling poses one of the key technical challenges in the successful development of a muon collider to explore high energy physics at the energy frontier. The same technology will be essential to the development of a muon-based Higgs factory to study physics at the intensity frontier. A twin helix channel implementing the principle of PIC has the potential to improve emittance reduction beyond simple ionization cooling methods and is a strong candidate for final 6D cooling in such colliders. Other candidate final cooling techniques include using lithium lenses [28] or extremely high field solenoids that use new high-temperature superconductors operating at low temperatures [29].

The length of the period for the helical dipole harmonics in the basic twin helix channel was optimized; 20 cm was chosen based on reducing the spacing between wedge absorbers to minimize particle loss through decay. Simulations in COSY verified the induced resonances in both horizontal and vertical dimensions. Wedge absorbers and RF cavities can be placed symmetrically in this channel. Field strengths for the helical quadrupole harmonic pairs were adjusted as necessary to trigger the resonance effects with the addition of absorbers and RF. Cooling in this optimized channel was verified with and without stochastic effects.

The effects of chromatic and spherical aberrations in this optimized channel have been studied. This included comparisons of aberrations in both the basic and full twin helix channel. This comparison demonstrated that the aberrations are arising from the basic channel fields, and that correction effort could focus on this simple system that does not have induced parametric resonances, wedge absorbers or RF cavities. Using COSY to determine a map of beam aberrations, the largest aberrations were identified. Simulations compared how various continuous magnetic multipoles and pairs of helical magnetic harmonics affected these aberrations. Using this information, a modified design successfully corrected major aberrations through 9th order. This permitted demonstration of the PIC cooling channel with the inclusion of the correction for aberrations. Unfortunately, the angular acceptance of this channel design was only about half of the equilibrium angular spread in the beam for a reference momentum of 250 MeV/c. By increasing the reference momentum to 1 GeV, the equilibrium angular spread in the beam was reduced to a point that was within the angular acceptance of the twin helix channel. Transmission in the twin helix with aberration correction was substantially improved.

ACKNOWLEDGEMENTS

Funding for this research was supported, in part, through DOE HEP STTR Grant No. DE-SC00005589, "Epicyclic Helical Channels for Parametric-resonance Ionization Cooling."

REFERENCES

[1] C.M. Ankenbrandt, et al., "Status of Muon Collider Research and Development and Future Plans", Phys. Rev. ST Accel. Beams 2, 081001 (1999); R.P. Johnson et al., Recent Inovations in Muon Beam Cooling and Prospects for Muon Colliders, Proc. 2005 PAC, Knoxville, p. 419; International Committee for Future Accelerators, Beam Dynamics Newsletter, No. 55, pp. 32 (Aug. 2011).

[2] R.P. Johnson, et al., Conceptual Design of a Higgs Factory Muon Collider, Proc. NuFact 2012, Williamsburg, VA (July 2012).

[3] K. Paul, R.P. Johnson & V. Yarba, Summary of the Low-Emittance Muon Collider Workshop, WEPLS009, Proc. EPAC 2006, Edinburgh, Scotland p. 2412-14 (Feb. 2006).

[4] Ya.S. Derbenev and R.P. Johnson, Ionization Cooling Using a Parametric Resonance, TPPP014, Proc. PAC05, Knoxville, TN, p. 1374 (2005).

[5] Ya.S. Derbenev and R.P. Johnson, Parametric-Resonance Ionization Cooling and Reverse Emittance Exchange for Muon Colliders, AIP Conf. Proc., 821, 420, p. 421 (2006).

[6] Ya.S. Derbenev et al., Parametric-Resonance Ionization Cooling of Muon Beams, arXiv: 1205.3476v1, p. 6 (2012).

[7] V.S. Morozov, et al., Epicyclic Twin-Helix Magnetic Structure for Parametric-Resonance Ionization Cooling, MOPEA042, Proc. IPAC 2010, Kyoto, Japan, p.166 (2010).

[8] J.A. Maloney, et al., EPIC Muon Cooling Simulations using COSY Infinity, MOP050, Proc. PAC 2011, New York, USA, p. 190 (2011).

[9] V.S. Morozov, et al., Twin Helix Channel for Parametric Resonance Ionization Cooling, AIP Conf. Proc. 1299, p. 664, 670 (2010).

[10] V.S. Morozov, et al., Epicyclic Twin-Helix Ionization Cooling Simulations, MOP036, Proc. PAC 2011, New York, USA, p. 163 (2011).

[11] V.S. Morozov, et al., Parametric-Resonance Ionization Cooling in Twin-Helix, WEPZ009, Proc. IPAC 2011, San Sebastian, Spain, p. 2784 (2011).

[12] V.S. Morozov, et al., Progress on Parametric-Resonance Ionization Cooling Channel Development, WEPPP005, Proc. IPAC 2012, New Orleans, LA, p. 2729 (2012).

[13] J.A. Maloney, et al., EPIC Muon Cooling Simulations using COSY Infinity, MOP050, Proc. PAC 2011, New York, USA, p. 190 (2011).

[14] M. Berz and K. Makino, COSY Infinity Version 9, Nuclear Instruments and Methods A558, 346-350 (2005).

[15] J.A. Maloney, et al., Parametric-Resonance Ionization Cooling for Muon Beams in the Twin Helix Channel, Doctoral Dissertation, Northern Illinois University, DeKalb, Illinois (2013)

[16] J.A. Maloney, et al., Studies of the Twin Helix Parametric-Resonance Ionization Cooling Channel with COSY Infinity, TUPPD011, Proc. IPAC 2012, New Orleans, LA, p. 1428 (2012).

[17] J.A. Maloney, Progress Towards Parametric-Resonance Ionization Cooling, Proc. NUFACT 2012, Williamsburg VA, p. 71 (2012).

[18] G4Beamline, http://g4beamline.muonsinc.com. T. Roberts, G4Beamline Validation (June 2012), http://muonsinc.com/muons3/g4beamline/G4beamlineValidation.pdf.

[19] J.A. Maloney, et al., Studies of the Twin Helix Parametric-Resonance Ionization Cooling Channel with COSY Infinity, TUPPD011, Proc. IPAC 2012, New Orleans, LA, p. 1428 (2012); J.A. Maloney, Progress Towards Parametric-Resonance Ionization Cooling, Proc. NUFACT 2012, Williamsburg, VA, p. 71 (2012).

[20] Ya.S. Debernev & R.P. Johnson, Six-dimensional muon beam cooling using a homogenous absorber: Concepts, beam dynamics, cooling decrements, and equilibrium emittance in a helical dipole channel, Phys. Rev. ST-AB 8, 041002 (2005); K. Yonehara, et al., A Helical Cooling Channel System for Muon Colliders, MOPD076, Proc. IPAC 2010, Kyoto, Japan, p. 870 (2010); C. Yoshikawa, et al., Complete Muon Cooling Channel Design and Simulations, TUPPD012, Proc. IPAC 2012, New Orleans, USA, p. 1433 (May 2012).

[21] Ya. S. Derbenev & R.P. Johnson, Ionization Cooling Using A Parametric Resonance, TPPP014, Proc. PAC 2005, Knoxville, Tenn. p. 1374-76 (2005).

[22] D. Neuffer, Ionization Cooling Introduction, presented at 4th Low Emittance Muon Collider Workshop, Fermilab, June 8, 2009; Handbook of Accelerator Physics and Engineering, Chapter 2.8.4, D. Neuffer, Ionization Cooling, p. 179.

[23] Ya.S. Derbenev and R.P. Johnson, Parametric-Resonance Ionization Cooling and Reverse Emittance Exchange for Muon Colliders, AIP Conf. Proc., 821, 420, p. 421 (2006); V. Ivanov, et al., Reverse Emittance Exchange for Muon Colliders, WE6PFP093, Proc. PAC 2009, Vancouver, Canada, p. 2721 (2009).

[24] V.S. Morozov, et al., Parametric-Resonance Ionization Cooling of Muon Beams, AIP Conf. Proc. 1507, 843 (2012).

[25] J.A. Maloney, et al., Parametric-Resonance Ionization Cooling for Muon Beams in the Twin Helix Channel, Doctoral Dissertation, Northern Illinois University, DeKalb, Illinois (2013).

[26] J.A. Maloney, et al., Studies of the Twin Helix Parametric-Resonance Ionization Cooling Channel with COSY Infinity, TUPPD011, Proc. IPAC 2012, New Orleans, LA, p. 1428 (2012).

[27] V.S. Morozov, et al., Parametric-Resonance Ionization Cooling of Muon Beams, AIP Conf. Proc. 1507, 843 (2012).

[28] V. Balbekov, Lithium Lenses Based Muon Cooling Channel, WPAE032, Proc. 2003 PAC, p. 2014.

[29] S.A. Kahn, et al., High Field Solenoid Magnets for Muon Cooling, WEPLS108, in proc. EPAC 2006, Edinburgh, Scotland, p. 2634 (Feb. 2006).